

BEC

BIOENERGETICS
COMMUNICATIONS

Mitochondrial Pathways and Respiratory Control

An Introduction to OXPHOS Analysis

Erich Gnaiger



Bioenergetics Communications 2020.2

Did you know that keeping your mitochondria fit is essential for quality of life, brain and muscle function, and resistance against preventable, immunological, and age-related degenerative diseases?

The capacity of cellular oxidative phosphorylation (OXPHOS) — a direct measure of mitochondrial function — is a result of evolution, age, gender, lifestyle, and environment (EAGLE). Increasingly, western lifestyle and aging contribute to mitochondrial dysfunction and the current epidemic of preventable diseases, including neurodegenerative and cardiovascular diseases, obesity, diabetes, and various types of cancer. The mitObesity epidemic leads to multimorbidity in aging and threatens to overwhelm the capacity of healthcare systems.

Training in mitochondrial physiology and bioenergetics, therefore, has high relevance to society. The *'Blue Book'* on *Mitochondrial Pathways and Respiratory Control* presents a fundamental introduction to OXPHOS analysis for students and researchers in life sciences — from evolutionary biology to medical and environmental applications. It combines concepts of bioenergetics and biochemical pathways related to mitochondrial core energy metabolism, provides the basis for substrate-uncoupler-inhibitor titration (SUIT) protocols, and updates the terminology consistent with the MitoEAGLE white paper on *Mitochondrial Physiology*.

It is now our responsibility to transfer the enthusiasm for innovation, reproducibility, and quality in science, and to translate mitochondrial research into visionary healthcare solutions.



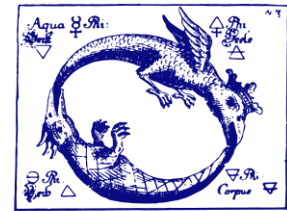
www.oroboros.at



BIOENERGETICS
COMMUNICATIONS

www.bioenergetics-communications.org

ISBN 978-3-9504814-2-6
BEC2020.2 doi:10.26124/bec:2020-0002



Mitochondrial Pathways and Respiratory Control

An Introduction to OXPHOS Analysis

Erich Gnaiger

Bioenergetics Communications 2020

©2020 The Author

Printed by Steiger Druck GmbH, Axams, Austria steigerdruck@tirol.com
Cover design: Paolo Cocco

5th edition 2020: 5000 prints

doi:10.26124/bec:2020-0002

ISBN 978-3-9504814-2-6

2014 4th edition: 4000 prints; ISBN 978-3-9502399-8-0

2012 3rd edition: 2400 prints; ISBN 978-3-9502399-6-6

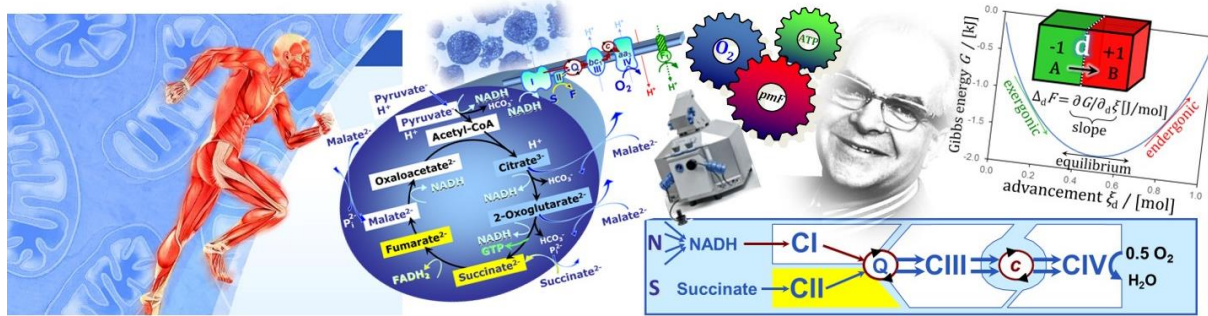
2007 1st edition: 1000 prints; electronic 1st edition, ISBN 978-3-9502399-0-4

Open Access:

https://www.bioenergetics-communications.org/index.php/Gnaiger_2020_BEC_MitoPathways

Oroboros Instruments GmbH
High-Resolution Respirometry
Schöpfstr. 18
A-6020 Innsbruck, Austria
erich.gnaiger@orooboros.at
www.orooboros.at

D. Swarovski Research Lab.
Dept. Visceral, Transplant and
Thoracic Surgery
Medical University of Innsbruck
A-6020 Innsbruck, Austria
www.bioblast.at



The four previous editions of the *Blue Book* are Open Access available on the Bioblast website. Three editions are printed as *Mitochondrial Physiology Network* publications. The 5th Open Access edition is published in the new journal *Bioenergetics Communications*. The previous chapters have gained as *living communications* from an informal ‘open review’ system. As a monograph communication the new chapters 7 and 8 of the *Blue Book* have not undergone peer review, but are open generally for feedback. The 5th edition was elaborated in the frame of the H2020 project NextGen-O2k, from which funding was received for the printed version. Information that is specific for the Oroboros O2k and NextGen-O2k is included here for scientific methodological purposes.



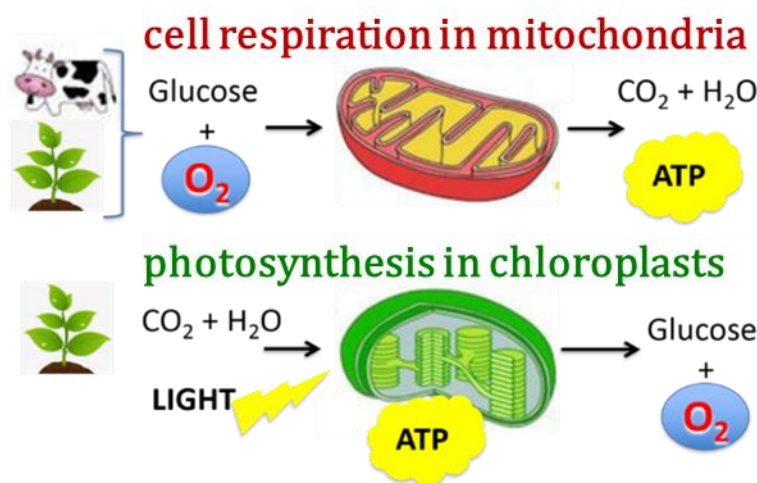
The project NextGen-O2k has received funding from the European Union’s Horizon 2020 research and innovation programme under grant agreement No 859770.



Competing financial interests: Erich Gnaiger is founder and CEO of Oroboros Instruments, Innsbruck, Austria.

Oroboros Instruments High-Resolution Respirometry

The Oroboros O2k-FluoRespirometer provides the basis for high-resolution respirometry (HRR). The O2k represents the technologically leading instrument for quantitative evaluation of mitochondrial function worldwide, represented in 49 countries with 680 O2k-Network Labs (2020). By integrating fluorometry into the O2k, HRR combines two instruments in one to explore O₂ consumption, H₂O₂ production, mt-membrane potential, ATP production, and Ca²⁺ concentration. Potentiometric and amperometric add-on modules support ion-selective electrodes (TPP⁺; pH) and NO, H₂S and H₂O₂ sensors.



Further extended by novel Q-redox and PhotoBiology modules, the NextGen-O2k is the all-in-one device for real-time monitoring of mitochondrial and microbial respiratory states and rates. Studies of oxygen consumption by the ‘bioblasts’ are extended to oxygen production by the chloroplasts. The NextGen-O2k innovations build upon the Oroboros O2k, distributed since 1992 and further

developed since 2001 as the signature of the Oroboros Ecosystem.



Figure 1. The *Blue Book: Mitochondrial Pathways and Respiratory Control* 1st edition. 1st Mitochondrial Physiology Summer School, MiPsummer July 2007, Schröcken, Austria.

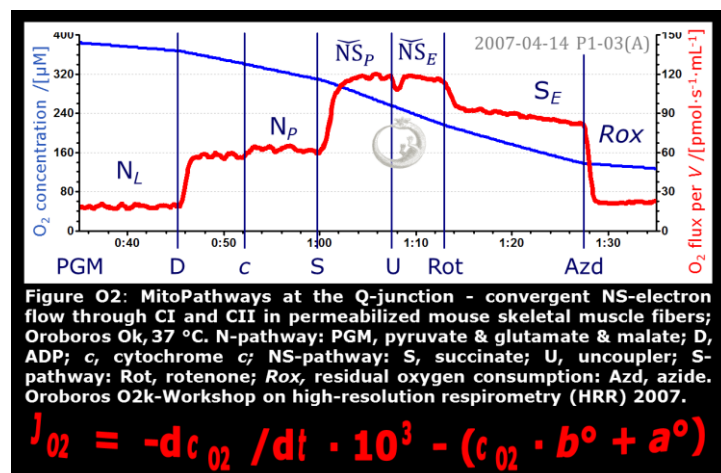
Mitochondrial Pathways and Respiratory Control

Preface

Mitochondrial physiology is part of our lives. Mitochondrial fitness — the capacity of oxidative phosphorylation (OXPHOS) — is essential for the quality of your life, for brain and muscle function, for resistance against preventable and age-related degenerative diseases. Evolutionary background, age, gender (sex), lifestyle, and environment (EAGLE) determine mitochondrial fitness, which is OXPHOS capacity and multiple mitochondrial functions. Comprehensive OXPHOS analysis is vital for understanding your cells, and for our health care systems. These deserve reliability of analytical and diagnostic methods.

The *Blue Book on Mitochondrial Pathways and Respiratory Control* presents a fundamental introduction to OXPHOS analysis. It combines concepts of bioenergetics and biochemical pathways related to mitochondrial (mt) core energy metabolism and provides the basis for the substrate-uncoupler-inhibitor titration (SUIT) protocols in high-resolution respirometry, which have been established since publication of the first edition of *MitoPathways* in 2007 (Figure 1).

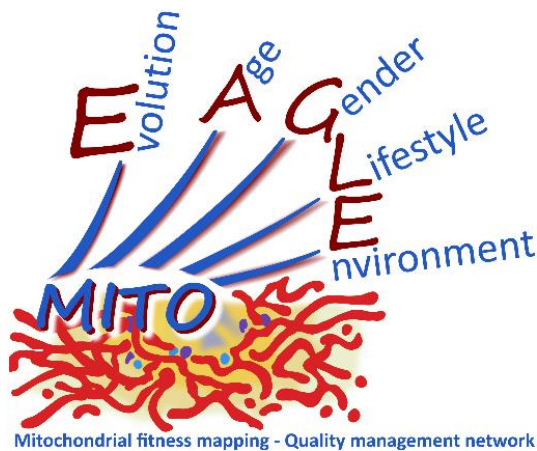
Figure 2. High-resolution respirometry (HRR) and OXPHOS analysis. O2k experiment performed at an O2k-Workshop (IOC39, April 2007, Schröcken, Vorarlberg, Austria).



SUIT protocols for real-time OXPHOS analysis are a component of metabolic phenotyping (Figure 2). OXPHOS analysis extends conventional bioenergetics to the level of mitochondrial physiology

for functional diagnosis in health and disease. The Oroboros O2k for HRR has the high signal stability and unrestricted flexibility of titrations suited for application of elementary and complex SUIT protocols. The emphasis on clarity, reproducibility, and innovation is matched by canonical referencing between chapters in the *Blue Book*, revealing isomorphic links between traditionally separated concepts.

Mitochondrial pathways integrate respiratory control with anaplerotic and cataplerotic metabolism as a communication network between mitochondria and the cell, which is a hallmark of mitochondrial physiology. Since 2007, research in mitochondrial physiology sparked a revolution of bioenergetics by experimental design that appreciates the convergent architecture of the electron transfer system (ETS) with multiple branches of mitochondrial pathways converging at the Q-junction, leading to a novel concept of *additivity* introduced in the new Chapter 7 of the *Blue Book*. These advancements are documented by >1,300 reports listed under 'NS-pathway control state' (https://wiki.oroboros.at/index.php/NS-pathway_control_state) in MitoPedia. To study respiratory control at the Q-junction, SUIT protocols are applied with physiological substrate cocktails, particularly NADH-linked substrates (N) in combination with succinate (NS), fatty acids (FNS), and glycerophosphate (FNSGp), which have been introduced for the first time in the 1st edition of *MitoPathways* (2007).



Since then, 'MitoPedia' was initiated and the COST Action MitoEAGLE flies. 666 coauthors joined forces to present a harmonized nomenclature on *Mitochondrial Physiology* (Bioenerg Commun 2020.1), with an emphasis on conceptual consistency for establishing a quality-controlled database on mitochondrial respiratory physiology. The 5th edition of *MitoPathways* gained from this collaboration. Many terms and symbols are simplified or presented in a more explicit form compared to the 2014 edition. Terms and iconic symbols develop meaning in context. Contextual meaning is best communicated by stories told in entertaining lectures, or by equations even if they turn off the most motivated student. Motivation is never enough. We need passion, persistence, resilience to transpose equations, terms and stories into the domain of personal experience, gaining perspective from perception to conception. The best scientific experience is the experiment driven by a hypothetical story written in clear words and forged into meaningful equations. This may provide a guideline to the critical discussion of the *ergodynamic* concept of the protonmotive force and protonmotive pressure, inspired by the *Grey Book* of Peter Mitchell and added as the new Chapter 8 of the *Blue Book*.

Mitochondria are the structural and functional elementary units of cell respiration. *MitoPathways* is an element of the Oroboros Ecosystem driven by high-resolution respirometry and shaping mitochondrial physiology. A mosaic evolves by combining the elements into a picture of modern mitochondrial respiratory physiology.

I thank all collaborators of the NextGen-02k project and the authors and coauthors of various publications emerging from international cooperations, particularly the Horizon 2020 funded COST Action CA15203 MitoEAGLE. Without the team of Oroboros Instruments, including our partners in electromechanical engineering (02k; WGT-Elektronik, Kolsass, Austria) and DatLab software development the experimental advances on *MitoPathways* would not have been possible.

Erich Gnaiger

Innsbruck, 2007 - 2020



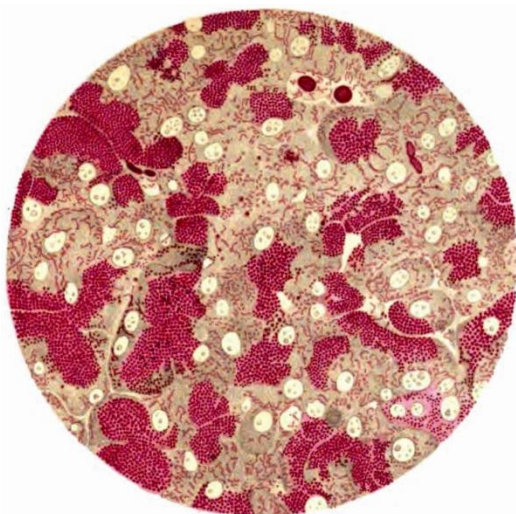
Contents

1. Real-time OXPHOS analysis	7
2. Respiratory states and rates: Coupling control	23
3. Normalization of rate: Flow, flux, and flux ratios	34
4. NADH-linked pathways through Complex CI: Respiratory pathway control with pyruvate, glutamate, malate	41
5. S-pathway through Complex CII, F-pathway through CETF, Gp-pathway through CGpDH	48
6. Convergent electron transfer at the Q-junction: NS-pathway through Complexes CI & CII	52
7. Additivity of convergent electron transfer	66
8. Protonmotive pressure and respiratory control	73
A. Conversions of metabolic fluxes	107
B. Substrates, uncouplers, inhibitors - SUIT	110
C. References	112

Citation

Gnaiger E (2020) Mitochondrial pathways and respiratory control. An introduction to OXPHOS analysis. 5th ed. Bioenerg Commun 2020.2:112 pp.

doi:10.26124/bec:2020-0002



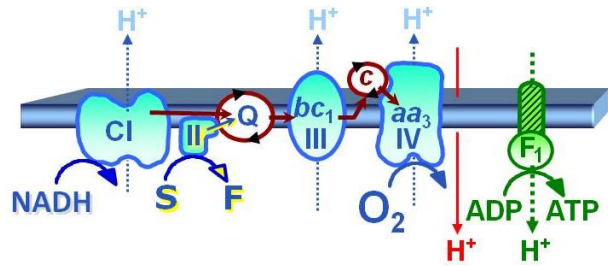
Bioblasts. *Left:* Richard Altmann (1894). *Right:* Odra Noel (2010) Homage to pioneers – Altmann’s bioblast (*MiPAr*t, Innsbruck, Austria).

A guide through the chapters

- 1. Real-time OXPHOS analysis.** — Richard Altmann's bioblasts are the systematic unit of bioenergetics and chemiosmotic coupling studied in living cells and mitochondrial preparations. A rigorous understanding of mitochondrial respiratory control relies on a clear concept of metabolic states and rates, accurate measurement and normalization of oxygen flux, and analysis of mitochondrial pathways.
- 2. Respiratory states and rates: coupling control.** — A concept-driven terminology frames our perception of the meaning of respiratory states and rates, from ROUTINE respiration of living cells to the capacity of oxidative phosphorylation (OXPHOS) determined in mitochondrial preparations, electron transfer (ET) capacity, LEAK respiration, and the distinction of uncoupled, noncoupled, or dyscoupled respiration.
- 3. Normalization of rate: flow, flux, and flux ratios.** — '*The challenges of measuring respiratory rate are matched by those of normalization*' (Gnaiger et al 2000). The effect of metabolic control variables on flow or flux can be expressed by normalization for rate in a *reference state*, and is evaluated relative to a *background state*. The concept of flux control efficiency is based on principles of thermodynamics and is guided by statistical considerations, to remove the bias of the classical respiratory control ratio.
- 4. NADH-linked pathways through Complex CI: respiratory pathway control with pyruvate, glutamate, malate.** — Substrate combinations feeding electrons into the ET system through NADH have been considered to reflect physiological respiratory states in mitochondrial preparations. These protocols ignored the importance of cataplerotic metabolite depletion in the tricarboxylic acid (TCA) cycle.
- 5. S-pathway through Complex CII, F-pathway through CETF, Gp-pathway through CGpDH.** — Succinate as the substrate of CII is at a level comparable to NADH as the substrate for CI. Too many textbooks and publications propagate the error of comparing NADH in the N-pathway with FADH₂ in the S-pathway — together with fumarate, FADH₂ is a product but not a substrate of CII.
- 6. $\bar{N}\bar{S}$ -pathway through Complexes CI & CII: convergent electron transfer at the Q-junction.** — The term 'electron transport chain' is a misnomer in bioenergetics, concealing the convergent pathway architecture of the electron transfer *system* (ETS). This has direct implications on the design of substrate-uncoupler-inhibitor titration (SUIT) protocols, for reconstitution of TCA cycle function, and sequential separation of branches of mitochondrial pathways for OXPHOS analysis.
- 7. Additivity of convergent electron transfer.** — OXPHOS capacity depends on the degree of additivity of pathways converging at the Q-junction. Paradoxically, current concepts on *interaction* do not agree whether to categorize incompletely additive effects as synergistic or antagonistic. A new mathematical definition of additivity bridges the gap between these apparently incompatible models of interaction.
- 8. Protonmotive pressure and respiratory control.** — Why is thermodynamics scary? The driving *force* of chemical reactions is confusingly called an energy (*Gibbs energy*), whereas it is actually an isomorphic force, linked to the chemical and electric terms of the protonmotive force. The gas law represents chemical force and gas pressure. Flux-force relations are non-linear. Why should we consider Fick's linear law of diffusion and protonmotive pressure in the control of flux?

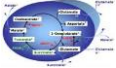
Chapter 1.

Real-time OXPHOS analysis



The protoplasm is a colony of bioblasts. Microorganisms and granula are at an equivalent level and represent elementary organisms, which are found wherever living forces are acting, thus we want to describe them by the common term bioblasts.

Richard Altmann (1894) Die Elementarorganismen und ihre Beziehungen zu den Zellen. Verlag Von Veit & Comp, Leipzig. 160 pp, 34 Tafeln.

Section		Page
	1.1. Chemiosmotic coupling	7
	1.2. Living cells and mitochondrial preparations	8
	1.3. From oxygen concentration to oxygen flux	10
	1.4. The sample in the chamber: count, volume, and mass.....	12
	1.5. Oxygen flow and flux: open the black box.....	14
	1.6. Fluxes and forces: coupling and efficiency	16
	1.7. Electron gating	17
	1.8. Convergent mitochondrial pathways: the Q-junction	17
	1.9. Biochemical thresholds and the Q-junction	20
	1.10. Boundary conditions	21

Oxidative phosphorylation (OXPHOS) is a key element of bioenergetics, extensively studied to resolve the mechanisms of energy transduction in the mitochondrial electron transfer system and to analyze various modes of mitochondrial respiratory control in health and disease. Respiratory flux control is exerted by (1) the density of mitochondria as the elementary units of cell respiration; (2) biochemical composition and structure of the mitochondrial-cytosolic network; (3) respiratory coupling and pathway control in substrate-uncoupler-inhibitor titrations (SUIT) with saturating substrate concentrations; and (4) allosteric kinetic and concentration-dependent substrate-uncoupler-inhibitor kinetic (SUIK) control.

1.1. Chemiosmotic coupling

Peter Mitchell's chemiosmotic coupling theory explains the general mechanism of mitochondrial, microbial and photosynthetic energy transformation. Thus Richard Altmann's 'bioblasts' are fundamentally appreciated to represent the systematic unit of bioenergetics and of the human symbiotic 'supraorganism' with microbial-mammalian co-metabolic pathways. The transmembrane protonmotive force pmF ("or, writing Δp , for the P.M.F.", Mitchell 1966), conceives H^+ translocation as the link between electron transfer and phosphorylation of ADP to ATP (Figure 1.1). Δp has a diffusive component ($\Delta_d F_{H^+}$, related to ΔpH) and an electric component of the pmF ($\Delta_{el} F_{p^+}$, equivalent to the mt-membrane potential difference $\Delta\Psi$),

$$\Delta p \equiv - \frac{2.3 \cdot RT}{F} \cdot \Delta pH + \Delta\Psi \quad [V] \quad 1.1$$

$$\Delta_m F_{H^+} = \Delta_d F_{H^+} + \Delta_{el} F_{p^+} \quad [V] \text{ or } [J \cdot \text{mol}^{-1}] \quad 1.2$$

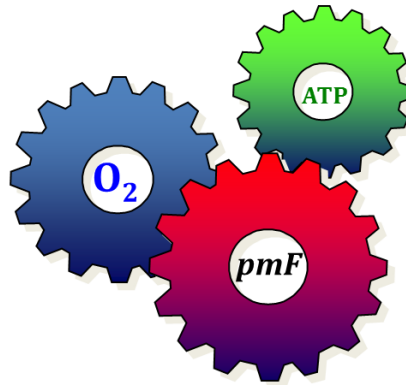
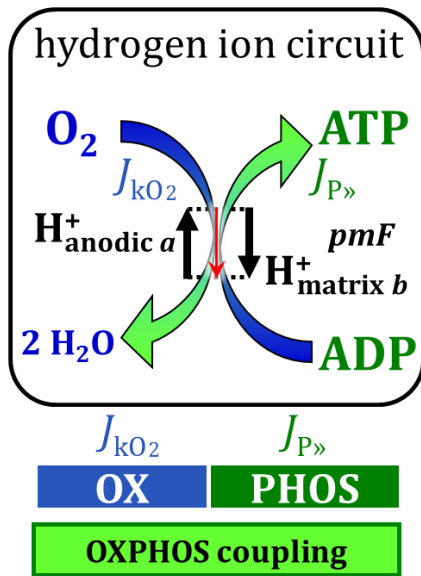


Figure 1.1. Coupling in oxidative phosphorylation is mediated by the protonmotive force pmF , linking electron transfer (catabolic O_2 flux J_{kO_2}) through the hydrogen ion H^+ circuit to phosphorylation $J_{P\gg}$ of ADP to ATP.

Physicochemical quantities — with symbols in *italics* — have magnitude and generalized or abstract units. These units are shown in brackets ([V] in Eq. 1.1). The rationale for distinguishing between equivalence (\equiv in Eq. 1.1) and equality ($=$ in Eq. 1.2) is elaborated in Chapter 8.

Mitochondrial respiration is the exergonic input of catabolism coupled to the endergonic output of phosphorylation. OXPHOS capacity P is measured at saturating ADP and P_i concentrations, which cannot be achieved in living cells. ET capacity E is quantified by titrations of an uncoupler (protonophore) to obtain maximum flux in mitochondrial preparations or living cells (Figure 1.2). E and P are numerically identical only if the phosphorylation system (adenylate nucleotide translocase, phosphate carrier, ATP synthase; Figure 2.7) does not exert control over coupled respiration. A shift towards control of OXPHOS by the phosphorylation system is observed particularly when ET capacity is increased by the additive effect of convergent electron transfer into the Q-junction.

LEAK respiration L is the oxygen flux compensating for leak, slip and cation cycling, with electron slip in ROS production usually exerting a minor effect on L . LEAK respiration is measured in the presence of fuel substrate(s) but absence of ADP or after inhibition of the phosphorylation system, usually by oligomycin or carboxyatractyloside (Figure 1.2). In this non-phosphorylating resting state a maximum pmF is maintained, exerting feedback control by depressing oxygen flux to a level determined mainly by ion leaks and the H^+/O_2 flux ratio. LEAK respiration measured in this state of maximum pmF represents the upper limit of the LEAK component in ADP-stimulated respiration; but then the pmF is reduced, thus reducing the LEAK component in the OXPHOS state.

1.2. Living cells and mitochondrial preparations

Living cells (ce) play an important role in mitochondrial physiology, since bioenergetic functions depend on cell vitality as much as cell vitality depends on mitochondrial function. While living cells are characterized by cell viability, mitochondrial integrity is maintained in mitochondrial preparations in which the plasma membrane is selectively permeabilized or removed (Table 1.1). In contrast to free-living bacteria, mitochondria (and chloroplasts and various parasitic microbes) are bioblasts which cannot *live*, but can *function* when properly isolated from their intracellular environment. Therefore, functional mitochondrial *fitness* rather than *viability* can be tested, progressing from the experimental level of quality control of the mt-preparation to the biomedical level of physiological fitness. Any loss of mitochondrial fitness induced artificially by the preparation procedure must be distinguished from pathophysiological mitochondrial dysfunction as a readout of real-time OXPHOS analysis and functional scoring.

Table 1.1. Mitochondrial preparations with integrity of mt-inner and outer membranes (mtIM and mtOM), versus living cells with intact plasma membrane barrier function

Symbol	Name and description
imt	isolated mitochondria
thom	tissue homogenate
pfi	permeabilized muscle fibers , selective permeabilization of the plasma membrane mechanically and with saponin, integrity of the mt-cytoskeletal structure
pti	permeabilized tissue , selective permeabilization of the plasma membrane mechanically and with mild detergents, integrity of the mt-cytoskeletal structure
pce	permeabilized cells , selective permeabilization of the plasma membrane with digitonin, integrity of the mt-cytoskeletal structure
ce	living cells , the population of living cells consists of viable cells (vce) but may contain a fraction of dead cells (dce; loss of plasma membrane barrier function)

The easily visible nuclei of dead cells (dce) but not of viable cells (vce) are stained with plasma membrane permeable dyes (e.g. trypan blue). In a population of living cells, $N_{ce} = N_{vce} + N_{dce}$, cell viability is scored as the fraction of cells with intact plasma membranes, N_{vce}/N_{ce} . A respirometric cell viability test (SUIT-003 O2 ce-pce D020) is based on the impermeability of cell membranes for ADP (general) and succinate in many types of living cells. Cell viability of 0.95 is frequently considered as a threshold for respirometry with living cells in healthy control groups. High Ca^{2+} concentrations in culture media cause swelling and disruption of mitochondria in dce and inhibit mt-respiration subsequently. When respiration corrected for residual oxygen consumption R_{ox} is expressed on the basis of the viable cell count N_{vce} , the assumption is made that non-viable cells (dce) contribute only to R_{ox} . Complex culture media or simpler respiration media (MiR05-Kit) are used, which may be supplemented with respiratory fuel substrates (such as pyruvate), to measure oxygen flux in the cellular ROUTINE state. In media without fuel substrates, cells respire on endogenous substrates. Different media and external substrate supply modify the potential limitation of ET capacity by intracellular substrates and influence the level of ROUTINE respiration. Definition of the 'basal metabolic rate' (BMR) of cells is open to a wide scope of speculation. If LEAK respiration is considered as 'basal' in mt-preparations, then — to be consistent — LEAK respiration should be referred to as 'basal' in living cells. In any case, aerobic and anaerobic metabolism contribute to ATP turnover and BMR in living cells.

Defined coupling states (Chapters 2 and 3) and pathway states (Chapters 4 to 7) are established in mt-preparations suspended in mt-respiration media. Coupling and pathway states are complementary (Figure 2.4). To remove the plasma membrane barrier in mt-preparations, the plasma membranes and organelles can be (1) separated by mechanical disruption, followed by low-spin centrifugation for crude enrichment (crude thom) and high-spin centrifugation for further isolation and purification (imt). (2) Alternatively, plasma membranes are selectively permeabilized by mechanical fracture (thom, pti, pce) or chemical permeabilization (pfi, pti, pce) with all intracellular structures remaining in the sample. Then soluble cytosolic components are either washed out (pfi, pti, pce) or highly diluted in mt-respiration medium (thom, pfi, pce). The quality of mt-preparations is evaluated by functional tests on the integrity of the mt-outer membrane (mtOM; cytochrome *c* test in specific respiratory states).

With careful preparation, the entire mt-population is recovered in thom and pti including pfi and pce. Then oxygen flux can be expressed on the basis of tissue wet mass m_w [mg] (Section 1.5). m_w is determined before (thom) or after preparation (pfi) before addition of samples to the experimental chamber. Tissue or cell protein mass can be determined in samples recovered from the O2k-chamber. The accuracy of measurement of tissue or protein content and mt-markers (e.g. CS activity) is limited by incomplete recovery from the chamber and large background corrections for protein (BSA and catalase in MiR06). Effects related to mt-density (mt-elementary markers per tissue mass) are separated from those related to mt-quality (function per mt-elementary marker) by mt-normalization (Figure 1.5).

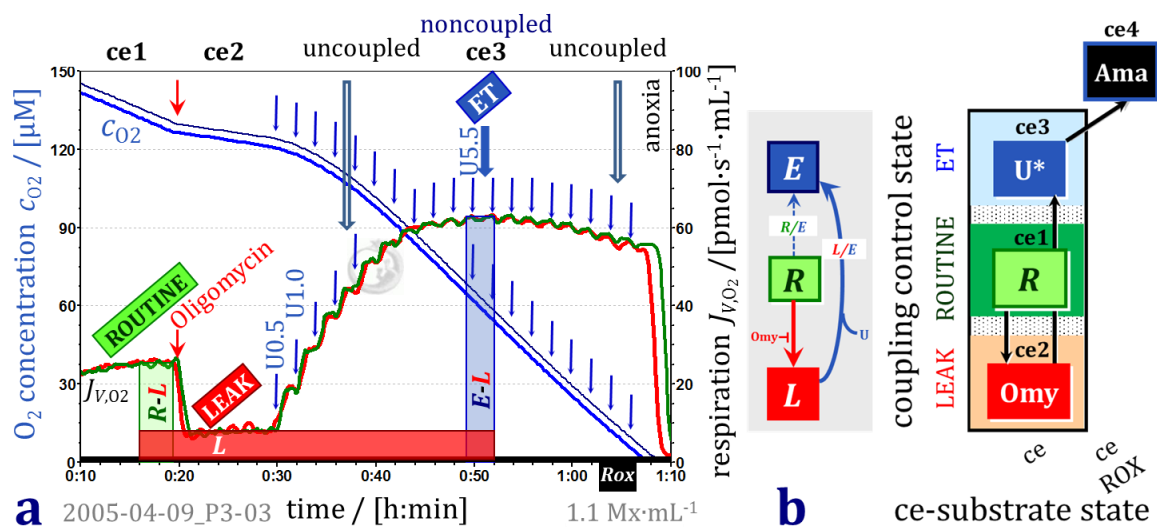


Figure 1.2. O₂ concentration and O₂ flux in living cells with a short coupling-control protocol CCP (SUIT-003). (a) High-resolution respirometry (Oroboros O2k with TIP2k) with parental hematopoietic 32D cells (1.1 Mx·mL⁻¹ = 1.1·10⁶ x·mL⁻¹) suspended in culture medium RPMI at 37 °C. Technical repeats (n=2) in 2-mL O2k-chambers. Superimposed plots of O₂ concentration c_{O_2} [μM = nmol·mL⁻¹], and volume-specific O₂ flux J_{V,O_2} , calculated real-time by DatLab as the negative time-derivative of c_{O_2} corrected for instrumental background O₂ flux ($J^{\circ}_{O_2}$): $J_{V,O_2} = -dc_{O_2}/dt \cdot 10^3 - J^{\circ}_{O_2}$ [pmol·s⁻¹·mL⁻¹]. J_{V,O_2} declines to zero at anoxia. (ce1) ROUTINE respiration R. (ce2) Inhibition of ATP synthase (manual titration of oligomycin) to induce non-phosphorylating LEAK respiration L. (ce3) Automatic uncoupler titrations (10 mM FCCP in the TIP2k) in steps of 0.1 μL corresponding to incremental steps of 0.5 μM FCCP at intervals of 120 s. Maximum noncoupled flux (electron transfer- or ET capacity E) is reached at 5.5 μM FCCP. Respiration is inhibited at higher [FCCP], corrected for sample dilution (<1 % effect). The E-L coupling efficiency, $j_{E-L} = (E-L)/E$, is 0.90. Modified after Gnaiger (2008) (O2k-Workshop IOC30). (b) Coupling-control states and rates in living cells. (ce4) Residual oxygen consumption Rox ($J_{V,Rox}$; ROX-state), induced by inhibition of CIII by antimycin A or myxothiazol.

1.3. From oxygen concentration to oxygen flux

Real-time OXPHOS analysis uses respirometry to study aerobic core metabolism, considering oxygen consumption as an element of mitochondrial fitness. Oxygen flux J_{kO_2} times the driving force of the oxidation reaction provide the input power into the OXPHOS system. In a closed respirometric chamber, the oxygen concentration declines over time

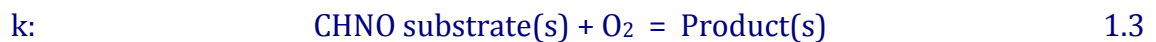
as a result of respiratory processes. The slope or time derivative, therefore, has a negative sign. Why is then the 'rate of oxygen consumption' not expressed as a negative value? Why do we use the term 'oxygen flux' in this context of chemical reactions? The rationale is based on fundamental concepts of physical chemistry and the thermodynamics of irreversible processes in open and closed systems (Gnaiger 1993).

Concentration c_{O_2} [$\text{mol}\cdot\text{L}^{-1} \stackrel{\text{def}}{=} \text{M}$] is the amount n_{O_2} of substance O_2 [mol], per unit volume V [L]. The amount of elemental oxygen n_{O_2} , dissolved per volume of aqueous medium is the O_2 concentration c_{O_2} or $[O_2]$, measured by the polarographic oxygen sensor in the O_2 -chamber as an electric current I [A], converted into a voltage [V]. This raw signal is calibrated to record $c_{O_2,t}$ over time t [s] (Figure 1.2). See Section A for units.

c_{O_2} in pure water at equilibrium with air at standard barometric pressure of 100 kPa is 254.8 and 207.3 $\mu\text{mol}\cdot\text{L}^{-1}$ at 25 °C and 37 °C. When aqueous medium is in equilibrium with a gas phase (air), the partial oxygen pressure p_{O_2} [kPa] is identical in the gas phase and aqueous phase. At equilibrium, the O_2 concentration in the gas phase is much higher than in aqueous solution. The concentration of dissolved O_2 is proportional to the partial O_2 pressure at constant temperature and composition of the aqueous medium. This proportionality is expressed as the O_2 solubility S_{O_2} [$\mu\text{M}\cdot\text{kPa}^{-1}$]. In pure water at 37 °C (25 °C), $S_{O_2(\text{H}_2\text{O})}$ is 10.56 (12.56) $\mu\text{M}\cdot\text{kPa}^{-1}$, but it is $0.89\cdot S_{O_2(\text{H}_2\text{O})}$ to $0.92\cdot S_{O_2(\text{H}_2\text{O})}$ in various culture and respiration media. The solubility factor F_M is 0.92 in MiR05 or MiR06.

Cell respiration is an exergonic process by which reduced CHNO-fuel substrates are oxidised. O_2 is consumed internally in exchange with the cellular environment. In the *closed* experimental chamber, which is sealed against the exchange of O_2 across the chamber boundaries, all O_2 consuming reactions cause a decline in c_{O_2} . If O_2 consumption is stimulated, then c_{O_2} falls off more steeply over time (Figure 1.2). The chamber has to be rigorously stirred to ensure a homogenous distribution of c_{O_2} in the entire volume and to avoid unstirred layers with O_2 diffusion gradients. When all processes reacting with O_2 are fully inhibited, c_{O_2} remains constant and the slope over time is zero. In practise, corrections have to be applied for O_2 diffusion and side reactions (Figure 1.3).

A constant decline of O_2 concentration with time in an ideally closed chamber results in a linear negative slope, indicating that the rate of the chemical reaction consuming O_2 is constant. Defining the catabolic reaction k as



then the O_2 consumption rate per unit volume (= volume-specific O_2 flux J_{V,O_2}) is proportional to the negative slope of $c_{O_2,t}$ with time. Take the difference of O_2 concentration (Y -axis in Figure 1.3a) between two time points (X -axis in Figure 1.3),

$$\text{Concentration axis:} \quad \Delta c_{O_2} = c_{O_2,2} - c_{O_2,1} \quad [\text{mol}\cdot\text{L}^{-1}] \quad 1.4a$$

$$\text{Time axis:} \quad \Delta t = t_2 - t_1 \quad [\text{s}] \quad 1.4b$$

The slope between these points is the rate of concentration change in *difference* format,

$$r_{O_2} = \Delta c_{O_2} / \Delta t \quad [\text{mol}\cdot\text{L}^{-1}\cdot\text{s}^{-1}] \quad 1.5$$

Catabolic flux (Eq. 1.3) is the *negative* slope, corrected for background flux $J^{\circ}_{O_2}$ and R_{ox} ,

$$J_{V,kO_2} = -(\Delta c_{O_2} / \Delta t) - J^{\circ}_{O_2} - J_{V,Rox} \quad [\text{mol}\cdot\text{s}^{-1}\cdot\text{L}^{-1}] \quad 1.6$$

In *differential* format (dt = infinitesimally small Δt), the expression becomes

$$\text{Closed system:} \quad J_{V,kO_2} = -(dc_{O_2} / dt) - J^{\circ}_{O_2} - J_{V,Rox} \quad [\text{mol}\cdot\text{s}^{-1}\cdot\text{L}^{-1}] \quad 1.7a$$

$$\text{General:} \quad J_{V,kO_2} = dn_{O_2}/dt \cdot v_{O_2}^{-1} \cdot V^{-1} = dk\xi_{O_2}/dt \cdot V^{-1} \quad [\text{mol}\cdot\text{s}^{-1}\cdot\text{L}^{-1}] \quad 1.7b$$

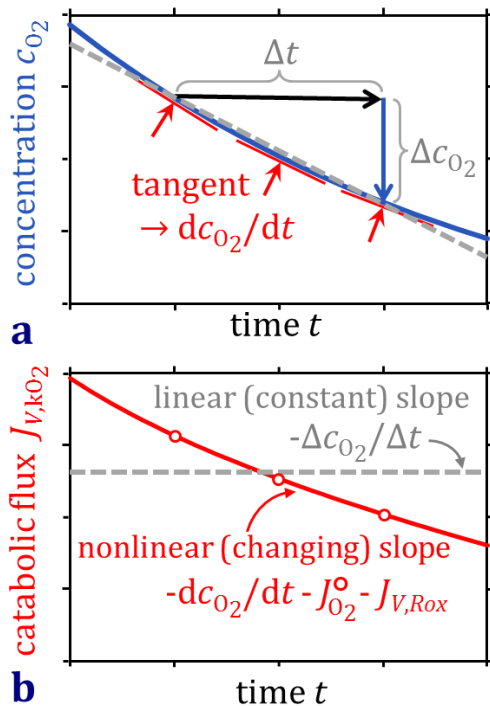


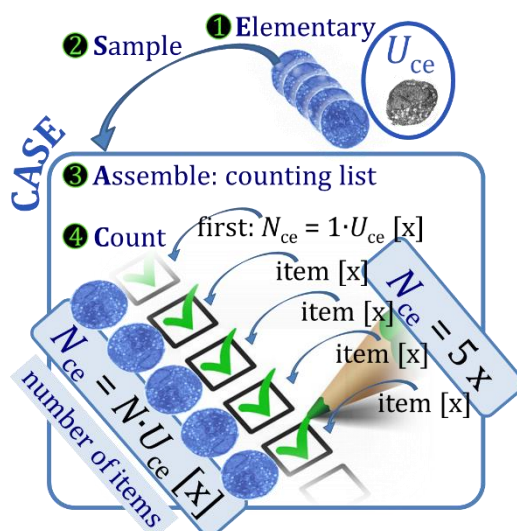
Figure 1.3. From concentration to flux in a closed chamber. (a) The slopes dc_{O_2}/dt of the tangents (arrows) are calculated to monitor flux. **(b)** Catabolic O_2 flux J_{v,kO_2} is corrected for instrumental background O_2 flux $J_{O_2}^o$ and Rox (Eq. 1.7a). $J_{O_2}^o$ is a linear function of $c_{O_2,t}$; $J_{O_2}^o = a^o + b^o \cdot c_{O_2,t}$. Multiplication by 10^3 converts units from $nmol \cdot s^{-1} \cdot mL^{-1}$ to $pmol \cdot s^{-1} \cdot mL^{-1}$ (Figure 1.2).

In contrast to a linear fit (Eq. 1.6), gradual changes of O_2 flux are resolved in the differential format (Eq. 1.7; Figures 1.2 and 1.3). A generalization to open systems is achieved by the concept of *advancement* of reaction, $d_k \xi_{O_2} = d_k n_{O_2} \cdot \nu_{O_2}^{-1}$ (Eq. 1.7b). The subscript O_2 in $d_k \xi_{O_2}$ defines the stoichiometric number of O_2 in reaction (1.3) as $\nu_{O_2} = -1$. Hence respiratory flux J_{v,kO_2} refers to a stoichiometric form of reactions where 1 mol of O_2 is consumed. Division by $\nu_{O_2} = -1$ yields positive values of $d_k \xi_{O_2}$ and J_{v,kO_2} .

Volume-specific O_2 flux J_{v,O_2} (Eq. 1.7; Figures 1.2 and 1.3) is a quantitative measure of the internal reaction per volume of the experimental chamber. What does it mean? The 'black box' is opened at three levels by expressing respiration per size of the sample or per individual object (mass-specific O_2 flux $J_{O_2/mce}$ or O_2 flow per cell $I_{O_2/ce}$; Figures 1.4 and 1.5), and per mitochondrial elementary marker (mt-specific O_2 flux $J_{O_2/mtE}$; Figure 1.6).

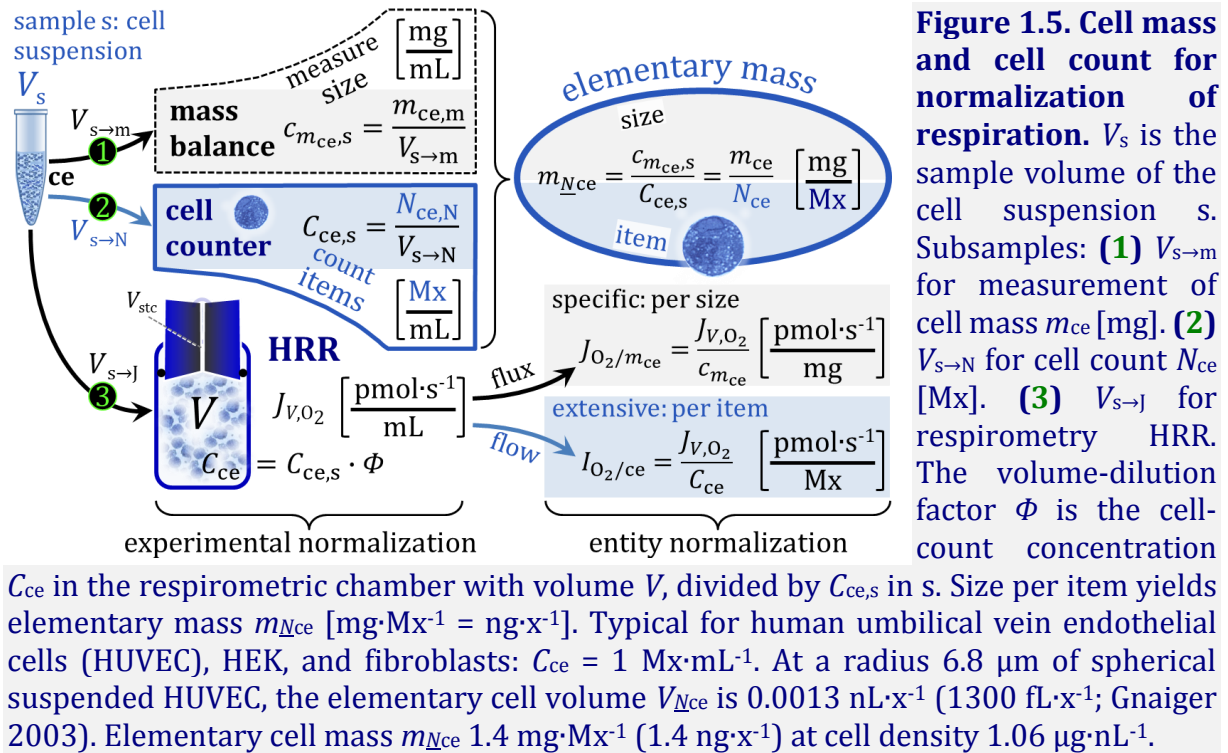
1.4. The sample in the chamber: count, volume, and mass

Consider cells (ce) – the cell count is the number of cells (Figure 1.4). Two fundamentally different quantities are determined of the sample of cells for normalization of respiratory rate (Figure 1.5): (1) The *size* of the sample is quantified by *measuring* extensive quantities such as mass m_{ce} [mg] or volume V_{ce} [μ L] of the pure sample of cells. The pure sample S of cells is ce . Normalization for the extensive quantity sample size yields size-specific flux J_{O_2} . The SI base unit of mass [kg] is the *abstract* unit, applicable to any kind of sample or entity X .



(2) Cells belong to the subset of entities X which are countable objects: A sample of cells can be expressed as a *count*, as the number of single individual items. The elementary entity U_{ce} is the specific *material* unit (Euclidean unit) of a cell count. The single individual cell defines the elementary U_{ce} ; U_{org} is the single individual organism. The cell count N_{ce} is an elementary quantity obtained by counting the number N of cells U_{ce} , item after item (Figure 1.4).

Fig. 1.4. Count, assembly, sample, elementary (CASE). The elementary entity *cell*, U_{ce} , is the *material unit* of the cell count N_{ce} , expressed in the *abstract unit* [x] with the meaning 'one item'.



A count N_X is the product of a number N and the elementary U_X (a multitude of items X),

$$N_X = N \cdot U_X \quad [x] \quad 1.8$$

The extensive quantity *mass* and the elementary quantity *count* are expressed in the abstract units *kilogram* [kg] and *elementary unit* [x], respectively. The abstract unit [kg] is applicable to the mass of all types of entities X . Likewise, the abstract unit [x] applies to the count of all types of elementary entities U_X . In contrast, U_X as the ‘real unit’ is specific for a defined entity type X : U_{ce} is the real unit of the cell count with abstract unit x.

The cell-mass concentration c_{mce} and cell-count concentration C_{ce} in the experimental chamber with volume V are,

$$c_{mce} = m_{ce} \cdot V^{-1} \quad [\text{mg} \cdot \text{mL}^{-1}] \quad 1.9a$$

$$C_{ce} = N_{ce} \cdot V^{-1} \quad [\text{Mx} \cdot \text{mL}^{-1}] \quad 1.9b$$

Any accuracy in the method of respiration and any high number of technical repeats in multiple chambers are in vain, if the normalization quantity – such as mass or count – is unreliable. There are growing concerns about the accuracy and comparability of different cell counters. Yet there is surprisingly little concern about the quantity *count* and its abstract elementary unit [x] in general. We are used to express a cell-count concentration as ‘ $0.8 \cdot 10^6$ cells $\cdot \text{mL}^{-1}$ ’. Do you realize, however, that the unit [$\text{cells} \cdot \text{mL}^{-1}$] is a formally inconsistent mix-up of real things [cells] and an abstract unit [mL]? Like mL or mg, the elementary unit [x] can be used with SI prefixes (mega M; Section A4): $0.8 \cdot 10^6 \text{ x} \cdot \text{mL}^{-1} = 0.8 \text{ Mx} \cdot \text{mL}^{-1}$.

Cell mass – like body mass – has dual meanings. Cell mass with symbol m_{ce} [mg] indicates the mass of a sample of cells. When m_{ce} is divided by the cell count N_{ce} , then we obtain the mass per single individual cell. This gives an entirely different meaning to ‘cell mass’. The term *elementary mass* (Gnaiger et al 2000) and iconic symbol $m_{Nce} \stackrel{\text{def}}{=} M_{ce}$ [$\text{mg} \cdot \text{x}^{-1}$] indicate the cell mass m_{ce} per cell count N_{ce} , or mass per elementary cell,

$$m_{Nce} = m_{ce} \cdot (N \cdot U_{ce})^{-1} \quad [\text{mg} \cdot \text{Mx}^{-1}] \quad 1.10a$$

$$m_{ce} = N_{ce} \cdot m_{Nce} \quad [\text{mg}] \quad 1.10b$$

1.5. Oxygen flow and flux: open the black box

(1) Flow per object: Normalization for a count yields *flow* $I_{O_2/ce}$ expressed in units [$\text{amol}\cdot\text{s}^{-1}\cdot\text{x}^{-1}$] ($=10^{-18} \text{ mol}\cdot\text{s}^{-1}\cdot\text{x}^{-1}=\text{pmol}\cdot\text{s}^{-1}\cdot\text{Mx}^{-1}$; Section A4). O_2 flow per cell is obtained when dividing chamber volume-specific flux J_{V,O_2} [$\text{pmol}\cdot\text{s}^{-1}\cdot\text{mL}^{-1}$] by cell-count concentration $c_{Nce} \stackrel{\text{def}}{=} C_{ce}$ [$\text{Mx}\cdot\text{mL}^{-1}$]. $I_{O_2/ce}$ is a measure of aerobic cell performance. Flow (per object) is an *extensive* quantity that changes with the size of the object (Figure 1.6).

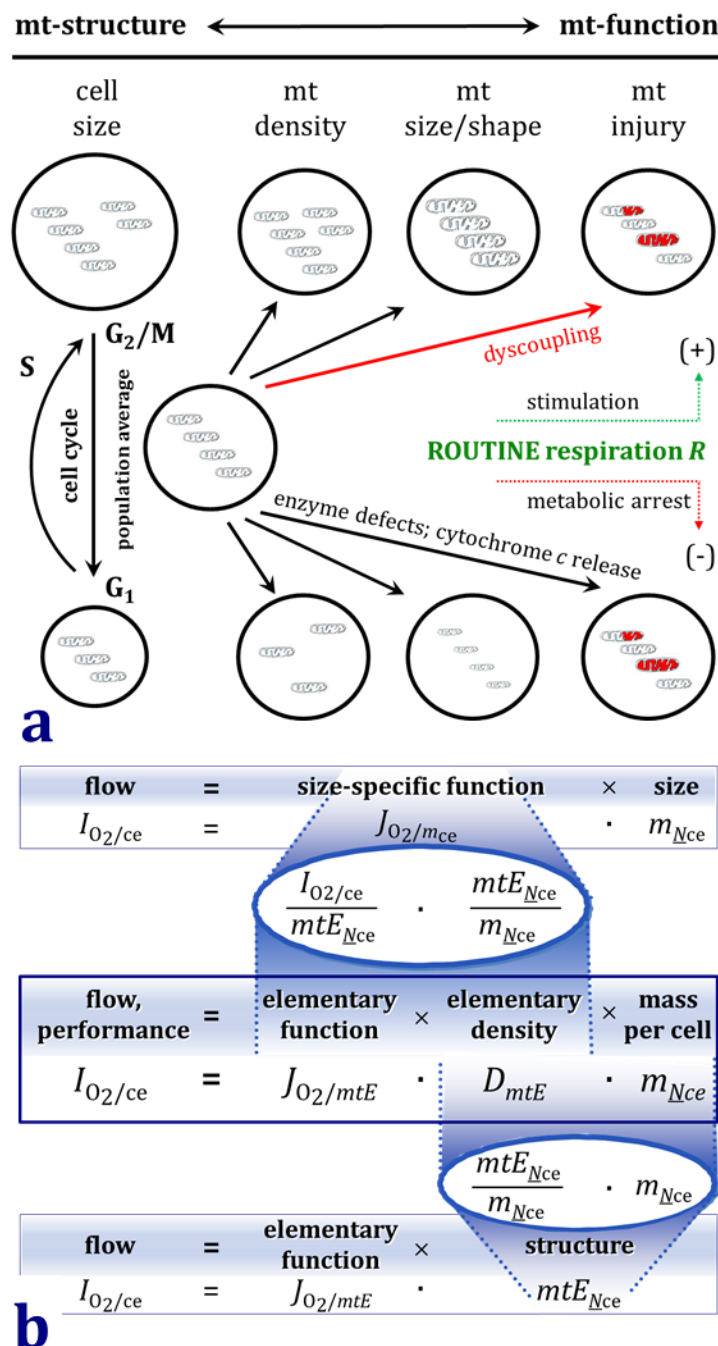


Figure 1.6. From O_2 flow $I_{O_2/ce}$ per cell to cell-size specific O_2 flux $J_{O_2/mce}$ per cell mass, and mt-specific O_2 flux $J_{O_2/mtE}$ per mt-marker.

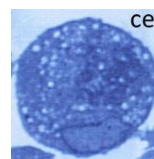
Catabolic flows and fluxes, I_k and J_k , baseline-corrected for R_{ox} . (a) O_2 flow depends on cell size, mt-density and mt-quality. ROUTINE respiration is a function of metabolic state. Modified after Renner et al (2003).

(b) Structure-function analysis: Aerobic performance $I_{O_2/ce}$ is the product of performance per mt-elementary marker ($J_{O_2/mtE} = I_{O_2/ce} \cdot mtE_{Nce}^{-1}$), elementary density ($D_{mtE} = mtE_{Nce} \cdot m_{Nce}^{-1}$) and mass per cell ($m_{Nce} = m_{ce} \cdot N_{ce}^{-1}$),

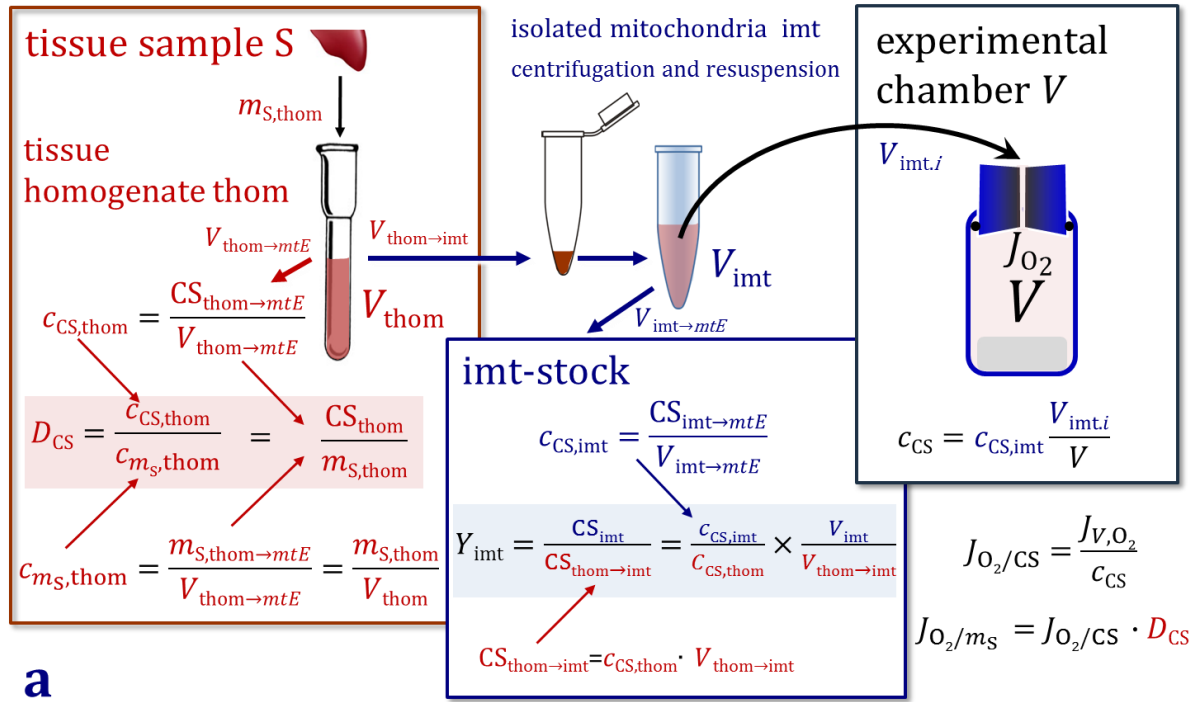
$$I_{O_2/ce} = J_{O_2/mtE} \cdot D_{mtE} \cdot m_{Nce}$$

Cell-mass specific O_2 flux $J_{O_2/mce}$ is the product of mt-quality (mtE function) and specific mt-density:

$$J_{O_2/mce} = J_{O_2/mtE} \cdot D_{mtE}$$



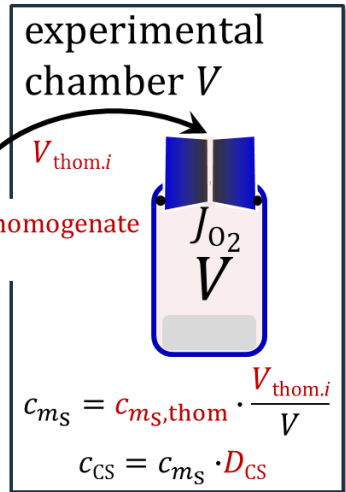
(2) Unstructured analysis: *Cell-mass specific* O_2 flux $J_{O_2/mce}$ [$\text{pmol}\cdot\text{s}^{-1}\cdot\text{mg}^{-1} = \text{amol}\cdot\text{s}^{-1}\cdot\text{ng}^{-1}$] is obtained when the extensive quantity flow per cell $I_{O_2/ce}$ [$\text{amol}\cdot\text{s}^{-1}\cdot\text{x}^{-1}$] is divided by *object size* (mass per cell m_{Nce} [$\text{ng}\cdot\text{x}^{-1}$]). O_2 flux is a *size-specific* quantity. Similarly, $J_{O_2/mce}$ is obtained when chamber volume-specific flux J_{V,O_2} [$\text{pmol}\cdot\text{s}^{-1}\cdot\text{mL}^{-1}$], is divided by mass concentration c_{mce} (cell mass per chamber V [$\text{mg}\cdot\text{mL}^{-1}$]; Figure 1.5).



a

Symbol Definition [Units]

c_{CS}	c_{mtE} ; mitochondrial concentration in chamber [$mtEU \cdot L^{-1}$]
c_{m_S}	tissue mass concentration in chamber [$g \cdot L^{-1}$]
$c_{m_S,thom}$	tissue mass concentration in homogenate [$g \cdot L^{-1}$]
D_{CS}	D_{mtE} ; specific mt-density per tissue mass [$mtEU \cdot g^{-1}$]
J_{O_2/m_S}	tissue mass-specific O_2 flux [$nmol \cdot s^{-1} \cdot g^{-1}$]
$J_{O_2/CS}$	$J_{O_2/mtE}$; mitochondria-specific O_2 flux [$nmol \cdot s^{-1} \cdot mtEU^{-1}$]
CS	mtE ; amount of mitochondrial elementary marker [$mtEU$]
$m_{S,thom}$	tissue mass of sample S in the homogenate [g]
Y_{imt}	recovery of isolated mitochondria
Y_{imt/m_S}	yield of isolated mitochondria; $Y_{imt/m_S} = Y_{imt} \cdot D_{mtE}$ [$mtEU \cdot g^{-1}$]



b

Figure 1.7. Normalization of flux of isolated mitochondria and tissue homogenate. (a) Recovery Y_{mtE} in preparation of isolated mitochondria. $V_{thom \rightarrow imt}$ and $V_{imt,i}$ are the subsamples transferred from V_{thom} and V_{imt} , respectively. $CS_{thom \rightarrow imt}$ is the subsample of mitochondrial elementary marker in the volume used for mt-isolation, $V_{thom \rightarrow imt}$. (b) Subsample of the homogenate $V_{thom,i}$ transferred directly into the respirometric chamber.

(3) Structured analysis: Mitochondria are the structural and functional elementary units mtE of cell respiration. O_2 flux can be normalized for a mt-marker mtE (Figures 1.6 and 1.7). Commonly used mt-markers are activities of citrate synthase (mt-matrix marker), cytochrome c oxidase (mtIM marker), or mt-protein mass for isolated mitochondria, expressed in their specific mitochondrial elementary units [$mtEU$]. Mitochondrial markers are used to determine the mt-concentration c_{mtE} [$mtEU \cdot mL^{-1}$] per

chamber volume, specific mt-density D_{mtE} [$mtEU \cdot mg^{-1}$] in cells and tissues, or mt-content per cell, $mtE_{N_{ce}} = mtE \cdot N_{ce}^{-1}$ [$mtEU \cdot x^{-1}$]. Flux control ratios are based on a *functional* mt-marker (Chapter 3).

Part of the mitochondria from the tissue is lost during preparation of isolated mitochondria. The fraction of mitochondria obtained is expressed as mt-recovery (Figure 1.7). At a high mitochondrial recovery the sample of isolated mitochondria is more representative of the total mitochondrial population than in preparations characterized by low recovery. Determination of mitochondrial recovery and yield is based on measurement of the concentration of a mitochondrial marker in the tissue homogenate, $C_{mtE,thom}$, which simultaneously provides information on the specific mitochondrial density D_{mtE} in the tissue. Thus, isolated mitochondria are referred to the context of the tissue or cell of origin (Figure 1.7).

Real-time OXPHOS analysis gains power by combining measurement of flows (electron transfer quantified by O_2 flow as input, ATP flow as output) and forces, such as $\Delta_{el}F_{p^+}$ ($\Delta\Psi$; Eq. 1.1), in the O2k using either potentiometric or fluorometric signals to study the equilibrium distribution of ions across the mtIM. The chemical ΔpH component of the pmF must be determined separately, or is diminished by incubation conditions including a high inorganic phosphate concentration and nigericin, which catalyzes K^+/H^+ antiport.

1.6. Fluxes and forces: coupling and efficiency

The flux ratio between ATP production J_{P^+} and O_2 consumption J_{kO_2} is the P^+/O_2 flux ratio (or P^+/O ratio with atomic oxygen as a reference). This is frequently referred to as the ‘coupling efficiency’, with focus on metabolic fluxes in real-time OXPHOS analysis. Coupling efficiency is quantified by the simultaneous determination of input and output fluxes, e.g. by measurement of O_2 flux and ATP flux in the O2k-FluoRespirometer, using Mg-green as a fluorophore.

A short circuit or leak dissipates the exergy of the translocated hydrogen ions H^+ , which otherwise is used to phosphorylate ADP to ATP, with an output force of 52 to 66 kJ/mol P^+ under intracellular conditions. The efficiency of coupling is diminished further by potential pump slips of the charge-exergy conserving pumps (Complexes CI, CIII and CIV). While the ionic leak depends on the pmF and is a property of the mtIM including the boundaries between membrane-spanning proteins and the lipid phase, pump slip is a property of the H^+ pumps when the charge slips back to the matrix side within the H^+ pumping process and is thus mainly dependent on flux. Electron leak with formation of reactive oxygen species ROS is another component reducing the coupling between O_2 flux and ATP turnover.

An indirect estimate of coupling efficiency is obtained by sequential measurement of LEAK respiration L and ET capacity E , which can be obtained in living cells (Figure 1.2). $E-L$ coupling efficiency is then expressed as the $E-L$ net ET capacity divided by ET capacity, $(E-L)/E = 1-L/E$, which is 0.0 at zero coupling ($L=E$) and 1.0 at the limit of a fully coupled system ($L=0$).

Conditions vary for measurement and expression of respiration (flux J_{kO_2} ; flow I_{kO_2}). If these conditions are defined and remain consistent within a given context, then the symbols for respiratory rates (P, R, E, L) can be used to substitute the explicit expressions for flows or fluxes, and the subscript k — implicit in P, R, E, L — may be omitted (Figure 1.6).

$$P, R, E, L = I_{O_2P}, I_{O_2R}, I_{O_2E}, I_{O_2L}; \text{ or } J_{O_2P}, J_{O_2R}, J_{O_2E}, J_{O_2L}$$

Efficiency is well defined in thermodynamics based on the entropy law, as an output/input power ratio with a maximum of 1.0. Metabolic power [$\text{W} \stackrel{\text{def}}{=} \text{J}\cdot\text{s}^{-1}$] is not identical to metabolic flow [$\text{mol}\cdot\text{s}^{-1}$]. Classical thermodynamics considers efficiency as a ratio of output in the form of work and input in the form of exergy (ergodynamic efficiency) or work and input in the form of enthalpy (caloric efficiency of the heat engine).

Efficiency in the thermodynamics of irreversible processes takes into account fluxes and forces (power = flow times force). Ergodynamic efficiency is the product of coupling efficiency (flux ratio) and a conjugated force ratio. Ergodynamic efficiencies require the combined information on coupling efficiency and force ratios, including evaluation of redox potentials, chemiosmotic potentials and phosphorylation potentials (isomorphic Gibbs forces). From [Figure 1.1](#), calculation of ergodynamic OXPPOS efficiency requires simultaneous measurement of input O_2 flux and force and output ATP flux and force. The Gibbs force of O_2 consumption is typically -470 kJ/mol O_2 . Maximum efficiency can be obtained only by compromising speed and slowing down when approaching equilibrium, whereas maximum power is achieved at the cost of exergy required for fast but less efficient processes ([Figure 1.8](#)).

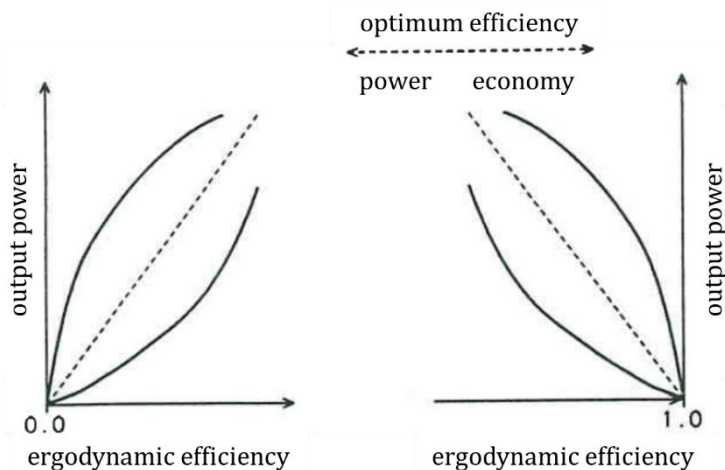


Figure 1.8. Optimum efficiency depends on the strategy of maximizing output power or economy. From Gnaiger E (1993) Efficiency and power strategies under hypoxia. Is low efficiency at high glycolytic ATP production a paradox? In: *Surviving Hypoxia: Mechanisms of Control and Adaptation*. Hochachka et al eds. CRC Press, Boca Raton, Ann Arbor, London, Tokyo:77-109.

1.7. Electron gating

Electrons flow to oxygen along linear thermodynamic cascades (electron transfer chains) with either three coupling sites when reducing Q through CI, or with two coupling sites through CII and other respiratory complexes which do not have a roman numeral. The mitochondrial pathways of electron transfer are conventionally separated by using either NADH-linked substrates (N-pathway), such as pyruvate & malate, or the classical succinate and rotenone combination (S-pathway), to analyze site-specific H^+/O and $\text{P}\gg/\text{O}$ ratios, or to study defects of specific respiratory segments in functional diagnosis. Electron gating is the experimental separation of various electron transfer pathways converging at the Q-junction ([Figure 1.9](#)). Even without having been properly recognized and defined by a term, electron gating is common to the extent of establishing a bioenergetic paradigm in studies of OXPPOS with isolated mitochondria or permeabilized cells.

1.8. Convergent mitochondrial pathways: the Q-junction

Metabolic pathways are defined by a network of enzymes and metabolites. The enzymes generate the catalytic capacity of the biochemical path. The travelers on the way

are the metabolites, converted from substrates through intermediates to products. For orientation it is helpful to signpost the metabolic highways with street names. The terminology for mitochondrial pathways of energy metabolism was focused on the respiratory Complexes catalyzing the entry of electrons into the Q-junction (Figure 1.10). Thus, CI-linked respiration indicates the electron transfer from N-type substrates through CI into Q and further through CIII to CIV and O₂. Succinate is the substrate for CII-linked respiration. The CI- and CII-linked pathways were then abbreviated as CI and CII. The lack of distinction between the abbreviation of a respiratory Complex (CI, CII) and a pathway (CI, CII) explains the widespread misconception to interpret a diminished OXPHOS capacity of the CI-pathway as a defect of *Complex I*. Of course, any other enzyme upstream or downstream of CI, depletion of co-enzyme pools (NAD⁺/NADH, Q, cytochrome *c*), or damage in the phosphorylation system can cause a decline of OXPHOS capacity in the N-pathway (CI-linked pathway).

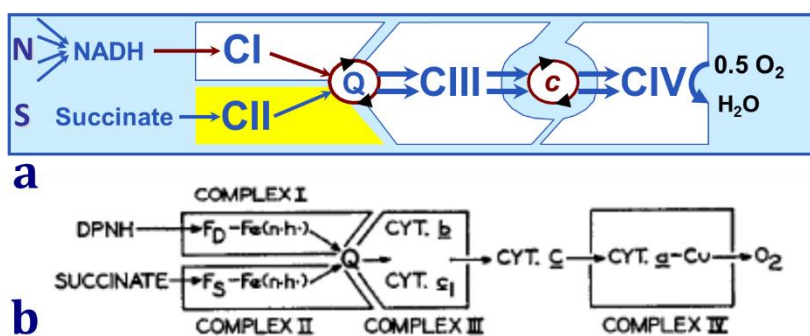


FIG. 5. Schematic representation of the four functional primary complexes and their sequential arrangement in the electron transfer system. *F_D*, DPNH dehydrogenase flavoprotein; *F_S*, succinic dehydrogenase flavoprotein.

To avoid confusion, a terminology focused on substrate type was introduced more recently for mitochondrial pathways. Mitochondrial pathways are stimulated by CHNO-fuel substrates feeding electrons into the ETS at different levels of integration and in the presence or absence of inhibitors acting on specific enzymes which are gate-keepers and control various pathway segments. Distinction of five ET-substrate types linked to ET-pathway levels provides the rationale for defining categories of SUIT protocols.

(1) CIV: Electron flow through CIV (cytochrome *c* oxidase) is measured in mitochondrial preparations after inhibition of CIII by antimycin A or myxothiazol, and addition of ascorbate (As) and the artificial substrate TMPD (Tm). Ascorbate has to be

Figure 1.9. Convergent NS-pathway of electron transfer at the Q-junction, exerting an additive effect on flux, versus electron gating for separation of single input pathways. (a) Gnaiger 2009. (b) Hatefi et al 1962. DPNH is the former abbreviation for NADH.

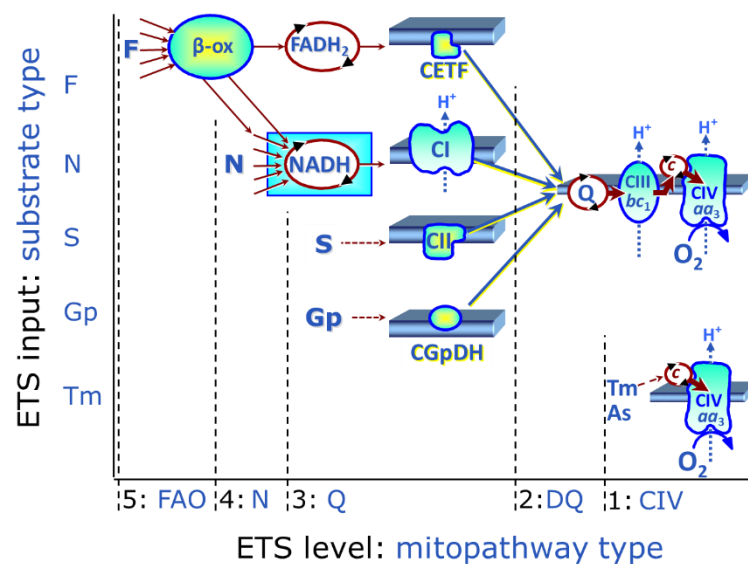


Figure 1.10. ET-substrate types are linked to ET-pathway types in substrate-uncoupler-inhibitor tritration (SUIT) protocols.

titrated first. It reduces TMPD, which further reduces cytochrome *c*, which is the substrate of CIV. Since CIV is a H⁺ pump of the electron transfer-pathway, CIV-linked respiration (*L*, *P* and *E*) can be measured in different coupling states. Measurement of CIV-activity (CIV_E) requires uncoupler titrations to eliminate any potential control by the phosphorylation system, and a cytochrome *c* test to avoid any limitation by cytochrome *c* release. Total oxygen uptake in the ascorbate & TMPD(& *c*) stimulated state (T_m) has to be corrected for chemical background O₂ consumption.

(2) DQ: ET-pathway level 2 is stimulated by duroquinol (DQ) feeding electrons into Complex III (CIII) with further electron transfer to CIV and O₂.

(3) Q: Level 3 ET pathways feed electrons from NADH, succinate, FADH₂, glycerophosphate into respiratory Complexes at the Q-junction. In mammalian mitochondria, neither NADH (the substrate of CI, reacting on the inner side of the mt-inner membrane, mtIM) nor FADH₂ (the substrate of electron transferring flavoprotein CETF, localized on the inner side of the mtIM) are transported across the mtIM and are, therefore, not suitable as level 3 substrates. Succinate is readily transported across the mtIM and is the substrate of succinate dehydrogenase (SDH, CII) localized on the inner side of the mtIM. Fumarate and FADH₂ are the products of CII, whereas FADH₂ is the substrate of CETF. Glycerophosphate dehydrogenase Complex (CGpDH) localized on the outer face of the mtIM. Choline and dihydro-*o*-rotate are the type 3 substrates of choline dehydrogenase and dihydro-*o*-rotate dehydrogenase, respectively. Sulfide-ubiquinone oxidoreductase oxidizes H₂S with electron transfer into Q and subsequent reduction of O₂ by CIV, associated with a dioxygenase consuming twice the amount of O₂ per H₂S.

(4) N: Level 4 ET pathways feed electrons into dehydrogenases and enzyme systems upstream of pathway level 3. Electron transfer from type 4 substrates (N) converges at the N-junction. Representative N-junction substrates are pyruvate, glutamate and malate, and also citrate, oxoglutarate and the ketone bodies acetoacetate and β-OH-butyrate. The corresponding dehydrogenases (PDH, GDH, MDH and mtME; IDH, OgdH) generate the CI substrate NADH.

(5) F: Fatty acids supporting converging electron transfer to the F-junction are catabolized by carnitine-dependent β-oxidation. β-oxidation of fatty acyl-CoA yields trans-2-enoyl-CoA catalyzed by acyl-CoA dehydrogenases, reducing FAD which accepts two electrons and two protons generating FADH₂. FADH₂ is the substrate of electron transferring flavoprotein (CETF) localized on the inner side of the mtIM. Fatty acid oxidation (FAO) not only depends on electron transfer through the F-junction (which is typically rate-limiting relative to the N-pathway branch), but simultaneously generates NADH from NAD⁺ in the step catalyzed by 3-hydroxy-acyl-CoA dehydrogenases. FAO thus depends on the obligatory combination of the F-junction and N-junction pathway branches. Hence FAO can be inhibited completely by inhibition of CI. In addition and independent of this source of NADH, the N-junction substrate malate is required at low concentration (0.1 mM) as a co-substrate for FAO in mt-preparations, since accumulation of acetyl-CoA inhibits FAO in the absence of malate. Malate is oxidized in a reaction catalyzed by malate dehydrogenase to oxaloacetate (yielding NADH), which then stimulates the entry of acetyl-Co into the TCA cycle catalyzed by citrate synthase. Malate is not required for FAO in liver mitochondria, which form ketone bodies from acetyl-CoA.

Addressing the functional design of the OXPPOS system requires a shift from the paradigm of electron transfer as a *chain* (ETC) to recognizing the convergent structure of the electron transfer *system* (ETS; [Figure 1.9](#)). Electron transfer capacity of cells *in vivo* is underestimated on the basis of the 'State 3' and conventional respiratory protocols with

single substrate types. OXPPOS analysis extends this bioenergetic paradigm to a perspective of mitochondrial physiology emerging from a series of studies based on high-resolution respirometry and SUIT protocols.

Reconstitution of citric acid cycle function in mt-preparations requires the combined application of N-type substrates and succinate. Then electron flow converges at the Q-junction from the upstream branches of the N- and S-pathway and exerts an additive effect on respiratory flux through the common pathway section downstream of Q. Flux through the convergent pathway system, $\bar{N}\bar{S}$ -pathway capacity (Figure 1.9), is distinguished from the arithmetic sum of the capacities of each pathway measured separately, $N+S$. Interactions of intermediates in convergent pathways explain incomplete additivity, $\bar{N}\bar{S} < N+S$. Complete additivity, $\bar{N}\bar{S} = N+S$, is indicative of tight channelling of flux through non-interactive supercomplex pathways (Chapter 7). Operation of OXPPOS in top gear resolves discrepancies between living cells and mitochondrial preparations, with profound implications on evaluation of biochemical thresholds, apparent excess capacities and flux control coefficients of various mitochondrial enzyme systems. The additive effect of convergent electron input indicates down-stream excess capacities of respiratory complexes, including cytochrome *c* oxidase CIV, over the separate branches upstream of the Q-junction (Figure 1.10).

1.9. Biochemical thresholds and the Q-junction

The additive effect of convergent electron transfer at the Q-junction is highest when electron channelling through supercomplexes is tight (Figure 1.9). The apparent excess capacity of a downstream step, such as the terminal cytochrome *c* oxidase CIV, must then be high when related to a single input pathway (N or S; Figure 1.10). This does not represent a functional excess capacity, however, which can only be evaluated relative to the reconstituted pathway flux ($\bar{N}\bar{S}$; Figure 1.11).

Convergent e-input into Q elicits the most pronounced stimulatory effect on coupled respiration when the phosphorylation system exerts low flux control. Convergent $\bar{N}\bar{S}$ e-input corresponds to the operation of the citric acid cycle and mitochondrial fuel substrate supply *in vivo*. Importantly, by establishing the reference state of maximum coupled respiration, convergent e-input provides the proper basis for (1) quantifying excess capacities of Complexes CIII and CIV, (2) interpreting flux control by various components such as the phosphorylation system or CIV, and (3) for evaluation of specific enzymatic defects in the context of mitochondrial respiratory physiology and pathology.

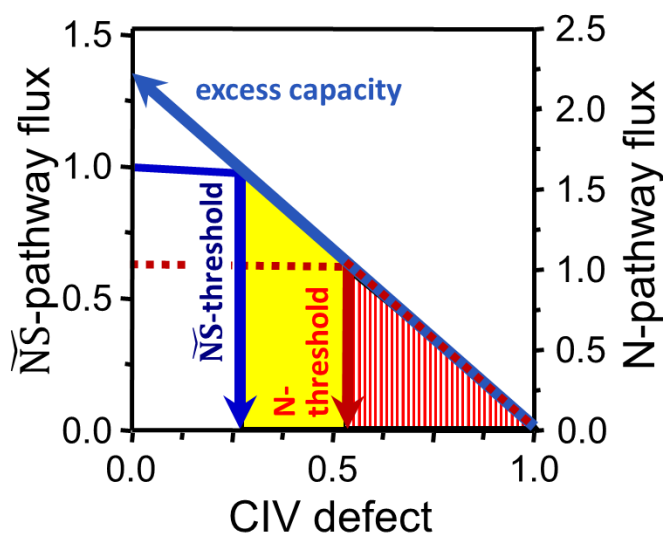


Figure 1.11. Biochemical threshold plot for convergent $\bar{N}\bar{S}$ -pathway flux (horizontal full line, left; the flux control coefficient is the slope) and N-pathway flux based on electron gating (horizontal dotted line, right). A defect of a single enzyme step (CIV) exerts no or little effect on pathway flux (horizontal lines) up to a threshold. Beyond the threshold a linear slope is obtained towards zero CIV-activity. Extrapolation to the left Y-axis yields the apparent excess capacity of the single step (arrow to Y-axis).

1.10. Boundary conditions

1.10.1. Respiration medium

Respiration medium MiR05 contains 10 mM inorganic phosphate P_i and 3 mM Mg^{2+} . Kinetically saturating ADP concentrations are added to evaluate OXPPOS capacity. P_i concentrations <10 mM and $[ADP] <0.4$ mM limit OXPPOS respiration in isolated heart mitochondria. In permeabilized muscle fiber bundles of high respiratory capacity, the apparent K_m for ADP increases up to 0.5 mM. This implies that >5 mM ADP is required to obtain >90 % of maximum rate. Hence, many studies using lower ADP concentrations in permeabilized tissues and cells may underestimate OXPPOS capacity. Saturating ADP concentrations are essential for evaluation of flux control exerted by the capacity of the phosphorylation system (ATP synthase, adenine nucleotide translocase and phosphate carrier), which is indicated if noncoupled respiration is higher than OXPPOS capacity.

1.10.2. Temperature

Experimental temperature is best chosen at or near physiological conditions, else care must be taken when extrapolating results obtained at a different temperature (Section A3).

1.10.3. Oxygen concentration

O_2 concentration is not limiting respiration of isolated mitochondria and small cells even at $20 \mu M$ (Figure 1.12; 20- to 50-fold above the apparent K_m for dissolved O_2). In permeabilized muscle fiber bundles, however, diffusion restriction increases the sensitivity to O_2 supply 100-fold (human vastus lateralis, rat soleus, rat heart). It is recommended, therefore, to apply O_2 levels in the range of 500 to $>250 \mu M$ to respiratory studies of muscle fibers, since OXPPOS flux may be O_2 limited below air saturation (about $200 \mu M O_2$).

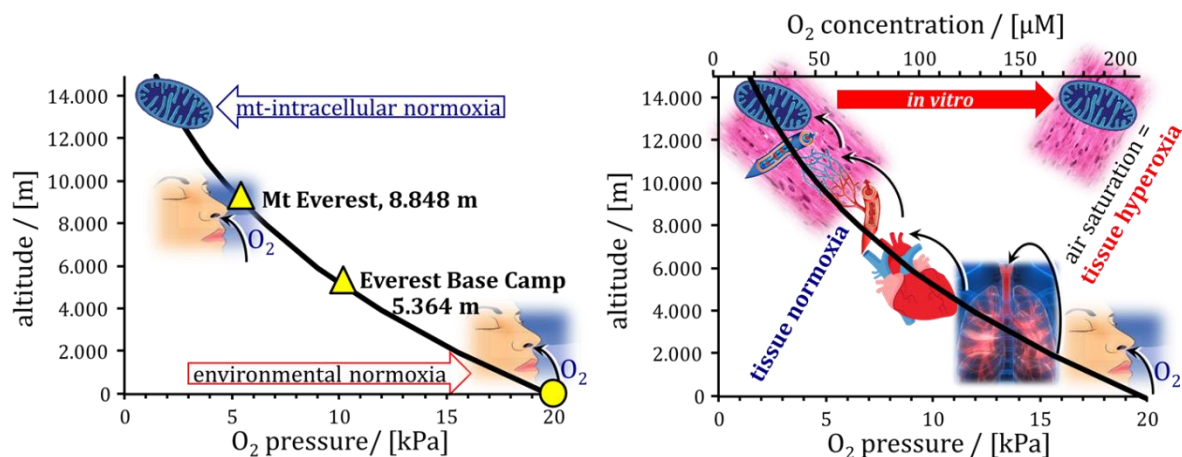


Figure 1.12. From environmental normoxia to hypoxia as a function of altitude versus tissue normoxia in the mitochondrial intracellular milieu.

1.10.4. Fuel substrate concentrations

Substrates feeding into the TCA cycle are generally added at saturating concentrations for measurement of mitochondrial respiratory capacity, providing a buffer against CHNO-fuel substrate depletion in the course of the experiment (Tab. A2.1). During exercise, there is an increase in the concentrations of TCA cycle intermediates, which are

not limiting in contracting skeletal muscle. Important anaplerotic reactions, replenishing the pools of metabolic intermediates in the TCA cycle, are catalyzed by malic enzyme and pyruvate carboxylase in the mitochondrial matrix, which synthesize pyruvate from malate and oxaloacetate from pyruvate, respectively. Balanced anaplerosis and cataplerosis (entry and exit of TCA cycle intermediates) is responsible – particularly in metabolism of amino acids and gluconeogenesis (export of malate) and lipogenesis (export of citrate) – for maintaining TCA cycle intermediates at steady states which shift under changing metabolic conditions of activity and starvation.

1.10.5. Cytochrome *c* release

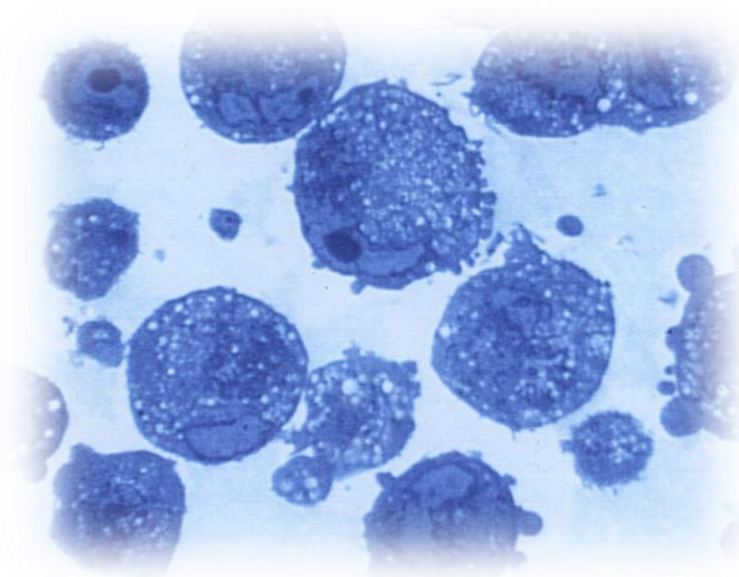
Release of cytochrome *c* – either under pathophysiological conditions of the cell or as a result of sample preparation – may limit active respiration. This specific effect can be separated from other OXPHOS defects by addition of cytochrome *c* (10 μM), which thus provides an essential aspect of quality control of isolated mitochondria or permeabilized tissues and cells (cytochrome *c* control efficiency; [Chapter 3](#)).

1.10.6. Ca^{2+}

Ca^{2+} at optimum concentration is an activator of dehydrogenases and oxidative phosphorylation. Free calcium in MiR05 is kept low by 0.5 mM EGTA. A modest increase of free calcium concentration may stimulate respiration. The mitochondrial Ca^{2+} uniporter is inhibited by ruthenium red.

1.10.7. Sample storage

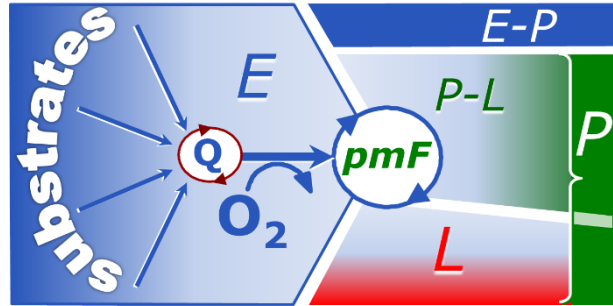
Short-term preservation of mt-preparations including isolated mitochondria on ice in a specific preservation medium increases respiratory capacity in the ADP-activated state when compared to storage in typical isolation medium, and addition of antioxidants even in the isolation medium has a significant beneficial effect.



Human umbilical vein endothelial cells HUVEC in suspension

Chapter 2.

Respiratory states and rates: coupling control



'The growth of any discipline depends on the ability to communicate and develop ideas, and this in turn relies on a language which is sufficiently detailed and flexible.'

Simon Singh (1997) *Fermat's last theorem*. Fourth Estate, London.

Section	2.1. Coupling in oxidative phosphorylation	23	Page
	2.2. Respiratory steady-states	24	
	2.3. OXPHOS capacity <i>P</i>	28	
	2.4. ROUTINE respiration <i>R</i> of the living cell	29	
	2.5. Electron transfer capacity <i>E</i>	30	
	2.6. LEAK respiration <i>L</i>	31	
	2.7. Uncoupled – noncoupled – dyscoupled?	33	
	2.8. Residual oxygen consumption <i>Rox</i>	33	

2.1. Coupling in oxidative phosphorylation

In oxidative phosphorylation OXPHOS, exergonic electron transfer to O₂ is coupled to endergonic phosphorylation of ADP to ATP. The H⁺ pumps generate and utilize the protonmotive force *pmF* in a hydrogen ion H⁺ circuit across the mt-inner membrane mtIM. The H⁺ circuit is partially uncoupled by leaks and decoupled by pump slip (Figure 1.1). Coupling and uncoupling are key components of mitochondrial respiratory control.

Table 2.1. Mitochondrial and cellular respiratory rates in coupling-control states

Symbol	Definition	mt-Preparations, ET-competent pathway states	Living cells, exogenous or endogenous substrates
rate	J_{kO_2} or I_{kO_2}		
<i>P</i>	OXPHOS capacity , coupled, <i>pmF</i> supports $J_{P\gg}$	saturating ADP and P _i , or J_{max} from ADP kinetics	can saturating [ADP] and [P _i] be achieved?
<i>R</i>	ROUTINE respiration , physiological control of energy turnover in the range from <i>L</i> to <i>P</i> , variable <i>pmF</i>	limiting steady-state ADP levels simulating ROUTINE respiration above <i>L</i> and below <i>P</i>	physiological control of cellular substrate uptake, intermediary metabolism and energy turnover
<i>E</i>	ET capacity , electron transfer capacity, noncoupled, very low <i>pmF</i>	optimal uncoupler concentration for maximum respiration	optimal uncoupler concentration for maximum respiration
<i>L</i>	LEAK respiration , nonphosphorylating, maximum <i>pmF</i>	<i>L</i> (n) and <i>L</i> (O _{my}): general; <i>L</i> (T): excluding ATPase activity	<i>L</i> (O _{my})
<i>Rox</i>	residual oxygen consumption , <i>pmF</i> collapsed or driven by reverse F-ATPase	substrate depletion, or inhibition of CI to CIV	inhibition of CI to CIV

2.2. Respiratory steady-states

Respiratory steady-states have been defined by Chance and Williams (1955 I, III) according to a classical Oxygraph protocol with isolated mitochondria (Figure 2.1; Table 2.1).

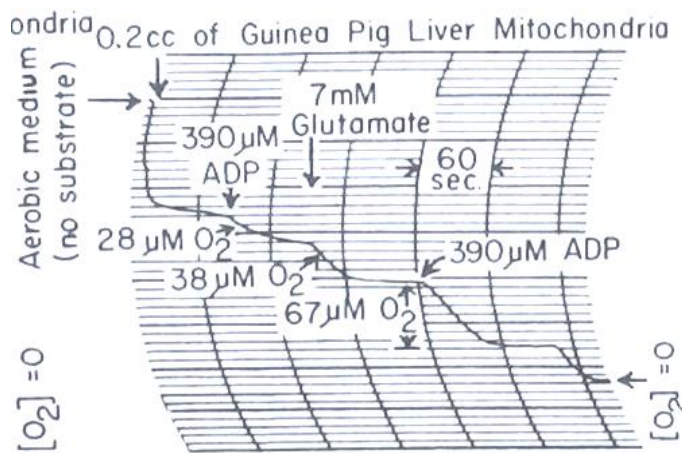


Figure 2.1. Respiratory states. Coupling control in isolated mitochondria: endogenous fuel substrates and added ADP (States 1 and 2), glutamate and respiratory control ratio (RCR=State 3/ State 4); zero oxygen calibration at State 5 (Chance and Williams 1955 I; Figure 4B).

The titration protocol (Figures 2.1 and 2.2a) starts with addition of imt to air-saturated isotonic medium with inorganic phosphate in State 1 (en, endogenous substrates; no adenylates, subscript N). ADP (D) induces a transient activation to effectively exhaust endogenous fuel substrates, after which State 2 is a CHNO substrate-depleted state of residual O₂ consumption (Rox). Addition of substrate (Figure 2.1: glutamate G) stimulates respiration while ADP is 'high', G_D (State 3, not showing kinetic saturation of OXPHOS capacity). When ADP is depleted by phosphorylation to ATP, respiration drops in the transition to State 4, which is an ADP-limited resting state, G_{L(T)} (LEAK), in the presence of ATP. A second ADP titration is followed by another State 3→4 transition while sufficient oxygen is available to allow calculation of the P»/O ratio (Figure 6.4). Finally, respiration becomes O₂ limited in the aerobic-anoxic transition (→anox, State 5; Table 2.1).

The titration protocol (Figures 2.1 and 2.2a) starts with addition of imt to air-saturated isotonic medium

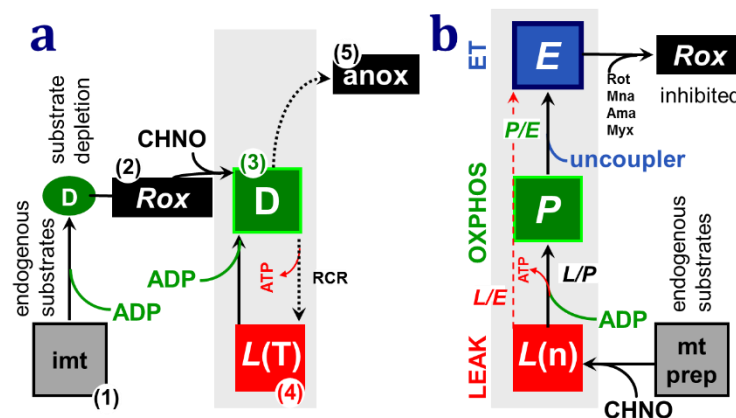


Figure 2.2. Coupling-control protocols. (a) Classical sequence from States 1 to 5 (numbers in parentheses): Addition of ADP to imt is followed by State 2 (residual oxygen consumption, Rox). CHNO-fuel substrates stimulate respiration in State 3 (D). After ADP→ATP phosphorylation (P») is complete, State 4 is a LEAK state with rate L(T). State 5 is anoxia. (b) Initial addition of CHNO substrates to induce a LEAK state in the absence of adenylates, L(n). Saturating ADP supports OXPHOS capacity P. Uncoupler titration to maximum O₂ flux induces the noncoupled state of electron transfer capacity E followed by inhibition of respiratory complexes to determine residual O₂ consumption Rox for correction of fluxes in the mt-coupling-control states. An ET-competent pathway control state has to be applied by selecting appropriate CHNO substrate combinations.

In an alternative protocol for any mt-preparation (Figure 2.2b) fuel substrates are added first, inducing a LEAK state (rate L(n); no ADP; Figure 2.3: pyruvate & glutamate &

malate, $PGM_{L(n)}$; Figure 5.5: succinate, $S(Rot)_{L(n)}$). The 4-compartmental model of OXPHOS provides the guideline for experimental design (Figure 2.4). The coupling-control steps include testing for saturating [ADP] (1D) to quantify OXPHOS capacity, uncoupler titrations (2U) to determine ET capacity, and inhibition of E to correct total O_2 uptake (L', P', E') for residual O_2 consumption, e.g., $L=L'-Rox$ and $E=E'-Rox$ (Figure 2.3).

The original definition of State 2 (Table 2.2) is opposite to the state obtained in the absence of ADP but presence of fuel substrate (Figure 2.3). 'We have sought independent controls on whether State 2 corresponds to complete oxidation of the system. It is logical that this be so, for respiration is zero in State 2 because substrate, not phosphate acceptor, is limiting' (Chance and Williams 1955). Residual oxygen consumption Rox in the absence of fuel substrate may be compared to Rox measured in the presence of inhibitors of the ETS (Section B) when various fuel substrates are added with or without uncoupler.

Table 2.2. Metabolic states of mitochondria (Chance and Williams 1956; TABLE V)

State	[O ₂]	ADP level	Substrate level	Respiration rate	Rate-limiting substance	Comments
1	>0	low	low	slow	ADP	endogenous substrates, no ADP
2	>0	high	~0	slow	substrate	Rox with ADP
3	>0	high	high	fast	respiratory chain	OXPHOS capacity ADP-limited
4	>0	low	high	slow	ADP	LEAK, if no ATPase activity
5	<0	high	high	0	oxygen	anoxic, but O ₂ backdiffusion

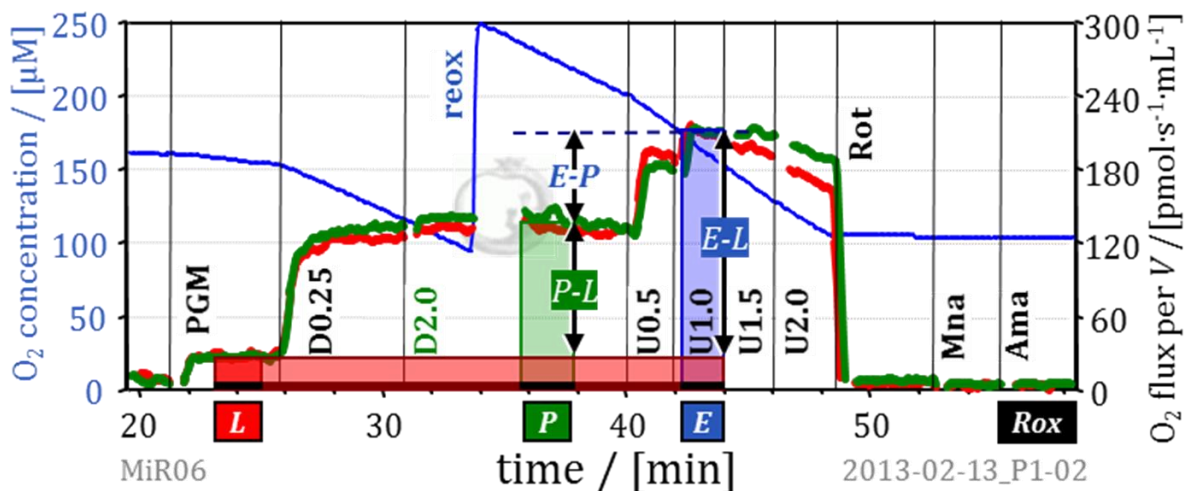


Figure 2.3. High-resolution respirometry and E-P-L coupling-control protocol (mouse brain homogenate in MiR05). O_2 concentration (blue line; left axis) for one chamber; O_2 flux (red and green lines) superimposed for the two chambers of the Oroboros O2k. N-type substrates pyruvate, glutamate and malate $PGM_{L(n)}$ (5, 10 and 2 mM; LEAK, without adenylates), 0.25 mM ADP (D0.25, nonsaturating; State 3), 2 mM ADP (OXPHOS capacity P). Uncoupler titration (U, 0.5 to 2.0 μ M FCCP) yields maximum flux at 1.0 μ M FCCP (ET capacity E). Residual O_2 consumption (Rox ; for correction of total O_2 flux) measured after inhibition of Complexes CI (rotenone, 0.3 μ M), CII (malonate, 5 mM), and CIII (antimycin A; Ama, 2.5 μ M). Reoxygenation with 3 μ L H_2O_2 (200 mM stock) in MiR06 containing catalase (280 U/mL). Safranin (2 μ M) added initially for simultaneous fluorometric measurement of $\Delta\Psi$ (not shown) specifically inhibits the phosphorylation system to a larger degree than N-ET capacity. This explains the large apparent E-P excess capacity (modified from Krumschnabel et al 2014).

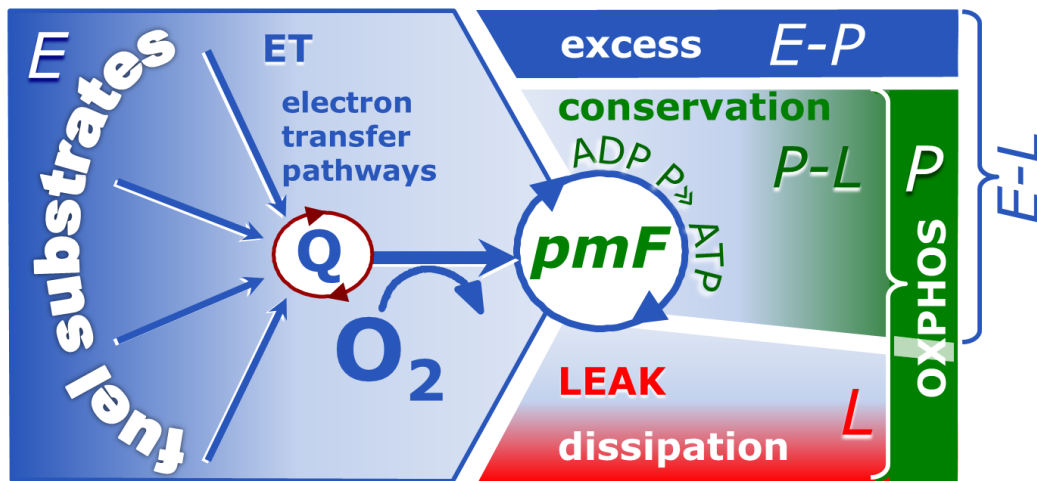


Figure 2.4. OXPHOS-, ET-, and LEAK states, respiratory capacities (P , E , L), and 4-compartmental OXPHOS model. (1) ET capacity E of the noncoupled electron transfer system ETS. OXPHOS capacity P is partitioned into (2) the dissipative LEAK component L , and (3) ADP-stimulated $P-L$ net OXPHOS capacity. $(P-L)/P$ is the OXPHOS $P-L$ control efficiency. (4) If $P-L$ is kinetically limited by a low capacity of the phosphorylation system to utilize the protonmotive force pmF , then the apparent $E-P$ excess capacity is available to drive coupled processes other than phosphorylation $P \gg$ (ADP to ATP) without competing with $P \gg$. $(E-P)/E$ is the kinetic $E-P$ control efficiency. The biochemical coupling efficiency or $E-L$ coupling efficiency, $(E-L)/E$, is independent of kinetic control by the phosphorylation system, which may decrease the $P-L$ control efficiency, $(P-L)/P$.

Respiratory coupling states are integrated in the metabolic design of core mitochondrial pathways (Figure 2.4). Dissipative LEAK respiration L restricts the $E-L$ net ET capacity. $E-L$ is partitioned into the $P-L$ net OXPHOS module for phosphorylation $P \gg$, and the $E-P$ excess capacity module potentially available for additional ion transport. The $E-P$ excess capacity provides a tool for the diagnosis of a specific impairment of the phosphorylation system (Figure 2.5) in toxicological or pathological states (Figure 2.3). Diminished P at constant or less affected E causes $E-P$ to increase, which leads to the unequivocal distinction between defects of the electron transfer versus phosphorylation system. Both can potentially limit the vital $P-L$ net OXPHOS capacity (Figure 2.4).

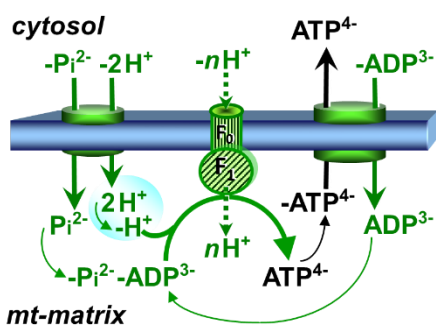


Figure 2.5. The phosphorylation system: ATP synthase, adenine nucleotide translocator and phosphate carrier. OXPHOS is electron transfer (OX) coupled through the H^+ circuit across the mt-inner membrane mtIM to the phosphorylation of ADP to ATP (PHOS; Figure 1.1). ATP, ADP and P_i are shown in a reference state of dissociation.

Pronounced differences in the magnitude of the $E-P$ excess capacity in healthy mitochondria from different species, tissues and life cycle stages challenge comparative mitochondrial physiology to the extent of a paradigm change. Mammalian myocardial mitochondria, particularly of mice and humans, but also skeletal muscle mitochondria, show unexpected diversity of respiratory control: $E-P$ control efficiency, $(E-P)/E$, ranges from 0.0 to 0.5. The $E-P$ excess capacity module needs functional interpretation: higher $E-P$ increases the $E-L$ net ET capacity which then is available to drive $\Delta\Psi$ or $\Delta\mu_{H^+}$ coupled transmembrane

processes without competing with phosphorylation: *pmF*-coupled ion transport, including fuel substrates and Ca^{2+} . The nature of these coupled processes needs to be identified to clarify the functional role of different apparent *E-P* excess in various species and tissues. Alternatively, the apparent *E-P* excess constitutes an actual reserve, and the substantial differences in this apparent reserve between species and tissues may then be related to differential challenges and evolutionary risk management.

Generations of students of bioenergetics have adopted a 3-compartmental model of mitochondrial respiration as a paradigm for functional separation of three OXPHOS modules (Figure 2.6): (1) Fuel substrate oxidation (ET chain), (2) the phosphorylation system (Figure 2.5) with energy (exergy) conservation as the efficient branch of OXPHOS, and (3) cation leak and other purely dissipative processes of heat production (dissipation) comprising the inefficient uncoupled respiration.

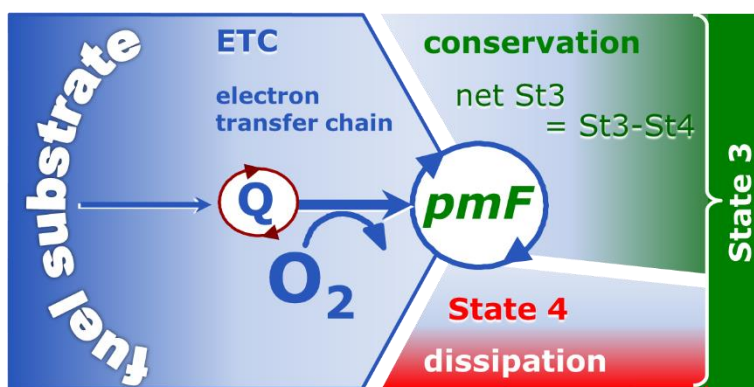


Figure 2.6. 3-compartmental OXPHOS model of respiration. Electron transfer coupled to phosphorylation in ADP-stimulated State 3, partially uncoupled in the dissipative State 4. State 3 respiration corrected for LEAK is potentially available for coupled phosphorylation of ADP to ATP ($P \gg$).

Compartmental OXPHOS analysis has been the basis of many important advancements in bioenergetics. However, the 3-compartmental OXPHOS model fails to consider the quantitative importance of the *E-P* excess capacity. This is reflected by the State 3/State 3u terminology which obscures the fundamental difference between ET- and OXPHOS capacities.

Limitations of the 3-compartmental OXPHOS model are tightly linked to traditional protocols restricted to respiratory States 3 and 4 (Figure 2.6). Experimentally, OXPHOS capacity P is underestimated at State 3, if the 'high' ADP concentration (Table 2.1) is kinetically not saturating. Then an *E-P* excess capacity above State 3 is due to kinetic limitation of respiration in contrast to differences in catalytic capacities.

Restricted substrate supply in the study of the electron transfer *chain* fails to reveal physiological ET capacity, since electron gating restricts electron transfer *system* capacity (Figure 1.9). Downstream excess capacity (CIII, CIV; Figure 1.11) is overestimated, but *E-P* excess capacity is underestimated without reconstitution of TCA cycle function by appropriate substrate supply to mt-preparations. Upstream substrate limitation does not push the capacity of the phosphorylation system to its limit and thus masks the functional gap between physiological ET capacity (noncoupled state) and OXPHOS capacity (coupled state).

Taken together, determination of respiratory capacities in specific coupling states (LEAK, OXPHOS, ET) requires electron transfer system (ETS) competent substrate states, including sufficient oxygen supply. Coupling states and fuel substrate states are complementary: both exert a mutual influence on respiratory control. ETS competence of fuel substrates depends on (1) transport of substrates across the mt-membranes or

oxidation by dehydrogenases localized at the outer face of the inner mt-membrane (e.g. glycerophosphate dehydrogenase complex), (2) oxidation in the mt-matrix (TCA cycle dehydrogenases) or on the inner face of the inner mt-membrane (CII, CETF), and (3) oxidation of substrates without accumulation of inhibitory endproducts (e.g. oxaloacetate inhibiting CII; NADH and oxaloacetate inhibiting malate dehydrogenase). Products must be either easily transported from the matrix across the mtIM in the process of cataplerosis (e.g. malate formed from succinate via fumarate), or metabolized as intermediates (e.g. malate to oxaloacetate forming citrate with Acetyl-CoA). These are fundamental topics of MitoPathways addressed in Chapters 3 to 5.

2.3. OXPHOS capacity *P*

P R E L - RoX

P OXPHOS capacity *P* is the respiratory capacity of mitochondria in the ADP-stimulated state of oxidative phosphorylation (OXPHOS), at saturating concentrations of ADP, inorganic phosphate, oxygen, and defined CHNO substrates. OXPHOS involves chemiosmotic in contrast to mechanistic coupling between electron transfer and the phosphorylation system. Mechanistic coupling is illustrated by a fully engaged clockwork gear wheel system. When loosening the fit of one gear wheel to the other, intrinsic uncoupling and dyscoupling lower the efficiency and contribute to the control of flux in the OXPHOS state (Figure 2.7).

OXPHOS capacity: saturating [ADP]

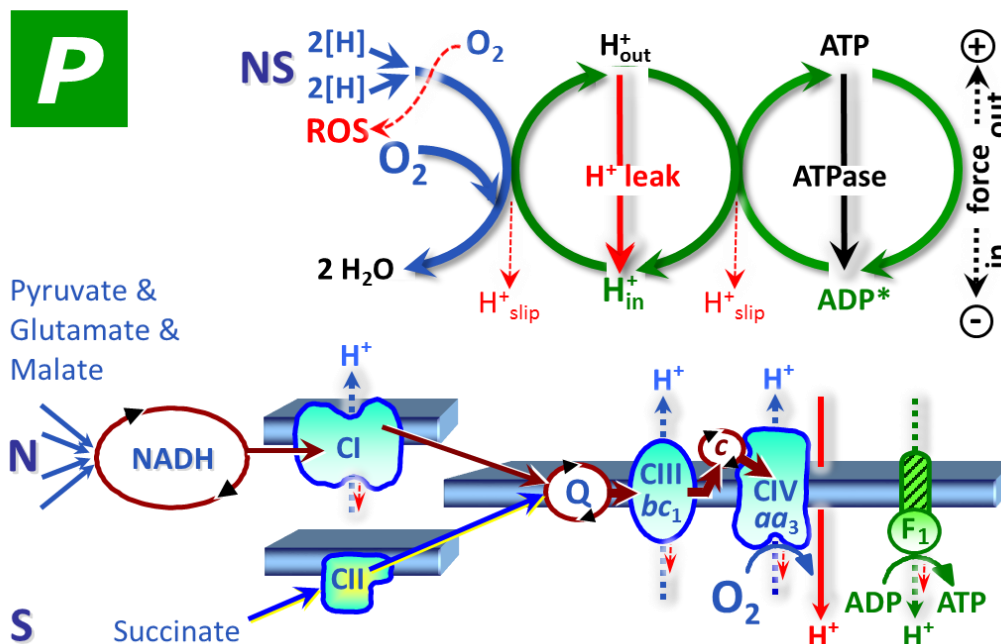


Figure 2.7. OXPHOS capacity *P*: Coupled energy cycles of oxidative phosphorylation stimulated by saturating concentrations of ADP and inorganic phosphate. $2[H]$ indicates the reduced hydrogen equivalents of CHNO fuel substrates and electron transfer to oxygen. H^+_{out} : H^+ pumped out of the matrix phase to the positive phase. H^+_{in} : H^+ flow to the negative matrix phase drives the phosphorylation of ADP to ATP. The capacity of the phosphorylation system may contribute to the limitation of flux. Cation leaks dissipate energy of translocated H^+ from the positive to the negative phase. Measurement of OXPHOS capacity is possible in mt-preparations at saturating ADP, supported by an ET-competent substrate state, for example in the NADH- and succinate-linked $\bar{N}\bar{S}$ -pathway. For further explanations, see Figure 1.1.

Mitochondria respiring at OXPHOS capacity generate a protonmotive force pmF by H^+ pumping through CI, CIII and CIV. The pmF in turn fuels the ATP synthase to drive phosphorylation (coupled respiration), facilitates transport of charged molecules, and is partially dissipated (uncoupled respiration). In the OXPHOS state, therefore, mitochondria are in a **partially coupled** (loosely coupled) state.

It is difficult to stimulate living cells to maximum OXPHOS activity, since ADP and inorganic phosphate do not equilibrate across plasma membranes, and thus saturating concentrations of these metabolites can hardly be achieved in living cells. Selective permeabilization of cell membranes with maintenance of intact mitochondria provides a model for biochemical *cell ergometry* (Figure 2.7; Figure 3.3).

2.4. ROUTINE respiration R of the living cell

R Cell respiration *in vivo* (in living cells, ce) is regulated according to physiological activity, at intracellular non-saturating ADP levels in ROUTINE states of activity (Figure 2.8).

ROUTINE respiration: living cells

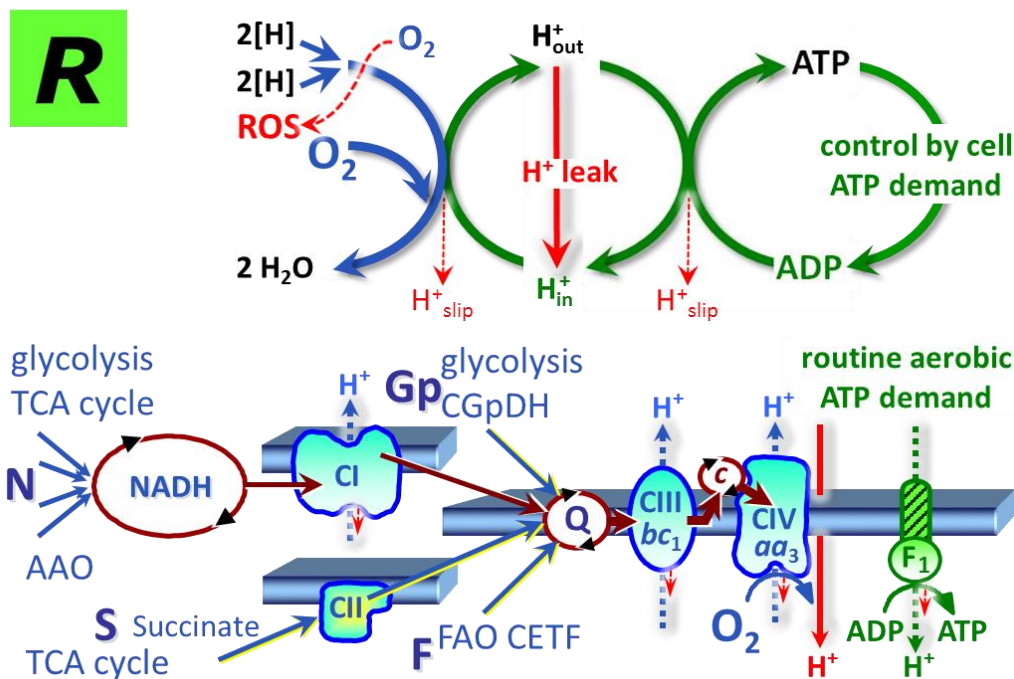


Figure 2.8. ROUTINE respiration R : Coupled energy cycles and hydrogen ion H^+ circuit of mitochondrial respiration in living cells controlled by aerobic ATP demand in the ROUTINE state of activity. $2[H]$ indicates the reduced hydrogen equivalents of a variety of CHNO energy substrates, from carbohydrates through glycolysis to the tricarboxylic acid (TCA) cycle and glycerophosphate dehydrogenase complex (CGpDH), amino acid oxidation (AAO) and fatty acid oxidation (FAO through the electron transferring flavoprotein complex, CETF). Compare Figure 2.7.

R increases or decreases under various conditions of pathophysiological activation or inhibition. The ROUTINE level of respiration R is corrected for residual O_2 consumption due to oxidative side reactions (Figure 1.2). At high glucose or fructose concentration, respiration may be suppressed by the Crabtree effect, when anaerobic catabolism

contributes significantly to ATP turnover. *R* may include aerobic energy requirements for cell growth when cells are incubated in culture medium. ROUTINE respiration is thus fundamentally different from the definition of basal metabolic rate (BMR). When incubated for short experimental periods in a medium devoid of fuel substrates, the cells respire solely on endogenous substrates at the corresponding ROUTINE state.

2.5. Electron transfer capacity *E*

E The capacity of the electron transfer system ETS is evaluated in an open-circuit operation of the transmembrane protonmotive force. The ET state is established experimentally by uncoupler titrations using protonophores (uncouplers, CCCP, FCCP, DNP) at optimum concentrations for stimulation of maximum flux (*noncoupled* state) in living cells (Figure 1.2) or mt-preparations supported by an ETS-competent substrate state (Figure 2.3). Protonophores do not uncouple electron transfer from H⁺ translocation, but dissipate energy of translocated H⁺ as a bypass of ATP synthesis (Figure 2.9).

In state *E* the mt-membrane potential is largely but not fully collapsed. Respiration is inhibited above optimum uncoupler concentrations. ET capacity potentially exceeds the OXPHOS capacity (Figure 2.3), since *E* is not limited by the capacity of the phosphorylation system (uncontrolled state).

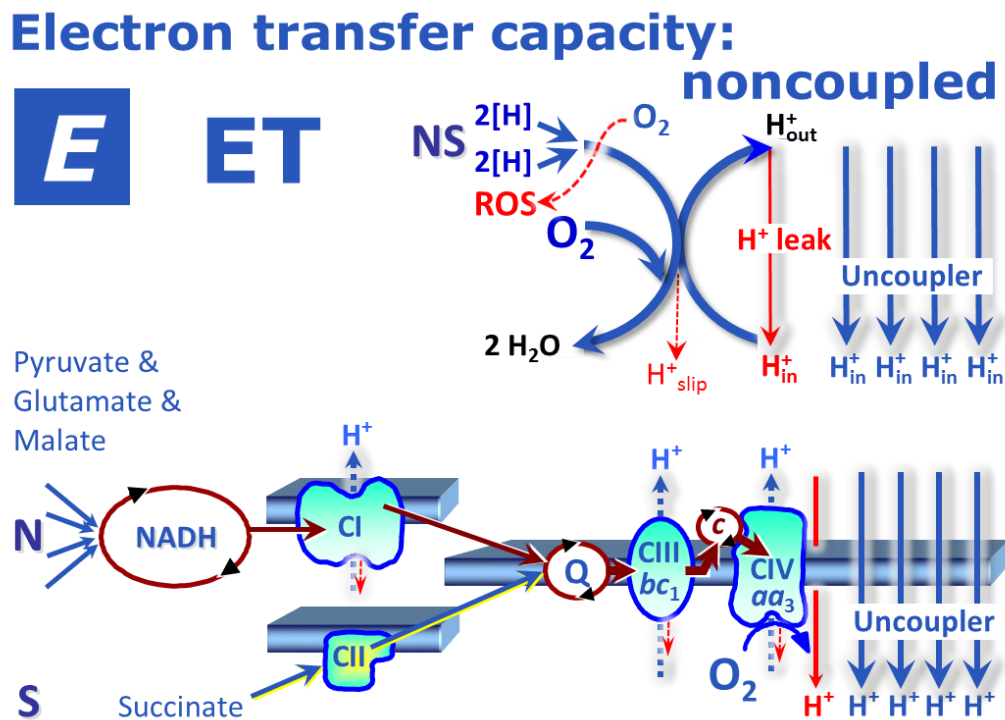


Figure 2.9. ET capacity *E*: Noncoupled respiration with a short circuit of the H⁺ cycle across the mtIM at optimum uncoupler (protonophore) concentration stimulating maximum O₂ flux. ET capacity depends not only on the inner membrane-bound ETS (mETS; with respiratory Complexes CI to CIV, electron-transferring flavoprotein complex, CETF, and glycerophosphate dehydrogenase complex, CGpDH), but also integrates transporters across the mtIM, the TCA cycle and other mt-matrix dehydrogenases.

2.6. LEAK respiration *L*

L LEAK respiration compensates for cation leak, pump slip, and cation cycling and is, to a small extent, influenced by electron leak linked to ROS production (Figure 2.10). LEAK is an acronym beyond the H^+ leak and is measured as mitochondrial respiration in the presence of CHNO-fuel substrate(s), absence of ADP, or after enzymatic inhibition of the phosphorylation system. The LEAK state is the *non-phosphorylating* resting state of intrinsic uncoupled or dyscoupled respiration when O_2 flux is minimized by the backpressure of a high protonmotive force generated when ATP synthase is not active. At a given leak, *L* depends inversely on the H^+/O_2 ratio and is thus lower in the N-pathway compared to the S-pathway. In the LEAK state at maximum *pmF*, LEAK respiration is higher than the LEAK component contributing to ROUTINE respiration or OXPHOS capacity. Therefore, *R-L* or *P-L* represent the lower limit of phosphorylation-linked net O_2 consumption.

LEAK respiration: dissipative

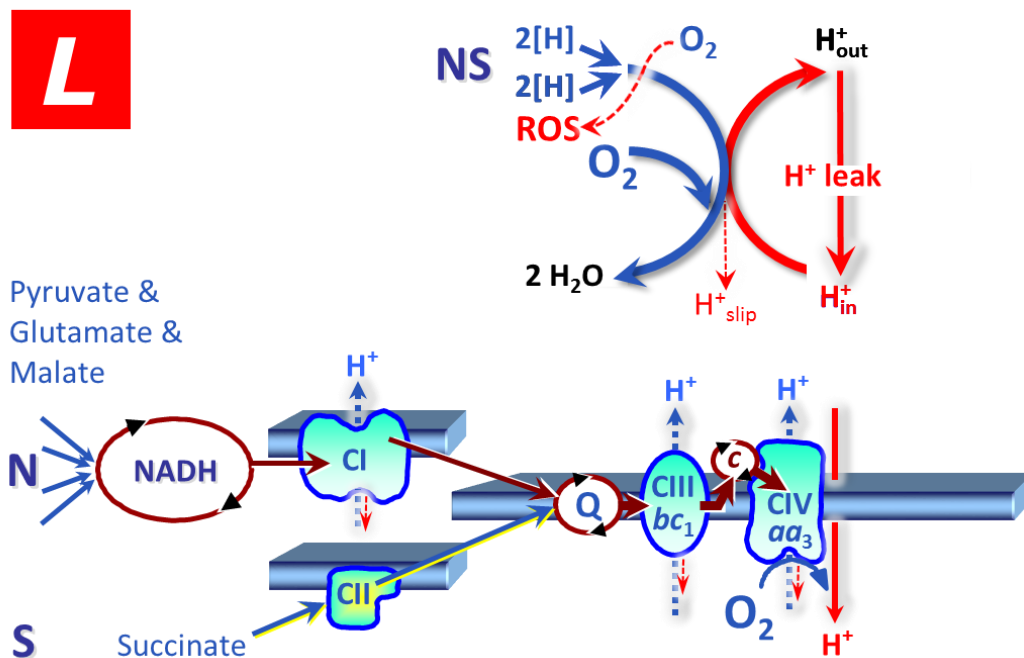


Figure 2.10. LEAK respiration *L*: Resting, non-phosphorylating electron transfer with a short circuit of the H^+ cycle across the inner mt-membrane due to intrinsic uncoupling or dyscoupling, but absence of utilization of the protonmotive force for driving ATP synthesis. Cation leak (a property of the inner mt-membrane) dissipates energy of translocated charges, whereas pump slip prevents full translocation of charge across the mt-inner membrane (a property of the H^+ pumps).

Three experimental LEAK states can be distinguished, which may yield identical estimates of LEAK respiration or may show deviations that help to critically assess the proper protocol to be applied in specific cases. Two LEAK states are based on elimination of the substrate ADP for phosphorylation, *L*(n) and *L*(T), with no adenylates (n) and with ATP (T) but no ADP, respectively. These ADP-limited LEAK states can be induced in mt-preparations but not in living cells. Effective elimination of inorganic phosphate is more difficult to achieve, exerts additional effects on the control of the *pmF* and substrate antiport, and is therefore not recommended. In living cells and all mt-preparations,

inhibitors of the phosphorylation system can be applied which are permeable through plasma- and mt-membranes. Oligomycin, an inhibitor of ATPsynthase, is currently the most frequently applied inhibitor inducing $L(Omy)$.

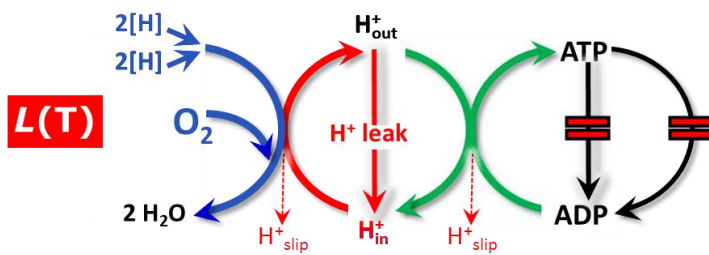


Figure 2.11. $L(T)$ in the LEAK state with ATP, which is the classical State 4 in isolated mitochondria after phosphorylation of ADP to ATP is completed (Figure 2.1).

Application: Highly purified intact imt; usually not suitable for tissue homogenate, permeabilized cells or tissues; not for living cells.

Caution: $L(T)$ represents intrinsic LEAK respiration only in the absence of ATPase activity, which would recycle ATP to ADP and thus stimulate coupled respiration. This is easily verified by unchanged respiration upon addition of ATP in the absence of adenylates, $L(n)$ to $L(T)$ transition; or after inhibition of the phosphorylation system, $L(T)$ to $L(Omy)$ transition. Phosphorylation of ADP to ATP must be completed before exhausting the O_2 concentration in the closed respirometer to zero. Hence 'high ADP' needs to be limited to concentrations <1 mM, which in many cases is not saturating the phosphorylation system for measurement of OXPHOS even in isolated mitochondria. Assume the O_2 concentration to be $\approx 200 \mu M$ O_2 at air saturation, then oxygen would be completely exhausted until 1 mM ADP is phosphorylated to ATP at a $P \gg O_2$ ratio of ≈ 5 .

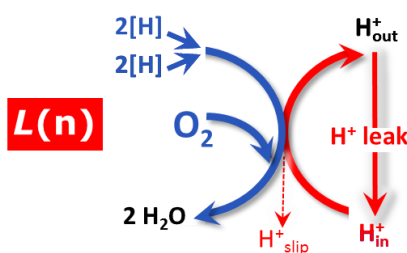


Figure 2.12. The LEAK state with no adenylates, $L(n)$ (protocol Figure 2.2b), is the state of substrate (ADP) limitation of the phosphorylation system, comparable to application of a specific inhibitor, $L(Omy)$.

Application: All mt-preparations; not in living cells.

Caution: Residual and endogenous adenylates may stimulate respiration above the actual LEAK state, which may be checked by addition of oligomycin.

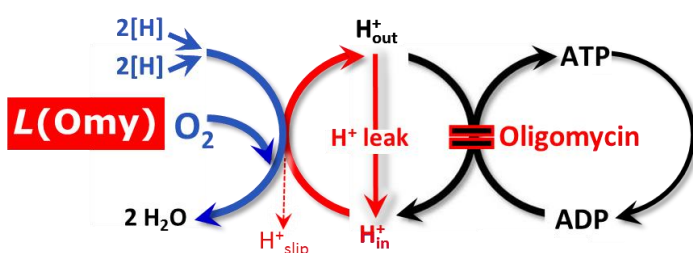


Figure 2.13. $L(Omy)$ in the LEAK state with oligomycin; the inhibitor of ATP synthase, Omy, is used to inhibit the phosphorylation system.

Application: $L(Omy)$ is frequently used in living cells, permeabilized cells and permeabilized tissue preparations or homogenate. It is also applicable for imt.

Caution: Permeabilized muscle fibers and living yeast cells respond to Omy very slowly, in contrast to isolated mitochondria and various living or permeabilized cells. Any subsequent measurements have to be evaluated critically, since cell metabolism may be dysregulated with the effect of deterioration of respiratory capacity. Experimental artifacts are readily apparent when uncoupler titrations after $L(Omy)$ cannot even restore previous OXPHOS- or ROUTINE levels of respiration. Avoid high Omy concentrations.

2.7. Uncoupled – noncoupled – dyscoupled?

Is LEAK respiration *uncoupled*? (1) **Yes**: with respect to the **process**, LEAK respiration is not coupled (non-phosphorylating respiration). (2) **No**: with respect to the **experimental state**, L and P are states of *coupled* mitochondria without addition of an uncoupler, in contrast to protonophore-stimulated ET capacity measured in the *uncoupled* (noncoupled) state E . (3) **Yes**: with respect to a **pathophysiological state**, in which coupling is lost, L and P can be observed in a state of *uncoupled* (dyscoupled) mitochondria. To address this confusing state, three different meanings of uncoupling (or coupling) are distinguished by defining intrinsically **uncoupled**, pathologically **dyscoupled**, and experimentally **noncoupled** states of respiration:

1. In the partially uncoupled (or partially coupled) state of respiration, *intrinsic uncoupling* under physiological conditions is a property of the mt-inner membrane (leak across the mtIM), H^+ pumps (pump slip; decoupling), and molecular uncouplers (uncoupling protein UCP1).
2. *Dyscoupled* respiration under pathological and toxicological conditions is related to states of mitochondrial dysfunction. An explicit distinction is made between physiologically regulated uncoupling and pathologically defective dyscoupling (analogous to distinguishing eustress versus distress, function versus dysfunction). Physiological uncoupling and pathological dyscoupling are evaluated under experimental conditions as respiration in the LEAK state in relation to ET capacity, i.e. the L/E coupling-control ratio, or as $E-L$ coupling efficiency, $1-L/E = (E-L)/E$.
3. *Noncoupled* respiration in the experimentally controlled uncoupled ($\stackrel{\text{def}}{=} \text{noncoupled}$) state is induced by application of established uncouplers (protonophores), with the aim of obtaining a reference state with reduced mt-membrane potential, for evaluation of the respiratory capacity through the electron transfer system (ET capacity; Figure 2.9).

2.8. Residual oxygen consumption *Rox*

KCN, H₂S and CO combine with some of the components of oxidase forming an inactive compound, with the result that cytochrome, or at least its components a' and c', as well as paraphenylenediamine added to the cells, are not oxidised. The respiratory process can be still carried out through the medium of some autoxidisable carriers such as haemochromogens, haematins, the component b' of cytochrome, or some as yet unknown autoxidisable substances. This residual respiration, according to the nature of the cell, may represent a larger or smaller fraction of the total respiration of the cell.

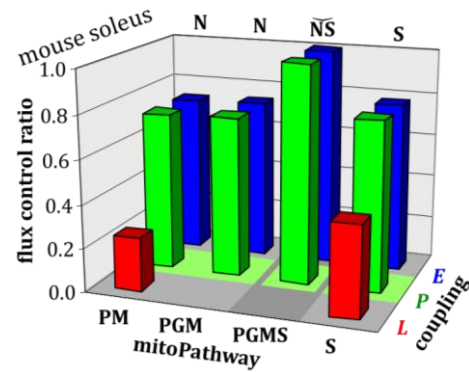
Keilin D (1929) Cytochrome and respiratory enzymes. Proc R Soc London Ser B 104:206-52.

Rox

Residual oxygen consumption *Rox* is the respiration due to oxidative side reactions in the ROX-state, after application of ET inhibitors acting downstream of any fuel substrates supplied to mitochondrial preparations or cells, or in mt-preparations incubated without substrates. Mitochondrial respiration is frequently corrected for *Rox*, then distinguishing *Rox*-corrected OXPHOS-, ET-, ROUTINE-, or LEAK-capacity (P, E, R, L) from the corresponding apparent fluxes that have not been corrected for *Rox* (P', E', R', L'). When expressing *Rox* as a fraction of total respiration (flux control ratio), apparent flux not corrected for *Rox*, $E(\text{tot})$ or E' , should be taken as the reference. *Rox* may be related to, but is of course different from ROS production and may exhibit oxygen kinetics very different from CIV-linked respiration.

Chapter 3.

Normalization of rate: flow, flux, and flux ratios



Section	3.1. Cell ergometry	34	Page
	3.2. Flux control ratio	38	
	3.3. Flux control efficiency	40	

3.1. Cell ergometry

Table 3.1 summarizes ET capacities of living cells, expressed as oxygen flow per cell. *R*, *L*, *E*, and *Rox* are determined in a sequence of coupling-control titrations (Figure 3.1), and normalized for ET capacity *E*. Internal normalization yields flux ratios, expressed either as flux control ratios (*R/E*; *Rox/E'*) or flux control efficiencies.

Table 3.1. Respiration corrected for *Rox* and coupling-control efficiency in living human cells (and 32D mouse cells). ET capacity *E* expressed as O₂ flow per cell *I*_{kO₂E}; residual oxygen consumption *Rox* is listed as a fraction of total ET capacity *E'*; *E-L* coupling efficiency is (*E-L*)/*E*; 37 °C; mean ±SD. References in Doerrier et al 2018 and https://wiki.oroboros.at/index.php/Gnaiger_2020_MitoPathways.

Cell type	ET (<i>E</i> , <i>I</i> _{kO₂E}) / [amol·s ⁻¹ ·x ⁻¹]	ROUTINE <i>R/E</i>	net ROUTINE (<i>R-L</i>)/ <i>E</i>	net ET (<i>E-L</i>)/ <i>E</i>	ROX <i>Rox/E'</i>
platelets	0.22 ± 0.03	0.33 ± 0.11	0.26 ± 0.11	0.93 ± 0.01	0.07 ± 0.03
PBMC	14 ± 1	0.27 ± 0.02	0.19 ± 0.01	0.92 ± 0.02	0.05 ± 0.01
HEK 293	47 ± 7	0.31 ± 0.03	0.23 ± 0.02	0.91 ± 0.00	0.01 ± 0.00
CEM, control	54 ± 11	0.40 ± 0.03	n.d.	n.d.	0.02 ± 0.03
CEM, G1-phase, apopt.	32 ± 6	0.41 ± 0.03	n.d.	n.d.	0.03 ± 0.03
CEM, S-phase, apopt.	85 ± 10	0.38 ± 0.03	n.d.	n.d.	0.01 ± 0.01
32D (mouse)	81 ± 11	0.39 ± 0.02	0.29 ± 0.02	0.90 ± 0.02	0.03 ± 0.01
HUVEC	114 ± 18	0.26 ± 0.02	0.13 ± 0.00	0.87 ± 0.02	0.05 ± 0.04
HPMC, control	181 ± 58	0.40 ± 0.09	0.31 ± 0.08	0.91 ± 0.01	0.01 ± 0.01
HPMC, +IL-1β	142 ± 47	0.41 ± 0.09	0.32 ± 0.08	0.92 ± 0.02	0.02 ± 0.01
fibroblasts, young-prolif.	111 ± 24	0.34 ± 0.03	0.20 ± 0.02	0.86 ± 0.02	0.07 ± 0.03
fibroblasts, young-arrest	138 ± 22	0.23 ± 0.01	0.18 ± 0.02	0.95 ± 0.01	0.05 ± 0.00
fibroblasts, senescent	285 ± 72	0.42 ± 0.05	0.21 ± 0.05	0.79 ± 0.04	0.07 ± 0.03

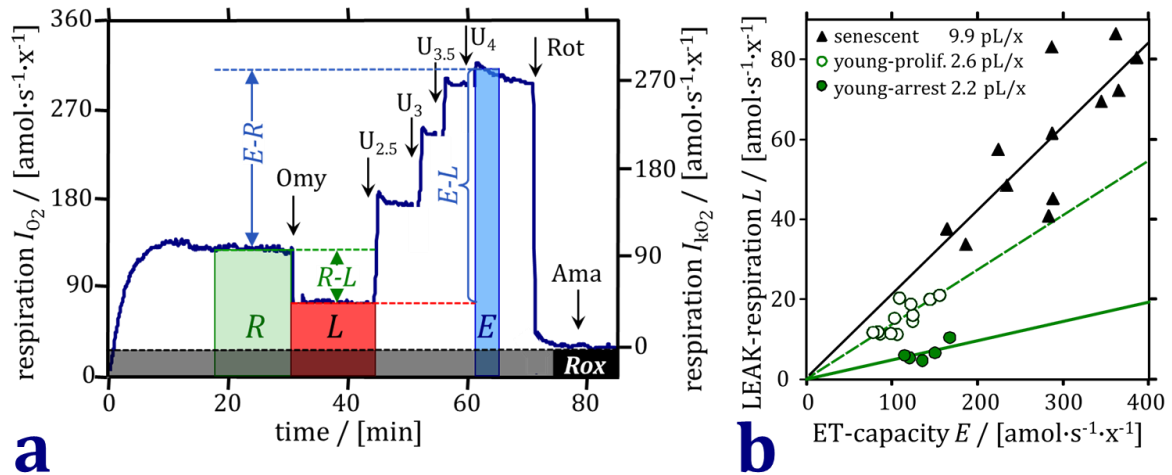


Figure 3.1. E-R-L coupling-control protocol in living cells (human foreskin fibroblasts). SUIT-003: respiration in cell culture medium DMEM, expressed as O_2 flow I_{O_2} per cell. Catabolic respiration I_{kO_2} (E , R , and L) corrected for residual oxygen consumption Rox . (a) HRR trace in growth-arrested senescent cells ($0.2 \text{ Mx}\cdot\text{mL}^{-1}$) with uncoupler titration (U ; FCCP 2.5-4 μM). Inhibition of CI by rotenone Rot blocks the TCA cycle in the living cell by redox control. Consequently succinate is not produced. When antimycin A (Ama , inhibitor of CIII) does not inhibit respiration further, CI-independent electron entries into Q are blocked. (b) Linear dependence of L on E , representing the L/E coupling-control ratio (slopes) independent of the effect of cell size (compare Figure 1.5) on respiratory flow (compare Figure 1.6; Table 3.1). Modified after Hütter et al 2004.

The extensive quantity oxygen flow I_{kO_2E} [$\text{pmol}\cdot\text{s}^{-1}\cdot\text{Mx}^{-1}$] varies 1300-fold from primary platelets to senescent fibroblasts (Table 3.1), whereas mass-specific oxygen flux $J_{kO_2E/m_{ce}}$ [$\text{pmol}\cdot\text{s}^{-1}\cdot\text{mg}^{-1}$] is confined to a 3.2-fold range (Table 3.2). Oxygen flow depends on cell size – volume per cell or mass per cell – not only between but also within cell types, as shown in fibroblasts and CEM cells (Figure 3.2). Normalization of rate for cell mass yields mass-specific flux $J_{kO_2/m_{ce}}$ of approximately 25 $\text{pmol}\cdot\text{s}^{-1}\cdot\text{mg}^{-1}$ in platelets and senescent fibroblasts and 40 to 80 $\text{pmol}\cdot\text{s}^{-1}\cdot\text{mg}^{-1}$ in PBMC, HEK, CEM, HUVEC, and young fibroblasts (Table 3.2). By comparison, OXPHOS capacity in human skeletal muscle ranges from 60 to 160 $\text{pmol}\cdot\text{s}^{-1}\cdot\text{mg}^{-1}$ based on wet muscle mass of permeabilized fibers (Figure 6.13) or isolated mitochondria related to the tissue mass of origin as illustrated in Figure 1.7 (Gnaiger 2009; compare Figure 6.14 for human heart muscle). This is a surprisingly small difference in respiratory capacity between muscle tissue and cultured human cells or primary blood cells – but are these values comparable?

There are practical limitations of the present comparison of respiratory capacity in tissue biopsies versus living cells, such as methodological differences in measurement of tissue mass and cell mass. In addition, theoretical arguments suggest to compare these respiratory capacities with caution: (1) Intracellular substrates and their concentrations are different in living cells and experimental substrate cocktails applied in mitochondrial preparations. (2) ET capacity may be up to two-fold higher than OXPHOS capacity (Chapter 2; Figure 6.12). The physiologically relevant OXPHOS coupling state cannot be established in living cells. (3) Intracellular mt-density is a vitally important component of mitochondrial fitness. Respiratory capacity per mass of muscle tissue varies >2.5-fold between sedentary and athletic physiological states, integrating mt-specific function and mt-density. Similarly, cell culture conditions modulate mass-specific cellular respiratory capacity. What are comparable sedentary and active lifestyle states of cultured cells?

Table 3.2. Cell size, and respiratory flow and flux of living human cells. See Table 3.1.

Cell type	Diameter / [μm]	$V_{U_{ce}}$ # / [$\text{pL}\cdot\text{x}^{-1}$]	$M_{U_{ce}}$ § / [$\text{mg}\cdot\text{Mx}^{-1}$]	Flow R, I_{O_2E} / [$\text{amol}\cdot\text{s}^{-1}\cdot\text{x}^{-1}$]	Flow E, I_{O_2E} / [$\text{amol}\cdot\text{s}^{-1}\cdot\text{x}^{-1}$]	Flux $E, J_{O_2E/m_{ce}}$ / [$\text{pmol}\cdot\text{s}^{-1}\cdot\text{mg}^{-1}$]
platelets	2.5	0.01	0.01	0.07	0.22	25
PBMC	7.4	0.21	0.22	4	14	62
HEK 293	13.0	1.2	1.2	15	47	39
CEM, control	11.4	0.77*	0.8	22	54	66
CEM, G1- phase, apopt.	10.6	0.63*	0.7	13	31	46
CEM, S- phase, apopt.	14.7	1.67*	1.8	32	85	48
HUVEC	13.6	1.3	1.4	30	114	82
fibroblasts, young-prolif.	17.1	2.6*	2.8	38	111	40
fibroblasts, young-arrest	16.1	2.2*	2.3	32	138	60
fibroblasts, senescent	26.6	9.9*	10.4	120	285	27

Elementary volume $V_{U_{ce}} = 4/3\cdot\pi\cdot(d/2)^3$, related to the diameter d of a sphere; $\mu\text{m}^3 = \text{fL}$ converted to pL (SI prefixes in Section A4).

* Volume determined by CASY1 TT cell counter (Schärfe System, Reutlingen, Germany).

§ Elementary mass $M_{U_{ce}}$ per cell is calculated assuming a cell density of $1.06 \mu\text{g}\cdot\text{nL}^{-1}$.

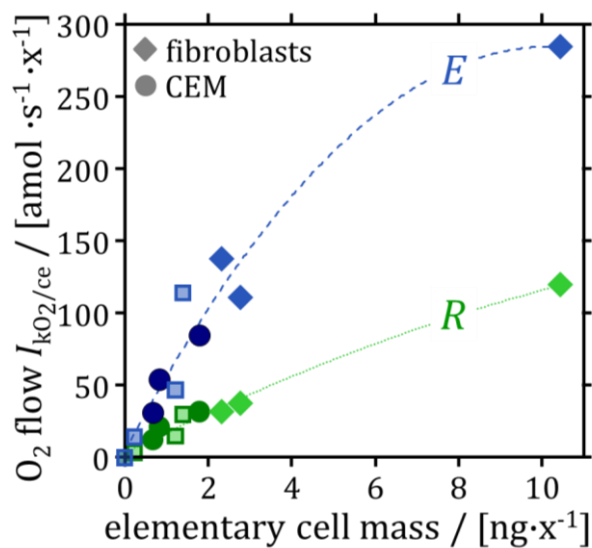
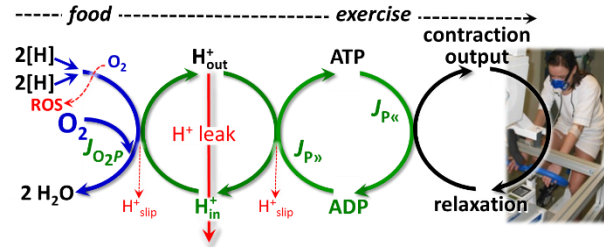


Figure 3.2. O₂ flow per cell as a function of cell size expressed as elementary wet mass $M_{U_{ce}}$. Average cell size depends not only on cell type (Table 3.2) but also on the distribution of growth states in the cell cycle of the cell population and growth conditions within cell types (fibroblasts, CEM). Normalization of rate represents a key for interpreting respiratory flow and distinguishing between the effects of cell size, mitochondrial density, and mitochondrial quality on respiratory performance (Figure 1.6). Polynomial fits for ROUTINE respiration R and ET capacity E , without implications on allometric scaling.

Analogous to ergometric measurement of $V_{O_2\text{max}}$ on a cycle or treadmill, cell ergometry is based on measurement of OXPHOS capacity J_{O_2P} [$\text{pmol O}_2\cdot\text{s}^{-1}\cdot\text{mg}^{-1}$], at the mitochondrial level (Figure 3.3). Whereas ET capacity is of fundamental importance in mitochondrial respiratory control, OXPHOS capacity and coupling control efficiency are the physiological determinants of mitochondrial fitness. The OXPHOS state is established experimentally in mt-preparations by the control of flux at kinetically saturating ADP and P_i concentrations, which is not possible in living cells. Fuel substrate combinations reconstitute physiological TCA cycle function in mt-preparations (Chapter 6).

Figure 3.3. Cell ergometry. OXPHOS analysis reveals the maximum aerobic capacity of well coupled cell respiration, in contrast to ET capacity based on uncoupler titrations.



Mitochondrial functional fitness is the product of mitochondrial density (per mass of tissue or cell) and elementary mitochondrial function (per mitochondrial unit). Elementary mitochondrial function is a property of mitochondrial quality independent of mitochondrial density.

When mitochondrial or cell respiration is measured in a sequence of respiratory states i in a substrate-uncoupler-inhibitor-titration (SUIT) protocol, internal normalization of rate Y_i yields flux ratios: (1) flux control ratios and (2) flux control efficiencies. Internal normalization uses the rate Z in a reference state as a functional mitochondrial marker. Flux ratios are independent of (1) cell count, wet or dry mass, (2) mt-content of cells or tissues, (3) purification in preparations of isolated mitochondria, and (4) assay conditions for determination of cell or tissue mass, or mt-markers external to a respiratory protocol (CS, protein, stereology, etc.; Figure 1.6b). Y and Z have to be expressed in the same units in a common format of flow or flux, but neither units nor format matter, nor is quantification required of the sample. For these methodological reasons, flux ratios are free of noise propagation encountered in external normalization, when a noisy marker inevitably causes noise in the marker-specific flux. Therefore, higher statistical resolution of changes in mt-quality is obtained by flux ratios compared to OXPHOS analysis based on external mt-markers, cell size, or cell count. Selection of the reference state for Z , however, is not arbitrary but decisive, and is controversial particularly with respect to the classical UCR and RCR (Table 3.3; Figures 3.4 and 3.5).

3.2. Flux control ratio

Flux control ratios FCR provide a fingerprint of respiratory control (Figure 7.2). FCR_i are internal normalizations of rates Y_i obtained in a sequence of respiratory states i , normalized for the rate Z in a fixed respiratory reference state common to all states i ,








$$\text{Flux control ratio:} \quad FCR_i = \frac{Y_i}{Z} \quad 3.1$$

The reference Z is typically the maximum or a high rate in a SUIT protocol, such as ET capacity (ce; Figure 3.1) or NS-ET capacity in mt-preparations (Figures 2.3, 6.4-6.5, 6.7-6.8). Coupling-control ratios are FCR at a constant mitochondrial pathway control state. E is the reference flux Z in the LEAK-, OXPHOS-, and ROUTINE-control ratios; P or R are Z in the L/P and L/R coupling-control ratios (Table 3.3; metabolic control variable X). Pathway control ratios are FCR at a constant coupling state (OXPHOS state in Figure 6.7).

3.3. Flux control efficiency

A step change of flow or flux, $Z_X - Y_X$, is the response of a rate to a specific metabolic control variable X . Table 3.4 summarizes $Z_X - Y_X$ derived from the $E-P-L$ coupling-control protocol applied to mt-preparations (Figure 2.3) and the $E-R-L$ coupling-control protocol applied to living cells (Figure 3.1). $Z_X - L_X$ net respiratory capacities are obtained by subtraction of LEAK respiration L . $E_X - Y_X$ is either the $E-P$ excess capacity, or the $E-R$ reserve capacity (Table 3.4).

Table 3.3. Flux control ratios related to coupling in mt-preparations and living cells

FCR	Coupling-control ratio Y_i/Z		X_i	Y_i	Z
<i>L/P</i>	L/P coupling-control ratio , 1/RCR, control by coupling and <i>P</i>		D	<i>L</i>	<i>P</i>
<i>L/R</i>	L/R coupling-control ratio , control by cell physiological state, mitochondrial coupling and <i>P</i>		Omy	<i>L</i>	<i>R</i>
<i>L/E</i>	L/E coupling-control ratio , 1/UCR, control by coupling and <i>E</i>		U	<i>L</i>	<i>E</i>
<i>P/E</i>	P/E control ratio , phosphorylation system control ratio, control by coupling and limitation by the phosphorylation system		U	<i>P</i>	<i>E</i>
<i>(P-L)/E</i>	net P/E control ratio		U	<i>P-L</i>	<i>E</i>
<i>R/E</i>	R/E control ratio , control by cell physiological state, coupling, <i>P</i> , and <i>E</i> -excess		U	<i>R</i>	<i>E</i>
<i>(R-L)/E</i>	net R/E control ratio		U	<i>R-L</i>	<i>E</i>

The flux control efficiency represents the fractional control of respiration in a *step* Z_X - Y_X . Low flux Y_X in the background state is increased under the influence of X to high flux Z_X in the reference state, $Z_X > Y_X$. The FCF_X is the dimensionless fractional increase of flux normalized for the higher flux Z_X ,

$$\text{Flux control efficiency: } j_{Z-Y} = \frac{Z_X - Y_X}{Z_X} = 1 - \frac{Y_X}{Z_X} \quad 3.2$$

Coupling-control efficiencies are determined in a constant ET-competent substrate state. On the other hand, pathway or substrate control efficiencies express the relative change of O_2 flux in response to transitions to another pathway or substrate in a defined coupling state.

Coupling-control efficiencies are integral components of thermodynamic efficiency, ranging from 0.0 (zero coupling) to 1.0 (the limit of a completely coupled system). The 4-compartmental OXPHOS model (Figure 2.4) provides the conceptual framework for coupling-control efficiencies summarized in Table 3.5.

The respiratory acceptor control ratio RCR and uncoupling-control ratios UCR are the inverse of the *L/P*, *L/E* or *R/E* control ratios (Table 3.3). UCR and RCR have been used to express coupling in living cells and isolated mitochondria. Figures 3.4 and 3.5 illustrate, why UCR and RCR (with ranges from 1 to ∞) should be replaced by flux control efficiencies (with corresponding ranges from 0 to 1). Additionally, kinetic limitation is distinguished from coupling: RCR and *P-L* control efficiency may be suppressed kinetically by the capacity of the phosphorylation system, if it limits the utilization of the *pmF*. *P-L* control efficiency and *E-L* coupling efficiency (j_{P-L} and j_{E-L}) are linearly related by inserting the *E-P* control efficiency j_{E-P} (Table 3.5),

$$P-L \text{ control efficiency: } j_{P-L} = j_{E-L} \cdot (1 - j_{E-P})^{-1} - j_{E-P} \cdot (1 - j_{E-P})^{-1} \quad 3.3a$$

$$E-L \text{ coupling efficiency: } j_{E-L} = j_{P-L} \cdot (1 - j_{E-P}) + j_{E-P} \quad 3.3b$$

3. Normalization

Figure 3.4. Uncoupling-control ratios UCR and flux control efficiencies. As $E-L$ coupling efficiency $(E-L)/E = 1-L/E$ approaches the maximum of 1, the $UCR = E/L$ increases to infinity, with asymmetric distribution of data points of UCR at a given efficiency. $(E-R)/E = 1-R/E$ is the $E-R$ control efficiency. For a wide range of low flux control efficiencies near 0.5, the UCR shows low sensitivity with a small variation around 2. Data points represent individual O2k-chambers with young and senescent fibroblasts. Data from Figure 3.1 (see Hütter et al 2004).

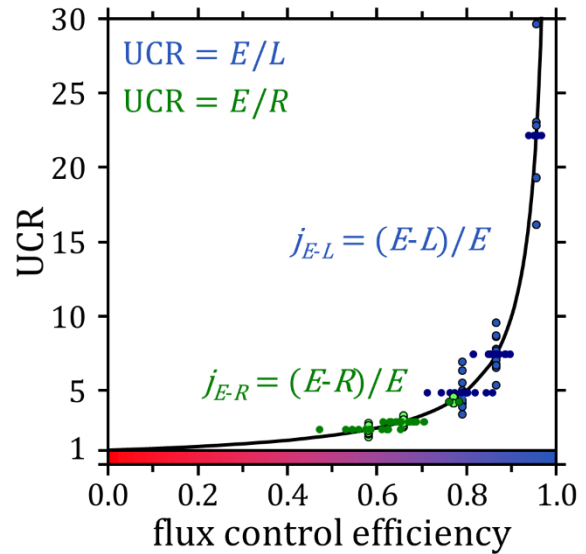


Table 3.4. Net, excess, and reserve capacities of respiration, in respiratory states of mt-preparations controlled by coupling in ET-competent pathway states, and living cells.

Net rate	Definition	mt-Preparations	Living cells
$Z_X - Y_X$		ET-competent pathway states	intracellular substrates, exogenous or endogenous
$P-L$ P-L	$P-L$ net OXPHOS capacity, coupled, pmF supports phosphorylation	saturation ADP and P_i ; or J_{max} from ADP kinetics, baseline L	constraints to induce accurately defined rate P in living cells
$R-L$ R-L	$R-L$ net ROUTINE capacity, physiological control in the range from minimum L (baseline) to maximum $P-L$, variable pmF	limiting steady-state ADP and P_i levels simulating ROUTINE respiration	physiological control of cellular substrate uptake, intermediary metabolism and energy turnover
$E-L$ E-L	$E-L$ net ET capacity, noncoupled, pmF is low but not zero	optimal uncoupler concentration for maximum respiration	optimal uncoupler concentration for maximum respiration
$E-P$ E-P	$E-P$ excess capacity	(see $P-L$)	(see $P-L$)
$E-R$ E-R	$E-R$ reserve capacity	(see $R-L$)	(see $R-L$)

Table 3.5. Flux control efficiencies related to coupling-control ratios. The terms *coupling efficiency* and *coupling-control efficiency* are used synonymously. See Table 3.3.

Rate, $Z-Y$	Name	$j_{Z-Y} = (Z-Y)/Z = 1-FCR$	X	Y_X	Z_X
net P , $P-L$	j_{P-L} $P-L$ control efficiency	$j_{P-L} = (P-L)/P = 1-L/P$	D	L	P
net R , $R-L$	j_{R-L} $R-L$ control efficiency	$j_{R-L} = (R-L)/R = 1-L/R$	Omy	L	R
net E , $E-L$	j_{E-L} $E-L$ coupling efficiency	$j_{E-L} = (E-L)/E = 1-L/E$	U	L	E
E -excess, $E-P$	j_{E-P} $E-P$ control efficiency	$j_{E-P} = (E-P)/E = 1-P/E$	U	P	E
E -reserve, $E-R$	j_{E-R} $E-R$ control efficiency	$j_{E-R} = (E-R)/E = 1-R/E$	U	R	E

Figure 3.5. Respiratory acceptor control ratio RCR, as a function of (a) P - L control efficiency j_{P-L} , and (b) biochemical E - L coupling efficiency j_{E-L} . RCR is the State 3/State 4 flux ratio, equal to P/L if State 3 refers to saturating [ADP] and [Pi]. RCR ranges from 1.0 to infinity and is highly non-linear in the typical experimental range of RCR from 3 to 10. When j_{P-L} increases from 0.8 to 0.9, RCR doubles from 5 to 10. RCR increases to infinity at the limit of $j_{P-L}=1.0$.

The P - L net OXPHOS capacity is potentially available for ATP production. To avoid overestimating the dissipative LEAK component, L can be measured during titration of an ET inhibitor to adjust the pmF to slightly lower values maintained in the OXPHOS state. Turnover-dependent components of cation leak and pump slip, however, are underestimated under these inhibited conditions.

The E - L coupling efficiency j_{E-L} decreases with increasing L or decreasing E . The P - L control efficiency j_{P-L} but not j_{E-L} decreases with specific inhibition of the phosphorylation system and increasing E - P excess capacity. j_{E-L} can be determined in living cells (Figure 3.1), whereas extended cell ergometry requires mt-preparations for determination of both j_{P-L} and j_{E-L} (Figures 3.5 and Figures 2.3, 6.5, 6.12, 6.14, 6.15).

j_{P-L} results from normalization of the measured P_{\gg}/O_2 ratio (P_{\gg}/P) by the mechanistic $P_{\gg}:O_2$ ratio (stoichiometric number ν_{P_{\gg}/O_2} of a fully coupled reaction). j_{P-L} is thus linked to the P_{\gg}/O_2 ratio by the approximation $\nu_{P_{\gg}/O_2} \approx P_{\gg}/(P-L)$,

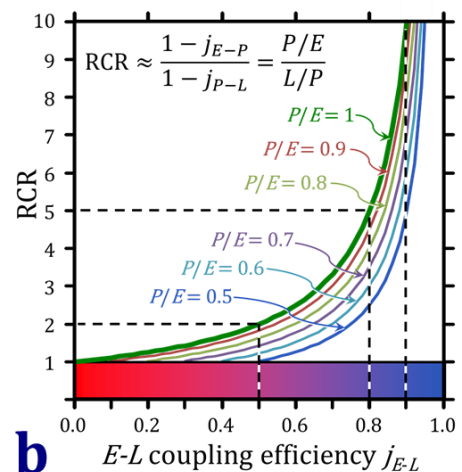
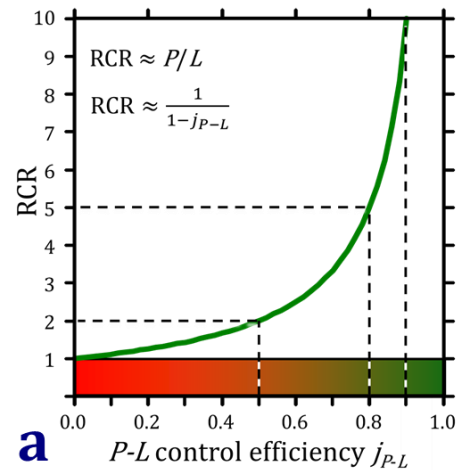
$$P-L \text{ control efficiency: } j_{P-L} = \frac{P_{\gg}/\nu_{P_{\gg}/O_2}}{P} \approx \frac{P-L}{P} = 1 - \frac{L}{P} = 1 - \frac{1}{RCR} \quad 3.4$$

ATP production P_{\gg} is converted to stoichiometrically equivalent P - L net O_2 consumption, which is the net OXPHOS capacity tightly coupled to phosphorylation (Figure 2.4),

$$P-L \text{ net OXPHOS capacity: } P - L \approx \frac{P_{\gg}}{\nu_{P_{\gg}/O_2}} \quad 3.5$$

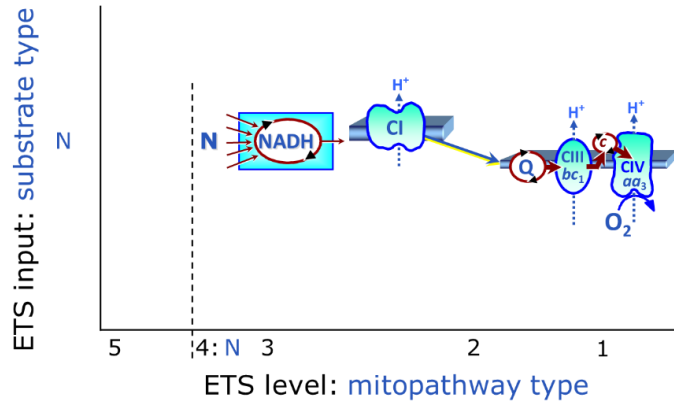
When X exerts a stimulatory effect – by a fuel substrate, ADP, or uncoupler – the background flux Y_X is measured first. In contrast, when X is an inhibitor, the reference flux Z_X is measured first. When a substance X is titrated to answer the question, if it acts as an inhibitor or activator, the results have to decide if Z_X is measured first or last in subsequent experiments. At the limit of a zero effect on flux, a consistent decision has to be taken on fixing the background Y_X as the flux measured first. For instance, the cytochrome c control efficiency may be zero with some \pm scatter, and Z_X should be defined always as J_{CHOc} (Eq. 3.2),

$$\text{Cytochrome } c \text{ control efficiency: } j_{cyt\ c} = \frac{J_{CHOc} - J_{CHO}}{J_{CHOc}} = 1 - \frac{J_{CHO}}{J_{CHOc}} \quad 3.6$$



Chapter 4.

NADH-linked pathways through Complex CI: respiratory pathway control with pyruvate, glutamate, malate



Section		Page
	4.1. Malate, M	42
	4.2. Pyruvate & Malate, PM	43
	4.3. Glutamate, G.....	44
	4.4. Glutamate & Malate, GM.....	45

Mitochondrial respiration depends on a continuous flow of CHNO-fuel substrates and products – with different degrees of reduction – across the mt-membranes between the matrix and cytosolic space. Glutamate and malate are anions which cannot permeate through the lipid bilayer of membranes and hence require carriers, which is also true for pyruvate. Anion carriers in the inner mt-membrane catalyze the transport of mitochondrial metabolites. Metabolite distribution across the mt-membrane varies mainly with ΔpH and not $\Delta\Psi$, since most carriers (but not the glutamate-aspartate carrier) operate non-electrogenic by anion exchange or electroneutral co-transport of H^+ .

Depending on the concentration differences, these carriers transport metabolites not only into mitochondria, but from the mitochondria into the cytosol, and thus cause the loss of intermediary metabolites into the incubation medium. Cataplerotic and anaplerotic transport of intermediates of the tricarboxylic acid (TCA) cycle plays an important metabolic role in the living cell. This must be considered when interpreting the effect on respiration of specific substrates used in studies of mitochondrial preparations.

Substrate combinations of pyruvate & malate (PM) and glutamate & malate (GM) stimulate dehydrogenases with reduction of nicotinamide adenine dinucleotide (NAD^+ to NADH), then feeding electrons into Complex I (CI, NADH-UQ oxidoreductase) and down the thermodynamic cascade through the Q-cycle and Complex III of the electron transfer system to Complex IV and O_2 . CI is present in most but not all mitochondria – not in yeast.

The NADH-linked pathway (N-pathway) and reverse electron transfer to NAD^+ (RET) are blocked by inhibition of the membrane-bound CI. Rotenone and the barbiturate amytal are semiquinone ($SQ^{\cdot-}$, partially reduced) antagonists that inhibit electron transfer from iron-sulfur centers to quinone by binding to the quinone (Q, fully oxidized) binding site of CI. In contrast, piericidin is both a quinone and semiquinone antagonist that competes with Q for binding sites. The CIII inhibitors myxothiazol and stigmatellin inhibit CI acting as quinol (hydroquinone H_2Q , fully reduced) antagonists. CI inhibitors stimulate or reduce ROS production depending on the mechanism of action and the types of added CHNO-fuel substrates.

4.1. Malate, M

Malate is typically used as a co-substrate with pyruvate or glutamate. OXPHOS capacity with malate alone is only 1.3 % of that with pyruvate & malate in isolated rat skeletal muscle mitochondria (Figure 4.1).

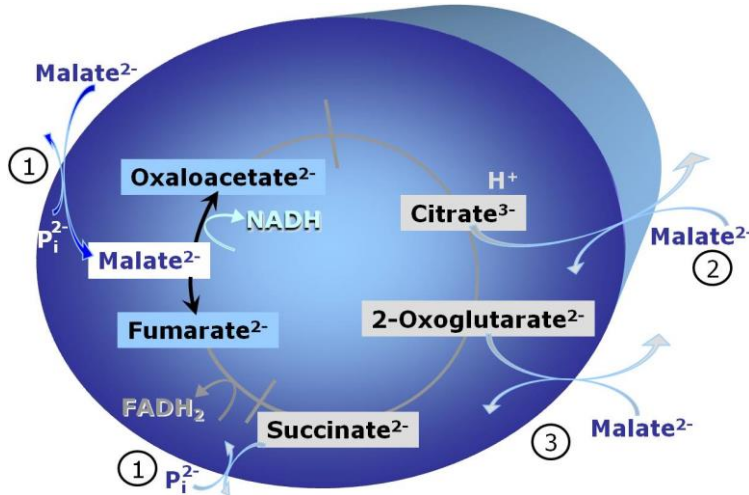


Figure 4.1. Malate, M alone does not support respiration of mt-preparations if oxaloacetate cannot be metabolized further in the absence of a source of acetyl-CoA. Transport of oxaloacetate across the inner mt-membrane is restricted particularly in liver. Mitochondrial citrate and 2-oxoglutarate (α -ketoglutarate) are depleted by antiport with malate. Succinate is lost from the mitochondria through the dicarboxylate carrier.

Carriers for malate (malic acid, C₄H₆O₅)

1. The dicarboxylate carrier catalyzes the electroneutral exchange of malate²⁻ or succinate²⁻ for HPO₄²⁻. It is more active in liver than heart mitochondria.
2. The tricarboxylate carrier exchanges malate²⁻ for citrate³⁻ or isocitrate³⁻ (with co-transport of H⁺). It is highly active in liver, but low in heart mitochondria.
3. The 2-oxoglutarate carrier exchanges malate²⁻ for 2-oxoglutarate²⁻.

Many mammalian and non-mammalian mitochondria have a mt-isoform of NADP⁺- or NAD(P)⁺-dependent malic enzyme (ME), the latter being particularly active in proliferating cells. Then malate alone can support high respiratory activities due to the simultaneous formation of pyruvate and oxaloacetate in the malate-anaplerotic pathway (Figure 4.2). Tartronic acid is an inhibitor of malic enzyme.

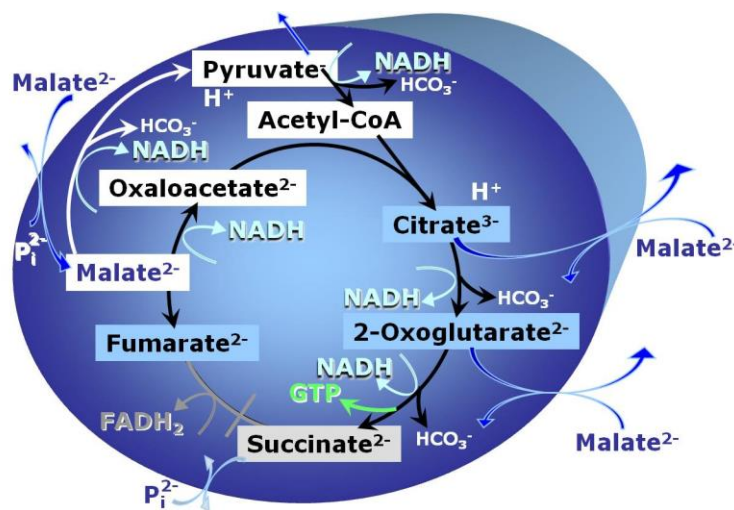


Figure 4.2. Malate, M, and mt-malic enzyme supporting the malate-anaplerotic pathway. Dismutation of malate by malate dehydrogenase (MDH) and mt-malic enzyme (mtME). Pyruvate accumulates in the medium or re-enters the TCA cycle via pyruvate dehydrogenase (PDH) and acetyl-CoA, thus supporting oxaloacetate consumption by citrate synthase.

Decarboxylase reactions catalyzed by PDH, isocitrate dehydrogenase, and 2-oxoglutarate dehydrogenase are shown with bicarbonate ion formation. Whether or not the carbonic anhydrase reaction $\text{CO}_2 \rightarrow \text{H}_2\text{CO}_3$ is required primarily remains an open debate (Swenson 2018). The hydrogen ion balance should be considered in detail.

4.2. Pyruvate & Malate, PM

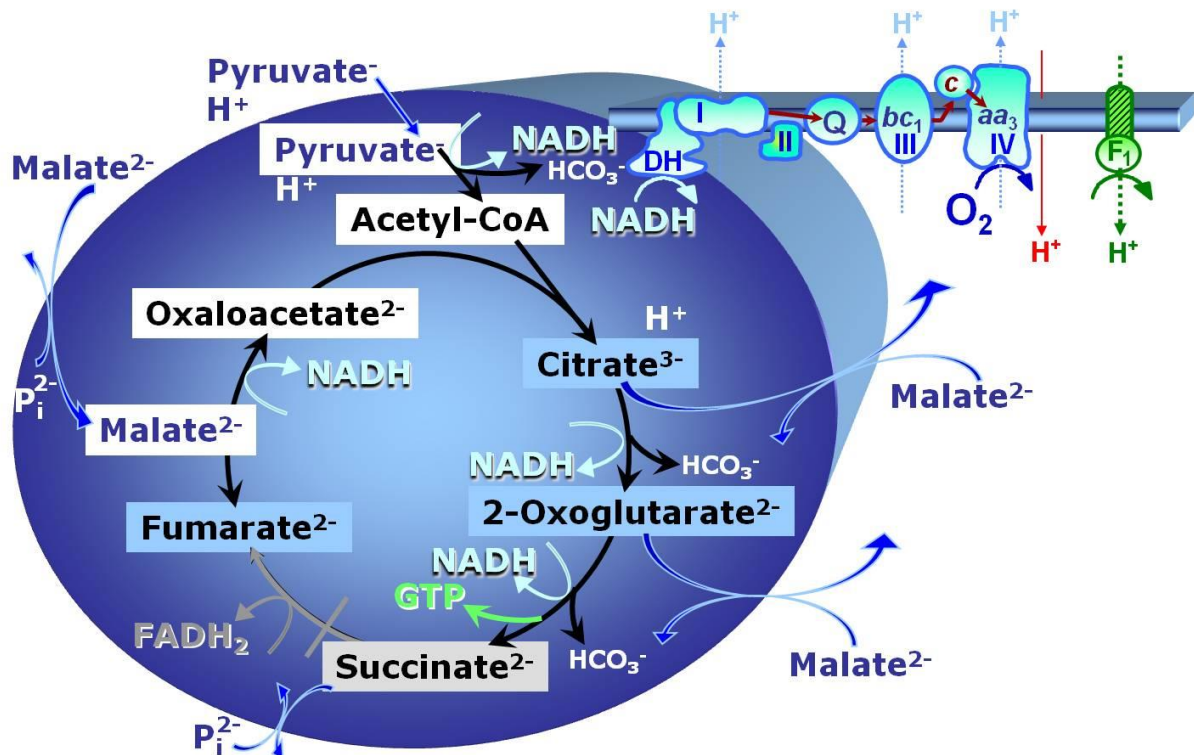


Figure 4.3. Pyruvate & malate, PM. Oxidative decarboxylation of pyruvate is catalyzed by pyruvate dehydrogenase (PDH) and yields acetyl-CoA. Several dehydrogenases catalyze the formation of NADH, the substrate of Complex I. Malate dehydrogenase (MDH) located in the mitochondrial matrix oxidizes malate to oxaloacetate. Condensation of oxaloacetate with acetyl-CoA yields citrate (citrate synthase CS). 2-oxoglutarate (α -ketoglutarate) is formed from isocitrate (isocitrate dehydrogenase IDH). Cataplerotic loss of TCA-cycle intermediates minimizes formation and further oxidation of succinate, thus diminishing the contribution of succinate-CoA ligase to substrate-level phosphorylation and production of ATP or GTP, and preventing electron flow through Complex II.

The pyruvate carrier (pyruvic acid, $C_3H_4O_3$)

The monocarboxylic acid pyruvate⁻ is exchanged electroneutrally for OH⁻ by the pyruvate carrier. H⁺/anion symport is equivalent to OH⁻/anion antiport. Above a pyruvate concentration of 5 mM (compare Table B1), pyruvate transport across the membrane is partially noncarrier-mediated due to a significant concentration of the non-dissociated acid. Hydroxycinnamate is an inhibitor of the pyruvate carrier, which cannot inhibit respiration above 10 mM pyruvate.

Pyruvate alone yields only 2.1 % of OXPHOS capacity with PM in rat skeletal muscle mitochondria. Pyruvate carboxylase synthesizes oxaloacetate from pyruvate and CO₂ as an anaplerotic reaction in the mitochondrial matrix of the liver and kidney of higher animals. Upon addition of malate, the malate-fumarate equilibrium is catalyzed by fumarase with an equilibrium ratio of malate to fumarate of 4.1. High added malate concentrations equilibrate with fumarate, which inhibits flux from succinate to fumarate in addition to any inhibition of succinate dehydrogenase by oxaloacetate. A kinetically significant mitochondrial succinate concentration can hardly be formed: Due to the high activity of the tricarboxylate carrier in liver mitochondria, citrate is lost from the mitochondria in exchange for malate, before it can be oxidized. In addition, 2-oxoglutarate and succinate are lost into the medium. Taken together, these are the arguments of using

a high malate concentration (2 mM; compare Table B1), particularly in studies of P_{i}/O_2 ratios of the N-pathway. Then Complex II is not or only to a small extent involved in respiration on pyruvate & malate (PM) in mitochondrial preparations (Figure 4.3). Malonate may be added to inhibit the succinate-fumarate reaction, which exerts only a minor effect on liver mitochondrial respiration.

On the other hand, cataplerotic efflux of 2-oxoglutarate can be reversed by using this intermediate as a NADH-linked fuel substrate. Reconstitution of TCA-cycle function by this approach is complicated due to competitive inhibition of Complex II by 2-oxoglutarate.

4.3. Glutamate, G

Glutamate derived from hydrolyzation of glutamine is an important aerobic substrate in cultured cells.

Carriers for glutamate (glutamic acid, $C_5H_9NO_4$)

1. The glutamate-aspartate carrier catalyzes the electrogenic antiport of glutamate $^- + H^+$ for aspartate $^-$. It is an important component of the malate-aspartate shuttle in many mitochondria. Due to the symport of glutamate $^- + H^+$, the glutamate-aspartate antiport is not electroneutral and may be impaired by uncoupling. Aminooxyacetate is an inhibitor of the glutamate-aspartate carrier.
2. The electroneutral glutamate $^- / OH^-$ exchanger is present in liver and kidney mitochondria.

In human skeletal muscle mitochondria, OXPHOS capacity with glutamate alone (Figure 4.4) is 50 % to 85 % of respiration with glutamate & malate (Figure 4.6). Accumulation of fumarate inhibits succinate dehydrogenase and glutamate dehydrogenase.

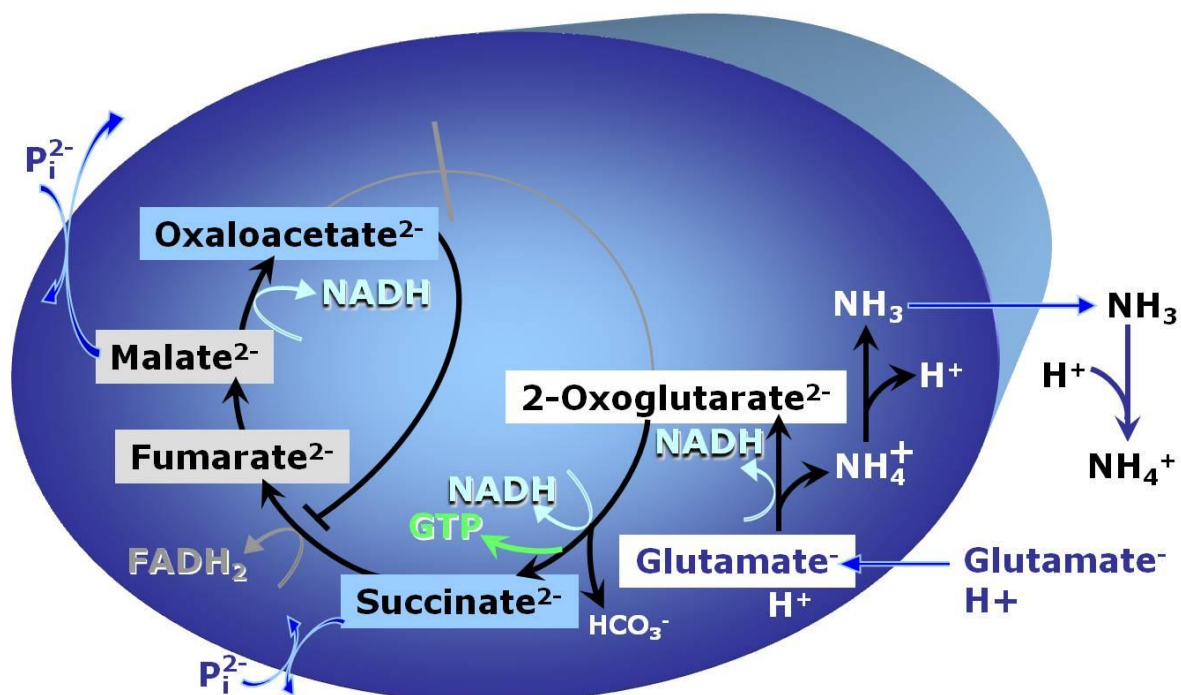


Figure 4.4. Glutamate, G as the sole fuel substrate is transported by the electroneutral glutamate $^- / OH^-$ exchanger, and is oxidized via glutamate dehydrogenase (GDH) in the mitochondrial matrix. Ammonia can pass freely through the mitochondrial membrane. Compare Figure 4.5.

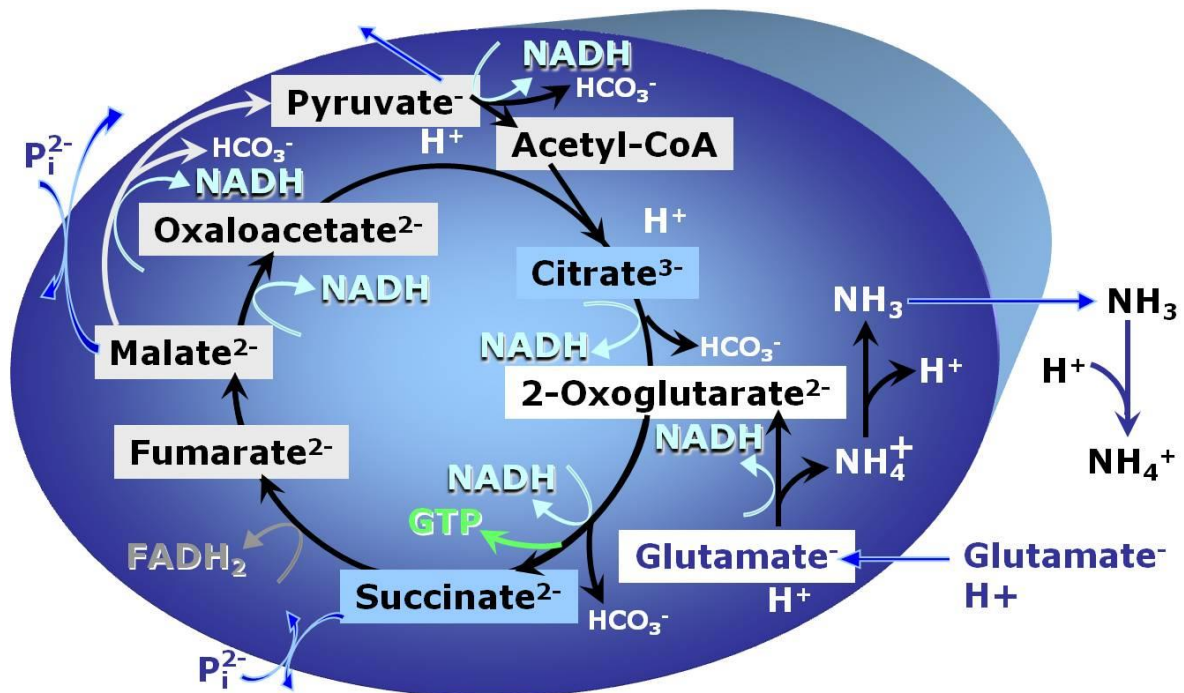


Figure 4.5. Glutamate, G, and mt-malic enzyme. Mitochondrial glutamate dehydrogenase is particularly active in astrocytes, preventing glutamate induced neurotoxicity. mtNAD-malic enzyme supports an anaplerotic pathway when carbohydrate is limiting.

Glutamine and glutamate in combination with mt-malic enzyme constitute a powerful anaplerotic system supporting biosynthesis and cell growth (Figure 4.5).

4.4. Glutamate & Malate, GM

In human skeletal muscle mitochondria, respiration with glutamate & malate (Figure 4.6) in the presence of ADP (GM_P) is identical or 10 % higher than with pyruvate & malate (PM_P). These results on isolated mitochondria agree with permeabilized fibers, although there are reports on respiratory capacity for PM_P being 16 % to 25 % higher than for GM_P. In fibroblasts, GM_P supports a higher respiratory flux than PM_P.

The PM_P/GM_P flux ratio shifts from <1 in white muscle to >1 in red skeletal muscle fibers from turkey. In rat heart mitochondria, respiration is 33 % higher for GM_P compared to PM_P, and OXPHOS with succinate and rotenone is marginally higher than with GM. 2-Oxoglutarate efflux with GM is limited at low malate concentrations, and is half-maximal at 0.36 mM. Glutamate & malate support a higher OXPHOS respiration (GM_P) than PM_P in rat liver mitochondria. The PM_P/GM_P ratio is strongly temperature dependent in permeabilized mouse heart fibers. Taken together, this suggests that a critical evaluation is required for interpreting CI-linked respiration on a particular N-type substrate in terms of limitation by CI.

Uncoupling stimulates respiration above OXPHOS capacity in human skeletal and cardiac muscle mitochondria, whereas respiration is not under the control of the phosphorylation system in mouse skeletal and cardiac muscle and red fiber type pigeon breast muscle mitochondria. GM_P is severely limited by the phosphorylation system in fibroblasts, since uncoupling exerts a strong stimulation above maximally ADP-stimulated respiration (compare Figure 6.12).

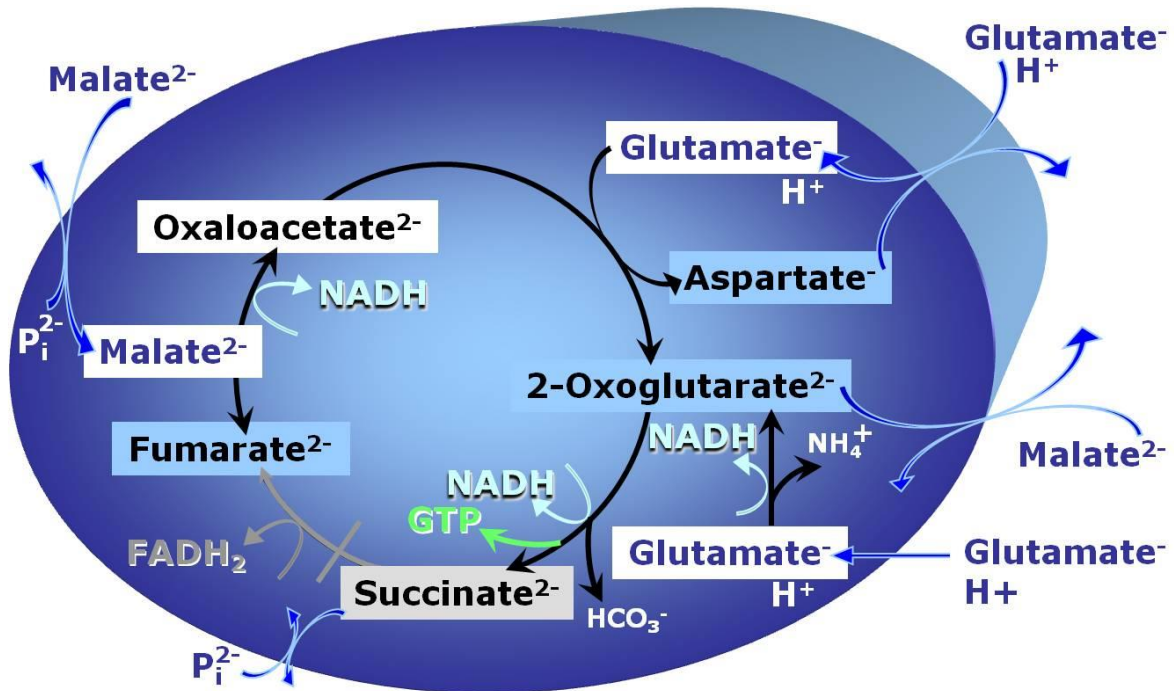


Figure 4.6. Glutamate & malate, GM. When glutamate & malate are added to mitochondrial preparations, glutamate and transaminase are responsible for the metabolism of oxaloacetate, comparable to the metabolism with acetyl-CoA and citrate synthase (Figure 4.3).

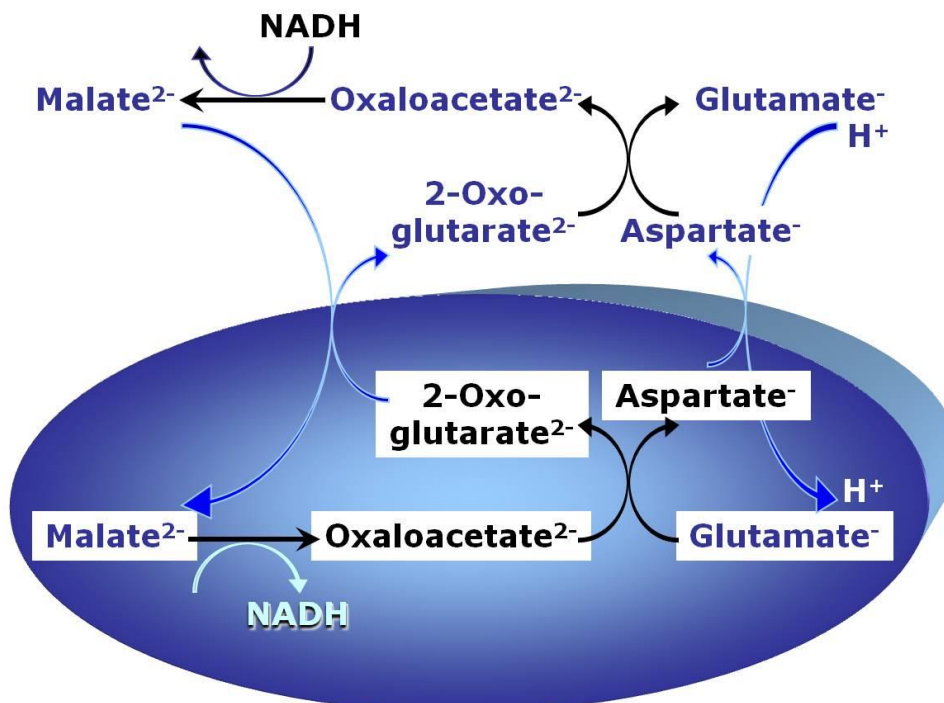


Figure 4.7. The malate-aspartate shuttle involves the glutamate-aspartate carrier and the 2-oxoglutarate carrier exchanging malate²⁻ for 2-oxoglutarate²⁻. Cytosolic and mitochondrial malate dehydrogenase and transaminase complete the shuttle for the transport of cytosolic NADH into the mitochondrial matrix. It is most important in heart, liver and kidney.

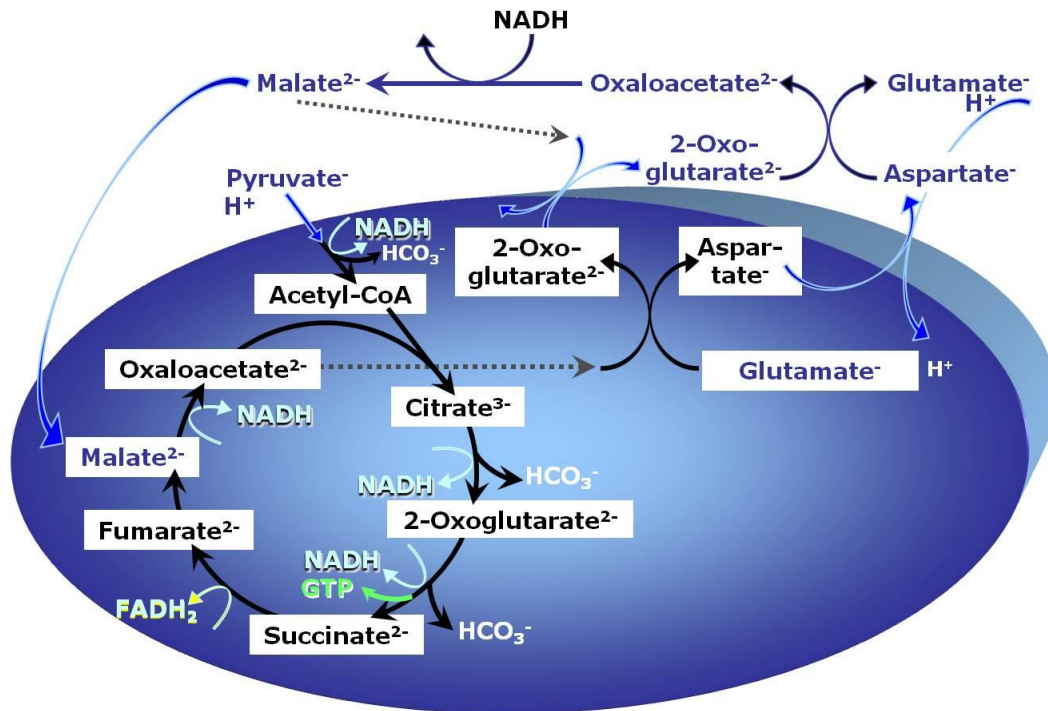


Figure 4.8. Malate-aspartate shuttle in the living cell. Cytosolic NADH is utilized for respiration at the cost of H⁺ transported along the electrochemical gradient back into the mitochondrial matrix. This reduces the effective P_o/O ratio.

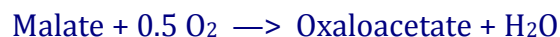
The overall reaction stoichiometry of the malate-aspartate shuttle is (Figure 4.7):



After transamination in the cytosol (Figure 4.8),



The net reaction is,

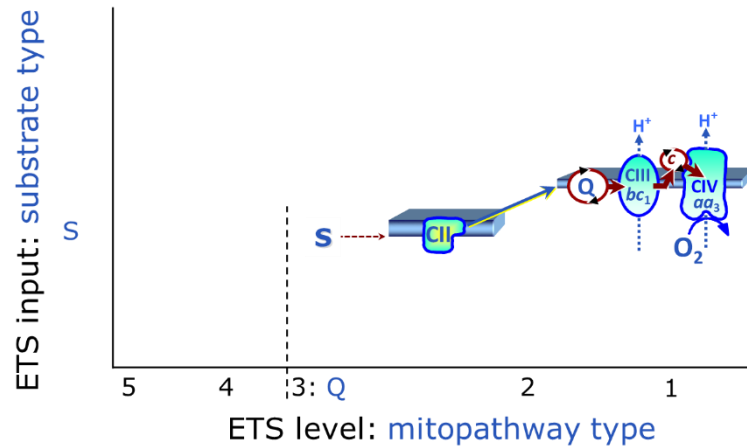


At high cardiac workload, the 2-oxoglutarate-malate transporter cannot effectively compete for the same substrate of the 2-oxoglutarate dehydrogenase. This limits the activity of the malate-aspartate shuttle and transfer of cytosolic NADH into the mitochondria. Then lactate is produced despite sufficient oxygen availability, when the cytosolic glutamate pool is diminished and cytosolic reoxidation of NADH is activated. Regulation of cytosolic NADH levels by the glutamate-aspartate carrier is implicated in glucose-stimulated insulin secretion in beta-cells.

Electron entry from succinate S through CII into the Q-junction is integral to the TCA cycle in the living cell, but plays no or minor roles in mt-preparations with NADH-linked substrate supply. Specific pathway control states are designed for studying the S-pathway alone (Chapter 5; including additional separate electron entries into Q) or in combination with the N-pathway for reconstituting the convergent pathway architecture of the ETS from CHNO-fuel substrates through the Q-junction into the downstream ET highway (Chapter 6).

Chapter 5.

S-pathway through Complex CII, F-pathway through electron-transferring flavoprotein, Gp-pathway through glycerophosphate dehydrogenase



Section		Page
5.1.	Succinate and rotenone, S(Rot)	48
5.2.	Succinate, S	49
5.3.	Glycerophosphate, Gp	50
5.4.	Electron-transferring flavoprotein, CETF	51

Complex II (CII) is the only membrane-bound enzyme in the tricarboxylic acid (TCA) cycle and is part of the electron transfer system. The flavoprotein succinate dehydrogenase (SDH) is the largest polypeptide of CII, located on the matrix face of the mt-inner membrane. The substrate of CII is succinate, which is oxidized forming fumarate while reducing flavin adenine dinucleotide FAD to FADH₂, with further electron transfer to the quinone pool. Whereas reduced NADH is a *substrate* of Complex I linked to dehydrogenases of the TCA cycle and mt-matrix *upstream* of CI, reduced FADH₂ is a *product* of Complex II with *downstream* electron flow from CII to Q. NADH and succinate (not FADH₂) are the comparable substrates of CI and CII. Malonate is a competitive inhibitor of CII, and phenylsuccinate is a competitive inhibitor of succinate transport.

5.1. Succinate-pathway: succinate and rotenone, S(Rot)

Succinate, S(Rot), supports electron flux into the Q-junction through CII. After inhibition of CI by rotenone, the NADH-linked dehydrogenases become inhibited by the redox shift from NAD⁺ to NADH (Figure 5.1). Succinate dehydrogenase is activated by succinate and ATP, which explains in part the time-dependent increase of respiration in some isolated mitochondria after addition of rotenone (added first), succinate and ADP.

Carrier for succinate (succinic acid, C₄H₆O₄)

The dicarboxylate carrier catalyzes the electroneutral exchange of succinate²⁻ for HPO₄²⁻. Accumulation of malate formed from fumarate is prevented either by further oxidation in the TCA cycle or by antiport of malate and inorganic phosphate.

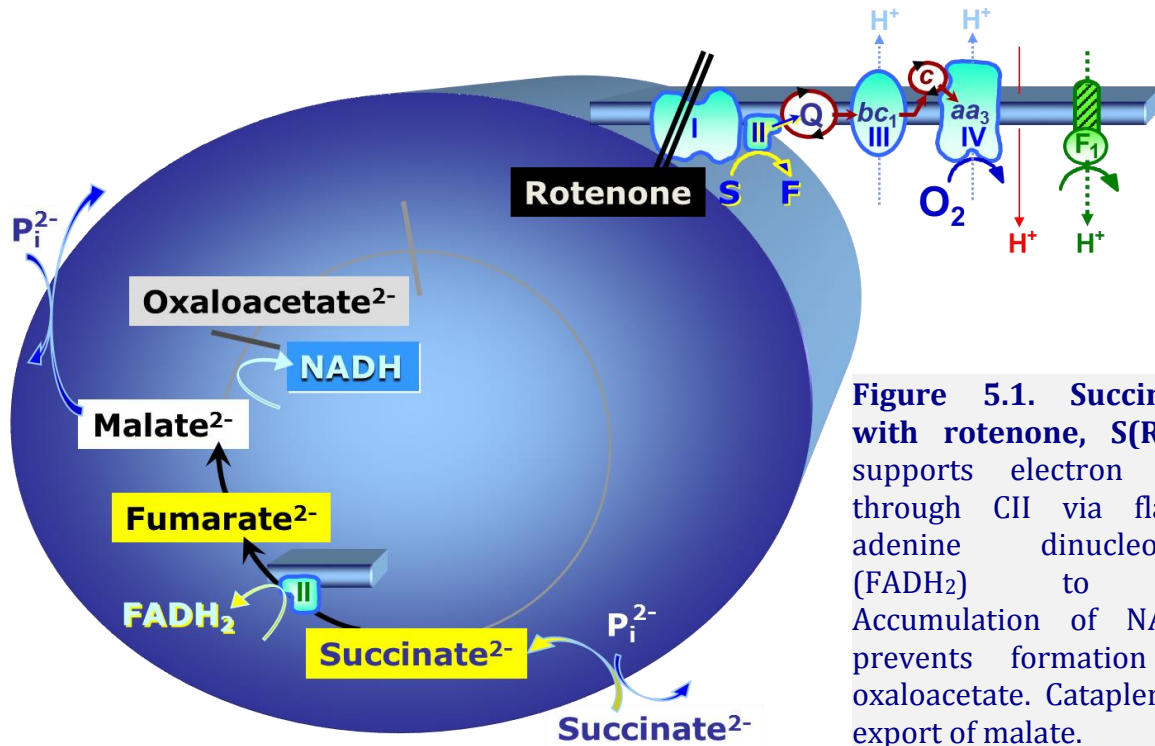


Figure 5.1. Succinate with rotenone, S(Rot), supports electron flux through CII via flavin adenine dinucleotide (FADH₂) to Q. Accumulation of NADH prevents formation of oxaloacetate. Cataplerotic export of malate.

5.2. Succinate-pathway: succinate without rotenone, S

When succinate is added without rotenone (Figure 5.2), oxaloacetate is formed from malate by the action of malate dehydrogenase. Oxaloacetate accumulates and is more potent even at small concentration as a competitive inhibitor of succinate dehydrogenase than malonate. Reverse electron transfer from CII to CI stimulates production of reactive oxygen species under these conditions to extremely high, non-physiological

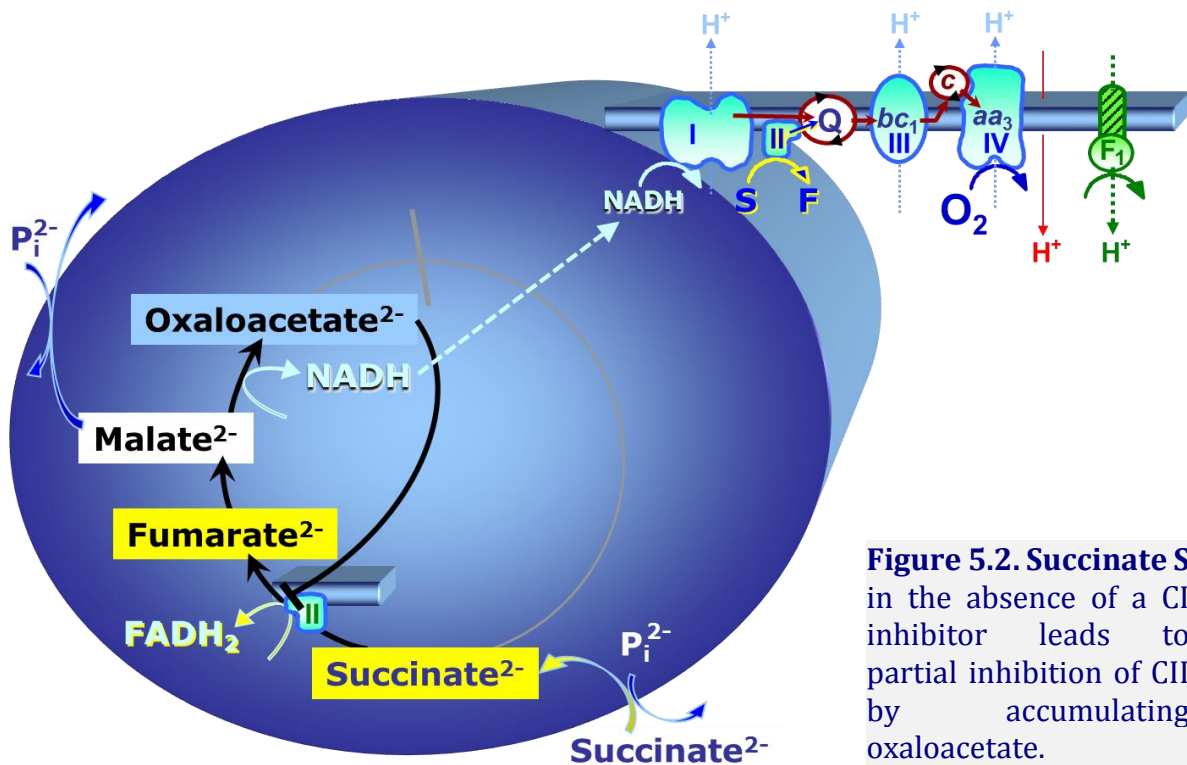


Figure 5.2. Succinate S in the absence of a CI inhibitor leads to partial inhibition of CII by accumulating oxaloacetate.

levels. Addition of malate reduces superoxide production with succinate, due to a shift in the redox state and inhibition of CII by oxaloacetate.

OXPHOS capacity S_P with succinate alone is 30-40 % lower than $S(\text{Rot})_P$ with succinate and rotenone in human and rat skeletal muscle mitochondria, due to inhibition of succinate dehydrogenase by accumulating oxaloacetate. This inhibition is similar in mammalian liver, where >90 % of malic enzyme is cytosolic, but is prevented by high activities of mt-malic enzyme.

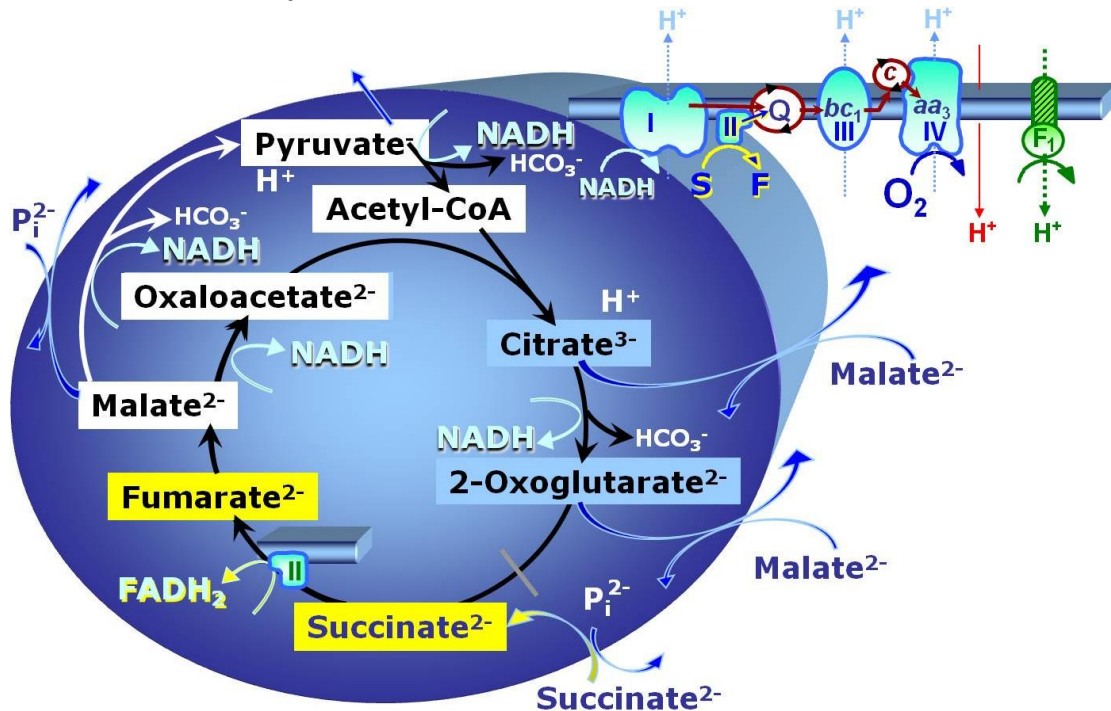


Figure 5.3. Succinate S and mtME. mt-Malic enzyme (mtME) catalyzes the formation of pyruvate from malate. Acetyl-CoA from pyruvate (PDH) is then available for removal of oxaloacetate through citrate synthase, thus preventing or reducing inhibition of succinate dehydrogenase by oxaloacetate.

Conditions with succinate as the sole substrate are different if mt-malic enzyme plays a significant role, as is the case in proliferating cells and many invertebrate mitochondria. $P \gg O_2$ ratios in the S-pathway with and without rotenone provide an indication of the extent to which CI is stimulated by NADH, which is generated through the anaplerotic malate-pathway in parallel with formation and removal of oxaloacetate through MDH and CS. The exported malate may be too dilute for an active antiport against citrate and 2-oxoglutarate (Figure 5.3; compare malate with mtME in Figure 4.2). S-pathway supported generation of NADH in the presence of mtME activity counteracts reverse CII to CI electron transfer and thus plays an important role in the regulation of ROS production under these experimental conditions.

5.3. Glycerophosphate-pathway, Gp

Glycerophosphate oxidation (Figure 5.4) is 10-fold higher in rabbit gracilis mitochondria (fast-twitch white muscle; 99 % type IIb) compared to soleus (slow-twitch red muscle; 98 % type I). Activity is comparatively low in human vastus lateralis. Gp is an important substrate for respiration in brown adipose tissue mitochondria.

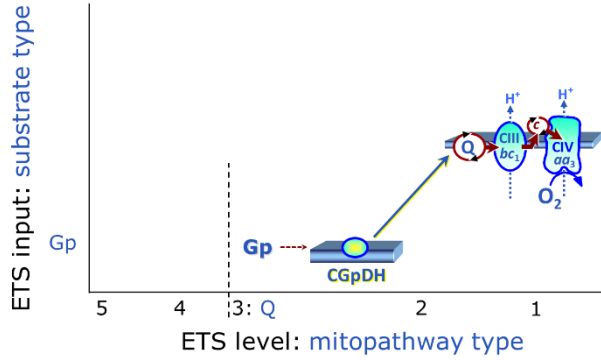
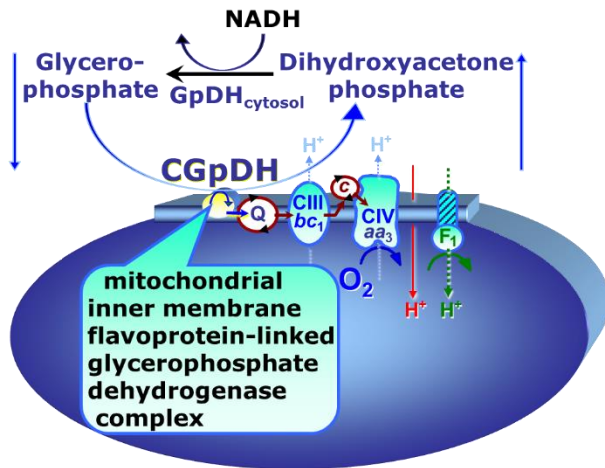


Figure 5.4. The glycerophosphate shuttle represents an important pathway, particularly in liver, of making cytoplasmic NADH available for mitochondrial oxidative phosphorylation. Cytoplasmic NADH reacts with dihydroxyacetone phosphate catalyzed by cytoplasmic glycerophosphate dehydrogenase. On the outer face of the mtIM, mitochondrial glycerophosphate dehydrogenase oxidizes glycerophosphate back to dihydroxyacetone phosphate, a reaction not generating NADH but reducing a flavin prosthetic group. The reduced flavoprotein donates reducing equivalents to the ETS at the level of Q.

NADH available for mitochondrial oxidative phosphorylation. Cytoplasmic NADH reacts with dihydroxyacetone phosphate catalyzed by cytoplasmic glycerophosphate dehydrogenase. On the outer face of the mtIM, mitochondrial glycerophosphate dehydrogenase oxidizes glycerophosphate back to dihydroxyacetone phosphate, a reaction not generating NADH but reducing a flavin prosthetic group. The reduced flavoprotein donates reducing equivalents to the ETS at the level of Q.

5.4. Fatty acid oxidation and the electron-transferring flavoprotein complex, F

Electron-transferring flavoprotein Complex (ETF) is located on the matrix face of the mtIM, and supplies electrons from fatty acid β -oxidation (FAO) to Q (Figure 5.5). FAO cannot proceed without a substrate combination of fatty acids & malate (0.1 mM), except with formation of ketone bodies in the liver. Fatty acids are split stepwise into two-carbon fragments forming acetyl-CoA, which enters the TCA cycle by condensation with oxaloacetate (CS reaction). As outlined in Chapter 1.8, FADH₂ and NADH formed in FAO imply convergent electron transfer into the Q-junction through ETF and CI (Figure 5.5). Inhibition of CI blocks FAO completely.

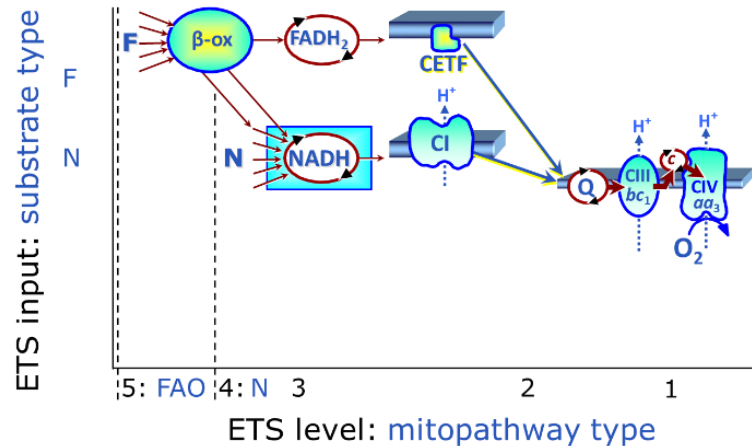
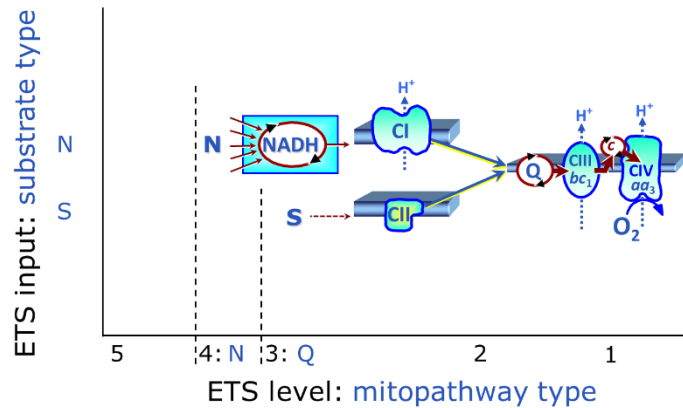


Figure 5.5. F-pathway in fatty acid oxidation, FAO.

Fatty acids (short-chain with 1–6, medium-chain with 7–12, long-chain with >12 carbon atoms) are activated by fatty acyl-CoA synthases (thiokinases) in the cytosol. The mtOM-enzyme carnitine palmitoyltransferase 1 (CPT-1) generates an acyl-carnitine intermediate for transport into the mt-matrix. Octanoate but not palmitate (eight- and 16-carbon saturated fatty acids) may pass the mt-membranes, but both are frequently supplied to mt-preparations in the activated form of octanoylcarnitine or palmitoylcarnitine.

Chapter 6.

Convergent electron transfer at the Q-junction: NS-pathway through Complexes CI & CII and additive effect of substrate combinations



..the O₂ uptake of intact cells represents the global result of the activity of several respiratory systems.

Keilin D (1929) Cytochrome and respiratory enzymes. Proc R Soc London Ser B 104:206-52.

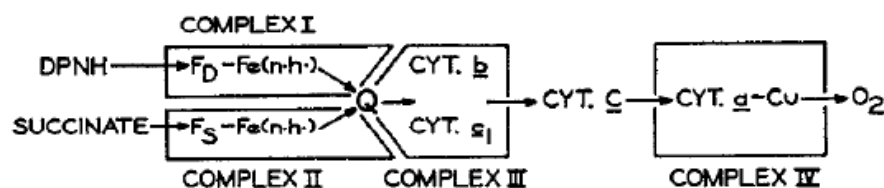
Section		Page
6.1.	Electron transfer system and ET chain: ETS and ETC	52
6.2.	Historical perspectives	54
6.3.	Pyruvate & Glutamate & Malate, PGM	57
6.4.	Pyruvate & Malate & Succinate, PMS	57
6.5.	Glutamate & Malate & Succinate, GMS.....	58
6.6.	Pyruvate & Glutamate & Malate & Succinate, PGMS	59
6.7.	Additive effect of Gp and FAO	60
6.8.	N/S flux ratios	60
6.9.	Mitochondrial pathways and coupling control	61
6.10.	Implications	65

6.1. Electron transfer-system and ET chain: ETS and ETC

The term ‘electron transport chain’ (ETC) is a misnomer. Understanding mitochondrial respiratory control has suffered greatly from this inappropriate terminology, although textbooks using the term ETC make it sufficiently clear that the electron transfer system is not arranged as a chain: the ‘ETC’ is in fact not a simple chain but an arrangement of electron transfer complexes in a non-linear, convergent electron transfer system (ETS). The convergent metabolic architecture at the Q-junction and its functional implication – the additive effect of NS-substrate combinations – were described already 50 to 60 years ago (Hatefi et al 1962; Gutman et al 1971; Figure 6.1).

Figure 6.1. Electron transfer system ETS:

The four primary Complexes and their arrangement in the electron transfer system.



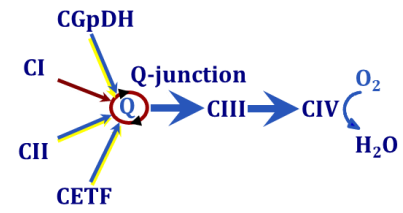
DPNH is NADH; from Hatefi et al (1962) Studies on the electron transfer system XLII. Reconstitution of the electron transfer system. J Biol Chem 237:2661-9.

Figure 6.2. ETC vs ETS. Electron transfer chain ETC (linear) versus electron transfer system ETS (convergent). CI to CIV, Complex I to IV; CGpDH, glycerophosphate dehydrogenase Complex; CETF, electron-transferring flavoprotein Complex. Convergent electron supply exerts an additive effect on ET capacity. Then electron gating – closing electron entries into Q (ETS to ETC) – limits flux upstream.

linear ETC



convergent ETS



Defining the electron transfer chain as being comprised of four respiratory Complexes has conceptual weaknesses. (1) In addition to Complexes CI and CII, further Complexes of mitochondrial electron transfer are involved in electron transfer to Q and CIII – for example, the Complexes glycerophosphate dehydrogenase CGpDH and electron-transferring flavoprotein CETF (Figure 6.2). (2) The term ‘chain’ suggests a linear sequence, whereas the functional structure of the electron transfer system can only be understood by recognizing the convergence of electron flow at the NADH- and Q-junctions, followed by electron transfer through CIII and CIV to O₂ (Figure 6.3).

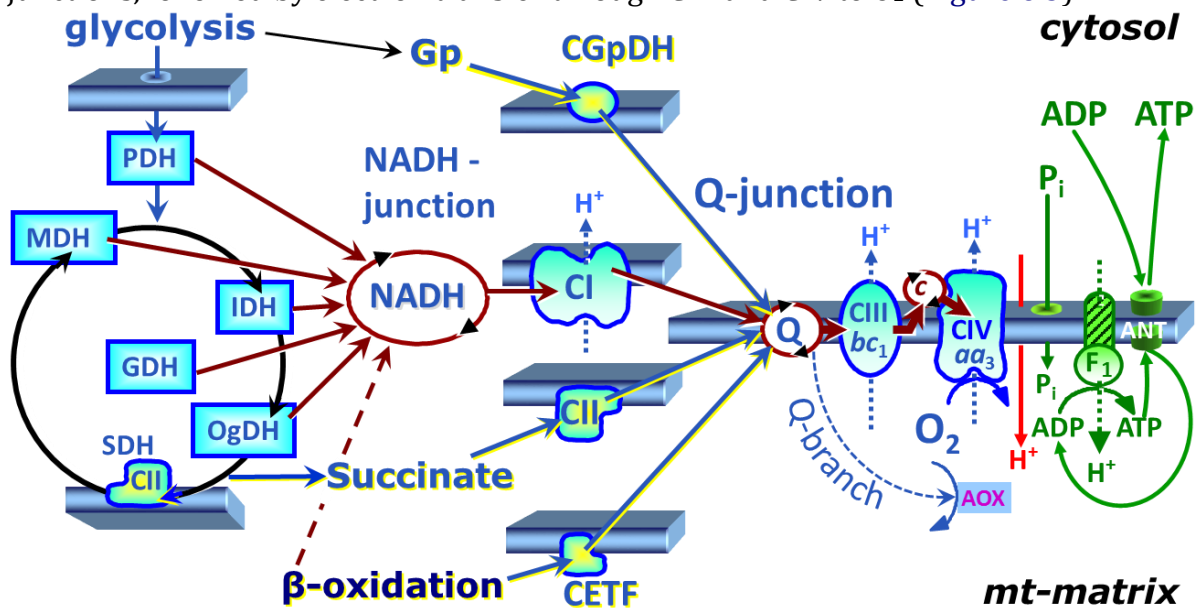


Figure 6.3. Convergent electron transfer at the NADH-junction and Q-junction. Dehydrogenases are PDH, pyruvate DH; MDH, malate DH; IDH, isocitrate DH; OgdH, 2-oxoglutarate DH; SDH, succinate DH – yielding a NADH:succinate ratio of 4:1 in the full TCA cycle. GDH, mt-glutamate DH. Q-branch to alternative oxidase AOX without H⁺ translocation, particularly in plant mitochondria. NADH- and Q-redox states reflect the pathway- and coupling states, the balance between upstream and downstream electron flow capacities, and flux control by the phosphorylation system (*E-P* control efficiency).

Electrons flow to oxygen from either Complex CI with three coupling sites in the N-pathway, or from Complex CII and other flavoproteins, providing multiple entries into the Q-cycle with two coupling sites downstream. Branching to AOX reduces mechanistic coupling. In the complete TCA cycle in the living cell with influx of pyruvate, electron flow into the Q-junction converges according to a NADH:succinate ratio of 4:1 (Figure 6.3). Advanced SUIT protocols are designed for reconstitution of TCA cycle function and sequential separation of segments of mitochondrial pathways for OXPHOS analysis.

6.2. Historical perspectives of protocols with substrate combinations: ETS concept versus ETC paradigm

Convergent NS-electron transfer is a complexity to be avoided for analyzing site-specific $H^+ : e$ and $P : O$ ratios (Figure 6.4). For this aim, segments of the convergent electron transfer system are separated into linear thermodynamic cascades, forming distinct electron transfer *chains*, using either NADH-linked substrates (N-pathway) or the classical succinate-rotenone combination (S-pathway). The experimental separation of convergent electron transfer by electron gating was common to the extent of establishing an 'ETC paradigm of bioenergetics'. The analytical approach pioneered by Chance and Williams (1955) has then been applied to the functional diagnosis of OXPHOS. This application, however, requires consideration of the ETS concept.

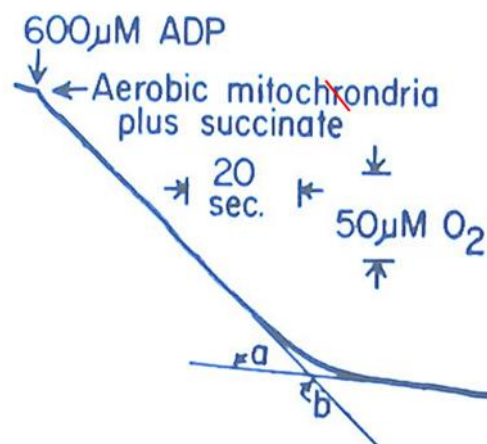


Figure 6.4. Recording of the kinetics of initiation and cessation of rapid respiration in rat liver mitochondria. Chance and Williams (1955 I; Fig. 5A).

6.2.1. Scattered observations with substrate combinations

It is difficult to trace the history of observations on mitochondrial respiration with specific substrate combinations that lead to convergent flow at the Q-junction (Hatefi et al 1962). The reason for this difficulty is related to the apparent lack of an explicit conceptual framework (Torres et al 1988), rendering valuable results scattered as observations without theoretical interpretation.

(1) The group of Alberto Boveris reports OXPHOS capacities P with glutamate & succinate (GS_P) which is 1.9-fold higher than glutamate & malate (GM_P) in rat heart mitochondria (Costa et al 1988). While no values were reported for S_P in heart, liver mitochondria were studied with succinate and rotenone, $S(Rot)_P$, and GM_P . The same group measured OXPHOS capacities GS_P and GM_P in rat muscle and liver mitochondria: The GM_P/GS_P flux ratios are 0.7 to 0.8 in liver (Llesuy et al 1994). No conclusion on an additive effect of the NS-pathway is possible, since succinate(rotenone) alone supports a higher flux than glutamate & malate in liver mitochondria and permeabilized liver tissue. In fact, the $GM_P/S(Rot)_P$ flux ratio is 0.6 (Costa et al 1988). Similarly, the GM_P/GS_P flux ratios of 0.5 and 0.8 for rat heart and skeletal muscle mitochondria cannot be interpreted without direct comparison to $S(Rot)_P$.

(2) Jackman and Willis (1996) report an additive effect of multiple substrates on flux: The sum of OXPHOS capacities with glycerophosphate (Gp_P) and pyruvate & malate (PM_P) adds up to respiration measured in state $PMGp_P$. The physiological importance of this additive effect of convergent electron flow can be evaluated only with information on the additive succinate effect, since addition of Gp to NS may exert a lower stimulatory effect on respiration from PMS_P to $PMSGp_P$.

(3) Kunz et al (2000) report a GM_P/GMS_P ratio of 0.7 in permeabilized human muscle fibers. The apparent excess capacity of cytochrome *c* oxidase is lower with reference to the higher flux GMS_P , compared to the lower GM_P reference flux. This finding was

interpreted by Kunz et al (2000) as a salient feature of permeabilized fibers (or living cells) in contrast to isolated mitochondria, rather than the actual consequence of the different pathway control states (Figure 1.11). A less misguided interpretation might have been obtained with reference to the data on mitochondria isolated from rat muscle (Llesuy et al 1994), and to the GM_P/GS_P ratio of 0.5 and 0.7 for isolated mitochondria from pigeon skeletal muscle and human vastus lateralis (Rasmussen, Rasmussen 1997; 2000).

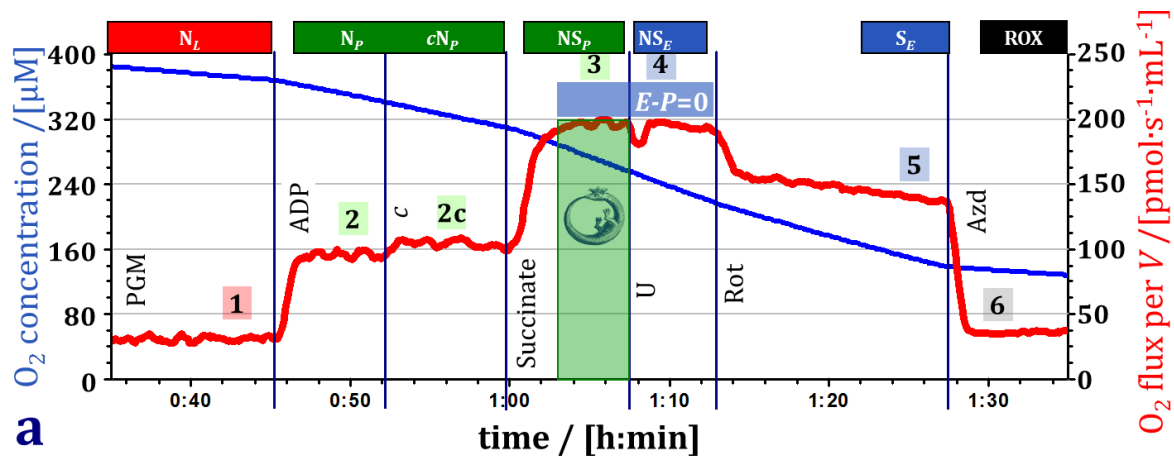
6.2.2. Maximum flux: functional assays and noncoupled cells

(4) Hans and Ulla Rasmussen (1997; 2000) developed the concept of '*functional assays of particular enzymes*' by using various substrates and substrate combinations in respiratory studies of mitochondria isolated from skeletal muscle. A functional assay is based on the stimulation of flux to a maximum, which then is limited by a particular enzyme or pathway segment. Their concept on the application of substrate combinations (glutamate & succinate) has been largely ignored in the literature, perhaps on the basis of the argument that flux control is distributed over several enzymes along a pathway. Limitation by a single enzyme, which then has a flux control coefficient of 1.0, is a rare event, even under conditions of a 'functional assay'. Importantly, however, the 1.4- or even 2.0-fold higher GS_P flux compared to the conventional State 3 paradigm based on PM_P , GM_P or $S(\text{Rot})_P$, raises the critical issue of the physiologically appropriate reference state for measuring flux control coefficients and excess capacities of a particular enzyme such as cytochrome *c* oxidase (Figure 1.11). For general consideration, Rasmussen et al (2001) state: "*The tricarboxylic acid cycle cannot be established in optimal, cyclic operation with isolated mitochondria, but parts of the in vivo reaction scheme may be realized in experiments with substrate combinations*".

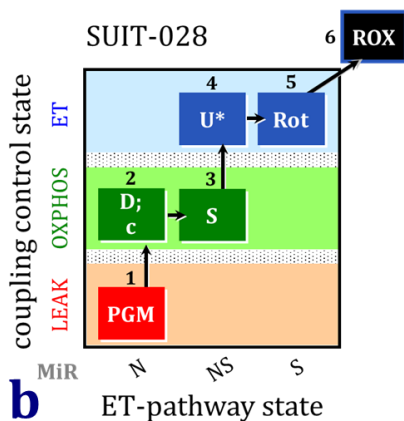
(5) Attardi and colleagues dismiss isolated mitochondria as a suitable model for respiratory studies, on the basis of the fact that 'State 3' in permeabilized cells (with NADH-linked substrates) is low compared to endogenous respiration of living cells, which then "*raises the critical issue of how accurately the data obtained with isolated mitochondria reflect the in vivo situation*" (Villani, Attardi 1997). Since low OXPHOS capacity may be related to artefacts in the isolation of mitochondria, the 'ETC paradigm of State 3' was converted into a paradigm of maximum flux, obtained by studying living cells in the noncoupled state (bold added): '*KCN titration assays, carried out on **intact uncoupled** cells, have clearly shown that the COX capacity is in low excess (16-40 %) with respect to that required to support the endogenous respiration rate*' (Villani et al 1998). As shown in Figure 6.12c, it is rather an issue of (1) physiological substrate combinations used with isolated mitochondria and permeabilized cells, and (2) a reliance on the three-compartment model of OXPHOS (Chapter 2), when comparing OXPHOS capacity in mitochondrial preparations with ET capacity in living cells. Uncoupling eliminates kinetic flux control by the phosphorylation system, hence only ET capacity in mt-preparations is comparable with ET capacity in living cells, unless the phosphorylation system exerts no control over coupled respiration.

6.2.3. Mitochondrial physiology and mitochondrial pathways

(6) A novel perspective of mitochondrial physiology and respiratory control by simultaneous supply of various fuel substrates emerged from a series of studies based on high-resolution respirometry. Substrate-uncoupler-inhibitor-titration (SUIT) protocols for real-time OXPHOS analysis (Figures 6.5, 6.12-6.15) are based on metabolic analysis of convergent pathways comprising the mitochondrial electron transfer system.



a



b

Figure 6.5. Substrate-uncoupler-inhibitor titration protocol for analysis of convergent NS-electron flow. Permeabilized mouse skeletal muscle fibers; O2k 2 mL, mitochondrial respiration medium MiR05, 37 °C. PGM pyruvate & glutamate & malate, c cytochrome c, U FCCP, Rot rotenone, Azd azide. **(a)** Blue plot: O₂ concentration; red plot: O₂ flux J_{V,O_2} . S stimulates flux two-fold, $(N/NS)_P=0.5$. The phosphorylation system is not limiting with zero *E-P* excess capacity (IOC39). **(b)** Coupling/pathway control diagram: 1PGM;2D;c;3S;4U;5Rot;6ROX.

A rapidly growing number of studies on various tissues and cells points to the importance of the additive effect of substrate combinations on OXPHOS capacity (Gnaiger 2009). Convergent electron flow to the Q-junction in the NS-pathway resolves discrepancies between living cells and mitochondria. This additive effect indicates a high downstream excess capacity of respiratory complexes including cytochrome *c* oxidase (CIV) over Complexes CI and CII. Convergent electron transfer yields a maximum (completely additive) effect on OXPHOS when CIII, CIV and the phosphorylation system exert a minimum (zero) flux control. Convergent electron transfer corresponds closely but not completely to the operation of the TCA cycle and mitochondrial substrate supply *in vivo*.

In isolated mitochondria and permeabilized cells or tissue, conventional measurements of State 3 with pyruvate & malate, glutamate & malate or succinate(rotenone) underestimate maximum OXPHOS capacity, since external succinate is required for reconstitution of the TCA cycle and stimulating convergent NS-electron flow under these conditions. By establishing the physiological reference state of maximum *coupled* respiration, convergent NS-electron flow provides the proper basis for (1) quantifying excess capacities and interpreting flux control by various enzymes such as cytochrome *c* oxidase and components such as the phosphorylation system, and (2) evaluation of specific enzymatic defects in mitochondrial respiratory physiology and pathology (Figure 1.11).

The concept on convergent electron transfer at the Q-junction (ETS) challenges conventional OXPHOS analysis based on the ETC terminology and a way of thinking about the mitochondrial ‘electron transfer chain’ (Figure 6.2).

6.3. Pyruvate & Glutamate & Malate, PGM

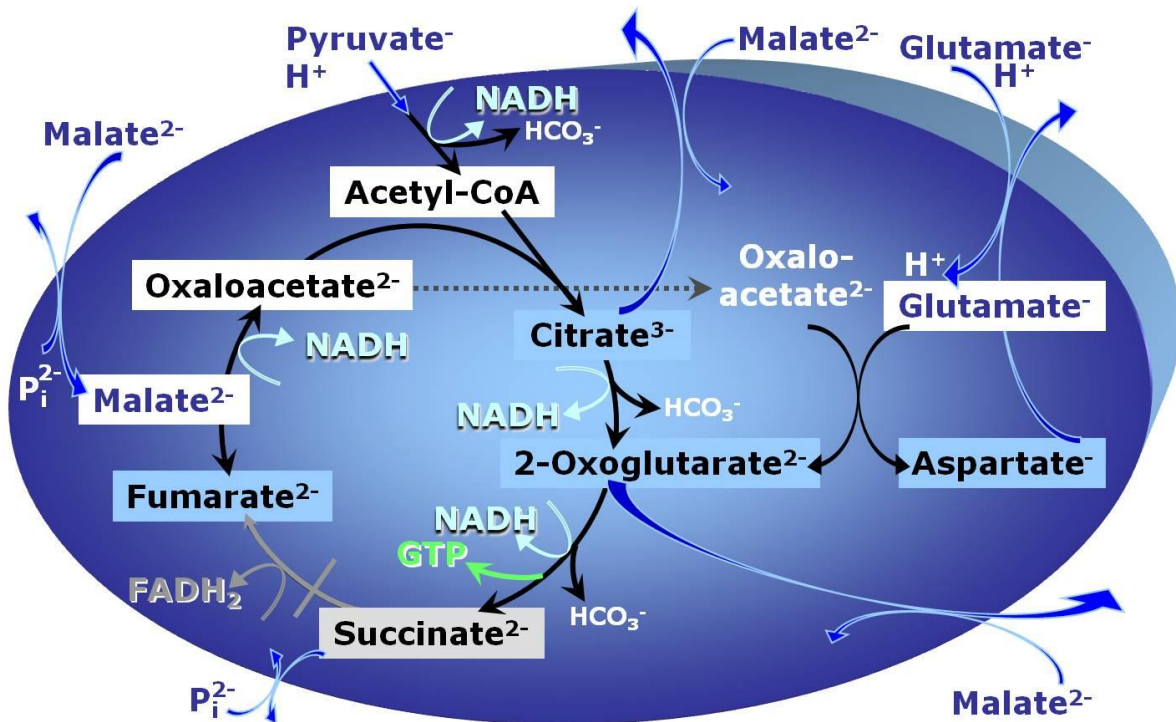


Figure 6.6. PGM. Respiratory capacity through Complex I may be limited by substrate supply. The addition of pyruvate and glutamate with malate (PGM) yields respiration in the presence of both pyruvate and the malate-aspartate shuttle.

Mitochondria from red muscle fibers (rabbit soleus) exhibit a 15 % higher flux in state PGM_P (Figure 6.6) compared to PM_P , whereas white muscle fiber mitochondria (rabbit gracilis) show a slight inhibition by glutamate added to PM_P (Jackman and Willis 1996). Paradoxically, a significant inhibition of flux by addition of pyruvate to GM_P was observed in horse skeletal muscle fibers (Votion et al 2012). Addition of glutamate to pyruvate & malate increases respiratory capacity in human skeletal muscle (Winkler-Stuck et al 2005; although PM_P is 16 % higher than GM_P). There is a strong additive effect of the PGM-substrate combination on respiratory capacity of mouse heart fibers (Lemieux et al 2006). High malate concentrations limit the flux through CII by product inhibition of SDH and thus support more specifically the N-pathway.

6.4. Pyruvate & Malate & Succinate, PMS

Reconstitution of TCA cycle function in isolated mitochondria or permeabilized tissues and cells requires addition of succinate to the conventional substrates for CI (Figure 6.7). The TCA cycle does not form a full functional loop when using the substrate combination pyruvate & malate, when citrate and 2-oxoglutarate are exchanged rapidly for malate by the tricarboxylate and 2-oxoglutarate carrier (Figure 4.3). Then succinate dehydrogenase activity is fully dependent on a high external succinate concentration.

Recent studies showed that S- and NS-OXPHOS capacities are inhibited partially by a concentration of 2 mM malate as applied in most SUIT protocols. This competitive inhibition is diminished at concentrations up to 50 mM succinate (Table B1).

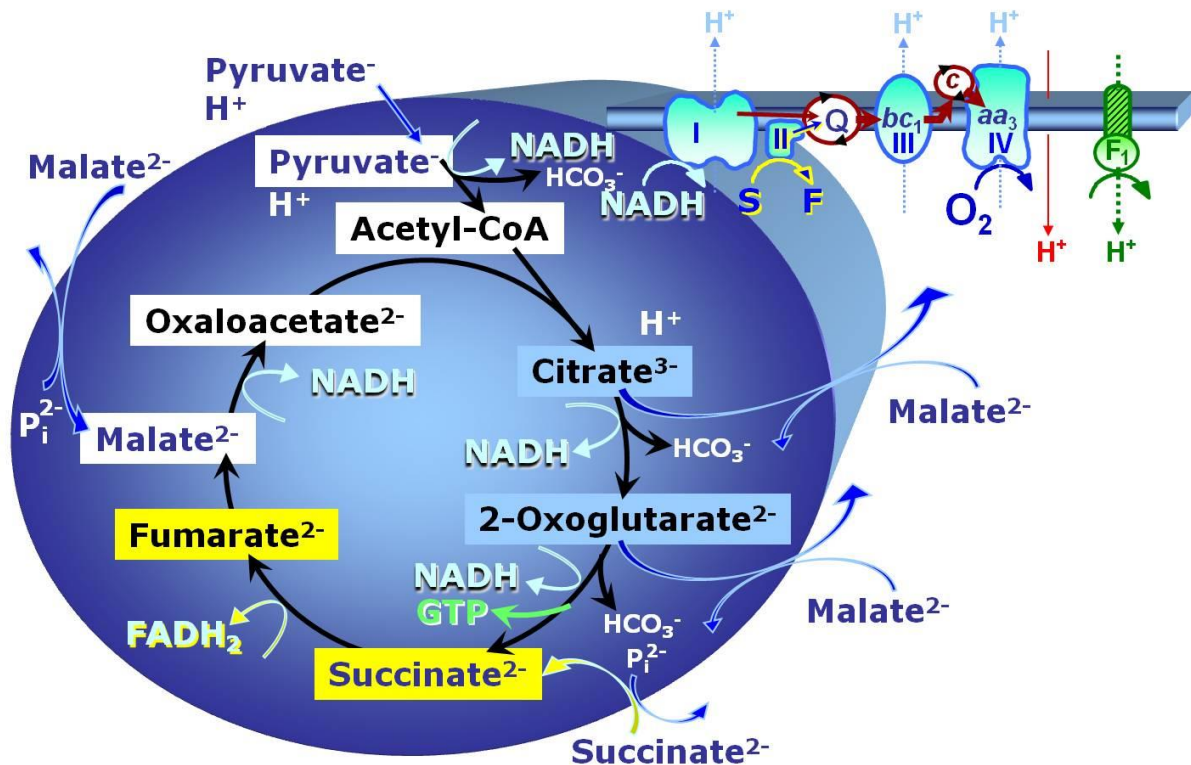


Figure 6.7. PMS. Convergent electron flow to the Q-junction with substrate combination pyruvate & malate & succinate.

6.5. Glutamate & Malate & Succinate, GMS

Transaminase catalyzes the reaction from oxaloacetate to 2-oxoglutarate, which then establishes a cycle without generation of citrate. OXPHOS is higher with glutamate & succinate (NS; Figure 6.8) compared to glutamate & malate (N) or succinate and rotenone (S). This documents an additive effect of convergent NS-electron flow to the Q-junction, with consistent results obtained with permeabilized muscle fibers and isolated mitochondria (Gnaiger 2009). In human skeletal muscle mitochondria (25 °C), Rasmussen and Rasmussen (2000) obtained N/NS flux ratios of 0.7 (0.6) for OXPHOS (or ET) with glutamate & malate (8+4 mM) and glutamate & succinate (4+8 mM), and S/NS flux ratios of 0.8 (0.6) for OXPHOS (or ET). The GM_P/GMS_E and $S(Rot)_E/GMS_E$ flux control ratios are 0.50 and 0.55 in human vastus lateralis (Pesta et al 2011).

Due to the lower H^+/O_2 stoichiometry of the succinate-pathway compared to the CI-linked N-pathway (two versus three coupling sites), the N/NS flux ratio is lower for LEAK respiration (0.3 to 0.4; Garait et al 2005) compared to OXPHOS capacity.

In human skeletal muscle, the phosphorylation system is more limiting at the highest OXPHOS activity with glutamate & succinate, at a P/E control ratio (GS_P/GS_E) of 0.69 versus 0.80 with glutamate & malate (Rasmussen and Rasmussen 2000). Failure of obtaining a further stimulation of coupled OXPHOS in human skeletal muscle mitochondria with GMS by uncoupling (Kunz et al 2000) can be explained by the high FCCP concentration applied (10 μ M) which inhibits respiration (Steinlechner-Maran et al 1996). In mouse skeletal muscle, however, the P/E control ratio is actually 1.0 (Aragones et al 2008), which contrasts with the significant limitation of OXPHOS capacity by the phosphorylation system in human muscle tissue (Gnaiger 2009).

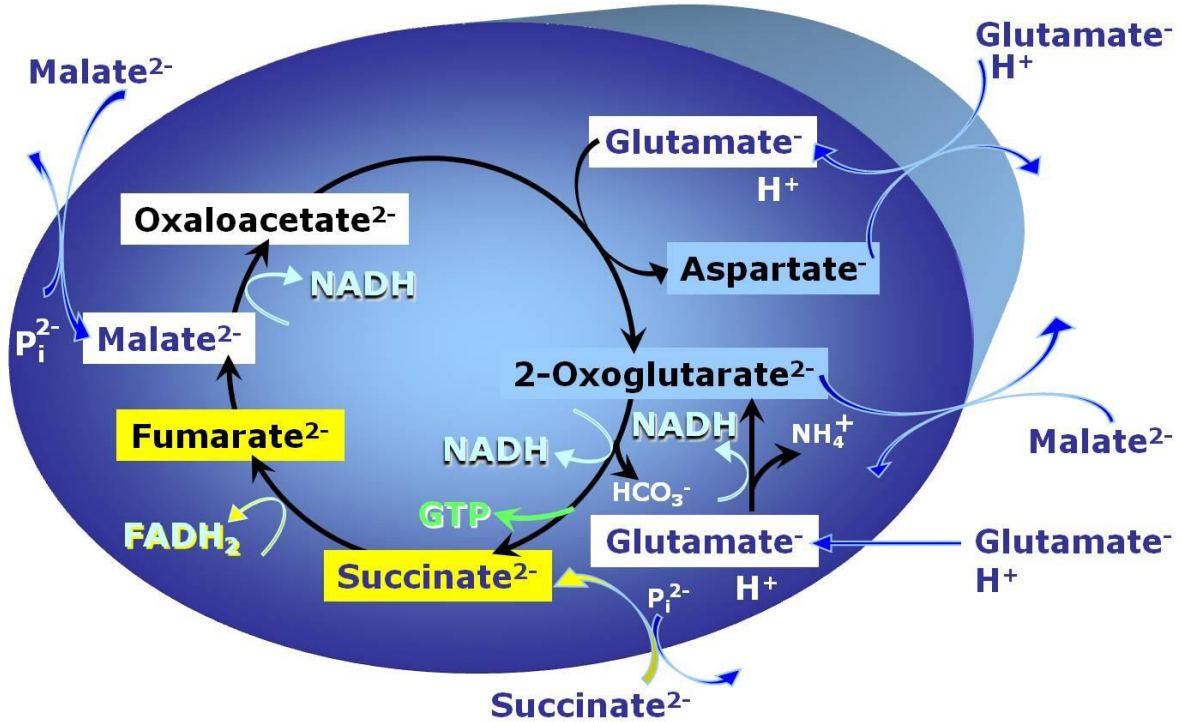


Figure 6.8. GMS. Convergent electron flow to the Q-junction with substrate combination glutamate & malate & succinate (GMS).

6.6. Pyruvate & Glutamate & Malate & Succinate, PGMS

2-oxoglutarate is produced through the citric acid cycle from citrate by isocitrate dehydrogenase, from oxaloacetate and glutamate by the transaminase, and from glutamate by the glutamate dehydrogenase. If the 2-oxoglutarate carrier does not outcompete these sources of 2-oxoglutarate, then the TCA cycle operates in full circle with external pyruvate & glutamate & malate & succinate (Figure 6.9).

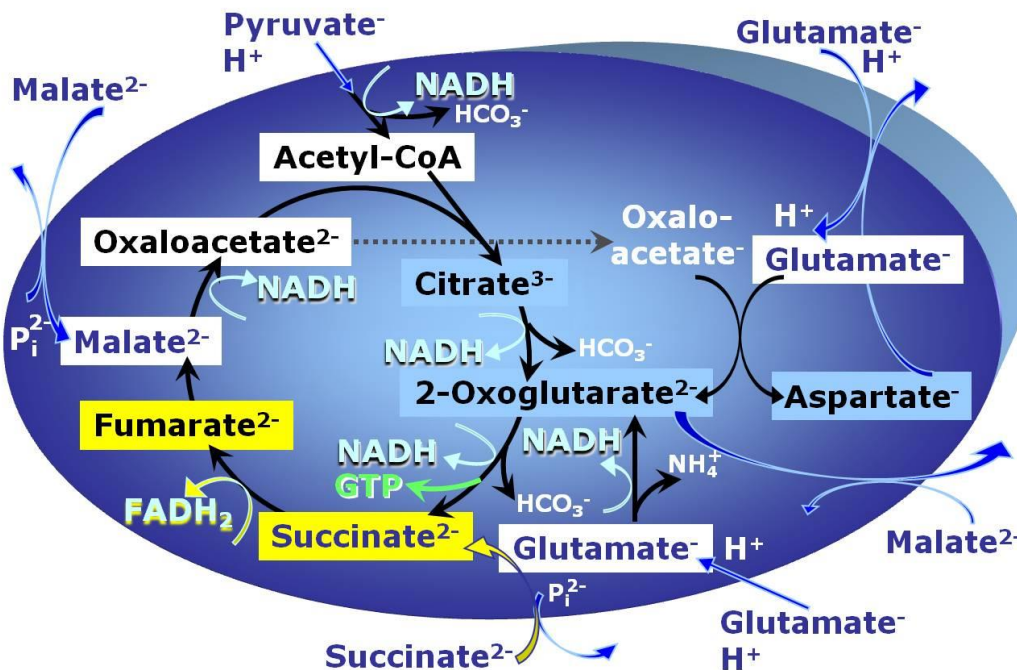


Figure 6.9. PGMS: Convergent electron flow to the Q-junction with substrate combination pyruvate & glutamate & malate & succinate (PGMS).

6.7. Additive effect of glycerophosphate dehydrogenase Complex and electron-transferring flavoprotein Complex

Glycerophosphate DH Complex CGpDH on the outer face of the mtIM oxidises glycerophosphate Gp to dihydroxyacetone phosphate, reducing a flavin prosthetic group that donates its reducing equivalents to the ETS at the level of Q. Electron-transferring flavoprotein Complex (CETF) is located on the matrix face of the mtIM, and supplies electrons from fatty acid β -oxidation to Q.

Gp oxidation in rabbit skeletal muscle (gracilis, fast-twitch white, 99 % type IIb; soleus, slow-twitch red, 98 % type I) exhibits an additive activity with pyruvate oxidation in the NGp-pathway (Jackman, Willis 1996; Figure 6.10a).

Gp flux increases after addition of succinate to brown adipose tissue mitochondria (Rauchova et al 2003). It has yet to be shown, if there is an additive effect of the two pathways (Figure 6.10b), or if respiratory capacity S(Rot) is already sufficient for supporting the maximum flux.

Rabbit muscle mitochondrial respiration is slightly increased by palmitoylcarnitine added to PM_P. Similarly, ATP production in human muscle mitochondria is higher with pyruvate & malate & 2-oxoglutarate & palmitoylcarnitine) supporting convergent FN-electron input into the Q-junction (Figure 6.10c), compared to electron flow through either the N- or S-pathway.

6.8. N/S flux control ratios

N/S flux ratios vary strongly between tissues and species. In human vastus lateralis, the N_P/S_P ratio is less than 1, with a wide scatter between studies but a consistent correlation between PM/S and GM/S flux control ratios (Figure 6.11; PM_P ~ GM_P). In pathologies or isolation artefacts, low N/S flux control ratios indicate defects in the N-pathway upstream of the Q-junction; then PM_P ~ GM_P points towards NADH depletion and CI as the targets. In human cardiac mitochondria, N_E/S_E ~ 2 in the ET-state (Figure 6.14). In contrast, N_E/S_E is as low as 0.5 to 1 in mouse heart mitochondria (Figure 6.15).

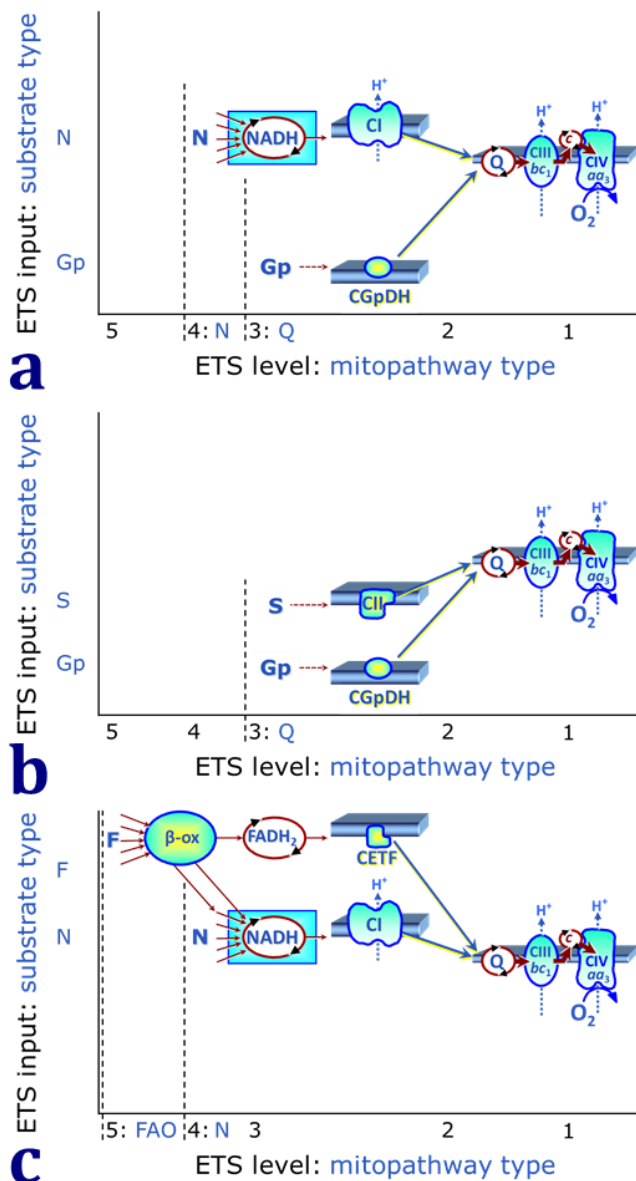
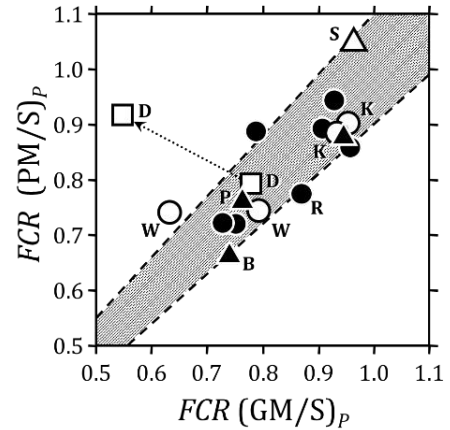


Figure 6.10. Combinations of convergent pathways. (a) NGp-, (b) SGp-, (c) FN-pathway.

Figure 6.11. Pathway flux control ratios $(PM/S)_P$ and $(GM/S)_P$ measured in parallel in the OXPHOS state. Human vastus lateralis with dominant S-pathway; Table 7.2. For symbols see on-line references.

The S-pathway is dominant in human, mouse, and rat liver, but not in trout liver mitochondria. Dominance of the N- or S-pathway has implications on kinetics and $\bar{N}\bar{S}$ -additivity (Chapter 7), which may help to relate the diversity of flux control ratios to adaptive strategies.



6.9. Mitochondrial N– $\bar{N}\bar{S}$ –S pathways and coupling control

SUIT protocols designed according to the pathway architecture of the Q-junction establish ET-pathway states in the sequence N– $\bar{N}\bar{S}$ –S (Figure 6.12). $\bar{N}\bar{S}$ and NS are used equally. NS_E but not NS_P or N_P capacity of permeabilized fibroblasts (pce) matches ET-capacity of living cells (ce), demonstrating the physiological relevance of the Q-junction.

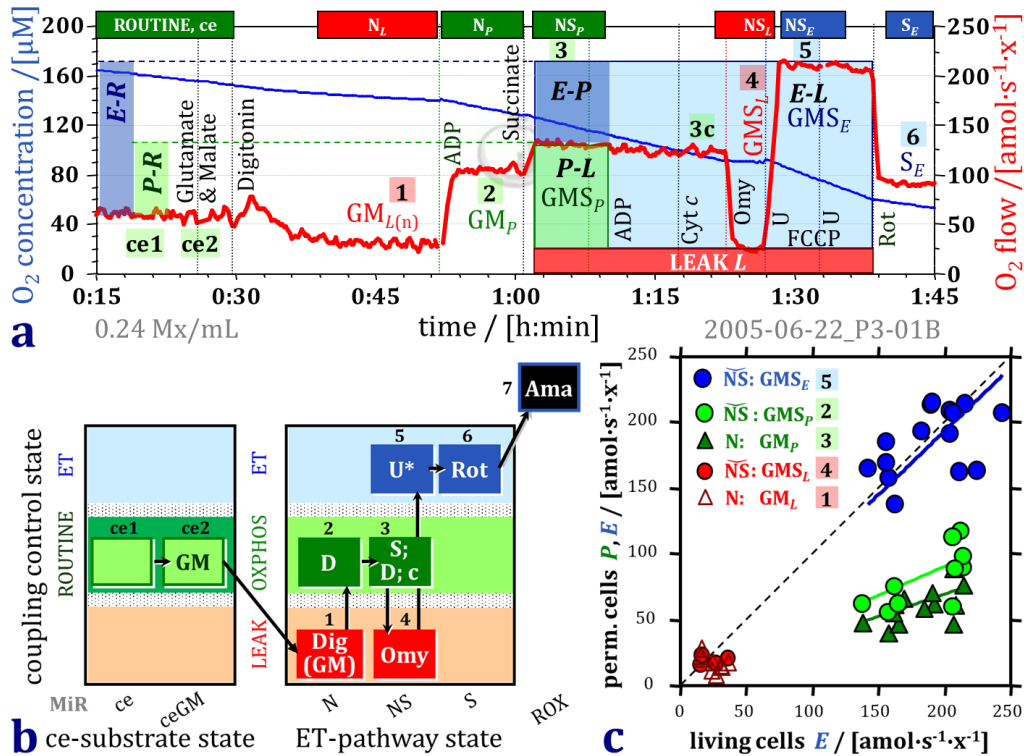


Figure 6.12. Convergent electron flow and E-P excess capacity. NIH3T3 fibroblasts; O₂k 2 mL, MiR05, 37 °C; plasma membrane permeabilization by digitonin. **(a)** Blue plot: O₂ concentration; red plot: O₂ flow $I_{kO_2/ce}$. $GM_{L(n)}$: LEAK, no adenylates; GM_P : 1 mM ADP; GMS_P : 3 mM ADP; 10 μM cytochrome c without stimulatory effect; $GMS_{L(Omy)}$: not higher than $GM_{L(n)}$, indicating suppression of the S-pathway by the N-pathway; GMS_E : high E-P excess capacity; E-L net ET capacity is nearly twice as high as P-L net OXPHOS capacity, comparable to human cardiac mitochondria (Figure 6.14); S(Rot)_E: low S-pathway capacity, S/NS flux control ratio <0.5. **(b)** Coupling/pathway control diagram: 1GM;2D;3S;D;c;4Omy;5U;6Rot;7Ama. **(c)** NS_E in permeabilized cells pce matches ET capacity in living cells ce harvested from the same culture plate, but NS_P and N_P are significantly lower. Similar E-L coupling efficiencies in pce and ce. Symbols show parallel measurements in MiR05 (pce) or DMEM (ce) of individual split culture dishes.

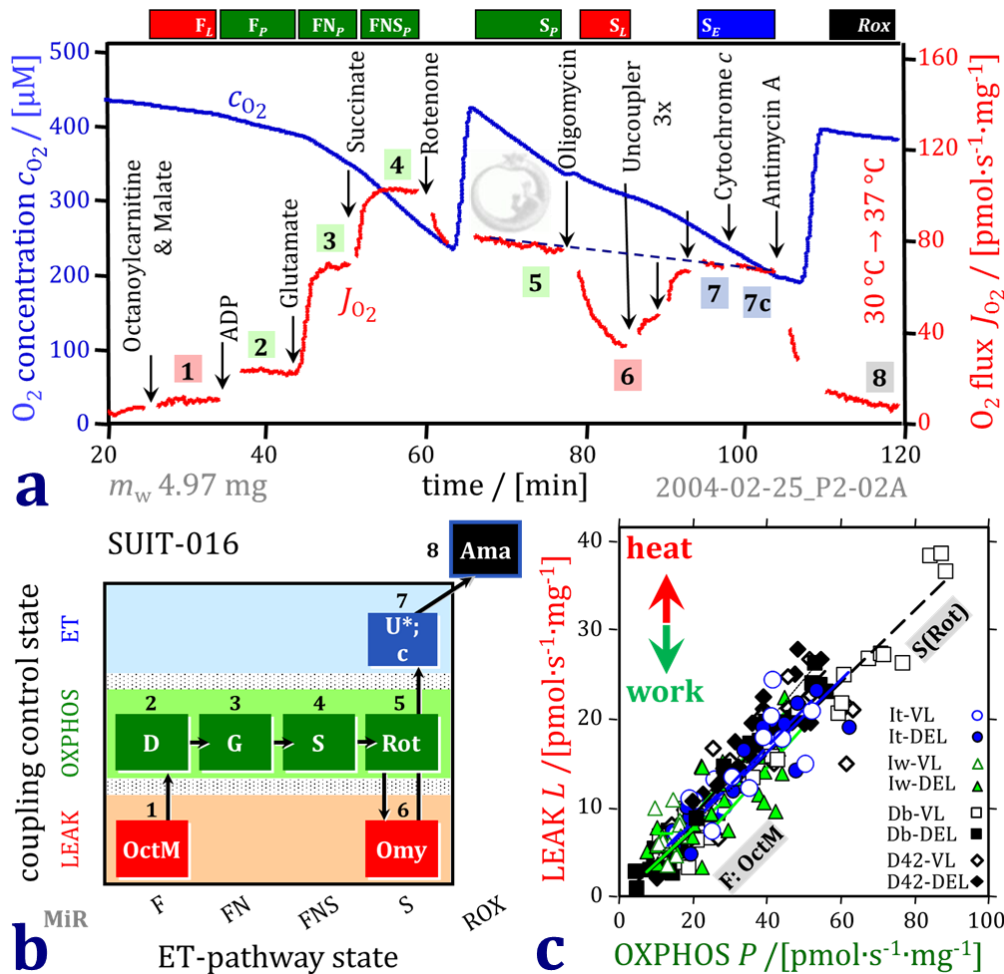
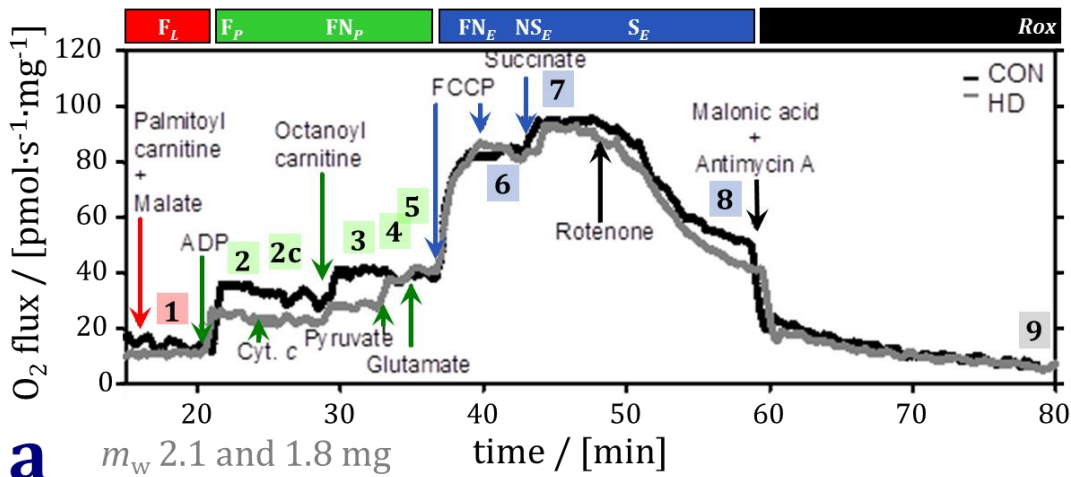
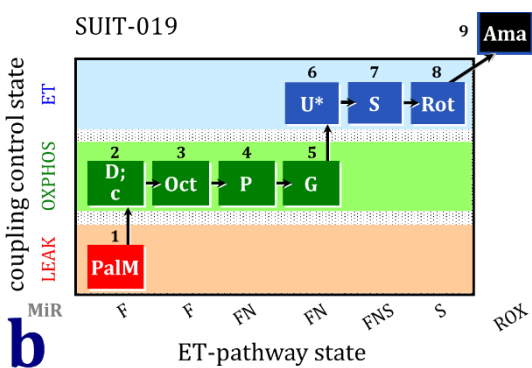


Figure 6.13. SUI protocol for analysis of P - L control efficiency, fatty acid oxidation, and additivity of convergent electron flow in the OXPHOS state. (a) Permeabilized human vastus lateralis fibers, O_2 flux per wet mass m_w measured at 30 °C, converted to 37 °C, MiR05, 2-mL O2k-chambers. Oct and 2 mM malate in human muscle support only the F-pathway. **(b)** Coupling/pathway control diagram. **(c)** Proportional dependence of LEAK respiration on OXPHOS capacity in Inuit and Danes across life styles and training (It and Iw, traditional hunters and westernized Inuit; Db and D42, Danes at baseline and after the 42-day sojourn in Northern Greenland winter), in leg (vastus lateralis VL) and arm muscle (deltoid DEL). Symbols represent the average of two measurements for each biopsy. Mean P - L control efficiencies were 0.57 ± 0.01 ($N = 91$) and 0.54 ± 0.01 (mean \pm SEM; $N = 69$) for F and S, respectively, indicating preserved coupling in the Inuit haplogroup across lifestyles in leg and arm. Modified from Gnaiger et al 2015.

SUIT protocols increase the information obtained from a limited amount of biological sample in a single assay, by sequential measurements of mitochondrial function in multiple pathway- and coupling control states. This allows calculation of statistically robust internal flux control ratios and flux control efficiencies, in contrast to independent assays used for normalization of rates (Chapter 3). SUIT protocols selected according to specific and interrelated questions reveal divergent OXPHOS-control patterns in different species, tissues, and cell types. Mitochondrial diversity has been largely masked by studies restricted to adenylate receptor control in N- and S-pathway states. SUIT protocols, therefore, extend the diagnostic scope and raise new questions on evolutionary strategies of contrasting mitochondrial respiratory control and pathologies linked to mitochondrial dysfunction or adaptive reprogramming (Figures 6.12 to 6.15).



a m_w 2.1 and 1.8 mg time / [min]



b ET-pathway state

Figure 6.14. SUIT protocol for OXPHOS analysis: human heart. Permeabilized myocardial fibers. **(a)** Superimposed traces of tissue mass-specific respiratory flux (at 500-200 μ M O_2) for a control and heart disease patient (CON and HD). Arrows indicate simultaneous titrations identical for both traces. Electron flux through fatty acid oxidation F; FN after addition of pyruvate & glutamate (high E - P excess capacity); FNS after addition of succinate (low succinate control efficiency); continued with ascorbate & TMPD (modified from Lemieux et al 2011). **(b)** Coupling/pathway control diagram.

The E - R reserve capacity in living cells (Figure 3.1) requires interpretation by OXPHOS analysis (Figure 6.12). In fibroblasts, this ‘reserve’ does not indicate a scope of ATP turnover, but mainly of uncoupling. Whereas noncoupled NS_E capacity matches the ET capacity of living cells, the NS_P OXPHOS capacity is half of NS_E . Therefore, the E - R reserve for uncoupling is larger than the P - R reserve for OXPHOS. Importantly, apparent discrepancies between respiratory capacities in living cells and isolated mitochondria are resolved on the basis of additivity of convergent pathways and E - P excess capacity.

Uncoupling stimulates OXPHOS- to ET respiration with pyruvate & malate in human vastus lateralis and rat skeletal muscle with an E - P control efficiency, $(E-P)/E$, of 0.15, and 0.35 to 0.40 in human heart. But E - P is close to zero in mouse skeletal and cardiac muscle (Figures 6.5 and 6.15). Does mouse muscle not require excess ET capacity for calcium handling, in contrast to rats and humans? The E - P excess capacity yields information on the limitation of OXPHOS capacity by the phosphorylation system and excess capacity for ion transport without competition with phosphorylation. Electron gating (ETC) limits flux artificially upstream of the Q-junction, thereby obscuring flux control by and injuries of the phosphorylation system (Figure 6.3).

Reproducibility is a critical issue in science. (1) A single SUIT protocol can be designed to test for reproducibility within an assay. Low mitochondrial coupling efficiency leading to higher heat dissipation has been a speculation in relation to the Northern Inuit haplogroups. This attractive hypothesis was rejected by results on coupling control in the F- and S-pathway within the same assay, demonstrating preserved coupling in muscle mitochondria between Inuit and European populations, in addition to exploring metabolic reprogramming of fatty acid oxidative capacity (Figure 6.13). (2)

Different SUIT protocols address specific aspects of mitochondrial respiratory control, and can be designed to test for reproducibility between assays by including common respiratory states (harmonization in the SUIT RP1 and RP2; Figure 6.15).

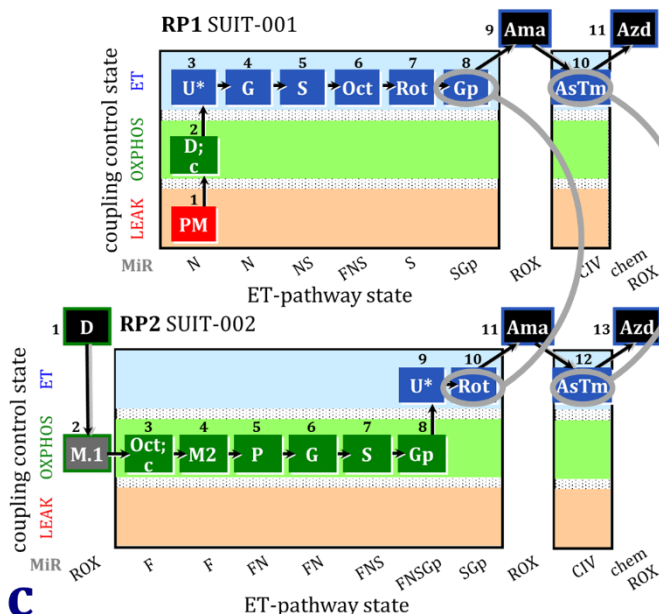
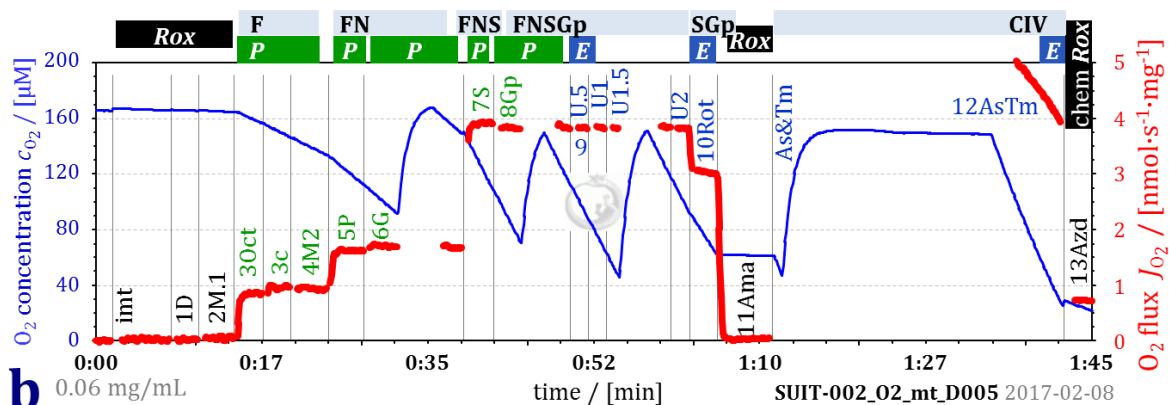
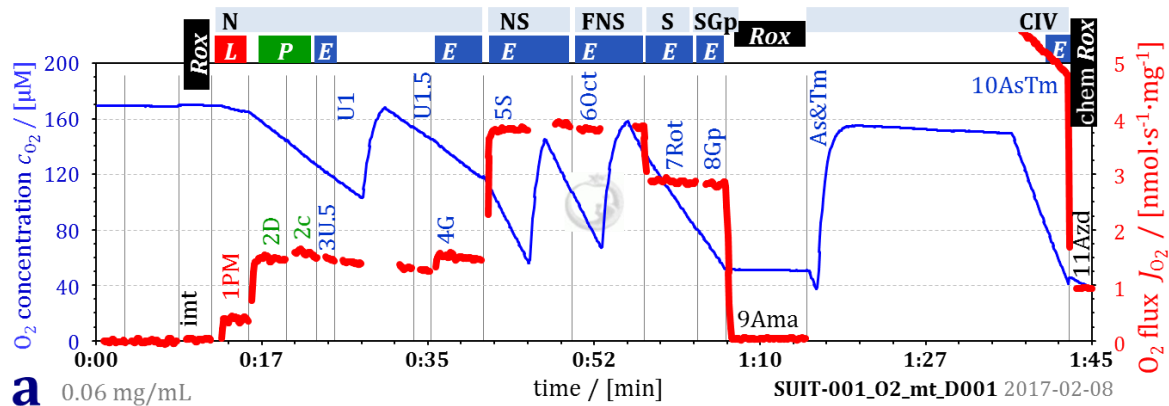


Figure 6.15. Reference protocols RP1 and RP2 for diagnostic OXPHOS fingerprinting. (a) and (b) HRR traces with isolated mouse heart mitochondria comparing RP1 and RP2; MiR05, 37 °C; mg protein. (c) Coupling/pathway control diagrams indicating the harmonized states with rates SGp_E (8 and 10) and CIV_E (10 and 12). Modified after Doerrier et al 2018.

The corresponding $\bar{N}\bar{S}$ -N flux control efficiency is high in mouse skeletal and cardiac muscle (Figure 6.5 and 6.15) and human skeletal muscle (Figure 6.13). In contrast, human heart mitochondria show an exceptionally low control efficiency of succinate added to the N- or FN-pathway state (Figure 6.14). Observations of striking diversities provide key models for testing hypotheses on the functional implications of complex respiratory control patterns compared across species, tissues, and cell types (Gnaiger 2009). Respiratory control patterns need to be compared with comparable protocols.

SUIT reference protocol RP1 represents N-pathway coupling control states $L-P-E$ (Chapter 2), followed by several pathway control steps, as shown for mouse heart mitochondria (Figure 6.15): $PM-PGM$ with low control by G (the reverse $GM-PGM$ reveals high control by P in mouse heart; Lemieux et al 2017); $PGM-PGMS$ showing high control by S; $PGMS-OctPGMS$ indicating no additive F-effect; $OctPGMS-S$ demonstrating high S-capacity and partial $\bar{N}\bar{S}$ additivity; $S-SGp$ indicating no additive Gp -effect. In contrast, RP2 evaluates fatty acid oxidation capacity after enhancing endogenous-substrate utilization by ADP. The rate with 0.1 mM malate is taken as a baseline for fatty acid-stimulated OXPHOS capacity. 2 mM malate is without effect in the absence of malate-anaplerotic capacity. $OctM-OctPM-OctPGM-OctPGMS$ reveal FN- and FNS-OXPHOS capacities (closely matched with PGM- and PGMS-ET capacities in mouse heart mitochondria). $OctPGMS_P-OctPGMS_E$ yields the $E-P$ control efficiency with four convergent electron entries into Q (Figure 1.10). CIV activity is measured – after addition of Ama, ascorbate & TMPD, and a chemical equilibration time of 20 min in the chamber with a gas phase of air – as the difference of flux before and after inhibition of CIV by azide within a very narrow O_2 concentration range (Figure 6.15 a, b).

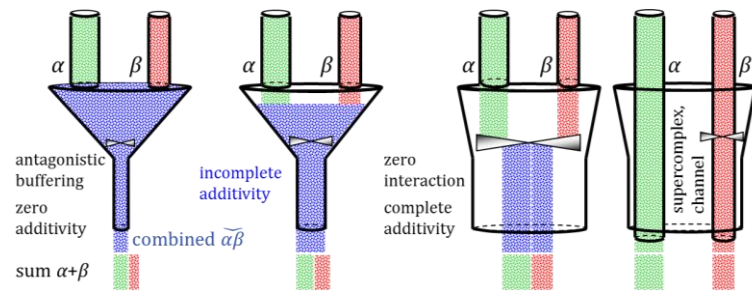
6.10. Implications

Application of physiological fuel substrate combinations is a hallmark of the extension of mitochondrial bioenergetics to mitochondrial physiology and real-time OXPHOS analysis. Conventional studies with N-type substrates for NADH-linked dehydrogenases prevent the simultaneous stimulation of CII or other convergent pathways into the Q-junction (Figure 6.3). Convergent electron input into the Q-junction characterizes mitochondrial function *in vivo*, with a minimum of $1/5^{\text{th}}$ to $1/4^{\text{th}}$ of electron flow through Complex II, for respiration on carbohydrate.

1. For appreciation of the diversity of mitochondrial function in different species, tissues, and cell types, mitochondrial respiratory capacity has to be assessed with application of substrate combinations for reconstitution of TCA-cycle function.
2. SUIT protocols need to be optimized by variation of substrate concentrations, including fatty acids, malate, and succinate. A compromise may be made between optimum conditions for F-, N- versus NS- and S-pathway respiration in a protocol.
3. Interpretation of excess capacities of various components of the electron transfer system and of flux control coefficients depends on the metabolic reference state. Appreciation of the concept of the Q-junction provides new insights into the functional design of the respiratory electron transfer system.
4. The conventional view of a drop of the pmF with an increase of flux from the LEAK- to OXPHOS state (high to moderate membrane potential) has to be modified, based on appreciation of pathway flux control. The relation between pmF and flux is reversed when an increase in flux is affected by a change in substrate supply.
5. Based on the relationship between ROS production and reversed electron flow from CII to CI, multiple substrates have been supplied in investigations of oxidative stress related to mitochondrial metabolism. The dependence of ROS production on pmF and metabolic state has to be investigated further, to resolve pertinent controversies on the role of mitochondria in cellular ROS production.
6. Supercomplex formation, metabolic channelling, and partially additive effects on flux suggest that convergent electron input into the Q-junction only partially proceeds through a common or free Q pool.

Chapter 7.

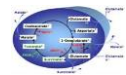
Additivity of convergent electron transfer



It is not at all easy to draw a sharp line between cases where what is happening could be called “addition”, and where some other word is wanted.

Douglas R Hofstadter (1979) Gödel, Escher, Bach: An eternal golden braid. A metaphorical fugue on minds and machines in the spirit of Lewis Carroll. Penguin Books.

Section	7.1. Intersubstrate competitions	66	Page
7.2. Types of interactions and additivity		67	
7.3. Additivity of convergent NS pathways		71	



Peter Mitchell (1979) defined the *physiological* level of the chemiosmotic theory as the aim to ‘*answer the question: What does it do?*’ More than 40 years later, a physiological perspective is emphasized in the study of oxidative phosphorylation, when asking: *How fast can it go?* This question gains perspective by considering the functional structure of the convergent electron transfer system, supercomplex formation, and dynamic network organization. Maximum aerobic flux depends on the degree of additivity of pathways converging at the Q-junction. Thus, additivity is essential in the control of oxidative phosphorylation. Incompletely additive effects are common in nature: When mixing equal volumes of ethanol and water, the volume of the mixed solution (incomplete additivity: $0.5+0.5=0.96$) is only 96 % of the volume calculated by addition of the volumes of the unmixed compounds. Paradoxically, current concepts on interaction do not agree whether to categorize incompletely additive effects as synergistic or antagonistic. The present analysis resolves these discrepancies by distinguishing incomplete additivity — in the numerical space between zero additivity ($0.6+0.4=0.6$) and complete additivity ($0.6+0.4=1.0$) — from antagonistic suppression and synergistic activation. The corresponding mathematical definition of additivity bridges the gap between incompatible models of interaction, with general implications on metabolic network analysis, traffic control, pharmacological combination therapy and epistatic interactions in all areas of biomedical, social and technological research.

7.1. Intersubstrate competitions

Restriction of permeability of the mt-inner membrane for various substrates of the TCA cycle raised the question on inter-substrate competition for transport, intramitochondrial concentrations and oxidation. Succinate accumulation is decreased by malate, and phosphate or malate inhibit respiration of rat liver mitochondria in the presence of succinate and rotenone (Harris, Manger 1968). In general, ‘*when two substrates are presented together the respiratory rate obtainable with maximal stimulation by uncoupler can exceed, be equal to or be less than the sum of the rates obtained with the respective substrates separately*’ (Harris, Manger 1969). Various mechanisms explaining these different effects have been recognized, in particular that ‘*the stimulation of the*

oxidation of either malate or succinate by the addition of glutamate is due to the removal of oxaloacetate by transamination' (Harris, Manger 1969; Figures 4.6 and 6.8). When β -hydroxybutyrate is added to N-type substrates (either citrate, malate, glutamate, oxoglutarate or pyruvate), then *'with these pairs the total rate of oxidation obtainable is equal to the sum of the respective rates measured separately'*. Since the *'respiratory rate obtainable from other pairs of substrates can be less than the sum of the separate rates, even though there is no known inhibition of the enzymes by the conjugate substances'*, the available conclusion was that *'in this circumstance mutual competition between the two anions for permeation and accumulation is presumed'* (Harris, Manger 1969).

Biochem. J. (1963) **86**, 432

Substrate Competition in the Respiration of Animal Tissues
 THE METABOLIC INTERACTIONS OF PYRUVATE AND α -OXOGLUTARATE
 IN RAT-LIVER HOMOGENATES

BY R. J. HASLAM* AND H. A. KREBS

*Medical Research Council Unit for Research in Cell Metabolism, Department of Biochemistry,
 University of Oxford*

(Received 23 July 1962)

A readily oxidizable substrate—an intermediate or a starting material—often inhibits the oxidation of other substrates when added to respiring material (Krebs, 1935; Edson, 1936). In terms of enzyme chemistry this means that oxidizable substrates

* Present address: Sir William Dunn School of Pathology, University of Oxford.

and intermediates derived from them compete with each other for the joint pathway of electron transport to molecular oxygen or for a shared co-factor. The present investigation is concerned with the detailed study of the competitive and other interactions of pyruvate, α -oxoglutarate and endogenous substrates in respiring rat-liver homogenates.

Importantly, these investigations were based on noncoupled flux, removing any downstream limitation of flux by the phosphorylation system. Without the concepts, however, of (1) a shift of flux control under different metabolic conditions of substrate supply to different enzyme-catalyzed steps, and (2) convergent versus linear pathways, interpretation of these results on rat liver mitochondria was only possible in terms of intersubstrate competition of substrate transport. The focus, therefore, was on inhibitory mechanisms (Section 6.4). Although respiration J_N with pyruvate of rat liver mitochondria was stimulated when adding succinate, J_{NS} (without using J_S with succinate & rotenone as a control to compare J_{NS} with J_{N+J_S}), the interpretation was that *'succinate oxidation did not inhibit pyruvate oxidation'* (König et al 1969). Although these early studies clearly showed that succinate plays an important regulatory role for mitochondrial respiration in the presence of NADH-linked substrates, they appear to have had little or no influence on later concepts on mitochondrial respiratory capacity and respiratory control.

7.2. Types of interactions and additivity

The degree of additivity of metabolic flux is the result of interactions between intermediates of the converging pathways. Three types of interaction are distinguished: synergistic, antagonistic, and no interaction. Interactions that lead to stimulation are categorized as *synergistic* — even if the effect is less than completely additive — based on a classical definition of additivity (Gaddum's highest single agent model; HSA model). The same stimulatory effect is paradoxically seen as *antagonistic* based on Loewe additivity, where the reference point of zero interaction is complete additivity: a sham combination of two doses of one and the same agent is completely additive (zero interaction; Fig. 7.1a).

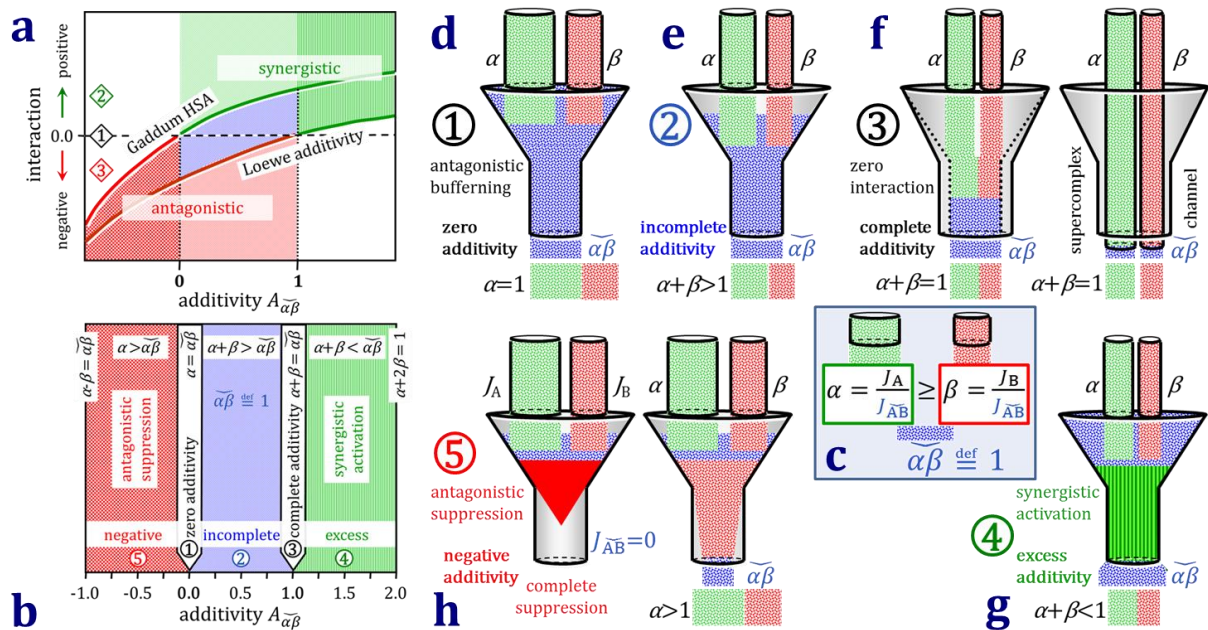


Figure 7.1. Additivity in convergent systems. (a) Zero or complete additivity are reference states of zero interaction of two component branches. Conflicting definitions of synergistic and antagonistic effects are a consequence of restriction to three types of interaction— 1: no interaction, 2: synergistic (positive), 3: antagonistic (negative). In the range of additivity 0 to 1, identical interactions change signs depending on the reference state of zero interaction at zero additivity (Gaddum’s model of non-interaction or highest single agent model, HSA; upper-left curve) versus complete additivity (models following Loewe additivity, lower-right curve). (b) Five types of interaction are distinguished by recognizing the two reference points of zero and complete additivity as upper and lower limits of antagonistic suppression and synergistic activation, respectively, separating incompletely additive interactions. (c) Definition of α and β (Eq. 7.1). (d) Zero additivity: the highest single agent A saturates downstream capacity. (e) Incomplete additivity: enhancement by combination, but $J_{AB} < J_A + J_B$. (f) Complete additivity: the combined effect is the linear sum of the component effects. Funnels represent the junction and downstream capacity, which exert a limiting effect on total flux at incomplete and zero additivity, but match (dotted funnel) or are in excess of pathway capacity at complete additivity. Functional channels (e.g. supercomplexes) yield complete additivity, imposing zero interaction. (g) Excess additivity: synergistic activation. (h) Negative additivity: antagonistic suppression, when components A and B, exerting an effect alone, suppress each other below the level of J_A , with the limiting case $J_{AB} = 0$ at complete suppression.

Table 7.1 Five types of interactions and additivity

Interaction	Additivity	Defintion
1. Antagonistic buffering	zero additivity	$A_{\alpha\beta} = 0$
2. Antagonistic: alleviating, antagonistic epistasis, positive epistasis, diminishing returns, partial suppressors	incomplete additivity	$A_{\alpha\beta} < 1$
3. Additive: no interaction	complete additivity	$A_{\alpha\beta} = 1$
4. Synergistic: aggravating, negative epistasis	excess additivity	$A_{\alpha\beta} > 1$
5. Antagonistic suppression	negative additivity	$A_{\alpha\beta} < 0$

Opposite to complete additivity, zero-additivity is considered as an alternative reference point for zero interaction (Table 7.1). This shifts the domain of antagonistic interactions below complete additivity into the category of synergistic interactions above zero additivity (Figure 7.1a). The effects of combined $\bar{N}\bar{S}$ -substrate supply qualify as antagonistic from the perspective of ‘smaller than completely additive’, although respiration is stimulated.

Alternatively, this would be synergistic when using zero-additivity as reference for non-interaction, which is the paradoxical consequence when generalizing any positive interaction as ‘synergistic’ (Gaddum’s model or highest single agent model; Berenbaum 1989; Lehár et al 2007) and is a deficiency in the model of Bliss independence (Boik et al 2008) (Figure 7.1a). On the other hand, using complete additivity as definition of zero-interaction has the consequence of viewing incompletely additive but enhancing effects as antagonistic (Figure 7.1a).

The strategy of using one index for amplification and another index for additivity (Figure 7.1a, left and right curve, respectively) is indicative of the limited scope of presently available additivity indexes to merely distinguish sub- from super-additive effects. A fourth type of interaction was introduced, by separating antagonistic effects below Loewe additivity (Figure 7.1a, right curve) into antagonistic suppression or hyper-antagonism (below zero additivity; Figure 7.1b) and antagonistic buffering (around zero additivity; Yeh et al 2009). The same categories of interaction can be defined from the perspective of multiplicative Bliss independence. The boundary between zero and completely additive effects, however, resides in a twilight zone with the problem of classifying incompletely additive interactions as antagonistic, when the combined effect is in fact enhanced above zero additivity. Surprisingly, an advanced mathematical definition of additivity remained inviolate.

These paradoxes and current disagreement on a strict mathematical definition of additivity (Boik et al 2008) are resolved by developing answers to three questions: (1) Where do the conflicting paradigms on interactions agree? As illustrated in Figure 7.1a, both models classify interactions as antagonistic below zero additivity (antagonistic suppression), and as synergistic above complete additivity (synergistic activation; Figure 7.1b). (2) Is there a conflict in choosing between the two alternative reference points of zero interaction? Such a conflict remains, if complete antagonistic suppression (Figure 7.1c) is considered as a basic cornerstone for defining additivity. When dropping this restriction, both states of zero interaction (zero and complete additivity) can be incorporated as reference states of additivity in a strictly phenomenological approach (Figure 7.1b). (3) Can additivity be generally defined in mathematical terms, based on the separate component effects, α and β (N- and S-pathway flux control ratios)? To do so, a distinction has to be made between the larger and smaller effect, which is implicit in several but not all models of additivity. Distinction of a dominant α and subdominant β component is obviously not necessary for complete additivity and synergistic activation, but is fundamental for defining the reference point of zero additivity (Figure 7.1d).

Using laboratory jargon, the ‘better’ substrate supports the higher flux with either NADH-linked substrates (N) or succinate (S; Figure 6.15a). The dominant α -substrate yields the higher flux, $J_A = \max\{J_N, J_S\}$. Succinate is frequently but not generally the α -substrate A (Table 7.2). α and β are the pathway control ratios of fluxes through the constituent pathways (N or S), normalized for flux with the $\bar{N}\bar{S}$ -substrate combination, $J_{\bar{A}\bar{B}}$ (Figure 7.1),

$$\alpha = \frac{J_A}{J_{\bar{A}\bar{B}}} \geq \beta = \frac{J_B}{J_{\bar{A}\bar{B}}} \quad 7.1$$

Pathway-control ratios are calculated for either OXPPOS- or ET capacities, with variation of pathway states (N, $\bar{N}\bar{S}$, S) at constant coupling-control states.

This sets the stage for a generalized mathematical definition of additivity, $A_{\alpha\beta}$, distinguishing five categories. (1) At zero additivity ($A_{\alpha\beta}=0$), the α -component A masks the effect of B completely (buffering), such that flux with the α -substrate A is as high as

flux with the substrate combination \overline{AB} (Figure 7.1d). (2) *Incomplete additivity* ($A_{\overline{\alpha\beta}} < 1$) is defined as an enhancement that is less than the linear sum of the components (Figure 7.1e). (3) At *complete additivity* ($A_{\overline{\alpha\beta}} = 1$), the combination yields the linear sum of the components, hence the component control ratios add to 1, $\alpha + \beta = 1$ (Figure 7.1f). (4) *Synergistic activation* at excess additivity ($A_{\overline{\alpha\beta}} > 1$) leads to higher than completely additive effects (Figure 7.1g). It is equally important to make a definitive distinction between incomplete additivity and (5) *antagonistic suppression* with negative additivity ($A_{\overline{\alpha\beta}} < 0$), when the combination yields a decreased effect compared to the maximum obtained separately by the α -component A (Figure 7.1h). Additivity $A_{\overline{\alpha\beta}}$ obeys these boundary conditions on the basis of the simple definition (Figure 7.2),

$$A_{\overline{\alpha\beta}} = \frac{J_{\overline{AB}} - J_A}{J_B} = \frac{\overline{\alpha\beta} - \alpha}{\beta} \quad \overline{\alpha\beta} \stackrel{\text{def}}{=} 1 \quad 7.2$$

Normalization for $J_{\overline{AB}}$ defines $\overline{\alpha\beta} = 1$. $\overline{\alpha\beta}$ indicates the combination, not a multiplication ($\alpha\beta$). $J_{\overline{AB}}$ is measured when a \overline{AB} substrate combination stimulates simultaneously the two branches converging in the common segment of the pathway (Figure 7.1).

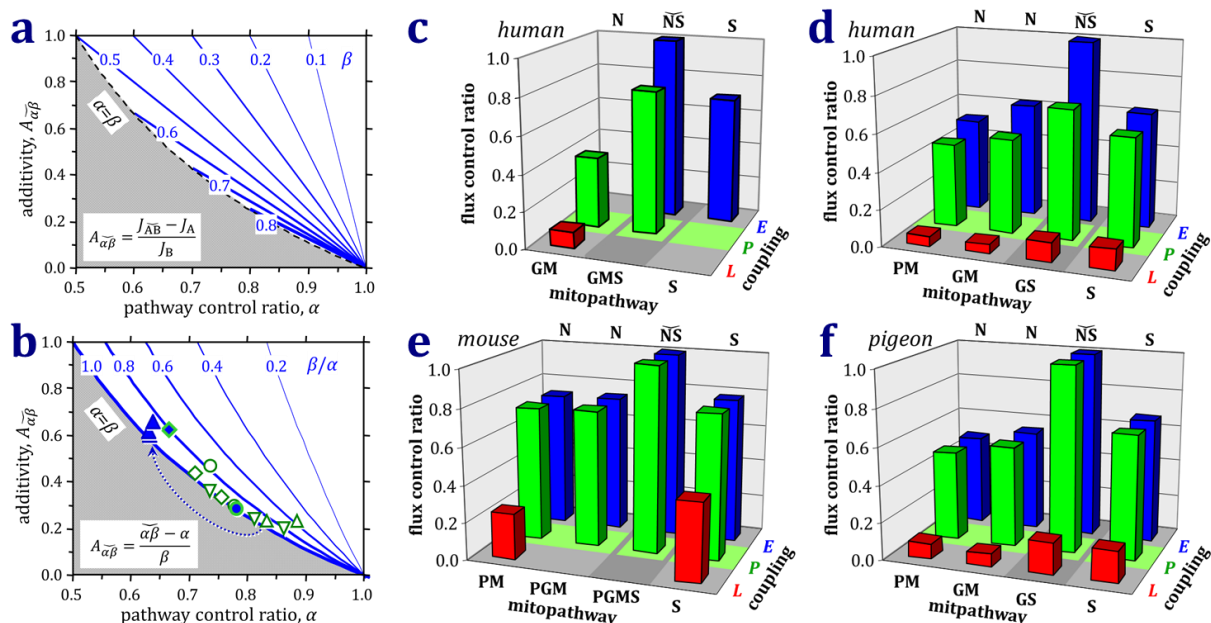


Figure 7.2. Incomplete additivity of convergent pathway capacities. (a) Interface between zero and complete additivity in convergent systems at lines of constant β and (b) constant β/α . Shaded regions are excluded by the restriction $\beta/\alpha \leq 1$. Extrapolations of continuous lines yield synergistic activation with decreasing α (additivity > 1) or antagonistic suppression with increasing α (additivity < 0). Additivity of respiratory capacity in skeletal muscle mitochondria for the N- and S-pathway (open symbols, OXPHOS-capacity, P; closed, ET-capacity, E; connected by dotted arrow). Triangles up – human vastus lateralis; triangles down – rat quadriceps; closed circle – mouse soleus (P and E identical), open circles – rat soleus and gastrocnemius; closed diamond – pigeon pectoralis (P and E identical); open diamonds – pig and rat biceps. (c) Permeabilized fibers and (d) isolated mitochondria from human skeletal muscle. (e) Permeabilized fibers from mouse soleus. (f) Isolated mitochondria from pigeon breast muscle. Flux control ratios normalized for \overline{NS} -ET-capacity ($\overline{\alpha\beta} \stackrel{\text{def}}{=} 1$). Limitation of OXPHOS-capacity by the phosphorylation system in skeletal muscle mitochondria in man (mixed fibre type in vastus lateralis) in contrast to slow oxidative mouse soleus muscle and red fiber type pigeon pectoralis. For details, see Table 7.2.

If the pathway control ratio of the subdominant β -pathway, β , is constant, then $A_{\alpha\beta}$ increases linearly with decreasing α , but α can decline in relation to β only to a minimum where $\alpha=\beta$ (Figure 7.2a; upper limit of the shaded area). Below this limit, the other component pathway gains dominance and takes over the role of α . At constant value of α , additivity increases with a decline of β . The minimum additivity, therefore, is obtained for any α , if the two separate pathways have identical capacities ($\beta/\alpha=1.0$; Figure 7.2b). At constant constituent pathway capacity of J_A or J_B , an increase of additivity effectively enhances the combined flux $J_{\overline{AB}}$ by an efficacy boost, whereas a potency shift allows reduction of J_A or J_B while maintaining $J_{\overline{AB}}$ constant.

Additivity (Eq. 7.2) is a quantitative index for the combination effect of bioactive compounds at fixed or saturating concentrations. No dose-response curves are implied, which are important, however, for describing combination effects in a variety of systems, from multiple inhibitors of a single enzyme to oncology and environmental toxicology. Dose additivity is important in pharmacology when drugs are administered in the form of cocktails and interactions between biologically active compounds are compared with responses to single components. Evaluation of combination therapies and synergistic toxicological effects is based on models of additivity, when applying drugs in a mixture of various concentrations of each component. Complete antagonistic suppression is obtained when the combined effect is fully inhibited to zero (Figure 7.1h). This point is frequently considered as a cornerstone for defining interaction coefficients and additivity as -1 . This is questionable as a general definition, since it applies to $A_{\alpha\beta}$ (Eq. 7.2) only in the special case when $\alpha=\beta$. With increasing potency of A, the weaker B must exert an increasing suppression potential to fully inhibit total flux. At complete antagonistic suppression ($J_{\overline{AB}}=0$), therefore, additivity is $A_{\alpha\beta} = -J_A/J_B$ (Eq. 7.2; fractions α and β are not defined at this point).

7.3. Additivity of convergent \overline{NS} pathways

Additivity $A_{\overline{NS}}$ (Eq. 7.2) in the OXPHOS-state is incomplete in many types of mitochondria, varying from 0.24 in human vastus lateralis to 0.62 in pigeon breast muscle (Table 7.2). Incomplete additivity of convergent \overline{NS} -OXPHOS capacity indicates the complexity of interactions in a system where flux control is shared between segments of the ETS upstream and downstream of the Q-junction and by the phosphorylation system (Figure 6.3). The relatively low additivity in human skeletal muscle is mainly due to the limitation of OXPHOS-capacity by the phosphorylation system, the control of which is stronger in the state of high flux with the combined substrates (NS) than in either state of low flux with the single components (N or S; Figure 1.9). Additivity of convergent electron flow in human skeletal muscle increases from 0.23 in the OXPHOS-state, to 0.62 in the ET-state (Figure 7.2b; arrow). In slow oxidative mouse soleus and fast oxidative glycolytic pigeon pectoris, additivities are 0.28 and 0.62, respectively (Figure 7.2e and f). In these muscles, no uncoupling effect is observed on ADP-stimulated respiration for all substrate combinations ($P/E=1.0$), hence additivities in OXPHOS- and ET-states are identical, and the large difference in the additive effect reflects the diversity of control in the ETS.

In liver mitochondria, succinate is the α -substrate compared to glutamate & malate or pyruvate & malate, and the N/S (GM/S) pathway control ratio is typically <0.8 for OXPHOS-capacity. In many muscle mitochondria, however, OXPHOS-capacity is similar with glutamate & malate versus succinate; the N/S (GM/S) pathway control ratio is 0.90 ± 0.15 for a wide range of muscle tissues (Table 7.2). The functional significance of the

N/S-pathway control ratio has not been an explicit subject of study, despite its central position in the structure of the ETS. When the TCA cycle is in full operation in the living cell with influx of pyruvate into the mitochondrial matrix, electron flow into the Q-junction converges according to a NADH:succinate ratio of 4:1 (Figure 6.3). The fact that such high ratios of N:S respiratory capacity are not observed (Table 7.2) suggests that a significant functional role is played by the apparent S-excess capacity above its relative contribution to integrated \overline{NS} -respiration. This is related most likely to the kinetic regulation of low succinate levels for the control of metabolite depletion into the cytosol, with direct implication on signaling and tumor formation by stabilizing HIF-1 α .

Table 7.2. Additivity of convergent \overline{NS} -electron flow in muscle mitochondria

Species	Muscle	Prep	<i>T</i>	\overline{NS}	N	S	N/\overline{NS}	S/\overline{NS}	$A_{\alpha\beta}$	Ref
h. ath.	vastus	imt	25	GS_P	GM_P	$S(Rot)_P$	0.73	0.83	0.23	1
h. sed.	vastus	pfi	37	GMS_{CP}	GM_{CP}	$GMS(Rot)_{CE}$	0.50	0.88	0.23	2
h. ob.	vastus	pfi	37	$PGMS_P$	PGM_P	--	0.48	--	--	3
h. pat.	vastus	pfi	25	GMS_P	GM_P	--	0.74	--	--	4
rat W	quad.	imt	30	GMS_P	GM_P	$S(Rot)_P$	0.81	0.78	0.24	5
rat L	quad.	imt	30	GMS_P	GM_P	$S(Rot)_P$	0.73	0.74	0.36	5
rat W	quad.	imt	25	GS_P	GM_P	--	0.54	--	--	6
mouse	soleus	pfi	37	$PGMS_{CP}$	PGM_{CP}	$PGMS(Rot)_{CP}$	0.74	0.78	0.28	7
rat W	gastr.	imt	30	GMS_P	GM_P	$S(Rot)_P$	0.78	0.76	0.29	8
rat	soleus	imt	25	GS_P	GM_P	$S(Rot)_P$	0.57	0.74	0.47	1
rat S	sm	imt	30	GS_P	GM_P	--	0.78	--	--	9
rat	biceps	imt	25	GS_P	GM_P	$S(Rot)_P$	0.67	0.71	0.43	1
pig	biceps	imt	25	GS_P	GM_P	$S(Rot)_P$	0.76	0.74	0.33	10
pigeon	bm	imt	25	GS_P	GM_P	$S(Rot)_P$	0.54	0.67	0.62	11
rat	heart	imt	30	GS_P	GM_P	--	0.54	--	--	12

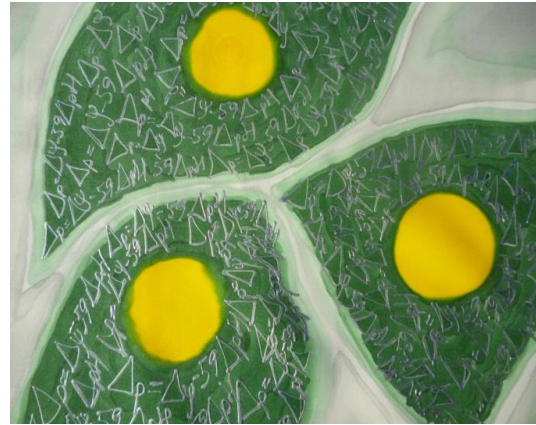
N/\overline{NS} and S/\overline{NS} are pathway control ratios of oxygen flux with substrate types provided separately for the N- and S-pathway, normalized for flux through the combined \overline{NS} -pathway. P – pyruvate; G – glutamate; M – malate; S – succinate; *c* – cytochrome *c*; subscript *P* - ADP-stimulated OXPHOS-capacity; subscript *E* – uncoupler-induced noncoupled ET-capacity. Additivity $A_{\alpha\beta}$ is calculated from Eq. 7.2.

h. – human; ath – athletic; sed. – sedentary; ob. – obese; pat. – retrospective control patient, without myopathy; rat strains: L, Lou/C; S, Sprague-Dawley; W, Wistar. Muscles: quad. – quadriceps, including the vastus lateralis (50 % type I in young trained subjects; towards 40 % type I in young untrained subjects); gastr. – gastrocnemius, and soleus (both form the calf muscle; typically slow oxidative); sm – skeletal muscle; biceps (pig: fast glycolytic, 80 % type IIb fibre type; rat: fast oxidative glycolytic); bm – breast muscle (fast oxidative glycolytic, very pure type IIb fibre type). Prep – preparation: imt, isolated mitochondria; pfi, permeabilized fibres. *T* – experimental temperature [°C]. Ref – references: (1) Rasmussen et al 2004. (2) Boushel et al 2007. (3) Raboel et al 2009. (4) Kunz et al 2000. (5) Garait et al 2005. (6) Fritzen et al 2007. (7) Aragonés et al 2008. (8) Capel et al 2005. (9) Llesuy et al 1994. (10) Rasmussen et al 1996. (11) Rasmussen, Rasmussen 1997. (12) Costa et al 1988.


The additive effect indicates a down-stream excess capacity of respiratory complexes including cytochrome *c* oxidase (CIV) over CI and CII. Convergent electron transfer yields a maximum (additive) effect on OXPHOS-capacity when cytochrome *c* oxidase and the phosphorylation system exert a minimum (zero) flux control (Figure 1.11). Comparative studies are required on the additive effect of \overline{NS} -electron input in different tissues and species, to advance our understanding of the physiological implications on tissue-specific respiratory control patterns and their effects on mitochondrial diseases.

Chapter 8.

Protonmotive pressure and respiratory control



Mitchell's dream by Odra Noel

Section	8.1. Vectorial and scalar forces and fluxes	75	Page
	8.2. Why is thermodynamics scary?	79	
	8.3. Protonmotive force and motive units	91	
	8.4. Protonmotive pressure linearity	96	

The chemiosmotic theory represents one of the most fundamental concepts in biology, impacting on modern medicine and biotechnology to an unprecedented extent. The chemiosmotic theory on the protonmotive force pmF is based on Peter Mitchell's famous theorems on four integrated coupling modules. **Module 1:** the reversible H^+ translocating F-ATPase; **Module 2:** the respiratory redox H^+ pumps; **Module 3:** the coupling of hydrogen ion translocation to electroneutral and reversible proton charge exchange of cations against H^+ ions and of anions against OH^- ions; **Module 4:** the coupling membrane, in which the three coupling modules reside, with no or low permeability for ions. Coupling Module 1 utilizes the pmF ; Module 2 generates the pmF ; Module 3 modulates the pmF ; and Module 4 is the coupling membrane as the structural and functional backbone of chemiosmotic energy transformation.

Paving the way towards acceptance of the chemiosmotic theory has been a monumental task, as summarized in the *Grey Book* (Mitchell 1966). Attempts to translate the arcane language of bioenergetics for communication across disciplinary fields are neither consistent nor complete. The terminology of physical chemistry is not accommodated by common language. There is an unresolved clash of classical thermodynamics when taking a narrow view on *closed* systems — as reflected in IUPAC recommendations (Cohen et al 2008) — and the nomenclature in thermodynamics of irreversible processes in *open* systems (Prigogine 1967; Gnaiger 1993a). It is, therefore, appropriate to reflect the thermodynamic and electrochemical basis of the concept of the protonmotive force, and to introduce constructive terminology and iconic abbreviations.

Section 8.1: Concentration or potential differences with vectorial fluxes and forces in discontinuous compartmental systems are distinguished from electrochemical potential gradients with fluxes and forces as vectors.

Section 8.2: Isomorphic forces including the pmF ($\Delta_m F_{H^+}$) are defined as partial derivatives of Gibbs energy (exergy) per advancement, introducing the stoichiometric number ν_{H^+} into the pmF equation. Advancement per time $d_m \xi_{H^+}/dt$ is flow I_{mH^+} (Eq. 1.7b).

Section 8.3: The diffusive and electric components of the pmF , $\Delta_d F_{H^+}$ and $\Delta_{el} F_{p^+}$, are presented as partial isomorphic forces. The stoichiometric number ν_{H^+} and the charge number z_{H^+} are made explicit in the pmF equation. This links the pmF equation to the

fundamental constants comprising the backbone of physical chemistry and the SI system: (1) the Boltzmann constant k , with kT [$\text{J}\cdot\text{x}^{-1}$] as the motive force quantum in the particle or molecular count format: x is the motive unit MU for the count N_{H^+} of H^+ ; (2) the Avogadro constant N_{A} , with $k\cdot N_{\text{A}}\cdot T = RT$ [$\text{J}\cdot\text{mol}^{-1}$] as the motive force quantum in the molar amount format: the mole is the MU for amount n_{H^+} of H^+ ; and (3) the elementary charge e , with $k\cdot e^{-1}\cdot T = fT$ [$\text{J}\cdot\text{C}^{-1}$] as the motive force quantum in the electrical charge format: the coulomb is the MU for electric charge Q_{p^+} , and exergy per charge is the voltage [V]. Imparting on z_{H^+} the deserved visibility in conjunction with e and N_{A} leads to the expression zeN_{A} . The notion of zeN_{A} conveys meaning to the pmF equation. This long journey sets the stage for applying the pmF equation to the topic of respiratory control.

Section 8.4: Proton leak flux in LEAK respiration is a non-linear function of the pmF . How can we explain the non-ohmic nature of this flux-force relation? *Four protonmotive theorems* are derived from first principles and integrated in the development of the concept of protonmotive *pressure*, to explain the observed convex shape of the dependence of LEAK respiration on protonmotive *force* (Figure 8.12).

1. The molecular or microscopic approach of Boltzmann has been pursued by Einstein, Smoluchowski and Sutherland in their analyses of diffusion gradients, providing a quantum mechanical or statistical explanation for the non-linear dependence of steady-state flux of diffusion on the chemical potential gradient $d\mu_{\text{X}}/dz$ [$\text{J}\cdot\text{mol}^{-1}/\text{m}$]. For entity X as an uncharged particle, the chemical potential gradient is the driving *force* of vector diffusion. This provides a link between thermodynamics and kinetics. Fick's law of diffusion relates flux linearly to the *concentration* gradient, which is recognized by introducing the motive force quantum kT (or RT) into Fick's diffusion equation: $J_{\text{dX}} = -D\cdot dc_{\text{X}}/dz = -u\cdot RT\cdot dc_{\text{X}}/dz = -u\cdot d\mu_{\text{X}}/dz$. The pressure gradient is $d\Pi_{\text{X}}/dz = RT\cdot dc_{\text{X}}/dz$ [$\text{Pa}\cdot\text{m}^{-1}$]. Flux is a linear function of the diffusive *pressure* gradient $d\Pi_{\text{X}}/dz$, proportional to the mobility u .
2. van't Hoff's concept of osmotic pressure in a compartmental system with a semipermeable membrane requires integration of the pressure gradient across the compartmental boundary, obtaining the osmotic *pressure difference* $\Delta_d\Pi_{\text{X}}$ [Pa]. This isomorphic diffusion pressure is proportional to the concentration difference Δc_{X} [mol], and Fick's law maintains linearity. Integration of the diffusive potential gradient, however, reveals a non-linear dependence of flux on the driving force $\Delta_d\mu_{\text{X}}$ [$\text{J}\cdot\text{mol}^{-1}$] of diffusion, where the diffusive *potential difference* is the isomorphic force.
3. The concept of protonmotive force is extended to protonmotive pressure. In addition to the partial diffusion pressure difference there must be an isomorphic partial electric pressure difference. This follows from Mitchell's Module 3 and the Nernst equation, coupling H^+ translocation to counterion translocation and thus incorporating the total electric p^+ potential difference in addition to H^+ and ΔpH into the concept of protonmotive pressure. Thus a non-linear dependence of flux on protonmotive force can be predicted from first principles. The shape, however, is concave – in plain contrast to all experimental evidence on a convex relationship.
4. A concave shape is obtained when calculating the relation between force and pressure in a compartmental electrochemical system with equal volumes on either side of the semipermeable membrane. Why are mitochondria small? Expanding the extramitochondrial volume fraction, the concave shape is gradually converted into a convex relation between compartmental H^+ flux and protonmotive force, thus explaining experimental observations on the basis of the four protonmotive theorems summarized as the concept of protonmotive pressure.

8.1. Vectorial and scalar flows and forces

8.1.1. The protonmotive force and forces in physics

The protonmotive force pmF across the mtIM is a characteristic of respiratory states, is maximum in the resting LEAK state, high in the OXPHOS state to drive phosphorylation of ADP to ATP, and is largely dissipated in the noncoupled ET state (Table 2.1). The pmF is the sum of two partial isomorphic forces: $\Delta_d F_{H^+} + \Delta_{el} F_{p^+}$. The force $\Delta_d F_{H^+}$ of H^+ diffusion (d) is linked to the *diffusive* H^+ potential difference $\Delta\mu_{H^+}$. The electric force $\Delta_{el} F_{p^+}$ is linked to the *electric* potential difference $\Delta\Psi_{p^+}$ expressed per proton charge p^+ . The symbol $\Delta_m F_{H^+}$ for the pmF includes the subscript m for *motive*. The motive flux is driven by the partial forces of H^+ diffusion and electric p^+ propulsion, summarized in the pmF equation,

$$\Delta_m F_{H^+} = \Delta_d F_{H^+} + \Delta_{el} F_{p^+} \quad [J \cdot mol^{-1}] \text{ or } [J \cdot C^{-1}] \quad 8.1$$

The iconic symbols in Eq. 8.1 can be translated into various more conventional symbols of the pmF , considering two equivalent formats: $\Delta\tilde{\mu}_{H^+}$ [$J \cdot mol^{-1}$] and Δp [V],

$$\text{amount format:} \quad \Delta\tilde{\mu}_{H^+} \equiv \Delta\mu_{H^+} + \Delta\Psi_{p^+} \cdot (z_{H^+} \cdot F) \quad [J \cdot mol^{-1}] \quad 8.2a$$

$$\text{charge format:} \quad \Delta p \equiv \Delta\mu_{H^+} \cdot (z_{H^+} \cdot F)^{-1} + \Delta\Psi_{p^+} \quad [J \cdot C^{-1}] = [V] \quad 8.2b$$

$$\text{conversion:} \quad \Delta\tilde{\mu}_{H^+} = \Delta p \cdot (z_{H^+} \cdot F) \quad [J \cdot mol^{-1}] \quad 8.2$$

The charge format of Δp (exergy per motive charge of H^+ [$J \cdot C^{-1}$]) is converted into the amount format $\Delta\tilde{\mu}_{H^+}$ (exergy per motive amount of molecules H^+ [$J \cdot mol^{-1}$]), by multiplication with the product $(z_{H^+} \cdot F)$. z_{H^+} is the proton p^+ charge number of the hydrogen ion H^+ . The Faraday constant F (ratio of chemical and electrical units [$\frac{J \cdot mol^{-1}}{V} = \frac{C}{mol}$]) converts the chemical unit [$J \cdot mol^{-1}$] to the electrical unit [V]=[$J \cdot C^{-1}$].

Physicochemical equality (=; Eq. 8.1) is distinguished from merely numerical equivalence (\equiv ; Eq. 8.2), where the stoichiometric numbers ν_i are missing (Eq. 8.25). Compared to the classical Eq. 1.1, the charge number of H^+ , $z_{H^+} = 1$, is included in Eq. 8.2. Mathematically, multiplication or division by 1 can be dropped, but physicochemically, consideration of the dimensionless terms $z_{H^+} = 1$ and $|\nu_i| = 1$ is far from trivial.

According to its definition in physics, a potential difference and as such neither the pmF nor $\Delta\mu_{H^+}$ and $\Delta\Psi_{p^+}$ are forces *per se* (IUPAC: Cohen et al 2008). Forces as defined in physics, F [$N \stackrel{\text{def}}{=} J \cdot m^{-1} = m \cdot kg \cdot s^{-2}$], describe the interaction between particles as vectors with direction of a gradient in space. These forces cause an acceleration — a change in motion, thus increasing the velocity of the particles in the spatial direction of the force. The three fundamental forces are the gravitational, electroweak (combining electromagnetic and weak nuclear) and strong nuclear forces. In contrast to the forces of physics with *spatial direction* in gravitational and electromagnetic fields, isomorphic *motive forces* (1) are not necessarily directed in geometrical but alternatively in compartmental space, (2) are expressed in different formats, and (3) have format-specific units different from F [N]. Motive forces include the compartmental forces $\Delta_{tr} F_X$ with *compartmental direction* of the energy transformation (Figure 8.1) and probabilistic microscopic distribution of particles X in motion without macroscopic drive of external fields. Localized electric fields are involved, when charged particles translocate across compartmental barriers. $\Delta_{el} F_{p^+}$ is an internal electric force due to internal, compartmental proton charge distribution, whereas external electric and gravitational fields are not considered.

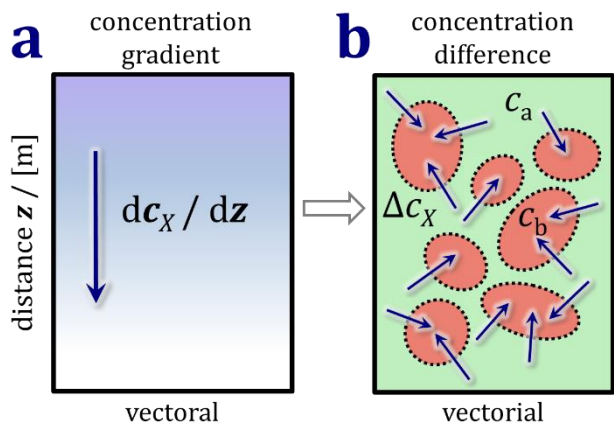


Figure 8.1. Diffusion in continuous and discontinuous systems. (a) Concentration gradient of substance X with spatial direction, $dc_X/dz < 0$ [mol·m⁻³/m] (only direction z is considered). (b) Concentration difference of substance X , $\Delta c_X = c_b - c_a$ [mol·m⁻³], with compartmental direction from the exit phase a (green) to the entry phase b (red) separated by semipermeable membranes. Arrows show net flux of motive entity $X_a \rightarrow X_b$.

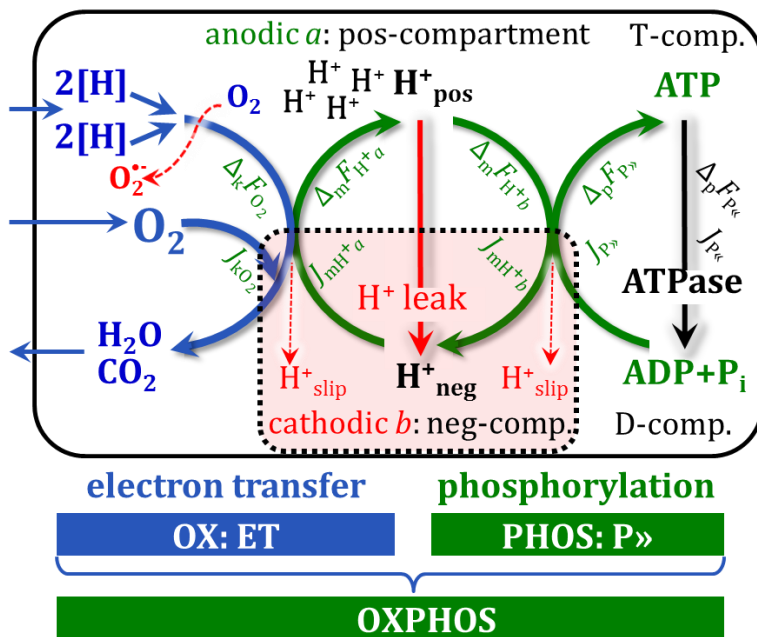


Figure 8.2. The hydrogen ion circuit and coupling in oxidative phosphorylation (OXPHOS). O_2 flux J_{kO_2} (catabolic ET pathway k), coupled to flux J_{pP} (phosphorylation pathway P) forming ATP from ADP. H^+ pumps of the ET pathway translocate H^+ into the positive (internal anodic a ; pos) compartment. J_{mH^+a} generates $\Delta_m F_{H^+a}$ as the output pmF . F-ATPase is coupled to inward H^+ flux J_{mH^+b} into the negative (cathodic b ; neg) compartment. Phosphorylation of ADP is

driven by the input pmF , $\Delta_m F_{H^+b} = -\Delta_m F_{H^+a}$. $2[H]$ indicates reduced hydrogen equivalents of CHNO-fuel substrates that provide the chemical input force $\Delta_k F_{O_2}$ [kJ/mol O_2] of the catabolic reaction k with oxygen (Gibbs energy of reaction per mole O_2 consumed in reaction k), typically in the range of -460 to -480 kJ/mol (-1.2 V). The output force is the phosphorylation potential difference $\Delta_p F_{P\gg}$ (ADP phosphorylated to ATP), which ranges *in vivo* from about 48 to 62 kJ/mol under physiological conditions (Gnaiger 1993b). Fluxes are expressed per volume V [m³] of the experimental system. The system defined by the boundaries (full black line) is not a black box, but is analysed as a compartmental system. The cathodic phase b (neg-compartment, enclosed by the dotted line) is the matrix space, separated by the mtIM from the anodic phase (pos-compartment). ADP+P_i and ATP are the substrate- and product-compartments (scalar D-comp. and T-comp.), respectively. Chemical potentials of all substrates and products involved in the scalar reactions are measured in the pos-compartment for defining the scalar forces of reactions k and p , $\Delta_k F_{O_2}$ and $\Delta_p F_{P\gg} = -\Delta_p F_{P\ll}$. Steady-state H^+ turnover $J_{H^+\infty}$ and steady-state ATP turnover $J_{P\infty}$ maintain a constant $\Delta_m F_{H^+}$ and $\Delta_p F_{P\gg}$, when $J_{mH^+\infty} = J_{mH^+a} = J_{mH^+b}$, and $J_{P\infty} = J_{pP} = J_{pP\ll}$.

It is important to distinguish between vectorial, vectorial, and scalar processes with isomorphic flows and forces: (1) *Vectorial* fluxes are translocations as functions of *gradients* with direction in geometric space in continuous systems (Figure 8.1a). Vectorial fluxes are normalized per cross-sectional area perpendicular to the gradient (Section

8.4.1). (2) *Vectorial* fluxes are translocations in discontinuous systems with *compartmental differences*. A membrane separates the compartments (*a* and *b*; Figure 8.1b and 8.2). The conjugated motive forces are due to potential *differences* between compartments, without any detailed information on the *gradients* across the mtIM nor its thickness (about 6 nm). (3) *Scalar* fluxes are transformations of chemical reactions in *homogenous* systems, where substrate and product compartments are separated energetically (Figure 8.3). In mt-electron transfer the catabolic flux of scalar reactions, collectively measured as O₂ flux J_{kO_2} , is coupled to vectorial transmembrane H⁺ flux J_{mH^+} through the H⁺ pumps CI, CIII and CIV (Figure 8.2). Vectorial and scalar fluxes [$\text{mol}\cdot\text{s}^{-1}\cdot\text{m}^{-3}$] are normalized per volume V [m^3] of the experimental system (Figure 8.3).

Both vectorial and scalar transformations have compartmental but not spatial direction. Arrows define the compartmental direction of translocation between the negative compartment (matrix space; negative, neg-compartment) and the positive compartment (pos-compartment; Figure 8.2). Arrows may point upwards or downwards, right or left, without implication on actual directions in space (Figure 8.1b to 8.3). The pos-compartment is neither above nor below the neg-compartment in a spatial sense, but is visualized in the upper position in Figure 8.2. Likewise, a chemical reaction does not proceed ‘from left to right’. We rely on spatial-mechanical analogies for graphical representations, atomic models for visualization, physicochemical equations for quantitative relations, and isomorphic analyses for unification of abstract concepts.

Complementary to the attempt towards unification of fundamental forces defined in physics, the concepts of Nobel laureates Lars Onsager, Erwin Schrödinger, Ilya Prigogine and Peter Mitchell unite — even if expressed in apparently unrelated terms — the diversity of *generalized* or *isomorphic flux-force* relationships, the product of which links to entropy production and the Second Law of thermodynamics (Schrödinger 1944; Prigogine 1967). A *motive force* is the derivative of potentially available or ‘free’ energy (exergy) per advancement of a *motive entity* (Eq. 1.7b). The first account of a *motive force* in energy transformation can perhaps be traced back to the Peripatetic school around 300 BC in the context of moving a lever, up to Newton’s motive force proportional to the alteration of motion (Coopersmith 2010). As a generalization, isomorphic motive forces are considered as *entropic forces* in physics (Wang 2010).

8.1.2. Stoichiometry and advancement in closed and open systems

Vectorial H⁺ translocation from the neg-compartment to the pos-compartment (Figure 8.2) is related to work (*erg* = work) that must be performed to lift the hydrogen ion H⁺ from the *ergodynamic* compartment with lower electrochemical potential to the compartment with higher electrochemical potential. The terms *compartment* and *phase* can be considered as synonyms, but their conventional meanings vary with isomorphic context. The direction of vectorial and scalar transformations is defined by arrows pointing from the exit phase to the entry phase ($A\rightarrow B$) or by stoichiometric numbers ν_i , that are negative for exit and positive for entry ($0=-1A +1B$; Figure 8.3). In a *scalar* chemical reaction substrates are assigned to the ergodynamic exit compartment, and products to the ergodynamic entry compartment. This is isomorphic to *vectorial* translocation of a substance *X* diffusing from the exit to the entry compartment (Figure 8.3). O₂ is a substrate in respiratory O₂ consumption, which together with the CHNO-fuel substrates comprises the substrate or exit compartment of the catabolic reaction (Figure 8.2). Scalar O₂ flux is coupled to vectorial translocation flux, which requires an isomorphic description of scalar and vectorial fluxes and the formal analysis of open systems.

Substance transformed in reaction (r) **Substance transferred in diffusion (d)**

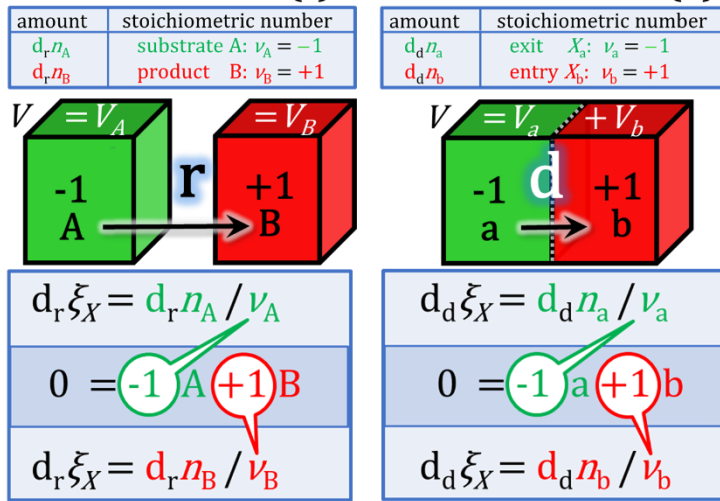


Figure 8.3. Stoichiometry and advancement in reaction r (A→B), and diffusion d of particles X from phase a to b (a→b). Stoichiometric numbers v_i ($0 = -1A + 1B$) define the direction from the exit to the entry phase (Eq. 8.4). A is the substrate and B the product of reaction. a and b are substance X in the exit and entry phase, respectively. $d_{tr}\xi_X$ is the advancement of reaction or diffusion (Eq. 8.5). V is the volume of the system; for aqueous reactions $V=V_A=V_B$, but for diffusion $V=V_a+V_b$.

The change $d_n n_X$ (indicating $d_n n_{X_a}$ or $d_n n_{X_b}$; briefly $d_n n_a$ or $d_n n_b$) in the amount of substance X in ergodynamic compartment a or b is distinguished from dn_X , which is the sum of all internal transformations $d_i n_X$ and external exchange $d_e n_X$ across the system boundaries. For an open system, this is written as a balance equation (Prigogine 1967):

$$\text{open:} \quad dn_X = d_i n_X + d_e n_X \quad [\text{mol}] \quad 8.3$$

The treatment of open versus closed systems separates apparently incompatible styles of thinking (Gnaiger 2009). As illustrated in Figure 8.3 for reaction and diffusion, the concept of open and closed systems with volume V is extended to compartments with volumes V_a and V_b . Open compartments may be contained in an open or closed system. In an open system at steady state, all changes due to internal transformations are compensated by external exchange, such that the properties remain unchanged in the system, $dc_X = dn_X/V = 0$, and in each compartment, $dc_a = dn_a/V_a = 0$ and $dc_b = dn_b/V_b = 0$. At steady state,

$$\text{steady state:} \quad d_i n_X = -d_e n_X \quad [\text{mol}] \quad 8.3a$$

The boundaries of a closed compartment are impermeable for all substances, such that all external exchanges are zero, $d_e n_X = 0$. For a closed (sub)system, therefore,

$$\text{closed:} \quad dn_X = d_i n_X \quad [\text{mol}] \quad 8.3b$$

$$\text{general:} \quad dn_X = \sum_j d_j n_X + d_e n_X \quad [\text{mol}] \quad 8.3c$$

Several transformations j — such as reaction r, diffusion d, or generally tr — proceed simultaneously in the cell. $d_i n_X = \sum_j d_j n_X$ is the sum of all partial transformations j exerting an effect on n_X in the system as a whole and in a particular compartment.

Subscript X in $d_r n_X$ represents substrate A or product B in Figure 8.3, whereas $d_a n_a$ and $d_b n_b$ represent substance X in compartment a or b. To simplify, upper case letters (A, B, X) may be used for reaction and diffusion in the general case of transformations tr. The *stoichiometric number* v_X yields a normalization of $d_{tr} n_X$ ($d_i n_X$ in Eq. 8.3):

$$\frac{d_{tr} n_A}{d_{tr} n_B} = \frac{v_A}{v_B} \quad v_A = \frac{d_{tr} n_A}{d_{tr} n_B} \cdot 1 \quad [v_B \stackrel{\text{def}}{=} 1] \quad v_A = \frac{d_{tr} n_A}{d_{tr} n_B} \cdot -1 \quad [v_B \stackrel{\text{def}}{=} -1] \quad 8.4$$

In a closed system (Eq. 8.3b), the amount n_A or n_a declines as the amount n_B or n_b increases as a function of the advancement of reaction or diffusion (tr; Figure 8.4a). If v_X is constant for a compound X under observation, then there is a fixed stoichiometry based on the conservation of mass and elemental composition. A→B can be written as $0 = -1 A + 1 B$

(Figure 8.3). Either A or B may be taken as a reference for normalization of changes in the exit and entry compartment. If B is taken as the reference and v_B is assigned the value +1, then B is defined as a product (entry phase; $A \rightarrow B$). Photosynthetic O_2 flux is typically expressed with O_2 as the reference and $v_{O_2}=+1$ (product, entry phase). For respiration J_{kO_2} , $v_{O_2}=-1$ (substrate, exit phase). The assignment +1 or -1 defines the compartmental direction of the transformation, $A \rightarrow B$ ($v_B=+1$) or $B \rightarrow A$ ($v_B=-1$). In addition, it also defines the stoichiometric form. Take oxidation of dissolved succinate S to malate M as example: $C_4H_4O_4^{2-}(aq) + 0.5 O_2(aq) \rightarrow C_4H_4O_5^{2-}(aq)$. Assignment $v_{O_2}=-1$ as a reference yields $v_S=-2$ and $v_M=2$, and the equation has the stoichiometric form $2 C_4H_4O_4^{2-} + 1 O_2 \rightarrow 2 C_4H_4O_5^{2-}$. When measuring $\Delta_k c_{O_2} = -100 \mu M$ for the S-pathway and observing complete conversion of succinate into fumarate and malate, then $\Delta_k c_S = -200 \mu M$ at $v_S = -2$. If the fumarate/malate ratio is not constant, then there is no fixed malate/ O_2 stoichiometry.

The stoichiometric number v_X is key for defining the isomorphic advancement of internal transformation $d_{tr}\xi_X$ and internal flow defined for closed and open systems,

$$d_{tr}\xi_X = d_{tr}n_X \cdot v_X^{-1} \quad v_X = |1| \quad [mol] \quad 8.5$$

The advancement may have a positive (forward) or negative (backward) sign for any reference stoichiometry. The corresponding flow of transformation is,

$$I_{trX} = d_{tr}\xi_X/dt = d_{tr}n_X/dt \cdot v_X^{-1} \quad v_X = |1| \quad [mol \cdot s^{-1}] \quad 8.6$$

Compartmental concentration changes in diffusion, $da_{Ca} = da_{na}/V_a$ and $da_{Cb} = da_{nb}/V_b$, are calculated for the compartmental volumes, but volume-specific flux $J_{d(a \rightarrow b)} = I_{d(a \rightarrow b)}/V$ is based on the total volume of the system, $V = V_a + V_b$ (Figure 8.3; Eq. 8.60).

8.2. Why is thermodynamics scary?

Our body has temperature sensors named temperature receptors. Therefore, temperature ‘makes sense’, but heat is a different story. Our bodies are chemical machines without specific organs to make sense of our chemistry — we can usually neither see nor hear or feel the ‘flow’ of a chemical transformation. Hence the world of biochemical transformations is abstract. Many terms of physical chemistry are borrowed from visible mechanics and perceptive fluid dynamics — such as flow (Eq. 8.6) —, but do not intuitively ‘make sense’. Typical simplified introductory chapters on thermodynamics in biochemistry and bioenergetics are not simple but are fundamentally wrong and do not make sense. Isothermal systems are considered here for simplification, with a focus on exergy transformations proceeding in open systems far from equilibrium at constant temperature. Enthalpy changes are the realm of calorimetry (Gnaiger et al 2000), but are not discussed here. Without covering measurements of heat (*therm-*), the focus is on work (*erg-*, exergy rather than energy). *Ergodynamics* is thus the more appropriate term compared to *thermodynamics*. In any case *dynamics* — as introduced by Gottfried Leibnitz — is the key, linked to power ($\deltaύναμις$; dynamis) and force. The term affinity for the force of chemical reactions can be traced back to alchemy. Affinity was conceived of as the disposition towards conjunction of two substances, which inspired Isaac Newton in his development of the concept of force. It took more than two centuries after the debate between Leibnitz and Newton to disentangle the concepts of force and energy in physics. Astonishingly, confusion remains up to now in physical chemistry when talking about reaction Gibbs energy mixed up with affinity, chemical potential, and the partial derivative of Gibbs energy per advancement of reaction (isomorphic force). This is scary.

8.2.1. Chemical potential derived from pressure

Diffusion of a dissolved substance X at high dilution is analysed on the basis of van't Hoff's concept of osmotic pressure Π_X [Pa], in terms of concentration of X , $c_X \stackrel{\text{def}}{=} n_X \cdot V^{-1}$ [mol·m⁻³], where the total volume V [m³] is approximately equal to V_{H_2O} , which is the volume of water as the solvent in dilute aqueous solutions,

$$\Pi_X = RT \cdot n_X \cdot V^{-1} = RT \cdot c_X \quad [\text{Pa} \stackrel{\text{def}}{=} \text{J} \cdot \text{m}^{-3}] \quad 8.7a$$

RT [J·mol⁻¹] — the product of the gas constant and absolute temperature — is pressure divided by concentration (Tables 8.2 and 8.3). Eq. 8.7a is isomorphic to the ideal gas equation, $p \cdot V = n \cdot RT$ [J], where p [Pa] is the gas pressure or barometric pressure in a total volume V containing a total of n moles of a pure ideal gas.

This section relates the concentration (strictly activity; Eq. 8.8) of a dissolved substance to its chemical potential, to (1) provide a direct link between experimental measurements — such as the activity of H⁺ determined with a pH electrode or dissolved O₂ measured with an electrochemical oxygen sensor — and chemical potential as one of the components of the protonmotive force and ergodynamic OXPHOS analysis (Table 8.4), (2) derive the logarithmic function in the expression of chemical potential from first principles (Eq. 8.9), and thus (3) set the stage for the concept of isomorphic force and pressure (Eq. 8.29; Eq. 8.53). The isomorphic method uses mathematical expressions complementary to a focus on the terms and units of physicochemical quantities. The ideal gas law at low pressure is taken as a reference for the analysis of dilute solutions. This yields an outline of the basic physicochemical concept, which then can be elaborated further with respect to details that are important at higher concentration and pressure.

The pressure p_X of a gas X is related to absolute temperature T [K] and concentration c_X [mol·m⁻³] by the ideal gas law,

$$p_X = RT \cdot \frac{n_X}{V} = RT \cdot c_X = RT \cdot \frac{1}{V_{nX}} \quad [\text{Pa} \stackrel{\text{def}}{=} \text{J} \cdot \text{m}^{-3}] \quad 8.7b$$

The gas equation (Eq. 8.7b) and the van't Hoff equation on osmotic pressure in aqueous solutions (Eq. 8.7a) are classical paradigms of isomorphic pressure-concentration relationships: the same formalism can be applied to gases and dilute solutions to derive the definition of chemical potentials. The inverse of concentration is the molar volume. V_{nX} is the iconic symbol for the volume per mole of the ideal gas X (Eq. 8.7b). The quantity and symbol V_{nX} (volume per amount X [m³·mol⁻¹]) is distinguished from V_X (volume of X [m³]). The subscript X indicates the nature of the gas in V_X , c_X and p_X , whereas the subscript nX indicates the normalization per mole X .

The relative activities a_X of a gas or a dissolved substance X are measured by polarographic oxygen sensors and ion selective electrodes (pH and TPP⁺),

$$a_X = \frac{c_X}{c^\circ} \cdot \gamma_X \quad [\text{mol} \cdot \text{L}^{-1} / \text{mol} \cdot \text{L}^{-1}] \quad 8.8$$

$c^\circ = 1 \text{ mol} \cdot \text{L}^{-1}$ is the standard concentration when concentration is expressed in the same units [mol·L⁻¹]. γ_X is the activity coefficient of X . Activities are numerically equal to concentrations when $\gamma_X = 1$, which applies to gases at low pressure and dissolved substances in dilute solutions (except for dissolved gases; see solubility in Chapter 1.3). Logarithmic functions of concentration must be expressed as dimensionless activities. However, the more familiar term concentration will be used, although chemical potentials are strictly defined in terms of activities. Even when concentrations deviate from activities, their ratios are entirely equivalent, if the activity coefficients are identical in both phases to which the quantities in the numerator and denominator of the ratios apply.

Pressure-volume work $p \cdot dV$ [J] performed by a reversible system of an ideal gas X and expressed per mol X , can be regarded as a 'molar exergy' $d_V \mu_X$ [J·mol⁻¹] (work per amount of gas, i.e. chemical potential), at constant temperature. The molar pressure-volume work is the integral at constant pressure, $p_X = \text{constant}$ [Pa] (e.g. O₂ pressure p_{O_2}), over the molar volume between initial and final molar volumes, V_{n1} and V_{n2} [m³·mol⁻¹],

$$-\Delta_V \mu_X = \int_{V_{n1}}^{V_{n2}} p_X \cdot dV_{nX} \quad [\text{J} \cdot \text{mol}^{-1}] \quad 8.9a$$

μ_X is the chemical potential of the gas; $\Delta_V \mu_X$ is the partial change of chemical potential in the system due to a change in molar volume, $\Delta V_{nX} = V_{n2} - V_{n1}$, as a function of pressure. With an increase in gas volume the $p \cdot dV$ work done on the surroundings is positive; therefore, $\Delta_V \mu_X$ seen from the point of view of the system is negative, i.e. exergonic. The chemical potential change of the gas (system) is reversibly transformed to the $p \cdot dV$ work received by the surroundings (environment). This is visualized in classical thermodynamics by a system consisting of a cylinder with the gas moving a frictionless piston of zero weight. The transformation is reversible when the process can be stopped and reversed, re-establishing all initial conditions for the system and the surroundings.

Substitute p_X from Eq. 8.7 into Eq. 8.9b,

$$\Delta_V \mu_X = -RT \cdot \int_{V_{n1}}^{V_{n2}} \frac{dV_{nX}}{V_{nX}} \quad [\text{J} \cdot \text{mol}^{-1}] \quad 8.9b$$

Integration in Eq. 8.9b uses the only more 'advanced' mathematical equation required in the present context, summarized in Section A1 on fundamental equations,

$$\int_{x_1}^{x_2} \frac{dx}{x} = \ln x_2 - \ln x_1 = \ln \frac{x_2}{x_1} \quad 8.10$$

This integration is the basis for the logarithmic relation between chemical potential and concentration or activity (Eq. 8.8),

$$\Delta_V \mu_X = -RT \cdot \ln \frac{V_{n2}}{V_{n1}} \quad [\text{J} \cdot \text{mol}^{-1}] \quad 8.11$$

$$\Delta_V \mu_X = RT \cdot \ln \frac{c_2}{c_1} = RT \cdot (\ln a_2 - \ln a_1) = RT \cdot \Delta_V \ln a_i \quad [\text{J} \cdot \text{mol}^{-1}] \quad 8.12$$

Since a_i is dimensionless, $\ln(c_i/c^\circ)$ is replaced by $\ln(a_i)$ in many equations, as required by the fact that logarithms can be calculated only for dimensionless ratios without units. Concentration ratios and activity ratios are equal and independent of the (frequently unknown) activity coefficient, if $y_1=y_2$ (Eq. 8.8).

$\ln \frac{V_{n2}}{V_{n1}}$ is positive for volume expansion ($\frac{V_{n2}}{V_{n1}} > 1$), negative for compression ($\frac{V_{n2}}{V_{n1}} < 1$), and zero for $\frac{V_{n2}}{V_{n1}} = 1$. In other words, the change of chemical potential in X is negative for expansion (exergonic dilution) and positive for compression (endergonic increase of concentration).

8.2.2. Chemical potential, stoichiometry, and metabolic force

The chemical potentials μ_A and μ_B (r: reactants; A→B) or μ_a and μ_b (d: motive substance X ; a→b) are a function of the standard potentials μ_X° in the standard state and the actual activities a_X (Figure 8.4b),

$$\mu_X = \mu_X^\circ + RT \cdot \ln a_X \quad [\text{J} \cdot \text{mol}^{-1}] \quad 8.13$$

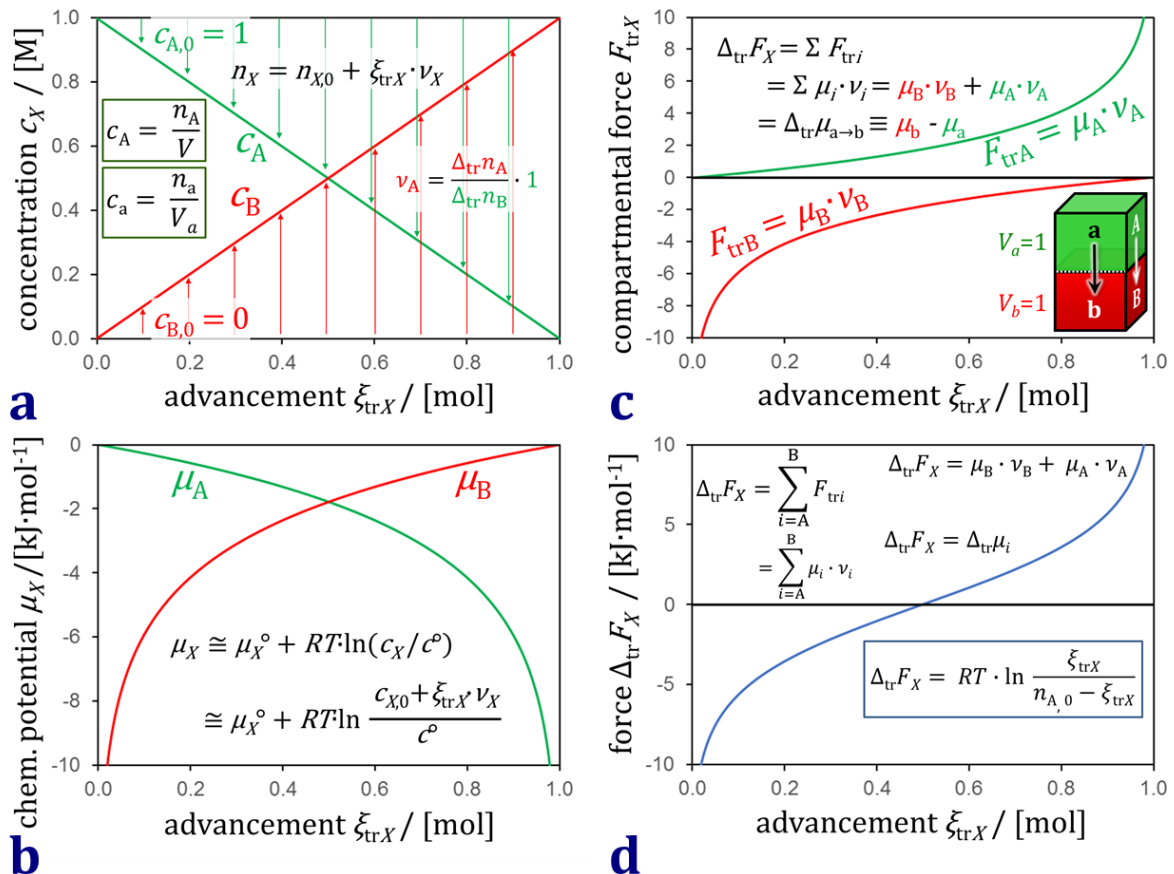


Figure 8.4. Concentration [mol·L⁻¹] and chemical potential [kJ·mol⁻¹] in A and B as a function of advancement in a closed system at constant temperature and pressure. The initial concentrations are $c_{A,0} = 1$ mol·L⁻¹, and $c_{B,0} = 0$ mol·L⁻¹. c_X/c° equals the relative activity a_X at an activity coefficient of 1; $c^\circ = 1$ mol·L⁻¹ is the standard concentration. The relations are shown for the simple case of $\mu_A^\circ = \mu_B^\circ = 0$; the equilibrium constant equals the ratio of activities at equilibrium, $K_{tr} = \frac{\bar{a}_B}{\bar{a}_A} = 1$ (Eq. 8.16b). The compartmental volumes V_i are identical; for tr=r: $V = V_A = V_B = 1$ L; for tr=d: $V = V_a + V_b = 2$ L (Figure 8.3).

In the initial state (Figure 8.4b), the chemical potential in B is negative infinite or undefined, when $c_{B,0} = 0$. The compartmental force in A and B is the *stoichiometric chemical potential* $F_{trX} = \mu_X \cdot \nu_X$ (Figure 8.4c). The force of reaction or diffusion is numerically equal to the difference of chemical potentials in B and A, $\Delta_{tr}F_X \equiv \Delta\mu_X = \mu_B - \mu_A$. This explains the Δ in the symbol $\Delta_{tr}F_X$. The equation, however, is physicochemically incomplete, since the stoichiometric number is missing. $\Delta_{tr}F_X \equiv \Delta\mu_X$ has to be replaced by the isomorphic motive force equation, retaining the delta in the symbol $\Delta_{tr}F_X$, but defining the forces of compartmental transformation as sums of *stoichiometric potentials* (Figure 8.4d),

$$\Delta_{tr}F_X = \sum_i \mu_i \cdot \nu_i = \left(\frac{\partial G}{\partial_{tr}\xi_X} \right)_{T,p} \quad [\text{J} \cdot \text{mol}^{-1}] \quad 8.14$$

The forces of vectorial diffusion and scalar chemical reactions are isomorphic. *Protonmotive (pm)* means that there is a potential for the movement of H⁺, and *force (F)* is a measure of the potential for motion. Motion is relative and not absolute (Principle of Galilean relativity); likewise there is no absolute potential, but the *pmF* — an isomorphic force — is a stoichiometric potential difference. Inserting Eq. 8.13 into Eq. 8.14 yields (for logarithmic functions, see Section A1),

$$\Delta_{tr}F_X = \sum_i (\mu_i^\circ \cdot \nu_i) + \sum_i RT \cdot \ln a_i^{\nu_i} = \Delta_{tr}F_X^\circ + \Delta_{tr}F_X^\# \quad [\text{J} \cdot \text{mol}^{-1}] \quad 8.15$$

The force is partitioned into two terms: (1) a concentration-independent part on the standard state at standard concentrations, $\Delta_{tr}F_X^\circ = -RT \cdot \ln K_{tr}$, linked to the equilibrium constant K_{tr} ; (2) a concentration-dependent part $\Delta_{tr}F_X^\#$ linked to the mass action ratio M_{tr} . At equilibrium the force is zero, $\Delta_{tr}F_X = 0$, at the minimum of Gibbs energy (exergy; Figure 8.5). Then the two terms in Eq. 8.15 are zero, or they cancel, $K_{tr} \stackrel{\text{def}}{=} M_{tr,eq}$. Equilibrium activities are \bar{a}_X . In general, close or far from equilibrium,

$$\Delta_{tr}F_X^\circ = -RT \cdot \ln K_{tr} \qquad \Delta_{tr}F_X^\# = RT \cdot \ln M_{tr} \quad [\text{J} \cdot \text{mol}^{-1}] \quad 8.16a$$

$$K_{tr} = \prod_i \bar{a}_i^{v_i} \qquad M_{tr} = \prod_i a_i^{v_i} \quad 8.16b$$

$$\kappa_{tr} \stackrel{\text{def}}{=} \frac{M_{tr}}{K_{tr}} \quad 8.16c$$

$$\Delta_{tr}F_X = RT \cdot (\ln M_{tr} - \ln K_{tr}) = RT \cdot \ln \frac{M_{tr}}{K_{tr}} = RT \cdot \ln \kappa_{tr} \quad [\text{J} \cdot \text{mol}^{-1}] \quad 8.16$$

For diffusion between homogenous compartments *a* and *b* (Figure 8.4), the standard chemical potential of *X* is identical in the two phases, $\mu_a^\circ = \mu_b^\circ$, hence $K_d = 1$ and $\Delta_d F_X^\circ = 0$, which yields $\kappa_d \equiv M_d \equiv \frac{a_b}{a_a}$, and the force, $\Delta_d F_X \equiv RT \cdot \ln \frac{a_b}{a_a}$. The activity coefficients cancel in the ratio, if they are equal in the two phases, which justifies the approximation by concentration ratios (Eq. 8.8).

Assigning the stoichiometric numbers as $v_a = -1$ and $v_b = 1$ defines the direction of diffusion as (*a* → *b*). Distinguished from ΔpH , the *stoichiometric* pH difference $\Delta_{\text{d}} \text{pH}$ in compartmental diffusion and the logarithmic concentration ratio $\Delta_{\text{d}} \ln c_X$ are,

$$\Delta_{\text{d}} \text{pH} \stackrel{\text{def}}{=} \text{pH}_a \cdot v_a + \text{pH}_b \cdot v_b = -\log(c_a^{v_a} \cdot c_b^{v_b}) \equiv -\log \frac{c_b}{c_a} \quad 8.17a$$

$$\Delta_{\text{d}} \ln c_X \stackrel{\text{def}}{=} \ln c_a \cdot v_a + \ln c_b \cdot v_b = \ln(c_a^{v_a} \cdot c_b^{v_b}) \equiv \ln \frac{c_b}{c_a} \quad 8.17b$$

For arithmetic equations see Section A1. The partial diffusive force of H^+ transduction is the *chemical stoichiometric potential difference* $\Delta_d F_{\text{H}^+}$:

potential: $\mu_{\text{H}^+} = RT \cdot \ln a_{\text{H}^+} = -RT \cdot \ln(10) \cdot \text{pH} \quad [\text{kJ} \cdot \text{mol}^{-1}] \quad 8.18a$

difference: $\Delta \mu_{\text{H}^+} = -RT \cdot \ln(10) \cdot \Delta \text{pH} = -RT \cdot 2.303 \cdot (\text{pH}_b - \text{pH}_a) \quad [\text{kJ} \cdot \text{mol}^{-1}] \quad 8.18b$

force: $\Delta_d F_{\text{H}^+} = \mu_{\text{H}^+ \cdot a} \cdot v_a + \mu_{\text{H}^+ \cdot b} \cdot v_b = -RT \cdot 2.303 \cdot \Delta_{\text{d}} \text{pH} \quad [\text{kJ} \cdot \text{mol}^{-1}] \quad 8.18c$

8.2.3. Force and Gibbs energy

A glorious didactic pitfall in most famous textbooks of biochemistry and bioenergetics — and even of physical chemistry — is the confusing presentation of ΔG , propagating a mix-up of Gibbs *energy* change [J] and *force* of chemical reactions [J·mol⁻¹]. Using the symbol ΔG for the ‘*change in Gibbs energy for the reaction*’ [J·mol⁻¹] (Alberty and Daniels 1980) or $\Delta_r G$ for the ‘*reaction Gibbs energy*’ [J·mol⁻¹] (Cohen et al 2008) entails a confusion between force and energy, causes students to fail in making a distinction between intensive and extensive quantities, without recognizing the important difference of units, and ultimately leads to the unbelievable paradox of equating a *difference* and a *partial differential*, “ $\Delta G = \left(\frac{\partial G}{\partial \xi}\right)_{T,p}$ ”. Do not consider this as an equation, it is just scary.

In the present context, the IUPAC symbol $\Delta_r G$ is replaced by $\Delta_r F$ [J·mol⁻¹], with the name *Gibbs force of reaction* (Gnaiger 1993) or *affinity* (with a negative sign, $\Delta_r F = -A$; Prigogine 1967). In contrast, dG , ∂G , ΔG or $\Delta_r G$ [J] indicate (partial) Gibbs energy changes (frequently called Gibbs free energy or free energy) of the (closed) system or of the transformation in open systems at constant temperature and pressure under further specified conditions (Figure 8.5).

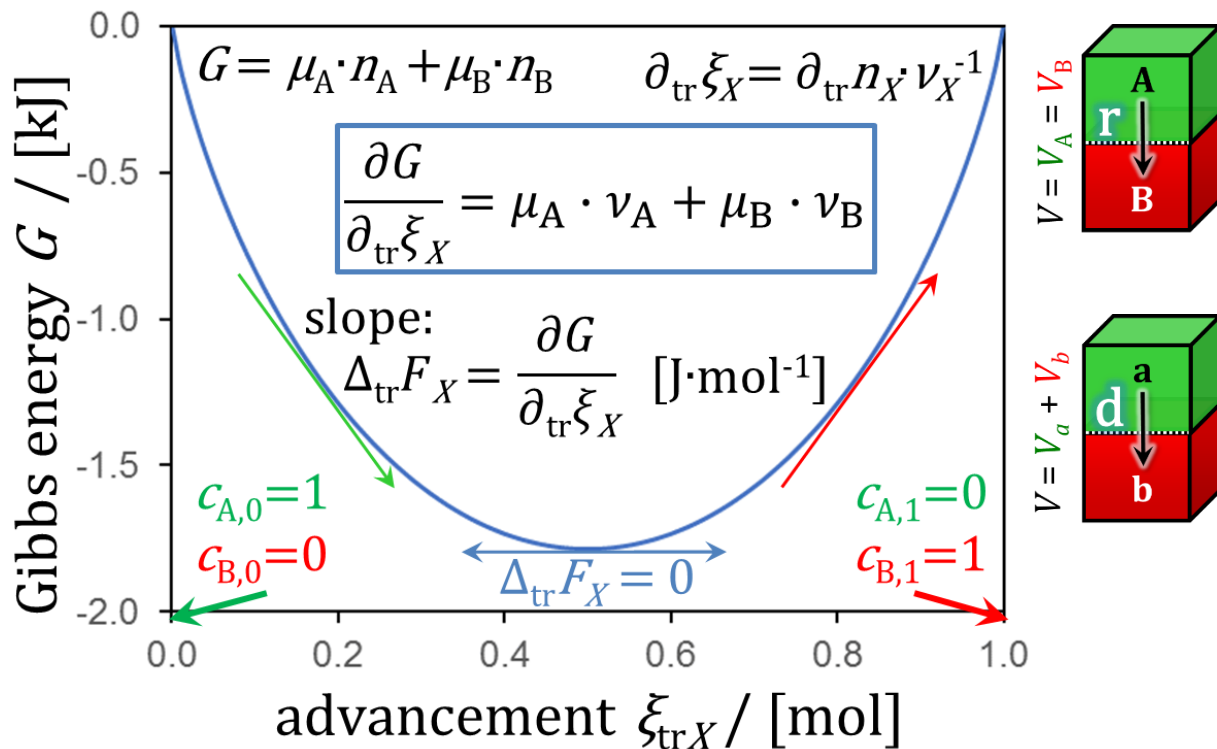


Figure 8.5. Gibbs energy as a function of advancement of transformation in a closed isothermal system at constant pressure. Force $\Delta_{\text{tr}}F_X = \partial G / \partial_{\text{tr}} \xi_X$ is the slope of Gibbs energy (exergy) of the system per advancement. For $\text{tr}=\text{r}$: advancement of reaction in a homogenous volume of 1 L. For $\text{tr}=\text{d}$: advancement of diffusion of an uncharged substance between homogenous compartments, $\text{a} \rightarrow \text{b}$, of equal volumes, $V_a = V_b = 1$ L. Equilibrium constants are $K_r = 1$ and $K_d = 1$ (Figure 8.4). At a negative slope of the transformation, the force $\Delta_{\text{tr}}F_X$ is negative such that the transformation is exergonic and proceeds spontaneously in the forward direction, $\text{A} \rightarrow \text{B}$. Equilibrium is obtained at the minimum of Gibbs energy, when $\Delta_{\text{tr}}F_X = 0$. In a closed system, the change $d_{\text{tr}}n_X$ of n_A or n_B due to the transformation equals the changes dn_X in the system. The stoichiometric number ν_X is positive for B and negative for A. Concentrations c_X are considered to be numerically equal to activities $a_X \equiv c_X / c^\circ$, where c° is the standard concentration [$1 \text{ mol} \cdot \text{L}^{-1} \stackrel{\text{def}}{=} 1 \text{ M}$].

The isomorphic scalar forces in irreversible thermodynamics (ergodynamics) are partial changes (derivatives) of Gibbs energy per advancement, $\Delta_{\text{tr}}F_X = \partial G / \partial_{\text{tr}} \xi_X$ (Figure 8.5). These isomorphic forces are sums of stoichiometric potentials (Eq. 8.14), numerically equal to differences Δ of potentials in the ‘substrate’ or exit compartment and the ‘product’ or entry compartment only if $\nu_i = |1|$ (Gnaiger 1993a). Figures 8.4 and 8.5 and corresponding equations show the derivation of the equivalent forms of isomorphic forces, as the sum (Σ) of stoichiometric (ν_i) potentials (μ_i).

8.2.4. Power, energy, force, and flux

Power (exergy per time) is flow times force [W]. The product of flows and forces is the basis of efficiency or irreversible entropy production. For any transformation tr (Eq. 8.14),

$$\text{Flow times force: } P_{\text{tr}} = I_{\text{tr}} \cdot \Delta_{\text{tr}}F \quad [\text{W}] \quad I_{\text{tr}} = d_{\text{tr}} \xi / dt = d_{\text{tr}} n_i / dt \cdot \nu_i^{-1} \quad 8.19a$$

$$\text{Flux times force: } P_{V,\text{tr}} = J_{V,\text{tr}} \cdot \Delta_{\text{tr}}F \quad [\text{W} \cdot \text{m}^{-3}] \quad J_{V,\text{tr}} = d_{\text{tr}} \xi / dt \cdot V^{-1} \quad 8.19b$$

Compartmental electric flow and diffusion proceed between compartments A and B. Electric flow is the net current I_{el} of positive charge in units ampere [$A \stackrel{\text{def}}{=} C \cdot s^{-1}$]. The electromotive force $\Delta_{el}F_{p^+}$ of proton charge (units volt [$V \stackrel{\text{def}}{=} J \cdot C^{-1}$]) is related to the electric potential difference, equivalent to $\Delta\Psi_{p^+}$ in Eq. 8.2.

$$\text{electric, el:} \quad P_{el} = I_{elp^+} \cdot \Delta_{el}F_{p^+} \quad [W] \quad \Delta_{el}F_{ep^+} = \partial G / \partial_{el}\xi_{ep^+} \quad [J \cdot C^{-1}] \quad 8.20a$$

$$\text{diffusion, d:} \quad P_d = I_{dx} \cdot \Delta_d F_x \quad [W] \quad \Delta_d F_{dx} = \partial G / \partial_d \xi_{dx} \quad [J \cdot \text{mol}^{-1}] \quad 8.20b$$

$$\text{reaction, r:} \quad P_r = I_{rx} \cdot \Delta_r F_x \quad [W] \quad \Delta_r F_{rx} = \partial G / \partial_r \xi_{rx} \quad [J \cdot \text{mol}^{-1}] \quad 8.20c$$

The power P_{tr} of a transformation is the partial Gibbs energy change per time, $P_{tr} = \partial_{tr}G / dt$ [$W \stackrel{\text{def}}{=} J \cdot s^{-1}$]. The total Gibbs energy change dG is the sum of all partial energy transformations ($dG = \sum \partial_{tr}G = \partial_{el}G + \partial_d G + \partial_r G + \dots$), which is a concept of eminent importance in the chemiosmotic theory. When the Gibbs energy change dG (differential) is integrated over a defined period of time Δt , it becomes ΔG (difference; Eq. 1.7 and 1.6).

A redox potential difference expresses electric force on the basis of displaced (motive) proton charge [$V \stackrel{\text{def}}{=} J \cdot C^{-1}$]. The chemical potential difference expresses chemical force on the basis of diffusing (d) or reacting (r) *amount of substance* [$Jol \stackrel{\text{def}}{=} J \cdot \text{mol}^{-1}$]. The unit 'Jol' — a unit for chemical force in analogy to the unit volt — does not exist officially. Yet it facilitates the distinction between Gibbs energy change [J] and Gibbs force [Jol], comparable to electric energy [J] and electric force [V] and mechanical energy [J] and mechanical force [$N \stackrel{\text{def}}{=} J \cdot m^{-1}$]. Logically, a *force* cannot be an *energy* difference ΔG [J]. A voltage [V] is not an electric energy difference [J]. Gibbs force is a stoichiometric chemical potential 'difference' (actually: sum; $\sum \mu_i \cdot \nu_i$) which can be converted to a stoichiometric electric potential difference by multiplication with the number of charges and the Faraday constant, $F = 96\,485 \text{ C} \cdot \text{mol}^{-1}$ or $F = 0.096 \text{ kJol} \cdot \text{mV}^{-1}$ (Table 8.1).

Force, exergy and power are positive when work is conserved in H^+ pumped uphill from the negative to the positive phase (high to low pH, low to high a_{H^+}). Output power requires coupling to input power (Figure 8.2). Input force, input exergy and input power have a negative sign, indicating the spontaneous downward or dissipative direction of energy transformation or (positive) entropy production of irreversible processes. The thermodynamics of irreversible processes describes all partial, simultaneous fluxes and forces in a consistent format of the dissipation function (Prigogine 1967). Iconic symbols unify the description of chemical and electrochemical energy transformations, achieving not only clarification but also unification compared to the divergent symbols and sign conventions in classical descriptions (Gnaiger 1993a).

8.2.5. Coupling and efficiency

In energetics (ergodynamics), coupling is defined as an energy transformation fuelled by an exergonic (downhill) input process driving the advancement of an endergonic (uphill) output. The (negative) output/input power ratio is the efficiency of a coupled energy transformation. At the limit of maximum efficiency of a completely coupled system, the (negative) input power equals the (positive) output power, when total power approaches zero at the maximum efficiency of 1. The process is fully reversible without dissipation of exergy, i.e. without entropy production, and the further advancement and net flows are zero.

A chemical reaction is exergonic, if the Gibbs energy change (exergy) of the reaction is negative at constant temperature and pressure. The sum of Gibbs energy changes of all internal transformations in a system cannot ever be positive, i.e. exergy is irreversibly

dissipated. Endergonic reactions are characterized by positive Gibbs energies of reaction and cannot proceed spontaneously in the forward direction as defined. The endergonic reaction $P \gg$ is coupled to exergonic catabolic reactions k , such that the total Gibbs energy change is negative, i.e. exergy must be dissipated for the reaction to proceed (Figure 8.2).

Exergy can be lost, but energy cannot be lost or gained in any internal process, which is the key message of the First Law of thermodynamics. Thus mitochondria are the sites of energy transformation but not energy production. Open and closed systems can gain energy and exergy only by external fluxes, i.e. uptake from the environment. Exergy is the potential to perform work. In the framework of flux-force relationships, the *partial* derivative of Gibbs energy per advancement of a transformation is an isomorphic force $\Delta_{tr}F$ (Eq. 8.14). In other words, force is equal to exergy per advancement of a motive entity (in integral form, this definition takes care of non-isothermal processes). This formal generalization represents an appreciation of the conceptual beauty of Peter Mitchell's innovation of the *pmF* against the background of the established paradigm of the electromotive force (emf or *emF*) defined at the limit of zero current (Cohen et al 2008).

Energetic coupling means that two processes of energy transformation are linked such that the input power P_{in} is the driving element of the output power P_{out} , and the (negative) out/input power ratio is the efficiency. When describing a system with volume V without information on the internal structure, the output is defined as the *external* work performed by the *total* system on its environment. Such a system may be open for any type of exchange, or closed and thus allowing only heat and work to be exchanged across the system boundaries. This is the classical black box approach of thermodynamics. In contrast, in a colourful compartmental analysis of *internal* energy transformations (Figure 8.2), the system is structured and described by definition of ergodynamic compartments (with information on the heterogeneity of the system) and analysis of separate parts, i.e. a sequence of *partial* energy transformations tr . At constant temperature and pressure, power per unit volume of the experimental chamber, $P_{V,tr} \stackrel{def}{=} P_{tr}/V$ [$W \cdot m^{-3}$], is the product of a volume-specific flux $J_{V,tr}$ and its conjugated force $\Delta_{tr}F$, and is directly linked to entropy production, $d_iS/dt = \sum_{tr} P_{tr}/T$ [$W \cdot K^{-1}$], as generalized by the thermodynamics of irreversible processes (Prigogine 1967; Gnaiger 1993a,b). Volume-specific output power of H^+ translocation and catabolic input power are (Figure 8.2),

$$\text{output:} \quad P_{V,mH^+a} = J_{mH^+a} \cdot \Delta_m F_{H^+a} \quad [W \cdot m^{-3}] \quad 8.21a$$

$$\text{input:} \quad P_{V,kO_2} = J_{kO_2} \cdot \Delta_k F_{O_2} \quad [W \cdot m^{-3}] \quad 8.21b$$

$\Delta_k F_{O_2}$ is the exergonic input force with a negative sign. $\Delta_m F_{H^+a}$ (translocation in the direction of the positive anodic compartment a) is the endergonic output force with a positive sign. Ergodynamic efficiency is the ratio of output/-input power, or the flux ratio times force ratio (Gnaiger 1993a,b),

$$\text{efficiency:} \quad \varepsilon = \frac{P_{mH^+a}}{-P_{kO_2}} = \frac{J_{mH^+a}}{J_{kO_2}} \cdot \frac{\Delta_m F_{H^+a}}{-\Delta_k F_{O_2}} \quad 8.22$$

The concept of incomplete coupling relates exclusively to the first term, i.e. the flux ratio or H^+_a/O_2 ratio. Likewise, respirometric definitions of the $P \gg/O_2$ ratio and biochemical coupling efficiency consider flux ratios (Section 3.4). In a completely coupled process, the power efficiency ε depends entirely on the force ratio, ranging from zero efficiency at an output force of zero, to the limiting output force and maximum efficiency of 1.0, when the total power of the coupled process (the negative dissipation function), $P_t = P_{kO_2} + P_{mH^+a}$, equals zero, and any net flows are zero at ergodynamic equilibrium of a coupled process. Thermodynamic equilibrium is defined as the state when all potentials

(all forces) are dissipated and equilibrate towards their minima of zero. In a fully or completely coupled process, output and input fluxes are directly proportional in a fixed ratio technically defined as a stoichiometric relationship (a gear ratio in a mechanical system). Such maximal stoichiometric output/input flux ratios are considered in OXPHOS analysis as the upper limits or mechanistic H^+_a/O_2 and P_{\gg}/O_2 ratios (Figure 6.3).

To convert O_2 consumption into energy units of power (=exergy per time), aerobic catabolic flux ($J_{O_2\max}$ for cycle ergometry; J_{O_2P} for cell OXPHOS-capacity [$\text{nmol}\cdot\text{s}^{-1}\cdot\text{g}^{-1}$]) is multiplied by the catabolic Gibbs force $\Delta_k F_{O_2}$; typically -0.47 mJ/nmol O_2 (Eq. 8.21b). This yields the mass-specific aerobic input power [$\text{mW}\cdot\text{g}^{-1}$]. In cycle ergometry, the corresponding mechanical output power results in ergodynamic efficiencies ε of about 0.25. In OXPHOS analysis output power is the product of mitochondrial ATP production $J_{P_{\gg}}$ [$\text{nmol } P_{\gg}\cdot\text{s}^{-1}\cdot\text{g}^{-1}$] and Gibbs force of phosphorylation $\Delta_p F_{P_{\gg}}$. $\Delta_p F_{P_{\gg}}$ is typically 48 to 62 kJ/mol P_{\gg} . Power efficiency is partitioned into a flux ratio — the P_{\gg}/O_2 ratio ($J_{P_{\gg}}/J_{kO_2}$; ATP yield per O_2 consumed) — and force ratio. Ergodynamic efficiency not only depends on coupling of flux but also on the force ratio or force efficiency. Output fluxes vanish to zero not only at thermodynamic equilibrium but also at maximum efficiency of ergodynamic equilibrium, $\varepsilon=1.0$. Evolutionary adaptation, therefore, involves optimization of power as a compromise between maximum output power and efficiency (Gnaiger 1993b).

8.2.6. The elementary quantities and motive units: count, amount, and charge

Thermodynamics is less scary, when formal consistency between chemical, electrochemical, and statistical thermodynamics provides the glue between the diffusive and electric terms, $\Delta\mu_{H^+}$ and $\Delta\Psi_{p^+}$, of the protonmotive force. The fundamental constant k , which received its name from Ludwig Boltzmann as the pioneer of statistical thermodynamics, yields the particle or count format of isomorphic forces, $kT \cdot \ln \kappa_{tr}$ [$\text{J}\cdot\text{x}^{-1}$]. This represents the missing link between the chemical format $RT \cdot \ln \kappa_{tr}$ [$\text{J}\cdot\text{mol}^{-1}$] (Eq. 8.16) and electrical format $fT \cdot \ln \kappa_{tr}$ [$\text{J}\cdot\text{C}^{-1}$] of the protonmotive force (Tables 8.1 and 8.2).

Table 8.1: Fundamental physical formats, constants, and relationships between the units of the elementary quantities count, amount, and charge.

Format	Name	Definitions	Numerical value	Unit*
N	count, molecular #	count $N_X = N \cdot U_X$		$\triangleleft N$ MU = x
n	amount, molar	amount $n_X = N_X \cdot N_A^{-1}$		$\triangleleft n$ MU = mol
e	charge, electrical	charge $Q_{elX} = n_X \cdot z_X \cdot F$		$\triangleleft e$ MU = C
N	Boltzmann constant §	$k = f e = R/N_A = 1.380\,649 \cdot 10^{-23}$		$\text{J}\cdot\text{x}^{-1} \cdot \text{K}^{-1}$
n	gas constant	$R = f F = k \cdot N_A = 8.314\,462\,618$		$\text{J}\cdot\text{mol}^{-1}\cdot\text{K}^{-1}$
e	electromotive constant §	$f = k/e = R/F = 8.617\,333\,262 \cdot 10^{-5}$		$\text{J}\cdot\text{C}^{-1} \cdot \text{K}^{-1}$
N/n	Avogadro constant §	$N_A = R/k = F/e = 6.022\,140\,76 \cdot 10^{23}$		$\text{x}\cdot\text{mol}^{-1}$
e/N	elementary charge \$,@	$e = k/f = F/N_A = 1.602\,176\,634 \cdot 10^{-19}$		$\text{C}\cdot\text{x}^{-1}$
e/n	Faraday constant	$F = R/f = e \cdot N_A = 96\,485.332\,12$		$\text{C}\cdot\text{mol}^{-1}$

* The motive quantity with motive unit MU defines the physical format.

Count N_X is the number N of elementary entities U_X with the abstract elementary unit [x] (Gnaiger 2020).

§ Redefinition of SI base units came into force on 2019-05-20; Bureau International des Poids et Mesures (2019) The International System of Units (SI). 9th edition.

§ A name or symbol was not found in the literature for the electromotive constant f introduced here.

@ Elementary charge $e \stackrel{\text{def}}{=} Q_{elp^+}/N_{p^+} = Q_{Np^+}$ is charge per proton count or charge per elementary proton U_{p^+} .

The concept of the particle is a unifying principle in (quantum) physics. The number of particles X is the count N_X . The Boltzmann constant k introduces the particle format \underline{N} based on the Euclidean unit U_X of the count N_X (elementary unit $[x]$); the molar format \underline{e} is based on amount n_X (mole $[\text{mol}]$); the electrical format \underline{e} is based on charge $Q_{\text{el}X}$ (coulomb $[\text{C}]$). The same entity-type X – consider H^+ as X – is expressed in different formats. The *motive unit* MU chosen to quantify the *motive entity* X defines the format of the advancement and corresponding isomorphic force (Eq. 8.20). The MU-formats of elementary quantities are tightly linked by the fixed conversion constants N_A , e , and F (Table 8.1): count $N_X = n_X \cdot N_A$; charge $Q_{\text{el}X} = N_X \cdot z_X \cdot e$; and $Q_{\text{el}X} = n_X \cdot z_X \cdot F$ (Figure 8.6a).

The Avogadro constant $N_A = R/k$ $[\text{x} \cdot \text{mol}^{-1}]$ is count per amount, linking the gas constant R and Boltzmann constant k . Table 8.1 introduces the electromotive constant f to emphasize the interrelation between elementary quantities: count, amount, and charge. The elementary charge $e = k/f$ $[\text{C} \cdot \text{x}^{-1}]$ is charge per count, linking the Boltzmann constant k and electromotive constant f . The Faraday constant $F = R/f$ $[\text{C} \cdot \text{mol}^{-1}]$ is charge per amount, linking the gas constant R and electromotive constant f .

Why should we consider the count format \underline{N} (particle or molecular format) of quantum physics and statistical mechanics in mitochondrial physiology? At pH 8 in the mt-matrix the H^+ activity is 10^{-8} corresponding to a concentration of free H^+ (or H_3O^+) of $0.01 \mu\text{mol} \cdot \text{L}^{-1}$ (the count concentration is $6 \cdot 10^{15} \text{x} \cdot \text{L}^{-1} = 6 \text{Px} \cdot \text{L}^{-1}$; see SI prefixes in Section A4). For a mt-matrix volume per mitochondrion of $0.3 \mu\text{m}^3 \cdot \text{x}^{-1} \text{ mt}$ (Schwerzmann et al 1986; $0.3 \text{ fL} \cdot \text{x}^{-1} = 0.3 \cdot 10^{-15} \text{ L} \cdot \text{x}^{-1}$) the molar amount of H^+ is $3 \cdot 10^{-24} \text{ mol} \cdot \text{x}^{-1}$ ($3 \text{ ymol} \cdot \text{x}^{-1}$). Multiplied by the Avogadro constant ($6 \cdot 10^{23} \text{x} \cdot \text{mol}^{-1} = 0.6 \text{ Yx} \cdot \text{mol}^{-1}$), the number of H^+ per mitochondrion of this size is $\sim 2 \text{x} \text{H}^+ \cdot \text{x}^{-1} \text{ mt}$. A similar result of $6 \text{x} \cdot \text{x}^{-1}$ is obtained with reference to a mt-matrix volume per mt-protein of $1 \mu\text{L} \cdot \text{mg}^{-1}$ and $10^9 \text{x} \cdot \text{mg}^{-1}$ protein. Thus, we can expect only a few H^+ in a single mitochondrion on average at any point of time. Although this has been widely discussed, it should be given more thought in relation to fluctuations and mitochondrial heterogeneity, particularly in single cell analysis with typically 300 mitochondria per cell. Animated cartoons on the electron transfer system with many bouncing H^+ propagate a false image. How do the many H^+ pumps of the mtIM get their hydrogen ions? Which role is played by counterion and buffer concentrations?

At a mt-protein concentration of $0.1 \text{ mg} \cdot \text{mL}^{-1}$ in a respirometric chamber and a mt-matrix volume V_{mt} of $10^{-6} \text{ L} \cdot \text{mg}^{-1}$ protein, the volume fraction is 0.0001 or $0.1 \mu\text{L}$ mt-matrix $\cdot \text{mL}^{-1}$. At pH 8, $0.1 \mu\text{L}$ mt-matrix contain 10^{-15} mol H^+ equivalent to $6 \cdot 10^8 \text{H}^+$. Thus statistically relevant information can be obtained on the protonmotive force when using large numbers of mitochondria even at high dilution in a respirometric chamber of 2 mL, containing >1 billion H^+ in the mt-matrix. Because quantities are quantized, thermodynamic terms such as temperature, Gibbs energy, pH, and the protonmotive force pmF can be defined and accounted for only on the basis of large counts in ergodic systems.

8.2.7. The motive force quantum and motive units

Isomorphic forces are quantized according to the Boltzmann constant (Table 8.1). These motive forces are expressed in various *motive units* MU $[\text{J} \cdot \text{MU}^{-1}]$, depending on the energy transformation under study and the unit chosen to express the motive entity. Independent of MU, however, concentration times force yields pressure, as shown for gas pressure in Table 8.2. For the pmF the *motive entity* is H^+ . The Boltzmann constant k , the gas constant R , and the electromotive constant f represent the count-, amount-, and charge-formats, respectively, and define the numerical values and units of the motive force quantum (Table 8.3). These relationships are represented graphically in Figure 8.6.

Table 8.2: The gas equation expressed in molecular \underline{N} and molar \underline{n} formats with corresponding motive units MU: Concentration \times force quantum $F_q =$ pressure.

Format	Concentration	Unit MU·m ⁻³	F_q	Unit J·MU ⁻¹	Pressure	Unit
\underline{N}	$C_X = N_X \cdot V^{-1}$	x·m ⁻³	kT	J·X ⁻¹	$p_X = kT \cdot C_X$	J·m ⁻³ = Pa
\underline{n}	$c_X = n_X \cdot V^{-1}$	mol·m ⁻³	RT	J·mol ⁻¹	$p_X = RT \cdot c_X$	J·m ⁻³ = Pa

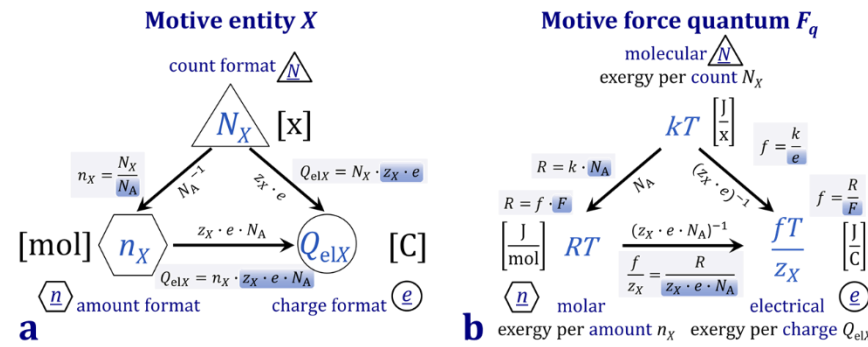


Figure 8.6. Boltzmann-Avogadro-Faraday plane of the motive entity (a) and motive force quantum (b). Formats \underline{N} , \underline{n} , and \underline{e} – count, amount, and charge – are expressed in the corresponding motive units MU and units J·MU⁻¹ of isomorphic motive forces.

Table 8.3: Motive force quantum F_q , expressed in different motive units MU corresponding to count, amount, and charge MU-formats

Format	Type	F_q	$T / [^{\circ}\text{C}]$ #	Numerical value	Unit *
\underline{N}	ln-molecular $F_{q\underline{N}}$ §	kT	25	= 4.1164	$\text{zJ} \cdot \text{x}^{-1}$
			37	= 4.2821	$\text{zJ} \cdot \text{x}^{-1}$
\underline{n}	ln-molar $F_{q\underline{n}}$	$RT = k \cdot N_A \cdot T$	25	= 2.4790	$\text{kJ} \cdot \text{mol}^{-1}$
			37	= 2.5787	$\text{kJ} \cdot \text{mol}^{-1}$
\underline{e} §	ln-electrical $F_{q\underline{e}}$	$fT = R \cdot F^{-1} \cdot T$	25	= 25.693	mV
			37	= 26.727	mV
\underline{N}	log-molecular $F_{q\underline{N}}$	$kT \cdot \ln(10)$	25	= 9.4784	$\text{zJ} \cdot \text{x}^{-1}$
			37	= 9.8599	$\text{zJ} \cdot \text{x}^{-1}$
\underline{n}	log-molar $F_{q\underline{n}}$	$RT \cdot \ln(10)$	25	= 5.7080	$\text{kJ} \cdot \text{mol}^{-1}$
			37	= 5.9377	$\text{kJ} \cdot \text{mol}^{-1}$
\underline{e} §	log-electrical $F_{q\underline{e}}$	$fT \cdot \ln(10)$	25	= 59.159	mV
			37	= 61.540	mV

25 °C = 298.15 K; 37 °C = 310.15 K; $\ln(10) = 2.302585$. The F_q on the basis of natural logarithms (ln) is converted to the basis of decimal logarithms (log) by multiplication with $\ln(10)$.
 * Suffix zepto $z = 10^{-21}$.
 § $(kT)^{-1}$ has the name ‘reciprocal temperature parameter’ in statistical thermodynamics (IUPAC).
 § For monovalent ions with $z_X = 1$.

$\Delta_{\text{d}}\text{pH} = 1$ implies a 10-fold difference in H^+ activity, a diffusive potential difference of -5.7 or -5.9 $\text{kJ} \cdot \text{mol}^{-1}$, and electric potential difference of -59 or -62 mV, at 25 or 37 °C.

The motive force quantum is exergy per elementary motive particle. In kT , the intensive quantity force is distinguished from the extensive quantity exergy [J] by the unit

[J·x⁻¹] – isomorphic to [J·C⁻¹ $\stackrel{\text{def}}$ V] and [J·mol⁻¹ $\stackrel{\text{def}}$ Jol] (Eq. 8.20). Unfortunately, the elementary unit [x] is not implemented in the SI nor by IUPAC (Gnaiger 2020). The SI unit of a count of particles, however, is the pure number 1, which is then dropped – mathematically: division by 1 is of no consequence. Based on this SI convention, the motive force quantum kT is expressed in the unit [J], indistinguishable from the unit [J] of energy – this is scary. – Or is it more scary, that the term *proton* is used ambiguously for the subatomic nuclear particle p and the free hydrogen ion H^+ or hydronium ion H_3O^+ ?

8.2.8 Remember ZEN, zeN_A

RM Pirsig (1974) *Zen and the art of motorcycle maintenance. An inquiry into values.* William Morrow & Company:418 pp. *Thermodynamics (motorcycle maintenance)* may be dull and tedious drudgery (without curiosity beyond “≡”) or a valuable and exciting art (if you seek for “=” ZEN). Transformation of dumb, dry and frigid equations into eloquent formulae radiating meaning and sparkling knowledge depends on motivation, skill and persistence (zeN_A).

Where is the charge number z_{H^+} of the hydrogen ion H^+ in the *pmF* equation (Eq. 1.1)? Omission of z_{H^+} is due to the trivial fact that $z_{H^+}=1$, which can be dropped mathematically. Picking up rather than dropping z provides meaning, consistency, and generalization. zeN_A connects the amount (n_X [mol]) and charge (Q_{elX} [C]) formats (Figure 8.6). zeN_A symbolizes a concept beyond mere numerical arithmetic solutions (Figure 8.7).

For ion X , the charge number $z_X = Q_{NX} \cdot e^{-1}$ is the molecular charge Q_{NX} (Q_{el} per ion X [C/x]) divided by elementary charge e (Q_{el} per p^+ [C/x]). z_X is, in turn, equal to the molar charge Q_{nX} [C/mol] divided by the Faraday constant F [C/mol] (Figure 8.7).

The charge number z_{H^+} is in the Nernst equation (Eq. 8.23), defining the electric potential generated by the charge distribution of a single type of ion X ,

$$\Delta\Psi_X = \frac{1}{z_X} \cdot \frac{RT}{F} \cdot \ln \frac{c_{X_b}}{c_{X_a}} = \frac{1}{z_X} \cdot \frac{RT}{F} \cdot \Delta \ln c_X \quad [J \cdot C^{-1}] \quad 8.23$$

The Nernst equation has the form of $RT \cdot \ln \kappa_{tr}$ (Eq. 8.16). The partial electrochemical potential for X alone contains a term for the diffusive chemical potential (Eq. 8.23a) and X -specific electric potential (Eq. 8.23b), inserting $f = R/F$,

$$\Delta\mu_X = RT \cdot \Delta \ln c_X = RT \cdot 2.303 \cdot \Delta pX \quad [J \cdot mol^{-1}] \quad 8.23a$$

$$\Delta\Psi_X = \frac{1}{z_X} \cdot fT \cdot \Delta \ln c_X = \frac{1}{z_X} \cdot fT \cdot 2.303 \cdot \Delta pX \quad [J \cdot C^{-1}] \quad 8.23b$$

Does X equilibrate – or not, such as H^+ – across the membrane? Neither H^+ nor protons are the full story of the *pmF*: the total proton electric potential is $\Delta\Psi_{p^+} = \Delta\Psi_{H^+} + \Delta\Psi_Z$, where $\Delta pH + \Delta pZ$ relates to the total proton charge ratio of hydrogen ions and counterions (Section 8.4.3).

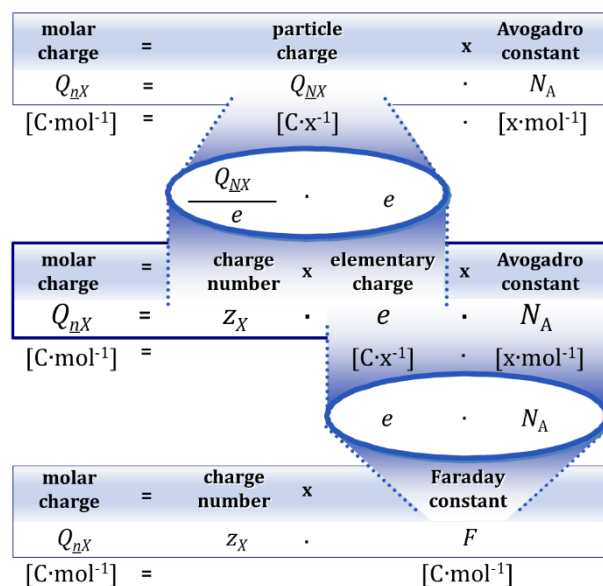


Figure 8.7. Relationships of zeN_A : Molar charge Q_{nX} is (1) molecular charge $Q_{NX} = z_X \cdot e$ times N_A ; (2) the product of the three terms of zeN_A ; (3) charge number z_X times the Faraday constant $F = e \cdot N_A$.

8.3. Protonmotive force and motive units

8.3.1. Why did Peter Mitchell use the symbol Δp ?

Peter Mitchell coined the term protonmotive force and introduced the symbol Δp . Δp is not related to *potentia hydrogenii* – hydrogenium power – in the *symbol* $\Delta p\text{H}$. What is the message of Δp ?

The term *proton* and symbol H^+ tend to be used synonymously in chemistry for the monovalent cations resulting from the dissociation of acids including water. The *hydrogen ion* H^+ is a bare atomic nucleus with only about 1/64 000 of the radius of a hydrogen atom. Therefore, H^+ is extremely reactive and becomes hydrated in aqueous solution, forming hydronium ions H_3O^+ and ions with higher levels of hydration. Collectively, these determine the acidity of dilute aqueous solutions. When the dissociation of water is simplified as $\text{H}_2\text{O} = \text{H}^+ + \text{OH}^-$, all levels of hydration of the hydrogen ion are represented by the (ambiguous) symbol H^+ . In contrast, $\text{H}_2\text{O} = \text{p}^+ + \text{OH}^-$ looks odd – and is odd.

p^+ or p is the IUPAC symbol for the proton. An *ion* is a molecule carrying net positive or negative electric charge. Molecules are made of atoms including subatomic particles: the central nuclear protons p^+ and neutrons n , and the peripheral electrons e^- . Whereas H^+ is a positively charged *molecule*, which is transformed to an electroneutral hydrogen atom when accepting an electron, p^+ is the positively charged *subatomic particle* occurring in all atoms and molecules. This distinction is explicit in the iconic symbols of the diffusive force $\Delta_{\text{d}}F_{\text{H}^+}$ (exergy per H^+) and electric force $\Delta_{\text{el}}F_{\text{p}^+}$ (exergy per p^+ ; Eq. 8.20). Adding the two partial forces, the *protonmotive force* $\text{pm}F$ is seen as $\Delta_{\text{m}}F_{\text{H}^+}$, in which the submolecular electric proton propulsion is superimposed on the molecular diffusive H^+ distribution.

$\Delta_{\text{m}}F_{\text{H}^+}$ is the iconic symbol for the $\text{pm}F$. This symbol can be read as "difference \ motive \ force \ for hydrogen ions". If you see the symbol Δp as frequently used in bioenergetics, the only iconic aspect is the Δ indicating a difference (an isomorphic 'delta-force'; Figure 8.4), whereas the full meaning of Δp has to be explained to any outsider. Outsiders are insiders in other fields: Δp [Pa] is a death penalty for professional and other high-risk divers, a pressure difference in respiratory medicine, cardiovascular physiology, and generally in fluid dynamics and the ideal gas equation, $\Delta p = n \cdot \Delta V^{-1} \cdot RT$. Why are we content with using a symbol for *pressure* when expressing the *protonmotive force*? To remove this aspect of ambiguity (= double meaning), Mitchell's classical Δp for the $\text{pm}F$ should be maintained instead of the italicized Δp , to read 'p' as the IUPAC symbol for the proton, instead of "p" for pressure. When Peter Mitchell used a typewriter for his *Grey Book* (1966), italic versus upright font was not a practical option — using underline in place of *italics* is tedious. Today, we should use the traditional symbol Δp for the $\text{pm}F$ with reference to the proton, and Δp for a pressure difference. Or do iconic symbols have an important advantage in general communication (Eq. 8.24)?

8.3.2. The chemical and electric partial forces of the $\text{pm}F$

The protonmotive $\text{pm}F$ is the sum of the partial diffusive and electric force of H^+ translocation across the mtIM, expressed with iconic symbols (Table 8.4),

$$\Delta_{\text{m}}F_{\text{H}^+} = \Delta_{\text{d}}F_{\text{H}^+} + \Delta_{\text{el}}F_{\text{p}^+} \quad [\text{J} \cdot \text{mol}^{-1}] \text{ or } [\text{V}] \quad 8.24$$

H^+ translocation combines the motive molecular and charge transfer. H^+ current I_{meH^+} [A $\stackrel{\text{def}}{=} \text{C} \cdot \text{s}^{-1}$] through an electrolytic conductor carries both matter — in the form of H^+ ions — and p^+ charge (Eq. 8.20a), in contrast to electric e^- current I_{el} [A] through electronic conductors.

Table 8.4. Protonmotive force and flux matrix. Rows: Compartmental H⁺ flux (rate) and protonmotive force (state). Count, amount and charge formats (\underline{N} , \underline{n} , \underline{e}) with motive units MU of the count N_X [x] of elementary entities X , amount of substance n_X [mol], and electric p⁺ charge Q_{elX} [C], respectively. Columns: The pmF , $\Delta_m F_{H^+}$, is the sum of two *partial isomorphic forces*, $\Delta_d F_{H^+} + \Delta_{el} F_{p^+}$. In contrast to force, the conjugated flux cannot be partitioned but is expressed in different MU-formats.

Name	Motive	= diffusive	+ electric	Unit	Notes
	M	d	el		
Rate isomorphic flux	J_{mH^+}			MU · s ⁻¹ · m ⁻³	1
\underline{N} count, molecular	J_{mNH^+}			x · s ⁻¹ · m ⁻³	1 \underline{N}
\underline{n} amount, molar	$J_{m\bar{n}H^+}$			mol · s ⁻¹ · m ⁻³	1 \underline{n}
\underline{e} charge, electrical	J_{meH^+}			C · s ⁻¹ · m ⁻³	1 \underline{e}
State isomorphic force	$\Delta_m F_{H^+}$	= $\Delta_d F_{H^+}$	+ $\Delta_{el} F_{p^+}$	J · MU ⁻¹	2
\underline{N} count, molecular	$\Delta_m F_{NH^+}$	= $\Delta_d F_{NH^+}$	+ $\Delta_{el} F_{Np^+}$	J · x ⁻¹	2 \underline{N}
\underline{n} amount, molar	$\Delta_m F_{\bar{n}H^+}$	= $\Delta_d F_{\bar{n}H^+}$	+ $\Delta_{el} F_{\bar{n}p^+}$	J · mol ⁻¹	2 \underline{n}
\underline{e} charge, electrical	$\Delta_m F_{eH^+}$	= $\Delta_d F_{eH^+}$	+ $\Delta_{el} F_{ep^+}$	J · C ⁻¹	2 \underline{e}
\underline{n} chemiosmotic potential	$\Delta\tilde{\mu}_{H^+}$	≡ $\Delta\mu_{H^+}$	+ $\Delta\Psi_{p^+ \cdot Z_{H^+} \cdot F}$	J · mol ⁻¹	3 3 \underline{n}
\underline{e} protonmotive force	Δp	≡ $\Delta\mu_{H^+} \cdot (Z_{H^+} \cdot F)^{-1}$	+ $\Delta\Psi_{p^+}$	J · C ⁻¹	3 \underline{e}

¹ The sign of J_{mH^+} depends on the compartmental direction of translocation. J_{mH^+a} into the positively (pos) charged internal anodic compartment a is >0 when the cations H^+_a are pumped into the anodic compartment a ($v_{H^+a} = 1$) while H^+_b is removed from the ‘cathodic’ negative compartment ($v_{H^+b} = -1$). Conversely, J_{mH^+b} is >0 when cations H^+_b move into the cathodic compartment b ($v_{H^+b} = 1$) while H^+_a is removed ($v_{H^+a} = -1$; Figure 8.2).

² Iconic symbols: $\Delta_m F_{H^+}$ is the pmF per entity H^+ (not per e^-) expressed in any MU-format. $\Delta_d F_{H^+}$ is the partial pmF specific for H^+ diffusion irrespective of charge. In contrast, $\Delta_{el} F_{p^+}$ is the partial pmF due to the total proton charge distribution across the mtIM, not specific for H^+ . The sign of the force $\Delta_m F_{H^+b}$ is negative for exergonic transformations in which exergy is lost or dissipated, and positive for endergonic transformations which conserve exergy in a coupled exergonic process, $\Delta_m F_{H^+a} = -\Delta_m F_{H^+b}$. An extended subscript a (or b) in $\Delta_{el} F_{p^+a}$ defines the compartmental direction. By definition, the product of flux and force is volume-specific power [$W \cdot m^{-3}$]: $P_{V,mH^+} = J_{m\bar{n}H^+a} \cdot \Delta_m F_{\bar{n}H^+a} = J_{meH^+a} \cdot \Delta_m F_{eH^+a}$ (compare Eq. 8.20).

³ Traditional representations: (\underline{n}) $\Delta\tilde{\mu}_{H^+} = \Delta_m F_{\bar{n}H^+}$; $\Delta\mu_{H^+} \equiv \Delta_d F_{\bar{n}H^+}$; (\underline{e}) $\Delta p = \Delta_m F_{eH^+}$; $\Delta\Psi_{p^+} \equiv \Delta_{el} F_{ep^+}$.

(1) $\Delta_d F_{H^+}$: The movement of the molecule H^+ – independent of its charge – is the focus of the chemical partial force of diffusion (d). $\Delta_d F_{H^+}$ contains the diffusive potential difference $\Delta_d \mu_{H^+}$, proportional to $\Delta_d pH = pH_a \cdot v_a + pH_b \cdot v_b$ (Eq. 8.18; Table 8.5),

$$\text{diffusive } d_{\underline{n}}: \quad \Delta_d F_{\bar{n}H^+} = RT \cdot (\ln a_{H^+a}) \cdot v_a + RT \cdot (\ln a_{H^+b}) \cdot v_b \quad [k] \cdot \text{mol}^{-1} \quad 8.25a$$

$$\Delta_d F_{\bar{n}H^+} = -RT \cdot 2.303 \cdot (pH_a \cdot v_a + pH_b \cdot v_b) \quad [k] \cdot \text{mol}^{-1} \quad 8.25b$$

(2) $\Delta_{el} F_{p^+}$: The electric partial force (el) relates to proton charge p⁺ irrespective of the nature of the charge-carrying ion (Eq. 8.20a). The net distribution of all ions – not restricted to hydrogen ions H^+ – generates an internal electric field in the compartmental system. $\Delta_{el} F_{p^+}$ contains the electric potential difference $\Delta\Psi_{p^+}$, which includes $\Delta\Psi_{H^+}$.

$\Delta\Psi_{H^+}$ is proportional to ΔpH generated by H^+ translocation resulting in the partial, H^+ -specific membrane potential difference (Table 8.5). According to Mitchell’s Module 3, H^+ pumping is coupled to electroneutral and reversible counterion exchange of cations against H^+ ions and of anions against OH^- ions. The mtIM has very limited permeability for

H⁺ and counterions. The charge distribution ΔpZ across the mtIM impermeable for counterions contributes to total charge distribution $\Delta pH + \Delta pZ$ and to $\Delta \Psi_{p^+} = \Delta \Psi_{H^+} + \Delta \Psi_{Z^+}$.

The chemiosmotic theory describes coupling in OXPHOS (Section 8.2.5). Thus, the question arises if the diffusive and electric parts of H⁺ translocation are coupled processes. This is not the case according to the definition of coupling. If the coupling mechanism is disengaged, the input process becomes independent of the output process, and both proceed in their downhill (exergonic) direction (Figure 8.2). In contrast, it is not possible to physically uncouple the diffusive and electric partial processes, which are only *theoretically* partitioned as chemical and electric components. The partial protonmotive forces, $\Delta_d F_{H^+}$ and $\Delta_{el} F_{p^+}$, can be measured separately. In contrast, the corresponding H⁺ flux J_{mH^+} is a non-separable flux of amount of H⁺ and proton charge of H⁺. Therefore, these are not *coupled*, but are defined as *bound* processes. The diffusive and electric parts are inseparably bound partial forces. Flux cannot be partitioned (Table 8.4, columns), but can be expressed in the count, amount, or charge format (Table 8.4, rows).

The additive *partial* diffusive and electric (distinguished from *electrical*) components of the *pmF*, $\Delta_d F_{H^+}$ and $\Delta_{el} F_{p^+}$, are different in nature. The chemical potential difference (diffusion, d) is strictly linked to ΔpH specific for the H⁺ cation, whereas the electric potential difference (el) is built up as net proton charge of all anions and cations involved (Table 8.4, columns). This *partial separation* is different from and entirely independent of the *format of expression*.

8.3.3. Conversion between amount format and charge format, and motive units

Diffusive and electric *forms* of exergy and force are transformed in electrochemical processes, whereas *MU-formats* are interconverted merely by arithmetic calculation (Eq. 8.2). For addition, the partial chemical and electric forces $\Delta_d F_{H^+} + \Delta_{el} F_{p^+}$ have to be expressed (1) in the same format with identical units and suffixes used with the units, and (2) in the same compartmental direction defining the signs of the stoichiometric numbers (Figure 8.3). In the amount format, the partial forces $\Delta_d F_{nH^+} + \Delta_{el} F_{np^+}$ [kJ·mol⁻¹] are given per *amount* of motive cations H⁺ [mol]. In the charge format, the partial forces $\Delta_d F_{eH^+} + \Delta_{el} F_{ep^+}$ [mV] are expressed per *charge* of motive protons p⁺ [C] (Table 8.4, rows). By setting $\nu_b = +1$, the compartmental direction is defined as H⁺_{a(exit)} → H⁺_{b(entry)} (proton leak in Figure 8.2). The compartmental direction of movement *into the positive compartment* is shown by subscript *a* (or *b*) for the force and flux: $\Delta_m F_{H^+a}$ and J_{mH^+a} (Figure 8.2). The sign of the force is positive, when Gibbs energy is conserved in proton pumping. When the direction of flux is defined as movement into the negative compartment, J_{mH^+b} , the force $\Delta_m F_{H^+b}$ has a negative sign in the dissipative direction.

The protonmotive force $\Delta_m F_{H^+}$ [J·MU⁻¹] is conjugated to the transmembrane H⁺ flux J_{mH^+} [MU·s⁻¹·m⁻³]. Comparable to the pair (d and el) of partial forces, a conjugated pair of flux and force is linked by the same MU. Taken together, the same MU-format has to be applied for (1) addition of partial forces to obtain the motive force, and (2) multiplication of flux and force to obtain power per volume (Eq. 8.21).

An electric force $\Delta_{el} F_{ep^+a} = 160 \text{ mJ} \cdot \text{C}^{-1}$ of positive charges (= 160 mV) in the charge format *e* corresponds to an electric force $\Delta_{el} F_{np^+a} = 15.4 \text{ kJ} \cdot \text{mol}^{-1}$ of positive charges in the amount format *n*. Considering a driving force of -470 kJ·mol⁻¹ O₂ for oxidation, the H⁺_a/O₂ ratio reaches the ergodynamic efficiency limit at 470/15.4 = 30, compared to a mechanistic stoichiometry of 20 in the N-pathway.

Table 8.5. Diffusive and electric partial forces of hydrogen ion distribution.

Term	Symbol	Definition	Unit	Notes
partial chemical force, \underline{n} at 37 °C	$\Delta_d F_{\underline{n}H^+}$	$= -RT \cdot \ln(10) \cdot \Delta_{dpH}$ $= -5.94 \cdot \Delta_{dpH}$	$J \cdot mol^{-1}$ $kJ \cdot mol^{-1}$	$1\underline{n}$
partial chemical force, \underline{e} at 37 °C	$\Delta_d F_{\underline{e}H^+}$	$= -fT \cdot \ln(10) \cdot \Delta_{dpH}$ $= -61.5 \cdot \Delta_{dpH}$	$V = J \cdot C^{-1}$ mV	$1\underline{e}$
partial electric force, \underline{n} at 37 °C	$\Delta_{el} F_{\underline{n}H^+}$	$= -RT/z_{H^+} \cdot \ln(10) \cdot \Delta_{elpH}$ $= -5.94 \cdot \Delta_{elpH}$	$J \cdot mol^{-1}$ $kJ \cdot mol^{-1}$	$2\underline{n}$
partial electric force, \underline{e} at 37 °C	$\Delta_{el} F_{\underline{e}H^+}$	$= -fT/z_{H^+} \cdot \ln(10) \cdot \Delta_{elpH}$ $= -61.5 \cdot \Delta_{elpH}$	$V = J \cdot C^{-1}$ mV	$2\underline{e}$

$1\underline{n}$: $RT = 2.479$ and 2.579 $kJ \cdot mol^{-1}$, $RT \cdot \ln(10) = 5.708$ and 5.938 $kJ \cdot mol^{-1}$, at 298.15 and 310.15 K (25 and 37 °C), respectively (Table 8.3). Replacing the gas constant R by the Boltzmann constant k converts the molar format \underline{n} [$J \cdot mol^{-1}$] into the particle format \underline{N} [$J \cdot x^{-1}$].

$1\underline{e}$: Replacing the gas constant R by the electromotive constant $f = R/F$ (Table 8.1) converts the molar format \underline{n} [$J \cdot mol^{-1}$] into the electrical format \underline{e} [$J \cdot C^{-1}$]. $fT = 25.7$ and 26.7 mV, and $fT/z_{H^+} \cdot \ln(10) = 59.2$ and 61.5 mV, (25 and 37 °C), respectively (Table 8.3). Although expressed in electrical format in units of joule per coulomb, the partial chemical force is not related to electric proton charge but to hydrogen ion particles.

2: $\Delta_{el} F_{H^+}$ is the partial contribution to $\Delta_{el} F_{p^+}$ of hydrogen ion distribution ($\Delta_{elpH} = \Delta_{dpH} = \Delta_{mpH}$). In a vectorial electric transformation (flux of charge, i.e. volume-specific current, from the matrix space to the intermembrane and extramitochondrial space), the motive force is the stoichiometric potential difference across the mtIM. The endergonic direction of translocation is defined in Figure 8.2 as $H^+_b \rightarrow H^+_a$. $z_{H^+} = 1$ is the proton charge number of the hydrogen ion H^+ . Note that ion selective pH electrodes respond to $\ln a_{H^+}$. $\Delta_{el} \ln a_{H^+} = -\ln(10) \cdot \Delta_{elpH}$.

For 1 unit of Δ_{mpH} , the partial forces $\Delta_d F_{\underline{n}H^+}$ and $\Delta_{el} F_{\underline{n}H^+}$ change by roughly 6 $kJ \cdot mol^{-1}$ in the amount format, and $\Delta_d F_{\underline{e}H^+}$ and $\Delta_{el} F_{\underline{e}H^+}$ change by about 61 mV in the charge format (Table 8.5). Therefore, 1 unit of Δ_{mpH} generates a pmF , $\Delta_m F_{\underline{n}H^+}$ of 12 $kJ \cdot mol^{-1}$ in the amount format or $\Delta_m F_{\underline{e}H^+}$ of 123 mV in the electrical format.

When different MU-formats are used, the format (\underline{N} , \underline{n} , \underline{e}) is indicated in the iconic symbol as an underlined subscript (Table 8.4). Other formats are theoretically possible, e.g. mass \underline{m} [kg], volume \underline{V} [m^3], or energy \underline{E} with further specification, such as heat or work [J]. Flow is advancement per time, $I_{tr} = d_{tr} \xi_i / dt = d_{tr} X_i / dt \cdot \nu_i^{-1}$ [$MU \cdot s^{-1}$] (Figure 8.3). X_{tri} is the generalized motive entity (*transformant*) involved in a transformation tr . X_{trni} is the motive entity expressed as amount of substance [mol]. X_{trei} denotes the same motive entity as charge [C] (Figure 8.6a). Accordingly, H^+ flow is expressed in various motive units [$MU \cdot s^{-1}$], with H^+ as the motive entity expressed as count N_{H^+} [x], amount n_{H^+} [mol], and charge Q_{elH^+} [C] (Figure 8.6a). Irrespective of format, H^+ is the current-carrying motive entity. H^+ flux (flow per volume) in the count, amount or charge formats has invariably the same meaning of H^+ translocation. The value, nature and meaning of H^+ flux remains identical when expressed in different units and corresponding numerical values. The product of the numerical value in N times the unit MU is the invariant value of the quantity flow. The independence of the value of a quantity from the numerical value times a corresponding unit is trivial, when using different units for a single quantity (e.g. time: 1 h = 3600 s). It is just the same, when we use different MU units for motive entities: 1 $mmol \cdot s^{-1} = 96.5$ $C \cdot s^{-1} = 96.5$ A for the flow of any ion X with $z_X = 1$ (Table 8.1).

8.3.4. Measurement of the *pmF*

$\Delta p\text{H}$ is measured with the use of radioactively labelled compounds (Canton et al 1995) or fluorescent dyes (Poburko et al 2011; Komlódi et al 2018). Methods for measurement of mt-membrane potential $\Delta\Psi_{p^+}$ are more generally available and simpler to use compared to measurement of $\Delta p\text{H}$. The contribution of $\Delta p\text{H}$ to the *pmF* is ignored in many studies reporting semi-quantitative measurements of $\Delta\Psi_{p^+}$, even in cases when a shift between the electric and diffusive partial forces cannot be excluded. This simple fact contributes to irreproducibility and explains several apparently paradoxical results.

The mtIM is nearly impermeable for the hydrophilic ions H^+ , OH^- and counterions Y^- , but is permeable for lipophilic cations X^+ . These equilibrate between the positive (anodic) compartment *a* and the negative matrix *b* (Figure 8.2). A cation does not neutralize H^+ , in contrast to a counterion Y^- , which reacts as $\text{H}^+ + \text{Y}^- = \text{HY}$. Therefore, the distribution of a lipophilic cation X^+ is used for measurement of $\Delta\Psi_{p^+}$ in the context of the *pmF*. Ideally X^+ does not undergo secondary reactions. In practice, however, corrections have to be applied for unspecific binding of X^+ particularly to membranes in both compartments.

The lipophilic cationmotive force $\Delta_m F_{\text{X}^+}$ is zero at equilibrium, when the chemical and electric partial forces compensate each other (compare Eq. 8.23):

$$\text{general:} \quad \Delta_m F_{\text{X}^+} = \Delta_d F_{\text{X}^+} + \Delta_{el} F_{p^+} \quad [\text{k}\cdot\text{mol}^{-1}] \quad 8.26$$

$$\text{equilibrium:} \quad \Delta_m \bar{F}_{\text{X}^+} = 0 = \Delta_d \bar{F}_{\text{X}^+} + \Delta_{el} F_{p^+}; \quad \Delta_{el} F_{p^+} = -\Delta_d \bar{F}_{\text{X}^+} \quad [\text{k}\cdot\text{mol}^{-1}] \quad 8.27$$

For compartmental distribution of cation X^+ , an equilibrium concentration ratio (activity ratio; Eq. 8.8) is obtained, $\bar{c}_{\text{X}^+}^b / \bar{c}_{\text{X}^+}^a$, the natural logarithm of which is $\Delta_m \ln \bar{c}_{\text{X}^+} = -2.303 \cdot \Delta p\text{X}$. Multiplication of $\Delta_m \ln c_{\text{X}^+}$ by RT [$\text{k}\cdot\text{mol}^{-1}$] yields the partial chemical force $\Delta_d F_{\text{X}^+}$, which at equilibrium is used to calculate $\Delta_{el} F_{p^+}$ for $z_{\text{X}^+} = 1$.

$$\text{calculate:} \quad \Delta_{el} F_{p^+} = -\frac{RT}{z_{\text{X}^+}} \cdot 2.303 \cdot \Delta_{el} p\text{X} \quad [\text{k}\cdot\text{mol}^{-1}] \quad 8.28$$

Due to the action of the respiratory H^+ pumps and the low permeability of the mtIM for H^+ , there is no equilibration of H^+ between the positive and negative compartments. Therefore, the protonmotive force $\Delta_m F_{\text{H}^+}$ is not zero, and $\Delta_{el} F_{p^+}$ cannot be calculated from the H^+ distribution as described for the equilibrating cation X^+ above.


Lipophilic cationic probes and ion selective electrodes are most commonly used to measure $\Delta \ln c_{\text{X}^+}$ as a basis for calculating the electric part of the *pmF* (Canton et al 1995; Rottenberg 1984; Divakaruni, Brand 2011; Nicholls, Ferguson 2013). Fluorescent probes are widely used as semi-quantitative indicators of $\Delta\Psi_{p^+}$. With additional measurements or assumptions, the fluorescent signals can be converted from relative to absolute values of $\Delta\Psi_{p^+}$ (Scaduto, Grotyohann 1999). The radioactive rubidium isotope is considered to provide the most reliable results on the partitioning between the matrix volume and the outer compartments (Rottenberg 1984), although the non-localized (Mitchell 1966) versus localized models remain open for discussion (Kell 1979). The mitochondrial matrix volume needs to be known either by direct measurement, or by reference to a range from 1 to 2 $\mu\text{L}/\text{mg}$ mt-protein. Measurement of mt-protein requires purification of mitochondria. Corrections are required for unspecific binding of lipophilic cationic probes. In mammalian isolated mitochondria the contribution of $\Delta p\text{H}$ to the *pmF* is smaller than that of $\Delta\Psi_{p^+}$ under typical experimental conditions (e.g. 10 mM P_i). The electroneutral H^+/K^+ antiporter nigericin shifts $\Delta p\text{H}$ further to counterion charge distribution $\Delta p\text{Z}$ and thus to $\Delta\Psi_{p^+}$ (Canton et al 1995; Komlódi et al 2018). Counterion proton charge in $\Delta p\text{Z}$ is distinguished from H^+ proton charge in $\Delta p\text{H}$.

8.4. Protonmotive pressure linearity

The concept of diffusion pressure in a gradient — related to force by local concentration — goes back to Einstein’s diffusion equation (Einstein 1905) referred to as the Einstein–Smoluchowski–Sutherland relation. Paradoxically, the quantity *pressure* has not gained sufficient attention as a fundamental concept beyond the context of the gas law (gas pressure) and van’t Hoff’s osmotic pressure. Throughout the historical record of physical chemistry, pressure has been mixed up with force. This may be explained by the gas equation (Eq. 8.7) that plays a singular and dominant role in physical chemistry (Table 8.1). In pressure-volume work, advancement of volume expansion or volume contraction can be defined as $dV\xi$ [m³]. Partial exergy changes are defined as force times advancement (Eq. 8.20). Consequently, pressure-volume work at constant temperature and pressure is: $\partial G = \Delta_V F \cdot \partial_V \xi$ [J]. Solving for the force,

The pressure-force confusion

On the Dynamical Theory of Gases. By J. CLERK MAXWELL
 Received May 16,—Read May 31, 1866.



James Clerk Maxwell (1831-1879)

This force is called the pressure of the gas.

$$\Delta_V F = \frac{\partial G}{\partial_V \xi} = \frac{\partial G}{\partial V} = p \quad [J \cdot m^{-3} = Pa] \quad 8.29$$

The accurate conclusion is: ‘*This force is called the pressure of the gas*’ (Maxwell 1866). A generalization of equating force and pressure (Eq. 8.29), however, leads to the pressure-force confusion with a remarkable inherent paradox. In physics, work [J] is force [N] times distance [m]. Therefore, force [J·m⁻¹ *def* N] is not the pressure of mechanics [N·m⁻² = J·m⁻³ *def* Pa]. Isomorphic forces are partial derivatives of exergy per advancement, $\partial G / \partial_{tr} \xi_X$, and are expressed in units of exergy per motive unit [J·MU⁻¹]. Pressure, in contrast, is always expressed in the unique SI unit Pa. Isomorphic *pressures* are generally defined for any transformation as the product of *force* [$\frac{J}{MU}$] times a concentration term: *free activity* α_X of the motive entity X. α_X has the units of a concentration of the motive entity [$\frac{MU}{m^3}$]; it is the local molecular concentration [x·m⁻³] or amount concentration [mol·m⁻³] in a diffusion gradient. This is a key message of Einstein’s diffusion equation (Gnaiger 1989).

Four *protonmotive theorems* introduce the concept of protonmotive pressure and predict the experimentally observed non-linear (non-ohmic) relationship between proton flux — proportional to LEAK respiration — and protonmotive force from first principles of physical chemistry, as summarized on [page 74](#) and below.

1. Diffusion gradients: Vector flux J_{ax} of diffusion of an uncharged particle X in the direction of a diffusion gradient in a continuous system is a non-linear function of the force daF_x (Einstein 1905). The force of diffusion is the chemical potential gradient $daF_x = da\mu_x/dz$ [J·mol⁻¹/m]. Vector force times *local concentration* c_x [mol·m⁻³] in the gradient yields the chemical pressure gradient: $c_x \cdot daF_x = da\Pi_x/dz = RT \cdot dc_x/dz$ [J·m⁻³/m = Pa/m]. Diffusion flux is linearly related to the chemical pressure gradient by the mobility u , or to the concentration gradient dc/dz by the diffusion constant, $D=u \cdot RT$: Fick’s linear law of diffusion is a flux-pressure law and yields a non-linear flux-force relation (see Eq. 8.40),

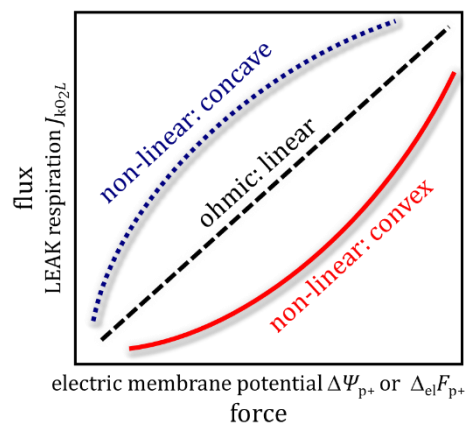
vector flux = -u × local concentration × chemical potential gradient
 $J_{ax} = -u \cdot c_x \cdot daF_x = -u \cdot da\Pi_x/dz = -u \cdot RT \cdot dc_x/dz \quad [mol \cdot s^{-1} \cdot m^{-2}]$

2. From gradients to compartments: Diffusion across a semipermeable membrane in a discontinuous system is driven by an isomorphic force of diffusion containing the chemical potential difference between the two compartments. Gas flow is a linear function of the gas pressure difference between two compartments. The osmotic pressure difference (van't Hoff) and diffusion pressure difference are linearly related to vectorial flux of diffusion across a semipermeable membrane. The concept of local concentration breaks down in a discontinuous system. It is replaced by *free activity* α_X [$\text{MU}\cdot\text{m}^{-3}$], which equals the ratio of pressure [$\text{J}\cdot\text{m}^{-3}$] and force [$\text{J}\cdot\text{MU}^{-1}$]. These first two theorems are well established for diffusion d (Gnaiger 1989), and need to be generalized for any transformation tr (Eq. 8.57),

$$\begin{aligned} \text{flux} &= -u_d \times \text{free activity} \times \text{compartmental force} = -u_d \times \text{pressure} \\ J_{dX} &= -u_d \cdot \alpha_X \cdot \Delta_d F_X = -u_d \cdot \Delta_d \Pi_X = -u_d \cdot RT \cdot \Delta_d c_X \quad [\text{MU}\cdot\text{s}^{-1}\cdot\text{m}^{-3}] \end{aligned}$$

3. Hydrogen ions and counterions: Extension of the concept of diffusion pressure to electron pressure requires consideration of translocation of H^+ and counterion charge Z^- based on the Nernst equation (Mitchell's Module 3; Section 8.1). The initial Δ_{CH^+} (expressed as ΔpH) results in an equivalent p^+ charge dislocation and charge difference Δ_{Cp^+} . Electroneutral H^+Z^- backflow reduces Δ_{CH^+} but maintains Δ_{Cp^+} . Therefore, the total electrochemical pressure can be calculated as the sum of the osmotic H^+ pressure and the electron pressure generated by H^+ translocation and ΔpH -compensating H^+Z^- backflow. Then a nonlinear (non-ohmic) flux-force relation is predicted. In a simple system as shown in Figure 8.3, however, the resulting steep part at low pmF with a concave shape is in direct contradiction to experimental evidence on a convex pattern with a steep increase of LEAK flux at high pmF (Figure 8.8).

Figure 8.8. Linear flux-force relation (Ohm's law) versus non-linear dependence of mitochondrial H^+ leak kinetics on the protonmotive force. LEAK respiration $J_{\text{kO}_2\text{L}}$ provides an indirect measure of vectorial H^+ flux in the absence of phosphorylation $\text{P}\gg$. The commonly observed convex non-linear shape is mainly reported for measurement of $\Delta_{\text{el}}F_{\text{p}^+}$ ($\Delta\Psi_{\text{p}^+}$) as an estimate of the pmF $\Delta_{\text{m}}F_{\text{H}^+}$, considering that ΔpH exerts a small effect (Table 8.5). If kinetic mechanisms modulate the H^+ conductance, then *specific* kinetic models are needed to explain the convex relationship (Garlid et al 1989). In contrast, the concept of protonmotive pressure derives flux-force non-linearity as a *general* feature from fundamental physicochemical principles.



4. Matrix volume fraction: Why are mitochondria and bacteria small? The mitochondrial volume is small with reference to the cytosolic volume, and particularly in comparison to the volume of the incubation medium used in respiratory studies of isolated mitochondria. At typical experimental dilutions of isolated mitochondria, the pattern of the flux-force relation as predicted by protonmotive pressure shifts from concave to convex, in agreement with experimental evidence (Figure 8.8).

Linking the equations of Fick, Einstein and van't Hoff on linear flux-pressure relations — in contrast to Ohm's law on a linear dependence of flux on force — opens the doors to a new understanding of proton leak flux and mitochondrial respiratory control.

8.4.1. Protonpressure theorem 1: Diffusion gradients, Einstein's equation, and Fick's law

The fundamental physico-chemical terms of the protonmotive force are linked to a classical treatment of diffusion, asking how H⁺ diffusing across the mtIM per unit time dt [s], i.e. H⁺ flow, is related to

$\Delta_m F_{H^+}$. Spontaneous translocation of H⁺ is driven by the protonmotive force pmF . A short-circuit of oxidative phosphorylation is caused by various uncoupling mechanisms and is compensated for and can be measured by LEAK-respiration, defined as the oxygen flux required to drive H⁺ across the redox pumps of the mtIM for maintaining the protonmotive force at steady state in the absence of phosphorylation of ADP to ATP. Diffusion of a dissolved substance X at high dilution is analysed on the basis of van't Hoff's concept of osmotic pressure Π_X [Pa], in terms of concentration of X (more strictly activity), $c_X \stackrel{\text{def}}{=} n_X \cdot V^{-1}$ [mol·m⁻³], where the total volume V [m³] is approximately equal to V_{H_2O} , which is the volume of water as the solvent in a dilute aqueous solution (Eq. 8.7),

$$\Pi_X = RT \cdot n_X \cdot V^{-1} = RT \cdot c_X \quad [\text{Pa} \stackrel{\text{def}}{=} \text{J} \cdot \text{m}^{-3}] \quad 8.30$$

Eq. 8.30 is isomorphic to the gas equation, $p \cdot V = n \cdot RT$ [J], where p [Pa] is the gas pressure or barometric pressure in a total volume V containing a total of n moles of a pure ideal gas.

When a vector force acts on a particle X in direction \mathbf{z} , it causes an acceleration, thus increasing the velocity of the particle up to a stationary state, when the effect of the force is counteracted by the frictional resistance (Figure 8.9). At this stationary state, the potential for performing work (*erg*; exergy) is not any longer conserved in kinetic exergy (acceleration), but is dissipated frictionally, such that the driving exergy is consumed only to maintain the particle at constant velocity. Then the motive particle has an average *velocity* \mathbf{v} in the z direction, relative to any reference velocity, irrespective of its speed following the pattern of Brownian motion. Since \mathbf{v} is a vector with magnitude and spatial direction, it is written in bold face,

$$\mathbf{v} \stackrel{\text{def}}{=} d\mathbf{z} \cdot dt^{-1} \quad [\text{m} \cdot \text{s}^{-1}] \quad 8.31$$

Similarly, the motive force $d\mathbf{a}F_{NX}$ of diffusion (units: newton per particle X [N·x⁻¹]) is a vector or gradient, taken here as being oriented in the \mathbf{z} direction only, effective for the motive particle X . The velocity at stationary state is proportional to the force, with the mobility u_{NX} [J⁻¹·m²·x·s⁻¹] as the proportionality constant,

$$\mathbf{v} = -u_{NX} \cdot d\mathbf{a}F_{NX} \quad [\text{m} \cdot \text{s}^{-1}] \quad 8.32N$$

First, the diffusive partial force in Eq. 8.24 is analyzed and linked to molecular diffusion. For a count N_X [x] of uncharged motive molecules localized in a gradient and diffusing at velocity \mathbf{v} [m·s⁻¹], the corresponding flow $I_{\mathbf{a}NX}$ of diffusion across a plane perpendicular to the gradient in direction \mathbf{z} is,

$$I_{\mathbf{a}NX} = N_X \cdot \mathbf{v} \quad [\text{x} \cdot \text{m} \cdot \text{s}^{-1}] \quad 8.33N$$

Subscript \mathbf{d} indicates vectoral diffusion. Subscript N for the molecular format expresses X as a count [x]. In turn, $n_X = N_X \cdot N_A^{-1}$ is the amount of X in the gradient expressed in the unit mole [mol] (Table 8.2). Then flow in the molar format \underline{n} is amount times velocity,

$$I_{\underline{n}X} = n_X \cdot \mathbf{v} \quad [\text{mol} \cdot \text{m} \cdot \text{s}^{-1}] \quad 8.33n$$

The pressure-force confusion


JACOBUS H. VAN'T HOFF

Osmotic pressure and chemical equilibrium

*Nobel Lecture, December 13, 1901**

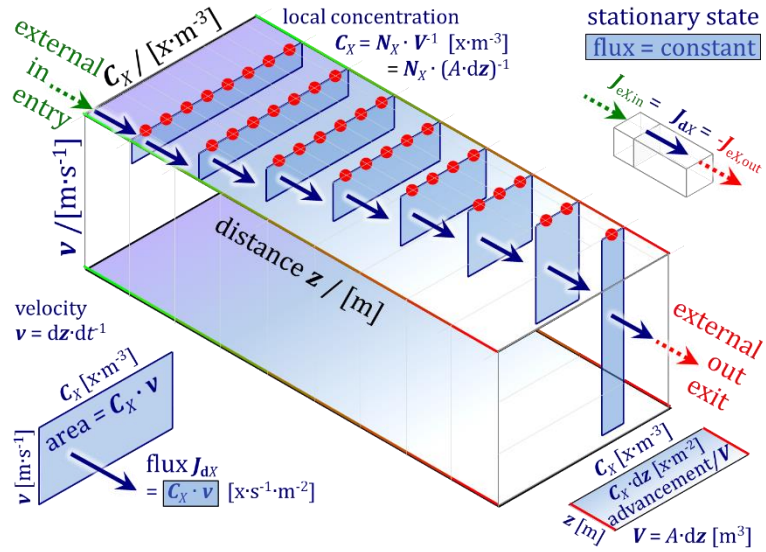
greater pressure on that side of the membrane to which the water is penetrating, i.e. to the solution side.
This pressure is osmotic pressure.

Osmotic forces are in fact unexpectedly great: with a 1% sugar solution they are equal to no less than 2/3 atm (68 kPa).



van't Hoff (1852-1911)

Figure 8.9. Vector flux and velocity: stationary state of diffusion in a linear concentration gradient. Local concentration C_X of particles X (red bullets) within each cross-sectional plane of area A and volume $V = A \cdot dz$. C_X declines linearly with diffusion distance z . External fluxes compensate for the loss of X in the entry plane and the gain of X in the exit plane. Internal fluxes maintain local steady states. As the number of X per V declines, the velocity v increases in indirect proportion, such that the product $C_X \cdot v = J_{dX}$ remains constant along the diffusion gradient. This constant vector flux is shown by areas $C_X \cdot v$ and also by arrows of constant length along the diffusion path. J_{dX} [$x \cdot s^{-1} \cdot m^{-2}$], C_X [$x \cdot m^{-3}$], and advancement per volume $da\xi_X \cdot V^{-1}$ [$x \cdot m^{-2}$] in count format are converted to amount format in Eq. 8.35 to 8.37.



To simplify symbols, the subscript \underline{n} is dropped, $I_{dX} \stackrel{\text{def}}{=} I_{d\underline{n}X}$. In the molar format, X is expressed as amount [mol] (Eq. 8.33n), compared to the molecular format (Eq. 8.33N). The definition of vector advancement of diffusion $da\xi_X$ is obtained by substituting in Eq. 8.33n the velocity from Eq. 8.31,

$$I_{dX} = (n_X \cdot dz) \cdot dt^{-1} \stackrel{\text{def}}{=} da\xi_X \cdot dt^{-1} \quad [\text{mol} \cdot \text{m} \cdot \text{s}^{-1}] \quad 8.34$$

$$da\xi_X \stackrel{\text{def}}{=} n_X \cdot dz \quad [\text{mol} \cdot \text{m}] \quad 8.35$$

Flux is flow per volume, $J_{dX} \stackrel{\text{def}}{=} I_{dX} \cdot V^{-1}$, where $V \stackrel{\text{def}}{=} A \cdot dz$ [m^3]. Therefore, vector flux J_{dX} in a gradient is the amount of X passing per unit time the unit cross-sectional area A , perpendicular to the gradient (Figure 8.9),

$$J_{dX} = n_X \cdot V^{-1} \cdot dz \cdot dt^{-1} = c_X \cdot v \quad [\text{mol} \cdot \text{m}^{-3} \cdot \text{m} \cdot \text{s}^{-1}] = [\text{mol} \cdot \text{s}^{-1} \cdot \text{m}^{-2}] \quad 8.36$$

c_X is the local concentration in the gradient ('local' is emphasized by **bold** face),

$$c_X \stackrel{\text{def}}{=} n_X \cdot V^{-1} \quad [\text{mol} \cdot \text{m}^{-3}] \quad 8.37$$

As a general definition, the work expended in any process is force times advancement. At constant barometric pressure and temperature, the maximum work that can be obtained is defined by the exergy or Gibbs energy transformed in a reversible process; or force is the partial derivative of exergy per advancement (Figure 8.5). Therefore, the force of diffusion in a gradient is in the molecular format \underline{N} and molar format \underline{n} ,

$$daF_{\underline{N}X} = \partial G \cdot \partial da\xi_{\underline{N}X}^{-1} = dG \cdot dz^{-1} \cdot N_X^{-1} \quad [N \cdot x^{-1} = J \cdot m^{-1} \cdot x^{-1}] \quad 8.38\underline{N}$$

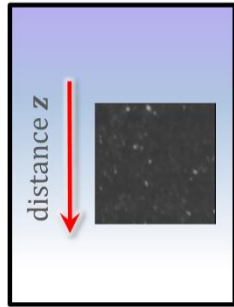
$$daF_X = \partial G \cdot \partial da\xi_X^{-1} = dG \cdot dz^{-1} \cdot n_X^{-1} \quad [N \cdot \text{mol}^{-1} = J \cdot m^{-1} \cdot \text{mol}^{-1}] \quad 8.38\underline{n}$$

$daF_{\underline{N}X}$ has the unit newton per particle [$N \cdot x^{-1}$]. With X expressed in moles [mol], the molar force daF_X is expressed in units [$N \cdot \text{mol}^{-1}$]. The molecular format of the mobility is changed to the molar format u [$J^{-1} \cdot m^2 \cdot \text{mol} \cdot s^{-1}$], such that velocity remains the same as in Eq. 8.32N,

$$v = -u \cdot daF_X \quad [\text{m} \cdot \text{s}^{-1}] \quad 8.39\underline{n}$$


From the linear velocity-force relation (Eq. 8.39) and the dependence of flux on local concentration and velocity (Eq. 8.37), we obtain flux J_{ax} as a function of: (1) mobility, (2) local concentration, and (3) force. This is Einstein's diffusion equation, with the mobility related to the Fick diffusion coefficient $D = u \cdot RT$ (Fick 1855; Einstein 1905; Einstein did not refer to Fick),

Flux and concentration gradient: flux / pressure gradient



$$J_{ax} = -D \cdot \frac{dc_x}{dz}$$

$$J_{ax} = -u \cdot \frac{RT \cdot dc_x}{dz}$$

$$J_{ax} = -u \cdot \frac{d_a \Pi_x}{dz}$$


Adolf Fick (1829-1901)

$$J_{ax} = -u \cdot c_x \cdot d_a F_x \quad [\text{mol} \cdot \text{s}^{-1} \cdot \text{m}^{-2}] \quad 8.40$$

We analyse further the product of local concentration c_x and force. The osmotic pressure equation (Eq. 8.30) is written in differential form of a pressure gradient,

$$d_a \Pi_x \cdot dz^{-1} = RT \cdot dc_x \cdot dz^{-1} \quad [\text{Pa} \cdot \text{m}^{-1}] \quad 8.41$$

Multiplication by $V \cdot dz$ yields the maximum pressure-volume work at constant volume in a reversible process, which is the exergy or partial Gibbs energy change $d_a G$,

$$d_a G \stackrel{\text{def}}{=} d_a \Pi_x \cdot V = RT \cdot dc_x \cdot V \quad [J] \quad 8.42$$

Inserting Eq. 8.42 into Eq. 8.38_n reveals the relationship between force and pressure gradient,

$$d_a F_x = \frac{d_a \Pi_x \cdot dz^{-1}}{c_x} = \frac{RT \cdot dc_x \cdot dz^{-1}}{c_x} \quad [\text{N} \cdot \text{mol}^{-1}] \quad 8.43$$

Since $dc_x \cdot c_x^{-1} = \ln a_x$ (compare Eq. 8.10),

$$d_a F_x = (RT \cdot \ln a_x) \cdot dz^{-1} \quad [J \cdot \text{mol}^{-1} \cdot \text{m}^{-1}] \quad 8.44$$

$RT \cdot \ln a_x$ is the concentration term of chemical potential μ_x (Eq. 8.13), and μ_x° cancels in the slope (gradient). The chemical force of vectorial diffusion is thus shown to be the chemical potential gradient,

$$d_a F_x = RT \cdot \frac{dc_x}{c_x} \cdot dz^{-1} = d_a \mu_x \cdot dz^{-1} \quad [\text{N} \cdot \text{mol}^{-1}] \quad 8.45$$

We can finally explain the product of local concentration and force, $c_x \cdot d_a F_x$ (Eq. 40), in terms of (1) c_x times the chemical potential gradient, (2) RT times the concentration gradient, and (3) the gradient of diffusion pressure,

$$c_x \cdot d_a \mu_x \cdot dz^{-1} = RT \cdot dc_x \cdot dz^{-1} = d_a \Pi_x \cdot dz^{-1} \quad [\text{Pa} \cdot \text{m}^{-1}] \quad 8.46$$

In summary, the force of vectorial diffusion is the chemical potential gradient (Eq. 8.45). Local concentration is the partial derivative of diffusion pressure per chemical potential,

$$c_x = \frac{d_a \Pi_x \cdot dz^{-1}}{d_a \mu_x \cdot dz^{-1}} = \frac{\partial_a \Pi_x}{\partial_a \mu_x} \quad [\text{mol} \cdot \text{m}^{-3}] \quad 8.47$$

Importantly, force and pressure are distinguished. The pressure gradient is the product of local concentration and force,

$$d_a \Pi_x \cdot dz^{-1} = c_x \cdot d_a F_x = c_x \cdot (d_a \mu_x \cdot dz^{-1}) \quad [\text{Pa} \cdot \text{m}^{-1}] \quad 8.48$$

At equilibrium, the local concentration times the force, $c_x \cdot d_a F_x$, is counterbalanced by the diffusion pressure gradient (Einstein 1905),

$$c_X \cdot d_d F_X - RT \cdot \frac{dc_X}{dz} = 0 \quad [J \cdot mol^{-1} \cdot mol \cdot m^{-3} \cdot m^{-1} = Pa \cdot m^{-1}] \quad 8.49$$

This summarizes the analysis of diffusion in a homogenous system, with a continuous concentration gradient (Figure 8.9), vectoral force and pressure, and vectoral flux. The next section explains the challenge of considering the protonmotive force as an isomorphic force applied to the analysis of a compartmental system, with a discontinuity represented by the semipermeable membrane (mtIM). Eq. 8.30 to 8.57 provide the detailed proof for the linearity of the flux-pressure relation for diffusion not only in a concentration gradient but also in a discontinuous compartmental system. Figure 8.10 summarizes the corresponding simple relation between diffusive flux and pressure related to Fick's law of diffusion. In contrast, the relation between flux and force is generally non-linear; it is near-linear only near equilibrium at a magnitude of the force $<RT$.

8.4.2. Protonpressure theorem 2: From gradients to compartments: diffusion and osmotic pressure

The difference of chemical potential $\Delta_d \mu_X$ of X between phase a and b is obtained by integration of Eq. 8.45 from concentration c_a to c_b , which are the homogenous concentrations of X in compartments a and b ,

$$\Delta_d \mu_X = RT \cdot \int_{c_a}^{c_b} \frac{dc_X}{c_X} \quad [J \cdot mol^{-1}] \quad 8.50$$

Integration of Eq. 8.50 is made again with Eq. 8.10,

$$\Delta_d \mu_X = RT \cdot \ln \frac{c_b}{c_a} = RT \cdot \Delta_d \ln c_X \quad [J \cdot mol^{-1}] \quad 8.51$$

Thus, the chemical force of compartmental diffusion is the chemical potential gradient integrated across the compartmental discontinuity. The chemical potential difference is equivalent to the sum of stoichiometric potentials, $\Delta_d \mu_X = \sum_i v_i \cdot RT \ln a_i$ (Figure 8.4). The diffusive forces can now be compared in a gradient (Eq. 8.45) and a compartmental discontinuity,

$$d_d F_X = d_d \mu_X / dz = RT \cdot \ln c_X / dz \quad [J \cdot mol^{-1} / m] \quad 8.52a$$

$$\Delta_d F_X = \Delta_d \mu_X = \sum_i RT \cdot \ln c_i^{v_i} \quad [J \cdot mol^{-1}] \quad 8.52b$$

Importantly, the product $c_X \cdot d_d F_X$ or $RT \cdot dc_X \cdot dz^{-1}$ (Eq. 8.46) is the pressure gradient, and pressure is the product of free activity and force,

$$d_d \Pi_X \cdot dz^{-1} = c_X \cdot d_d F_X = RT \cdot dc_X \cdot dz^{-1} \quad [(mol \cdot m^{-3}) \cdot (J \cdot mol^{-1} \cdot m^{-1}) = Pa \cdot m^{-1}] \quad 8.53a$$

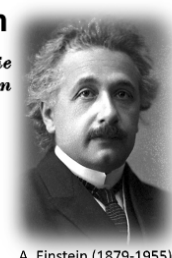
$$\Delta_d \Pi_X = \alpha_X \cdot \Delta_d F_X = RT \cdot \Delta_d c_X \quad [(mol \cdot m^{-3}) \cdot (J \cdot mol^{-1}) = J \cdot m^{-3} = Pa] \quad 8.53b$$

The pressure-force confusion

5. Über die von der molekularkinetischen Theorie der Wärme geforderte Bewegung von in ruhenden Flüssigkeiten suspendierten Teilchen;
von A. Einstein.

Bern, Mai 1905

$$K v - \frac{\partial p}{\partial x} = 0.$$



A. Einstein (1879-1955)

Die letzte Gleichung sagt aus, daß der Kraft K durch osmotische Druckkräfte das Gleichgewicht geleistet wird.

Pressure-forces ..

The pressure-force confusion

'It is quite natural to assume, at least close to equilibrium, that we have **linear relations between the rates and the affinities**. Such a scheme automatically includes empirical laws as Fourier's law for heat flow and **Fick's law for diffusion**.



Ilya Prigogine (1917-2003)

Introduction to
THERMODYNAMICS OF
IRREVERSIBLE PROCESSES
Third Edition

By I. PRIGOGINE
University of Brussels
Brussels, Belgium

Interscience Publishers,
a division of John Wiley & Sons
New York · London · Sydney
Copyright © 1967 by Charles C Thomas, Publishers; assigned to
I. Prigogine
Copyright © 1961, 1967 by I. Prigogine

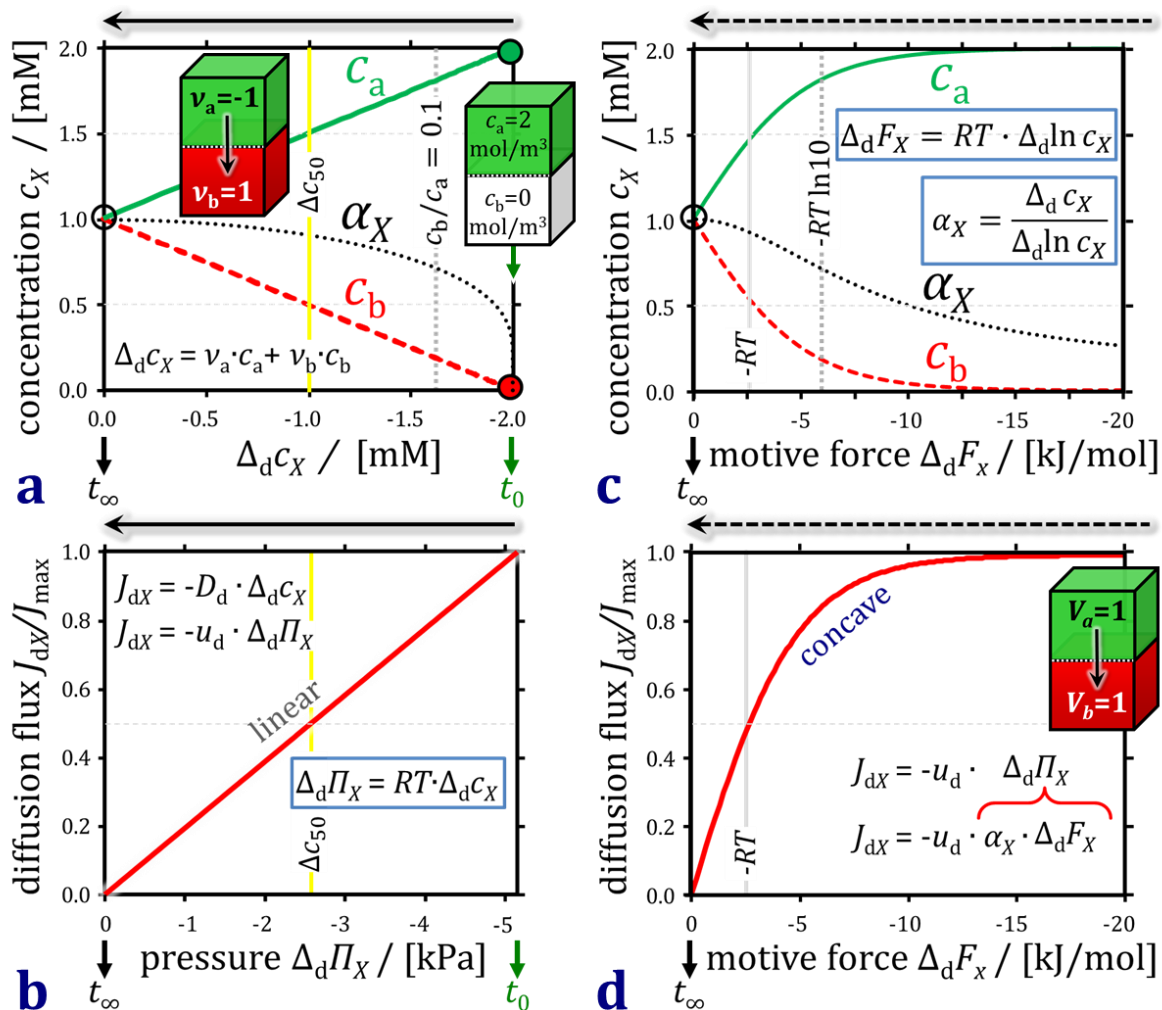


Figure 8.10. Compartmental diffusion of uncharged substance X. (a) The concentration difference $\Delta_d c_X$ has a negative maximum at time t_0 , when X is added to compartment a at high dilution (2 mM) and compartment b contains the pure solvent (t_0 , open system; primary kinetic state). The closed system advances to equilibrium at t_∞ . Δc_{50} at 50 % of the initial concentration difference corresponds to $c_b/c_a=0.33$. (b) Linear dependence of diffusion flux on diffusive pressure difference $\Delta_d \Pi_X = RT \cdot \Delta_d c_X$, representing Fick's law (Eq. 8.55). (c) The force of diffusion is undefined (infinite) in the primary state at t_0 , when free activity α_X approaches zero. At a concentration ratio $c_a/c_b = e$, the motive force (37 °C) is $-RT$ at $\ln(c_b/c_a) = \ln(1/e) = -1$ (Euler's number $e \approx 2.718$ and $1/e \approx 0.37$). The force equals $-RT \cdot \ln 10$ at $c_b/c_a = 0.1$. (d) The flux/force relation represents a pressure/force plot for diffusion. This is not a hyperbolic kinetic saturation curve, but the pressure/force relation in a system with equal compartmental volumes V_a and V_b .

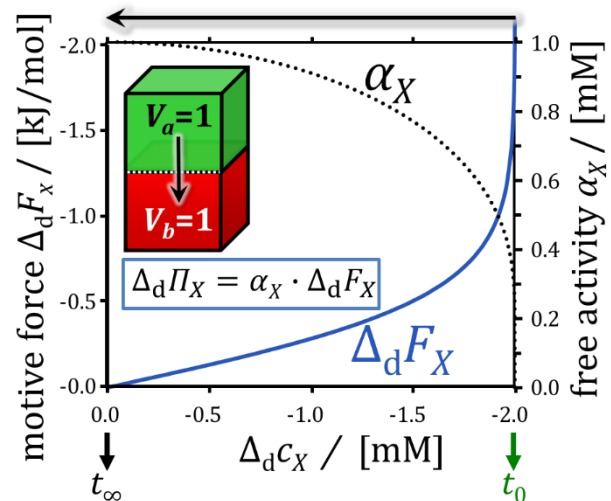
The local concentration c_X in Eq. 8.53a (more generally the local activity α_X) is replaced by the *free activity* α_X [mol] in Eq. 8.53b. A local concentration or activity at the discontinuity of the phase boundary cannot be defined. Isomorphic pressure [Pa], however, is defined as the product of force [$\text{J} \cdot \text{MU}^{-1}$] times the corresponding concentration or free activity [$\text{MU} \cdot \text{m}^{-3}$]. Rearranging Eq. 8.53 for c_X or α_X , we obtain the definition of free activity as a pressure/force ratio (Eq. 8.17; Gnaiger 1989),

$$c_X = \frac{\partial_d \Pi_X}{\partial_d F_X} = \frac{dc_X}{d \ln \frac{c_X}{c^\circ}} \quad [\text{mol} \cdot \text{m}^{-3}] \quad 8.54a$$

$$\alpha_X = \frac{\Delta_d \Pi_X}{\Delta_d F_X} = \frac{\sum_i v_i \cdot c_i}{\sum_i v_i \cdot \ln \frac{c_i}{c^\circ}} = \frac{\Delta_d c_X}{\Delta_d \ln c_X} \quad [\text{mol} \cdot \text{m}^{-3}] \quad 8.54b$$

Figure 8.11. Force and free activity. In a simple diffusion system (Figure 8.10), the increase of force is mirrored by the decline in free activity. Their product is diffusion pressure, which increases linearly with concentration difference as $RT \cdot \Delta_d c_X$.

The misleading name ‘mean of the concentrations of the solute in the two compartments’ (Kedem, Katchalski 1958) has been given to the term α_X . α_X is zero but not the mean in the primary kinetic state when c_b is zero. Then the isomorphic force $\Delta_d F_X$ is undefined at infinity, whereas pressure as the product $\alpha_X \cdot \Delta_d F_X$ has a well-defined value of $RT \cdot \Delta_d c_X$ (Figure 8.11).



From Eq. 8.53 and Eq. 8.54, chemical flux of diffusion is a linear function of pressure, $da\Pi_X \cdot dz^{-1}$ or $\Delta_d \Pi_X$ (Figure 8.10),

$J_{dX} = -u \cdot da\Pi_X \cdot dz^{-1} = -D \cdot dc_X \cdot dz^{-1}$	[mol·s ⁻¹ ·m ⁻²]	8.55a
$J_{dX} = -u_d \cdot \Delta_d \Pi_X = -D_d \cdot \Delta_d c_X$	[mol·s ⁻¹ ·m ⁻³]	8.55b

In contrast, the flux-force relationship is non-linear,

$J_{dX} = -L \cdot daF_X$	[mol·s ⁻¹ ·m ⁻²]	8.56a
$J_{dX} = -L_d \cdot \Delta_d F_X$	[mol·s ⁻¹ ·m ⁻³]	8.56b

L and L_d are known as the phenomenological coefficients, and flux-force relations are linear, if L and L_d are constant (Onsager 1931). However, $L = u \cdot c_X$ and $L_d = u_d \cdot \alpha_X$ vary as direct functions of the force (Eq. 8.54), which explains the non-linear behavior of diffusion in relation to force, in contrast to flux-pressure linearity (Eq. 8.55). Nearly perfect linearity is obtained, when the minimum compartmental $c_X > 0.5 \cdot |\Delta c_X|$, since then the force remains near equilibrium within $\pm 2.8 \text{ kJ} \cdot \text{mol}^{-1}$ (Figure 8.10d).

Considering the relation between the diffusion coefficient and mobility in a gradient, $D = u \cdot RT$, and in a compartmental system, $D_d = u_d \cdot RT$, we obtain Fick's law of diffusion, which in contrast to a flux-force relation (Eq. 8.56) is a flux-pressure relation (Eq. 8.55),

$J_{dX} = -u \cdot RT \cdot dc_X \cdot dz^{-1}$	[mol·s ⁻¹ ·m ⁻²]	8.57a
$J_{dX} = -u_d \cdot RT \cdot \sum_i \frac{c_i}{v_i} = -u_d \cdot RT \cdot \left(\frac{c_b}{v_b} + \frac{c_a}{v_a} \right) = -u_d \cdot RT \cdot \Delta_d c_X$	[mol·s ⁻¹ ·m ⁻³]	8.57b

Concepts of facilitated diffusion – the phosphocreatine/creatine kinase system for codiffusion with ADP, codiffusion with CO₂ in the carbonic acid/carbonic anhydrase system, facilitated H⁺ transport by diffusion of buffer molecules – are collectively based on the importance of concentration differences ($\cdot RT = \text{pressure}$) rather than concentration ratios (diffusive forces). Propulsion by electric potential differences has to be added.

8.4.3. Protonpressure theorem 3: Hydrogen ions and counterions: the Nernst equation and electrochemical pressure

The concept of electrochemical (electrolytic) pressure is not new, since it was introduced by Nernst 130 years ago: *‘In 1889 he elucidated the theory of galvanic cells by assuming an “electrolytic pressure of dissolution” which forces ions from electrodes into solution and which was opposed to the osmotic pressure of the dissolved ions’* (www.nobelprize.org/prizes/chemistry/1920/nernst). The challenge is to derive α_{p^+} .

In the LEAK state, the pmF contains a maximum electric potential difference $\Delta_{el}F_{p^+}$ of c. 200 mV, equivalent to 19.3 kJ/mol p^+ for H^+ moved from b (matrix) to a (internal anode; Figure 8.2). If Δ_{mpH} accounts for the entire $\Delta_m F_{H^+}$ of 200 mV, $\Delta_d F_{H^+}$ is 100 mV or 9.6 kJ/mol H^+ , with an equal contribution of 100 mV by $\Delta_{el}F_{p^+}$ (Table 8.5). The c_{H^+a}/c_{H^+b} ratio would have to be 42 and $\Delta_{mpH} = \log(42) = 1.6$.

Δ_{mpH} is reduced by electroneutral cotransport of counterion charge Z^- with H^+ from the anodic to the matrix phase b in the form of HY . The mtIM is impermeable for counterions Y^- (Mitchell's Module 3, p. 73). The total counterion charge distribution c_{Z^-b}/c_{Z^-a} is (at $z \stackrel{def}{=} z_{Z^-} = -1$),

$$\frac{c_{Z^-b}}{c_{Z^-a}} = e^{\frac{z \cdot \Delta_{el}F_{ep^+}}{fT}} = e^{\frac{z \cdot \Delta_{el}F_{np^+}}{RT}} \tag{8.58}$$

which amounts to 1778 at $\Delta_{el}F_{ep^+a} = 200$ mV at a theoretical $\Delta_{mpH} = 0$. Then $\Delta_{elpZ} = \log(1778) = 3.2$. With H^+_a electrically neutralized by counterion charge Z^-_a at the anodic $pH_a = pZ_a$ of 7.2 and $c_{Z^-a} = c_{H^+a} = 0.06 \mu M$, the corresponding c_{Z^-b} is 112.2 μM in the mt-matrix at the electric potential difference of 200 mV. The electric pressure difference is then calculated as $RT/z_{Z^-} \cdot \Delta_{el}c_{Z^-} = 0.29$ kPa (compare Eq. 8.53b). Pressure divided by force is the free charge activity α_{Z^-} of 15 μM (Eq. 8.54b), equivalent to α_{p^+} on account of $z_{Z^-} = -1$. At a force of 19.3 kJ the corresponding protonmotive pressure is 0.29 Pa.

The immediate implication for mitochondrial bioenergetics is a shift from Ohm's linear law on flux-force relations to the linear flux-pressure law, to explain the enigmatic nonlinear dependence of LEAK respiration on mitochondrial membrane potential. In the thermodynamics of irreversible processes, a paradigm shift is required from analysis of flux-force relations to the study of flux as a function of isomorphic pressure.

For the conditions described above in a system with $V_a=V_b$, the equilibrium concentration of H^+ and the counterion charge distributing between the anodic and cathodic phase is $(112.18+0.06)/2 = 56.12 \mu M$ ($pZ_a = pZ_b = 4.25$). The corresponding flux-force relation is highly non-linear or non-ohmic (Figure 8.12a). However, the concave shape is in direct contrast to experimental evidence on a convex flux-force relation of mitochondrial LEAK-respiration (Garlid et al 1989). Why are mitochondria small?

8.4.4. Protonpressure theorem 4: Matrix volume fraction and flux-force relation

The flux-force relation inverts from concave to convex with increasing anodic volume fraction $\Phi_a = V_a/V$ (Figure 8.12). The matrix volume fraction of isolated mitochondria in the experimental chamber of volume V is $\Phi_b = V_{mt}/V$. At a typical mt-protein concentration of 0.1 mg/mL, $\Phi_b = 0.0001$, and $\Phi_a = 1-\Phi_b = 0.9999$ (Section 8.2.6). The non-ohmic dependence of LEAK flux on the mt-membrane potential difference is explained for the first time by the convex shape of the pressure-force relation based on fundamental physicochemical principles (Figure 8.12d).

The pressure-force confusion

WALTHER NERNST

Studies in chemical thermodynamics

Nobel Lecture, December 12, 1921



Walther Nernst (1864-1941)

For, in the case of normal, i.e. non-electrolyte, dissolution, pressures are attained which, too, are enormous under certain circumstances. Let us for example consider the process when ice and sulphur trioxide dissolve in dilute sulphuric acid. During this process 38,000 calories are generated which, if electromotively active, would yield a galvanic cell with an e.m.f. of approximately

$$E = \frac{38,000}{23,050} = 1.65 \text{ volts}$$

From *Nobel Lectures, Chemistry 1901-1921*, Elsevier Publishing Company, Amsterdam (1966)

Figure 8.12. Protonmotive pressure – protonmotive force times free activity. The dependence of pressure – hence flux – on force shifts with increasing anodic volume fraction Φ_a and correspondingly small matrix volume fraction Φ_b from concave at equal volumes (a), to sigmoidal (b, c), and convex at $\Phi_a = 0.9999$ (d). Electroneutral H^+Z^- -counterion charge backflux into the matrix maintains Δ_{mpH} at zero. At $\Delta_{el}F_{p^+}$ of 200 mV, the anodic pH_a and pZ_a are 7.2 (0.06 μM). Then a negative charge concentration of 112.2 μM (pZ_b 3.95) is required for an electric cross-membrane potential difference of 200 mV. The equilibrium concentrations \bar{c}_{Z^-} are buffered by the high anodic volume at high Φ_a , and equal the free charge activity $\bar{\alpha}_{Z^-} = \bar{c}_{Z^-}$ at equilibrium (shown by symbols on the left Y-axis and numerical values). Protonmotive force and pressure calculated at 37 °C.

The equilibrium concentration is,

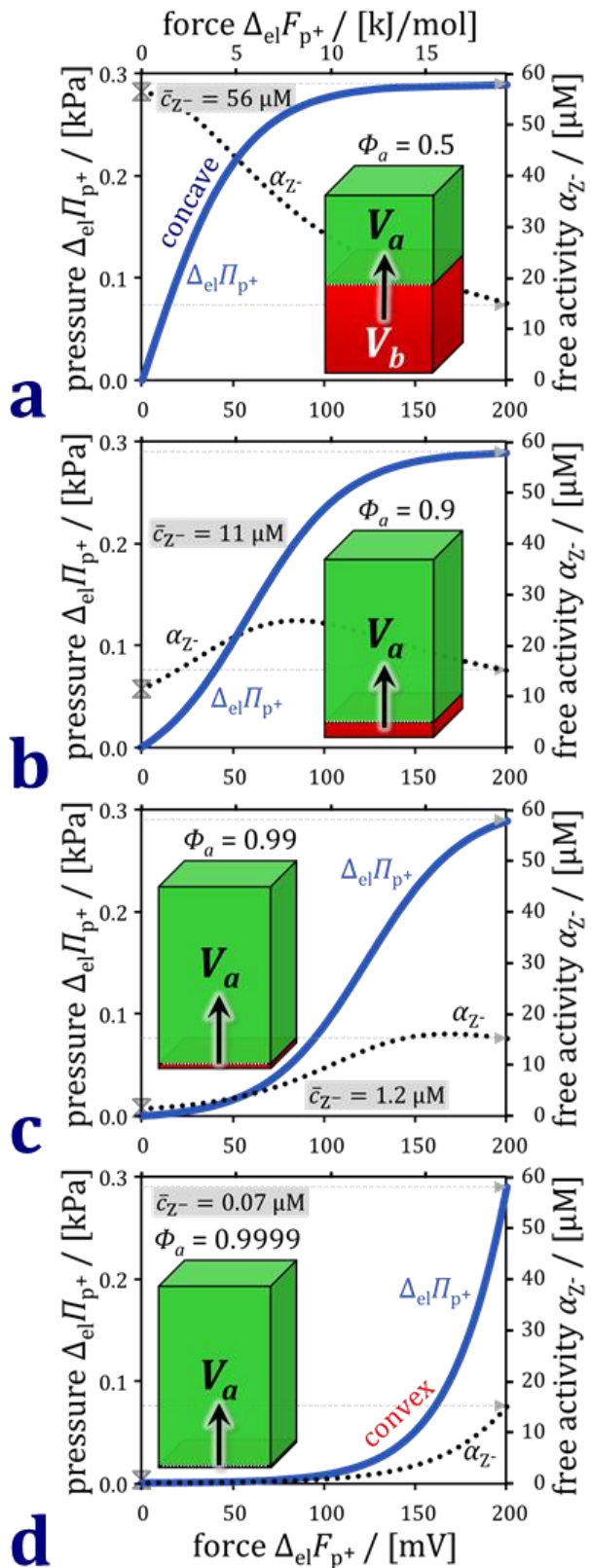
$$\bar{c}_{Z^-} = c_a \cdot \Phi_a + c_b \cdot \Phi_b \quad [\mu\text{mol} \cdot \text{L}^{-1}] \quad 8.59$$

The volume fraction takes the role of the stoichiometry ($\Phi_b \cdot \nu_b^{-1}$), when expressing diffusive advancement (Eq. 8.5) as volume-specific advancement $d_d \xi_{YX} = d_d \xi_X \cdot V^{-1}$, where $V = V_a + V_b$ and the compartmental concentration is $c_b = n_b \cdot V_b^{-1}$,

$$d_d \xi_{YX} = d_d c_b \cdot (\Phi_b \cdot \nu_b^{-1}) \quad [\mu\text{mol} \cdot \text{L}^{-1}] \quad 8.60$$

At high Φ_a (Figure 8.12d), the equilibrium concentration of 0.074 μM is close to the anodic counterion charge concentration of 0.063 μM at 200 mV. This ‘volume-fraction buffering’ in a closed compartmental system results in flux control states that are practically identical to an open system, when cytosolic (internal anodic) c_{Z^-} is maintained constant by external compensation while hydrogen ions H^+ are pumped into phase a and recycled with counterion charge translocation and accumulation of Z^- in the matrix phase b .

An inversion from concave to convex flux/force relations has been shown in an ergodynamic reaction kinetics analysis comparing a closed with an open reaction system. This has general implications for metabolism and OXPHOS flux control beyond LEAK respiration and the pmF (Gnaiger 1989).



For many decades the pressure-force confusion has blinded the most brilliant minds, reinforcing the expectation that Ohm's linear flux-force law should apply to the hydrogen ion circuit and protonmotive force. Fick (1855) compared 'hydrodiffusion' to Ohm's law, but did not refer to gas pressure. Isomorphic forces including electric, chemical and electrochemical potential differences are quantities of *intensity*, whereas osmotic and chemiosmotic pressure is related to *capacity*.

- **Intensity:** concentration ratios; exergy per advancement, expressed in units joule per motive unit [$\text{J}\cdot\text{MU}^{-1}$] – such as [$V = \text{J}\cdot\text{C}^{-1}$] – in line with the forces of physics: exergy per advanced distance in a gradient, expressed in units newton [$\text{N} = \text{J}\cdot\text{m}^{-1}$].
 - **Capacity:** concentrations; exergy per volume, expressed in units pascal [$\text{Pa} = \text{J}\cdot\text{m}^{-3}$].
- Physicochemical principles explain the highly non-linear flux-force relation in the dependence of LEAK respiration on the *pmF*. The explanation is based on an extension of Fick's law of diffusion and Einstein's diffusion equation, representing protonmotive pressure – isomorphic with mechanical pressure, hydrodynamic pressure, gas pressure, and osmotic pressure – which collectively follow the generalized linear *flux-pressure law*.

The hydrodiffusion across membranes might properly call far more attention of physicists than it received so far, not merely as one of the elementary factors of organic life but as a physical process of the highest interest by itself. .. The distribution of a dissolved particle in the solvent proceeds, as far as it takes place undisturbed under the exclusive influence of the molecular forces, according to the same law, which was established by Fourier for the distribution of heat in a conductor, and which Ohm has transposed with such brilliant success to the distribution of electricity (where it is of course not strictly correct, as is well known). - Fick Adolf (1855) Über Diffusion. Pogg Ann 94:59-86.

The 'ergodynamic flux-pressure hypothesis' bridges the gap between thermodynamics and kinetics. Further theoretical analyses will reveal limitations inherent in the present derivation of the four protonpressure theorems. Advanced experiments can be designed to directly test the quantitative hypotheses derived from them. A theory is not the final target, but provides the guideline for exploratory research and a deeper understanding, not limited to mitochondrial respiratory control. The formalization of isomorphic flux and pressure in relation to the isomorphic forces points to a generalized concept on the control of energy transformations and dynamic processes.

It is not that we can never observe the fate of a single small group of atoms or even a single atom. We can, occasionally. But whenever we do, we find complete irregularity, co-operating to produce regularity only on the average. .. The Brownian movement of a small particle suspended in a liquid is completely irregular. But if there are many similar particles, they will by their irregular movement give rise to the regular phenomenon of diffusion.

Schrödinger Erwin (1944) What is life? The physical aspect of the living cell. Cambridge Univ Press (1st edition).

The pressure-force confusion

*'.. the coupling membrane has a low permeability to ions generally and not only to protons, so that the electron transport and ATPase systems could be coupled through the sum of the **electrical pressure difference** and the **osmotic pressure difference** (i.e. the **electrochemical potential difference**) of protons that would thus be conserved across the membrane.'*



Peter Mitchell (1920-1992)

CHEMIOSMOTIC COUPLING IN OXIDATIVE AND PHOTOSYNTHETIC PHOSPHORYLATION
By PETER MITCHELL
 Glynn Research Ltd.
 Bodmin, Cornwall
 May, 1966.



Erwin Schrödinger (1887-1961)

A: Conversions of metabolic fluxes and forces

A1. Some fundamental equations and conversion factors (see Table 8.3)

$$\ln x + \ln y = \ln(x \cdot y) \quad \ln x_2 - \ln x_1 = \ln \frac{x_2}{x_1} \quad z \cdot \Delta \ln x = \ln \frac{x_2^z}{x_1^z} \quad \text{A1.1}$$

$$x \cdot \ln y = \ln \cdot y^x \quad -x \cdot \ln y = \ln \cdot y^{-x} = \ln \frac{1}{y^x} \quad \text{A1.2}$$

$$\int_{x_1}^{x_2} \frac{dx}{x} = \ln \frac{x_2}{x_1} = \ln x_2 - \ln x_1 \quad \int_{y_1}^{y_2} \frac{dy}{y} = \ln \frac{y_2}{y_1} = \ln \frac{x_1}{x_2} \quad \text{for } y = \frac{1}{x} \quad \text{A1.3}$$

$$\text{pH} = -\log a_{\text{H}^+} = -\frac{\ln a_{\text{H}^+}}{\ln 10} \quad a_{\text{H}^+} = 10^{-\text{pH}} \quad \ln a_{\text{H}^+} = -\ln 10 \cdot \text{pH} \quad \text{A1.4}$$

$$c_{\text{H}^+} [\text{M}] = 10^{-\text{pH}} \cdot c^\circ \quad c_{\text{H}^+} [\mu\text{M}] = 10^{6-\text{pH}} \cdot c^\circ \quad \text{A1.5}$$

$$\text{pH } 7 = 10^{-7} \text{ M H}^+ = 0.1 \mu\text{M H}^+ \quad \text{pX } 3 = 10^{-3} \text{ M X}^z = 1 \text{ mM X}^z \quad \text{A1.6}$$

absolute temperature, T	273.15; 298.15; 310.15 K	at 0; 25; 37 °C
RT	2.271; 2.479; 2.579 kJ·mol ⁻¹	at 0; 25; 37 °C
$\ln(10)$	2.302585	
$RT \cdot \ln(10)$	5.229; 5.708; 5.938 kJ·mol ⁻¹	at 0; 25; 37 °C
$fT \cdot \ln(10) = (RT/F) \cdot \ln(10)$	54.20; 59.16; 61.54 mV	at 0; 25; 37 °C
$1/(z_0 F)$	2.591 μmol/(4 C)	$z_0 = 4$
e elementary charge	1.602 176 634 · 10 ⁻¹⁹ C·x ⁻¹	
e Euler's number	2.718281828459	$\ln(e) = 1$

A2. Conversion factors for units of oxygen flux

Comparability of quantitative results on respiratory fluxes is aided by using common units. Considering the variety of units used in various disciplines of respiratory physiology (e.g. $V_{\text{O}_2\text{max}}$), a common basis may only be found with reference to SI units (Gnaiger 1983, 1993).

$$1 \text{ mL O}_2 \cdot \text{min}^{-1} \cdot \text{kg}^{-1} = 0.744 \mu\text{mol} \cdot \text{s}^{-1} \cdot \text{kg}^{-1} \text{ at STPD}$$

When respiratory activity is expressed per volume of the O₂k chamber or volume-specific O₂ flux, the base SI unit is [mol·s⁻¹·m⁻³]. Since O₂ concentration in pure water at equilibrium with air at standard barometric pressure of 100 kPa is 254.8 to 207.3 μmol·dm⁻³ (25 to 37 °C), it is most practical to express O₂ concentration in μM units,

$$1 \mu\text{mol O}_2/\text{L} = 1 \mu\text{mol}/\text{dm}^3 = 1 \mu\text{M} = 1 \text{ nmol}/\text{mL} = 1 \text{ nmol}/\text{cm}^3$$

Table A1. Conversion of various units into SI units when expressing respiration as mass-specific oxygen flux, $J_{\text{O}_2/m}$.

J	[Unit _{<i>i</i>}]	x	Factor	=	$J_{\text{O}_2/m}$ [μmol O ₂ ·s ⁻¹ ·kg ⁻¹]
12	ng·atom O·min ⁻¹ ·mg ⁻¹	x	8.33	=	100
12	μmol O·min ⁻¹ ·g ⁻¹	x	8.33	=	100
12 000	natom O·min ⁻¹ ·g ⁻¹	x	0.00833	=	100
6	nmol O ₂ ·min ⁻¹ ·mg ⁻¹	x	16.67	=	100
6	μmol O ₂ ·min ⁻¹ ·g ⁻¹	x	16.67	=	100
6	mmol O ₂ ·min ⁻¹ ·kg ⁻¹	x	16.67	=	100

The SI unit $\text{nmol O}_2 \cdot \text{s}^{-1}$ is used for the corresponding respiratory flow in the classical bioenergetic literature (Chance and Williams 1956). In the bioenergetic context of $\text{H}^+ / 2\text{e}$ or H^+ / O ratios (Mitchell and Moyle 1967) or $\text{P} \gg \text{O}$ ratios, corresponding fluxes were then frequently expressed as $J_{\text{P}} / J_{\text{O}}$, where $J_{\text{O}_2} = 2 \cdot J_{\text{O}}$, the latter in ‘bioenergetic’ units [$\text{natoms O} \cdot \text{s}^{-1}$] (Slater et al 1973). In bioenergetics a variety of expressions is used for units of amount of oxygen (natoms oxygen ; natoms O ; ng.atom O ; nmol O), with the identical meaning: 0.5 nmol O_2 .

A3. Temperature adjustment of flux

Manometric techniques (‘Warburg apparatus’) require good temperature control and were used extensively at 37°C for respirometry with mammalian cells up to the middle of the last century, and later occasionally with isolated mitochondria. Spectrophotometers and Clark-type Oxygraphs had comparatively poor or no temperature control and thus measurements were performed at room temperature (Chance and Williams 1955). This conceptually trivial (technically less simple) reason is largely forgotten, but a convention is continued, and frequently mammalian mitochondrial respiration is still measured at 25°C or 30°C in ‘modern’ bioenergetics. Mitochondrial physiology requires functional measurements at physiological temperature. A Q_{10} of 2 (multiplication factor for an increase by 10°C) is frequently assumed for adjustment to physiological temperature, but can be considered as an approximation only.

Metabolic reactions are not a linear function of temperature. $Q_{10} = 2$ (Eq. A3.1a) is an approximation for the temperature dependence of chemical reactions in general (Arrhenius equation) and metabolic fluxes in particular. To adjust flux, J_1 , measured at temperature T_1 (for instance, $T_1 = 25^\circ\text{C}$; Table A2) to the physiological temperature, $T_2 = 37^\circ\text{C}$, the exponential relation (Eq. A3.1) is used to calculate J_2 (37°C),

$$J_2 = 10^{\log J_1 - \log Q_{10} / (\frac{10}{T_1 - T_2})} \quad \text{A3.1}$$

The derivation is obtained from the definition of the Q_{10} ,

$$Q_{10} = \left(\frac{J_1}{J_2}\right)^{\frac{10}{T_1 - T_2}} \quad \text{A3.1a}$$

In log transformation, Eq. A3.1a is,

$$\log Q_{10} = (\log J_1 - \log J_2) \cdot \left(\frac{10}{T_1 - T_2}\right) \quad \text{A3.1b}$$

Division by the term $10 / (T_1 - T_2)$ yields,

$$\log Q_{10} / \left(\frac{10}{T_1 - T_2}\right) = \log J_1 - \log J_2 \quad \text{A3.1c}$$

and solving for $\log J_2$,

$$\log J_2 = \log J_1 - \log Q_{10} / \left(\frac{10}{T_1 - T_2}\right) \quad \text{A3.1d}$$

Eq. A3.1 is then obtained by inserting Eq. A3.1d into Eq. A3.1e,

$$J_2 = 10^{\log J_2} \quad \text{A3.1e}$$

For any given Q_{10} and temperature difference $\Delta T=T_1-T_2$, a multiplication factor $F_{\Delta T}$ can be calculated from Eq. A3.1 to obtain J_2 (Table A2),

$$J_2 = J_1 \cdot F_{\Delta T} \tag{A3.2a}$$

$$F_{\Delta T} = 10^{-\log Q_{10} / (\frac{10}{T_1 - T_2})} \tag{A3.2b}$$

The Q_{10} is the $F_{\Delta T}$ (Eq. A3.2b) for a temperature difference of 10 °C. Obviously, if T_2 is 37 °C and T_1 is 27 °C ($T_1-T_2=-10$), then the exponent in Eq. A3.2b is $\log Q_{10}$, and $F_{\Delta T} = Q_{10}$. For T_1 of 25 °C or 30 °C and $Q_{10}=2$, the ΔT -factor $F_{\Delta T}$ is 2.30 and 1.62, respectively. Clearly, if respiratory flux at physiological temperature is of interest, respiration should be measured at this temperature rather than adjusted on the basis of potentially inaccurate assumptions about the Q_{10} .

In HRR, experimental temperature is controlled in the range of 4 °C to 47 °C at a stability better than ± 0.002 °C.

Table. A2. Conversion of metabolic flux from experimental temperature T_1 to adjusted temperature T_2 , based on Q_{10} values of 2.0, 1.8 and 2.2.

Q_{10}	2.00			1.80			2.20		
T_1 °C	25	30	37	25	30	37	25	30	37
T_2 °C	$F_{\Delta T}$	$F_{\Delta T}$	$F_{\Delta T}$	$F_{\Delta T}$	$F_{\Delta T}$	$F_{\Delta T}$	$F_{\Delta T}$	$F_{\Delta T}$	$F_{\Delta T}$
25	1.00	0.71	0.44	1.00	0.75	0.49	1.00	0.67	0.39
30	1.41	1.00	0.62	1.34	1.00	0.66	1.48	1.00	0.58
35	2.00	1.41	0.87	1.80	1.34	0.89	2.20	1.48	0.85
37	2.30	1.62	1.00	2.02	1.51	1.00	2.58	1.74	1.00
38	2.46	1.74	1.07	2.15	1.60	1.06	2.79	1.88	1.08
39	2.64	1.87	1.15	2.28	1.70	1.12	3.02	2.03	1.17
40	2.83	2.00	1.23	2.41	1.80	1.19	3.26	2.20	1.27

A4. SI prefixes

10^{24}	yotta	Y	1 000 000 000 000 000 000 000 000
10^{21}	zetta	Z	1 000 000 000 000 000 000 000
10^{18}	exa	E	1 000 000 000 000 000 000
10^{15}	peta	P	1 000 000 000 000 000
10^{12}	tera	T	1 000 000 000 000
10^9	giga	G	1 000 000 000
10^6	mega	M	1 000 000
10^3	kilo	k	1 000
10^2	hecto	h	100
10^1	deca	da	10
10^{-1}	deci	d	0.1
10^{-2}	centi	c	0.01
10^{-3}	milli	m	0.001
10^{-6}	micro	μ	0.000 001
10^{-9}	nano	n	0.000 000 001
10^{-12}	pico	p	0.000 000 000 001
10^{-15}	femto	f	0.000 000 000 000 001
10^{-18}	atto	a	0.000 000 000 000 000 001
10^{-21}	zepto	z	0.000 000 000 000 000 000 001
10^{-24}	yocto	y	0.000 000 000 000 000 000 000 001



B: Substrates, uncouplers, inhibitors - SUIT

B1. O2k manual titrations: mitochondria, homogenate, permeabilized cells and tissues



Table B1. Manual titrations for O2k-chamber volume of 2.0 mL

Substrates	Event	Concentration in syringe (solvent)	Storage [°C]	Final conc. in 2 mL	Titration [μL]	Syringe [μL]
Pyruvate	P	2 M (H ₂ O)	fresh	5 mM	5	25
Malate	M	0.4 M (H ₂ O)	-20	2 mM	10	25
Malate	M	0.05 M (H ₂ O)	-20	0.05 mM	2	10
Glutamate	G	2 M (H ₂ O)	-20	10 mM	10	25
Succinate	S	1 M (H ₂ O)	-20	10 mM	20	50
Octanoylcarnitine	Oct	0.1 M (H ₂ O or DMSO)	-20	0.5 mM	10	25
Glycerophosphate	Gp	1 M (H ₂ O)	-20	10 mM	20	50
Ascorbate	As	0.8 M (H ₂ O)	-20	2 mM	5	25
TMPD	Tm	0.2 M (H ₂ O)	-20	0.5 mM	5	25
Cyt. c	c	4 mM (H ₂ O)	-20	10 μM	5	25
ADP+ Mg ²⁺	D	0.5 M (H ₂ O)	-80	1 - 5 mM	4 - 20	25
ATP+ Mg ²⁺	T	0.5 M (H ₂ O)	-80	1 - 5 mM	4 - 20	25
Uncoupler						
CCCP*	U	0.1 mM (EtOH)	-20	0.05 μM step	1 μL step	10
CCCP*	U	1.0 mM (EtOH)	-20	0.5 μM step	1 μL step	10
Inhibitors						
Rotenone	Rot	1 mM (EtOH)	-20	0.5 μM	1	10
Malonic acid	Mna	2 M (H ₂ O)	fresh	5 mM	5	25
Antimycin A	Ama	5 mM (EtOH)	-20	2.5 μM	1	10
Myxothiazol	Myx	1 mM (EtOH)	-20	0.5 μM	1	10
Sodium azide	Azd	4 M (H ₂ O)	-20	≥100 mM	≥50	50
KCN	Kcn	1 M (H ₂ O)	fresh	1.0 mM	2	10
Oligomycin	Omy	5 mM (EtOH)	-20	2.5 μM	1	10
Carboxyatractyloside	Cat	5 mM (H ₂ O)	-20	0.75 mM	2	10
Other						
Digitonin	Dig	10 mg/mL (DMSO)	-20	10 μg/Mx cells	1 μL/Mx	10
Catalase in MiR06	Ctl	112 000 U/mL	-20	280 U/mL	5	25
H ₂ O ₂ for reoxygenation	Hp	200 mM	fresh		1-3	10

* 0.1 mM stock for mt-preparations with high uncoupler sensitivity; 1 mM stock for mt-preparations with low uncoupler sensitivity, living cells in various culture media (e.g. RPMI, DMEM, EGC) and for TIP2k.

SUIT symbols have evolved for laboratory practice with the requirement to keep abbreviations short. They are not intended for use outside the SUIT framework.

Caution: When using the O2k-sV-Module (small-volume O2k-Chamber: 0.5 mL), titration volumes and stock concentrations have to be adjusted. *Further details:*

 http://www.bioblast.at/index.php/MiPNet09.12_O2k-Titrations

B2. Substrates of the TCA cycle and major entries

Single capital letters for the most commonly used fuel substrates

N	NADH-linked (N-) pathway, at a defined coupling state
S	S-pathway, at a defined coupling state
\overline{NS}	Convergent \overline{NS} -pathways, with N- and S-type substrates added in combination, at a defined coupling state
N+S	Flux or flow calculated as the arithmetic sum of N- plus S-pathway respiration measured separately
N/\overline{NS}	Pathway control ratio at a defined coupling state
FN	Pathway with a F- and N-competent substrate combination (e.g. OctGM)
P	Pyruvate; if added after GM: $FCF_P=1-GM/PGM$
G	Glutamate; if added after PM: $FCF_G=1-PM/PGM$
M	Malate; inhibition by Δ concentration Z to Y: $FCF_{\Delta c}=1-M_Y/M_Z$
S	Succinate; if added after N: $FCF_S=1-N/\overline{NS}$
F	Fatty acid supporting FA oxidation (e.g. OctM), involving Complexes CETF and CI
Fu	Fumarate
Og	Oxoglutarate
Oca	Octanoate
Paa	Palmitate
Oct	Octanoylcarnitine
Pal	Palmitoylcarnitine
As	Ascorbate
Tm	TMPD
c	Cytochrome c; c control factor: $FCF_c=1-J_{CHO}/J_{cCHO}$
Gp	Glycerophosphate



[http://www.bioblast.at/index.php/MitoPedia:Substrates and metabolites](http://www.bioblast.at/index.php/MitoPedia:Substrates_and_metabolites)

B3. Inhibitors of respiratory complexes, dehydrogenases or transporters

Atr	Attractyloside; ANT; $L(Atr)$
Ama	Antimycin A; CIII: inhibits electron transfer from heme b_H to oxidized Q (Qi site inhibitor); induces ROS production
Azd	Sodium azide; CIV
Hci	Hydroxycinnamate; pyruvate carrier
Kcn	KCN; CIV; competitive inhibitor; pyruvate and hyperoxia counteract inhibition
Mna	Malonate; CII; competitive inhibitor
Myx	Myxothiazol; CIII: binds to the Qo site of CIII (close to cytochrome b_L), inhibits electron transfer from reduced QH_2 to the Rieske iron sulfur protein; induces less ROS production compared to Ama.
Omy	Oligomycin; $L(Omy)$; inhibits ATP synthase by binding on the F_0 -subunit
Rot	Rotenone; CI; if added after NS: $FCF_N=1-S/NS$; binds on the ubiquinone binding site of CI



<http://www.bioblast.at/index.php/MitoPedia:Inhibitors>



<http://www.bioblast.at/index.php/MitoPedia:Uncouplers>

C: References

Open Access to the full list of references and notes:



http://www.bioblast.at/index.php/Gnaiger_2020_BEC_MitoPathways

Selected references, restricted to sources of figures, tables, and basic concepts:

- Chance B, Williams GR (1955) Respiratory enzymes in oxidative phosphorylation. III. The steady state. *J Biol Chem* 217:409-27.
- Doerrier C et al (2018) High-Resolution Fluorescence Respirometry and OXPHOS protocols for human cells, permeabilized fibers from small biopsies of muscle, and isolated mitochondria. *Methods Mol Biol* 1782:31-70.
- Einstein A (1905) Über die von der molekularkinetischen Theorie der Wärme geforderte Bewegung von in ruhenden Flüssigkeiten suspendierten Teilchen. *Ann Physik* 4, XVII:549-60.
- Fick Adolf (1855) Über Diffusion. *Pogg Ann* 94:59-86.
- Gnaiger E (1989) Mitochondrial respiratory control: energetics, kinetics and efficiency. In: *Energy transformations in cells and organisms*. Wieser W, Gnaiger E (eds), Thieme, Stuttgart:6-17.
- Gnaiger E (1993) Nonequilibrium thermodynamics of energy transformations. *Pure Appl Chem* 65:1983-2002.
- Gnaiger E (1993) Efficiency and power strategies under hypoxia. Is low efficiency at high glycolytic ATP production a paradox? In: *Surviving Hypoxia: Mechanisms of Control and Adaptation*. Hochachka PW, Lutz PL, Sick T, Rosenthal M, Van den Thillart G (eds) CRC Press, Boca Raton, Ann Arbor, London, Tokyo:77-109.
- Gnaiger E (2009) Capacity of oxidative phosphorylation in human skeletal muscle. New perspectives of mitochondrial physiology. *Int J Biochem Cell Biol* 41:1837-45.
- Gnaiger E (2020) Canonical reviewer's comments on: Bureau International des Poids et Mesures (2019) The International System of Units (SI) 9th ed. *MitoFit Preprint Arch* 2020.4 doi:10.26124/mitofit:200004.
- Gnaiger E et al (2015) Mitochondrial coupling and capacity of oxidative phosphorylation in skeletal muscle of Inuit and caucasians in the arctic winter. *Scand J Med Sci Sports* 25 (Suppl 4):126-34.
- Gnaiger E et al – MitoEAGLE Task Group (2020) Mitochondrial physiology. *Bioenerg Commun* 2020.1. doi:10.26124/bec:2020-0001.v1.
- Hatefi Y, Haavik AG, Fowler LR, Griffiths DE (1962) Studies on the electron transfer system. XLII. Reconstitution of the electron transfer system. *J Biol Chem* 237:2661-9.
- Lemieux H, Semsroth S, Antretter H, Höfer D, Gnaiger E (2011) Mitochondrial respiratory control and early defects of oxidative phosphorylation in the failing human heart. *Int J Biochem Cell Biol* 43:1729-38.
- Mitchell P (1966) *Chemiosmotic coupling in oxidative and photosynthetic phosphorylation*. Glynn Research Ltd, Bodmin:192 pp.
- Rasmussen UF et al (2001) Aerobic metabolism of human quadriceps muscle: in vivo data parallel measurements on isolated mitochondria. *Am J Physiol Endocrinol Metab* 280:E301-7.
- Renner K, Amberger A, Konwalinka G, Gnaiger E (2003) Changes of mitochondrial respiration, mitochondrial content and cell size after induction of apoptosis in leukemia cells. *Biochim Biophys Acta* 1642:115-23.



Winfried Platzgummer - Oroboros in thermodynamics (2010)